

Diss. ETH No. 9432

**GEOCHEMICAL AND MICROBIAL CONTROLS ON DOLOMITE FORMATION AND
ORGANIC MATTER PRODUCTION/PRESERVATION IN ANOXIC ENVIRONMENTS:
A CASE STUDY FROM THE MIDDLE TRIASSIC GRENZBITUMENZONE, SOUTHERN
ALPS (TICINO, SWITZERLAND)**

A dissertation submitted to the
SWISS FEDERAL INSTITUTE OF TECHNOLOGY ZURICH


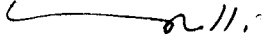
for the degree of
Doctor of Natural Sciences

presented by
Stefano Michele Bernasconi
Dipl. Natw. ETH-Zürich

born June 16, 1961

citizen of Magliaso TI

accepted on the recommendation of

Prof. D. Bernoulli, ETH-Zürich	examiner		
Prof. J. A. McKenzie, ETH-Zürich	co-examiner		
Dr. A. Riva, AGIP SpA, Milano	co-examiner		

1991

ABSTRACT

The Middle Triassic Grenzbitumenzone is a 16 m thick sequence of interbedded, finely laminated organic matter-rich dolomites and black shales. Organic carbon contents in the dolomites reach 10 wt%, whereas black shales have organic carbon contents of up to 40 wt%. Geochemical calculations based on trace metal concentrations in the black shales together with paleontological and sedimentological data indicate that the sediments of the GBZ were deposited at extremely low sedimentation rates (2 to 5 m/my) in a silled shallow marine basin (30-100 m deep) under permanently anoxic conditions. Sedimentary structures indicate that the dolomites are the product of periodic turbiditic transport of carbonate mud into the basin diluting a more or less constant organic matter-siliciclastic background sedimentation. Carbon isotope compositions of the dolomites range from -1.4 to -5.6‰ (PDB) indicating that dolomite was formed in the sulfate reduction zone of organic matter diagenesis. No organic or inorganic geochemical evidence for methanogenetic activity is found in the sediments, suggesting that dolomite may have formed before sulfate was completely depleted from the pore waters. Sedimentary structures and the small variations in carbon isotopic compositions suggest that dolomite is mostly of replacement origin.

Commonly, depth and temperature of dolomite formation are determined solely on the basis of oxygen isotope thermometry. However, because oxygen isotope compositions of dolomite can be modified by late diagenetic exchange with warmer fluids during burial, the determination of the depth of dolomite formation is always rather speculative. Synsedimentary slump structures in the Grenzbitumenzone, however, allow the depth of dolomite formation to be constrained and to evaluate the effect of burial diagenesis on its oxygen isotopic composition. The deformation behavior of various dolomite layers attest to early lithification, with extensive dolomitization occurring only a few centimeters to decimeters below the sediment-water interface. The oxygen isotope compositions of dolomites, however, show a relatively wide scatter and range from -0.4 to -6.5 ‰ (PDB). The $\delta^{18}\text{O}$ -values become more negative with increasing grain-size and percentage of late diagenetic dolomite cements. Fluid inclusion data from these cements indicate a maximum precipitation temperatures of approximately 70°C from fluids with salinities close to that of seawater. The range in oxygen isotopic compositions of the dolomites is therefore interpreted as the result of partial reequilibration of early formed dolomite during late diagenesis.

This study shows that the combination of slow sedimentation rates and high supply of organic matter are the main factors that favored extensive early diagenetic dolomitization in the GBZ. The slow sedimentation rate allowed enough time for magnesium and sulfate to diffuse into the pore waters. The high alkalinity produced by organic matter decomposition through sulfate reducing bacteria, combined with the

availability of magnesium, led to high dolomite supersaturation in the pore-waters and to the replacement of the abundant precursor calcium carbonate.

Organic geochemical data indicate that the organic matter is immature and primarily of marine origin with a high bacterial contribution and can be classified as type II. A high contribution of bacterial lipids to the kerogen is indicated by high hopane concentrations. Variations in maturity-dependent biomarker parameters, such as Ts/Tm and 20S/20R sterane isomerization ratios, observed over a depth range of a few meters, probably reflect changes in bacterial activity and/or redox conditions during deposition and early diagenesis and cannot be related to differences in maturity.

Carbon isotope compositions of total organic carbon are unusually light for marine organic matter and range from -27.5 to -31.8‰ (PDB); $\delta^{13}\text{C}$ -compositions of the saturated and aromatic extract fractions range between -28.1 and -32.9 ‰ and -27.6 and -32.9‰, respectively. The most ^{13}C -depleted samples are those which contain the highest concentrations of hopanes and have the highest Pr/n-C17 and Ph/n-C18 ratios. The relationship between carbon isotope depletion and biomarker concentrations indicates that bacteria which used a ^{13}C -depleted source of carbon for their metabolism are a significant contributor to the organic matter of the Serpiano oil shale.

A model is presented in which sedimentation and organic matter accumulation and preservation is dominated by two major factors: the periodic deposition of carbonate mud turbidites and the presence of a permanently stratified water column in which cyanobacteria and chemoautotrophic bacteria formed a bacterial plate at the anoxic-oxic interface.

RIASSUNTO

La Grenzbitumenzone (Scisti bituminosi di Besano) è composta da un'alternanza di dolomie laminate e argille bituminose di 16 metri di potenza. Il contenuto di carbonio organico delle dolomie raggiunge il 10% mentre le argille ne contengono fino al 40%. I dati geologici e geochimici indicano che i sedimenti della Grenzbitumenzone sono stati depositati molto lentamente (2.5 m/m.a.) in un bacino a circolazione ristretta con acque di fondo permanentemente anossiche. Sulla base di dati geologici la profondità del bacino è stimata tra 30 e 100 m. Le strutture sedimentarie presenti indicano che la maggior parte delle dolomie sono calciturbiditi che diluiscono una sedimentazione di materia organica e detrito siliciclastico. La composizione isotopica del carbonio delle dolomie varia tra -1.4 e -5.6‰ (PDB). Questo indica che la dolomite si è formata come conseguenza dell'attività di batteri solfato-riduttori nel sedimento. La completa assenza di segnali geochimici di metanogenesi indica che la dolomite si è formata prima che tutto il solfato fosse rimosso dalle acque di porosità. Le strutture sedimentarie e le piccole variazioni in composizione isotopica del carbonio indica che la dolomite rimpiazza un carbonato e non è precipitata direttamente da una soluzione.

La presenza di deformazioni sinsedimentarie indica che gli strati dolomitici si sono litificati pochi centimetri al disotto dell'interfaccia acqua-sedimento. La composizione isotopica dell'ossigeno delle dolomiti varia tra -0.4 e -6.5‰ (PDB). La variazione nella composizione isotopica dell'ossigeno è dovuta alla presenza di quantità minori di cementi tardo-diagenetici. Misurazioni di inclusioni fluide indicano che questi cementi sono precipitati a una temperatura di circa 70°C da acqua con composizione essenzialmente marina. La variazione della composizione isotopica dell'ossigeno delle dolomie è dunque dovuta ad una parziale cementazione e recristallizzazione della dolomite formata durante la diagenesi precoce. Questo studio mostra che la combinazione di una sedimentazione lenta associata all'accumulazione di grandi quantità di materia organica è determinante per una dolomitizzazione pervasiva di un sedimento subtidale. La sedimentazione lenta permette a una quantità sufficiente di magnesio di diffondere nel sedimento mentre la presenza di materia organica favorisce la presenza di un'abbondante fauna microbica che aumenta l'alcalinità e favorisce la supersaturazione e la precipitazione di dolomite.

Lo studio di geochimica organica indica che la materia organica è immatura e principalmente di origine marina (tipo II) e contiene una forte componente batterica. Questo è suggerito dalla presenza di grandi quantità di hopani. La variazione di parametri molecolari generalmente dipendenti solamente dalla maturità, segnatamente il rapporto Ts/Tm e il rapporto di isomerizzazione degli sterani, indica che l'attività batterica nel sedimento durante la diagenesi precoce può influenzare questi parametri in modo determinante.

La composizione isotopica del carbonio organico totale è molto negativa per un sedimento marino e varia tra -27.5 e -31.8‰ (PDB). La composizione isotopica degli idrocarburi saturi e aromatici varia tra -28.2 e -32.9‰ e 27.6 e -32.9‰, rispettivamente. I campioni con la composizione isotopica più negativa sono quelli caratterizzati dalla più alte concentrazioni di hopani e con in più alti rapporti Pr/n-C17 e Ph/n-C18. La relazione tra i parametri che indicano attività batterica e la composizione isotopica del carbonio indica che la materia organica della Grenzbitumenzone contiene un importante contributo di batteri che utilizzavano una sorgente di carbonio arricchita di ^{12}C .

La sedimentazione e la produzione/preservazione di materia organica nella Grenzbitumenzone erano controllate da due fattori principali: la deposizione periodica di calciturbiditi e la presenza di una colonna d'acqua stratificata nella quale cianobatteri e batteri chemoautotrofi formavano una "placca batterica" alla superficie della colonna d'acqua anossica.

AKNOWLEDGEMENTS

I would like to sincerely thank my advisors Prof. Dr. Daniel Bernoulli, Prof. Dr. Judith McKenzie and Dr. Angelo Riva for their competent advice, their support and their friendship. Prof. Dr. John D. Hudson, and Dr. Andrew Aplin kindly provided their unpublished sulfur isotope data of the Grenzbitumenzone, for which I am very grateful. I also would thank Prof. Luigi Mattavelli from AGIP, Milano. Without his collaboration and the collaboration of the whole staff of the organic geochemistry laboratory, especially Angelo Riva, Marta Gorzia and A. Caccialanza, the organic geochemical part of this thesis would have not been possible. Among the other people that helped me in the field or in many discussions I would like to thank Prof. Hans Rieber, Prof. Bob Garrison, Peter Brack, Helmut Weissert, David Hollander, Craig Glenn, Andrea Lini, Daniel Aritzegui, Maria Mutti.

A special thank goes to my girlfriend Gretchen Früh for her continuous support throughout the years of my thesis and for her patient help in transforming this manuscript into readable English.

TABLE OF CONTENTS

Abstract	
Riassunto	
Acknowledgements	
CHAPTER 1 SCOPE OF STUDY AND METHODOLOGY	1
1.1 The Grenzbitumenzone: Historical Overview	2
1.2 Summary of Research Objectives	3
1.3 Methods	5
CHAPTER 2 STRATIGRAPHIC FRAMEWORK	9
2.1 Introduction	9
2.2 General Evolution of the Middle Triassic	9
2.3 Description of Individual Formations.	11
2.3.1 Servino (Upper Permian? - Late Anisian?)	11
2.3.2 Lower Salvatore Dolomite	12
2.3.2.1 "Plattendolomite"	12
2.3.2.2 Diplopora Dolomite	13
2.3.3 Middle Salvatore Dolomite and Grenzbitumenzone	15
2.3.3.1 Middle Salvatore Dolomite	15
2.3.3.2 The Grenzbitumenzone	15
2.3.3.2.1 Dimensions of the GBZ basin	16
2.3.4 Upper Salvatore Dolomite and San Giorgio Dolomites	20
2.3.4.1 Upper Salvatore Dolomite	20
2.3.4.2 San Giorgio Dolomite	20
2.3.5 Lower Meride Limestone	22
2.3.6 "Dolomitband"	22
2.3.7 Upper Meride Limestone	23
2.3.8 "Kalkschieferzone"	23
2.3.9 Raibl Beds	23
CHAPTER 3 SEDIMENTOLOGY AND PETROGRAPHY	24
3.1 Introduction	24
3.1.1 The Grenzbitumenzone: General Description	24
3.2 Description of Lithologies	28
3.2.1 Rhythmic sediments	28
3.2.1.1 Laminated dolomites	28
3.2.1.2 Black shales	32

3.2.2	Non periodic events	36
3.2.2.1	White dolomite layers	36
3.2.2.2	Bentonites.	38
3.2.2.3	Cherts	38
3.2.2.4	Massive dolomites	39
3.2.2.5	Coarse resediments	39
3.2.3	Fossil content and preservation	39
3.3	Discussion: Depositional Environment	43
3.3.1	Origin of dolomite laminations	43
3.3.2	Origin of pure organic matter laminae.	44
3.3.3	Bathymetry	46
3.4	Synsedimentary Deformation Structures	48
3.4.1	General characteristics	48
3.4.2	Semi-ductile deformation features	49
3.4.3	Brittle deformation (Layers 140, 144u, 88)	51
3.4.4.	Interpretation of deformation structures	56
3.5	Dolomite Petrography and Cathodoluminescence (CL) Cement Stratigraphy	57
3.5.1	Grenzbitumenzone	57
3.5.2	San Giorgio Dolomites and Lower Salvatore Dolomite	60
3.5.2.1	Salvatore Dolomite	60
3.5.2.2.	San Giorgio Dolomite	60
3.5.3	Fluid inclusions	64
3.5.4	Summary	65
CHAPTER 4	INORGANIC GEOCHEMISTRY	66
4.1	Major and Minor Element Geochemistry	66
4.1.1	Introduction	66
4.1.2.1	Major Elements	67
4.1.2.2	Trace elements	67
4.1.3	Discussion	69
4.1.3.1	Source of trace metals.	69
4.1.3.2	Controls on V and Ni enrichment	71
4.1.3.3	Calculations of excess trace metals	72
4.1.3.4	Calculation of sedimentation rates and water residence times.	74
4.1.3.5	Calculation of primary productivity	77
4.1.4	Summary	79
4.2	Sulfur Geochemistry	79
4.2.1	Introduction	79

4.2.2	Results	81
4.2.3	Discussion	82
4.2.3.1	Controls on pyrite formation	82
4.2.3.2	Timing of pyrite formation	82
4.2.3.3	Sulfur incorporation in GBZ organic matter	85
4.2.4	Summary	88
4.3	Oxygen and Carbon Isotope Geochemistry of Dolomite	88
4.3.1	Introduction	88
4.3.2	Results	91
4.3.2.1	Dolomite crystallography and crystal chemistry	91
4.3.2.2	Isotope geochemistry of Grenzbitumenzone	92
4.3.2.3	Isotope geochemistry of Salvatore dolomite	94
4.3.2.4	Isotope geochemistry of San Giorgio Dolomite and Meride Limestone	94
4.3.3	Discussion: Origin of GBZ dolomites	96
4.3.3.1	Controls on the carbon isotope composition.	96
4.3.3.2	Possible temperature and composition of dolomitizing fluids	98
4.4	Carbonate fluorapatite isotope geochemistry	100
4.4.1	Results and Discussion	100
4.4.1.1	Carbon isotopes	100
4.4.1.2.	Oxygen isotopes	100
4.4.1.3	Carbonate substitution in the apatite lattice	101
4.5	Oxygen isotope geochemistry of cherts	102
4.5.1	Introduction	102
4.5.2	Results and discussion	102
4.6	Summary	103
CHAPTER 5 ORGANIC GEOCHEMISTRY		105
5.1	Introduction	105
5.2	Organic Petrology	106
5.2.1	Results	106
5.2.2	Discussion	106
5.3	Rock-Eval Pyrolysis	109
5.3.1	Definition of parameters	109
5.3.2	Results	109
5.3.3	Discussion kerogen type and organic matter preservation	114
5.3.4	Petroleum potential	117
5.4	Gas Chromatography - Mass Spectrometry Studies	117
5.4.1	Introduction	117
5.4.2	Composition of the extracts	118

5.4.3	Saturated Hydrocarbons	118
5.4.3.1	Normal alkanes and isoprenoid hydrocarbons	124
5.4.3.2	Terpenoids (hopanes, steranes)	127
5.4.3.2.1	Maturity parameters	129
5.4.3.2.2	Source parameters	131
5.4.4	Aromatic hydrocarbons	134
5.4.4.1	Maturity parameters	135
5.5	Organic Carbon Isotope Geochemistry	135
5.5.1	Total organic carbon	135
5.5.2	Saturated and aromatic hydrocarbon fractions	138
5.5.3	Discussion	143
5.5.4	Estimate of the bacterial contribution to total organic matter	146
5.6	Summary	147
CHAPTER 6	SUMMARY AND CONCLUSIONS	148
6.1	Introduction	148
6.2	The GBZ Depositional Environment and Basin Geometry	149
6.3	Sedimentation Rates	151
6.4	Origin of cyclicity	152
6.5	Controls on Organic Matter Accumulation and Preservation	153
6.6	Controls on Dolomite Formation in the GBZ.	156
	References	158
	Appendices	172
	Curriculum Vitae	196

CHAPTER 1

SCOPE OF STUDY AND METHODOLOGY

1.0 Introduction

The discovery of petroleum and its extensive use since the nineteenth century has dramatically changed our society and greatly influenced world politics. Oil has become the main world-energy source and is the main source of base chemicals for the production of a wide range of synthetic products ranging from the plastic bag to high tech medical products. The high costs involved with the search and development of new oil reserves and the predicted exhaustion of the known resources in the next 30 to 100 years has greatly stimulated research on the conditions which promote accumulation and preservation of organic matter in sediments. A positive by-product of this research is a better understanding of the interactions between atmosphere, biosphere and geosphere. This has led to a better understanding of the climatic evolution of the earth and gives us the tools to study the possible consequences of the increase in CO₂-content in the atmosphere from burning of fossil hydrocarbons.

Despite the intensive research, the biological, geochemical and physical factors that promote accumulation and preservation of high quantities of organic matter in sediments are still much debated (e.g. Demaison and Moore, 1980; Tissot and Welte, 1984; Bralower and Thierstein, 1987; Calvert, 1987; Pedersen and Calvert, 1990). The major controversies include: the relative importance of primary productivity vs. oxygen content of the bottom waters, the role of sedimentation rate, the role of aerobic and anaerobic bacteria in the degradation of organic matter synthesized by the primary producers and the importance of chemoautotrophic and photoautotrophic bacteria in the synthesis of organic matter from CO₂. The variety and complexity of the parameters controlling the accumulation of organic matter in sediments requires an interdisciplinary study which, with the integration of organic- and inorganic-geochemical and geological methods, can improve our ability to predict depositional conditions and locations of petroleum source rocks. In this study, the organic carbon-rich sediments of the Grenzbitumenzone (GBZ) in the Southern Alps of Switzerland and Italy are investigated. These sediments are pervasively dolomitized and offer a unique opportunity to combine studies of the processes of organic matter production and accumulation with processes of early diagenetic dolomitization.

With the discovery of Holocene dolomites associated with organic matter-rich sediments, the spectrum of environments leading to early diagenetic dolomitization has been enriched with a new actualistic model. Most studies of recent and ancient dolomites associated with organic matter-rich sediments, however, have concentrated on deep

marine settings with high sedimentation rates (e.g. many papers in Garrison et al. (eds), 1984; Shimmiel and Price, 1984; Burns and Baker, 1985; Burns et al., 1988; Botz et al., 1988). Moreover, in most known examples, dolomite represents only a few volume percent of the total sediment and is generally concentrated in beds or nodules of concretionary origin. Although these studies have led to a fairly good understanding of the factors controlling dolomite formation, a number of important aspects remain controversial. These include the depth and timing of dolomite formation, the role of dissolved sulfate as an inhibitor of dolomite crystallization and the source of magnesium.

The Middle Triassic Grenzbitumenzone (Frauenfelder, 1916), a 16 m thick sequence of laminated dolomites rhythmically interlayered with black shales, was chosen for this study as it offers a good opportunity to study pervasive early diagenetic dolomitization in a shallow marine basin where good controls on the timing and depth of dolomite formation are available. Moreover, the presence of extremely high concentrations of organic matter (up to 40 wt% TOC) suggest that the environmental conditions during the deposition of the Grenzbitumenzone were extreme and rather unusual in the rock record. Often the study of extreme and end-member situations enables a better understanding of processes that take place under more "normal" earth's surface conditions.

1.1 The Grenzbitumenzone: Historical Overview

The Grenzbitumenzone (GBZ) has been the subject of considerable interest to paleontologists for more than 150 years because of its abundant and well-preserved fauna of vertebrate fossils (e.g. Curioni, 1863; Bassani, 1886). As early as 1863, systematic excavations were undertaken by the Museum of Natural History of Milano to search for vertebrate fossils in the Grenzbitumenzone. Since then, many additional smaller field studies have been completed. In 1950, the University of Zürich began an extensive research program, which included an excavation over an area of approximately 250 square meters on Monte San Giorgio, whereby the Grenzbitumenzone was carefully quarried bed by bed. Through these excavations hundreds of complete and well-preserved skeletons of saurids and fish, as well as a considerable number of invertebrate fossils were recovered. As a consequence of this interest and the rich and varied fauna recovered, there is abundant literature on the paleontology of the Grenzbitumenzone, and a large number of the fossils still await examination or are currently being studied. A synthesis and extensive compilations of paleontological publications on the Grenzbitumenzone can be found in *Lexique Stratigraphique International*, I/II; Kuhn-Schnyder (1974), Rieber (1973), Rieber and Sorbini (1983) Zorn (1971) and Rieppel (1987). Although the paleontological significance of the Grenzbitumenzone has been well documented, the sedimentological, diagenetic (in

particular the problem of dolomitization) and geochemical aspects have received comparatively little attention. The only sedimentological study of the GBZ is that of Müller (1965) which was mainly limited to petrographic observations. Although an early diagenetic origin of dolomitization was recognized, Müller was unable to characterize the environmental controls on dolomite formation.

In contrast to the lack of extensive petrographic and sedimentological studies of the GBZ, some aspects of the organic geochemistry have been studied in more detail. In particular, the isolation and structural determination of porphyrins in the bitumens have received considerable attention (Blumer, 1950; Thomas and Blumer, 1964; Blumer and Omenn, 1961; Blumer and Snyder, 1966; Chicarelli and Maxwell, 1984; Chicarelli et al., 1984, 1987, 1990; Wolff et al., 1983, 1984). Moreover, McEvoy and Giger (1986) studied the distribution of hopanoids in the bitumen and recognized that the organic matter of the GBZ had a high contribution of bacterial biomass. However, a systematic geochemical and petrographic study to determine the petroleum potential and the environmental conditions that led to the deposition and preservation of these organic matter-rich sediments was still lacking. Thus, the main aim of this work is to integrate various modern-day geochemical, sedimentological and petrographic methods in order to better understand the depositional environment and the early and late diagenetic history of the Grenzbitumenzone, as well as to characterize the environmental controls on dolomite formation and organic matter preservation in anoxic environments.

The study area is located along the border between southern Ticino (Switzerland) and Italy. A schematic map of the area showing the outcrops of Middle Triassic rocks is presented in Fig 1.1.

1.2 Summary of Research Objectives

The present study is mainly concerned with the depositional and early diagenetic history of the Grenzbitumenzone and aims to characterize the source of organic matter and factors controlling its preservation in the sediments. Chapter 2 is an overview of the Middle Triassic stratigraphy of the Monte San Giorgio-Lugano region and provides a geological framework to understand the significance of the Grenzbitumenzone in the Middle Triassic evolution of the region.

Chapter 3 describes the sedimentology and petrography of the Grenzbitumenzone, the coeval Salvatore Dolomite and the overlying San Giorgio Dolomite. The sedimentological and petrographic characteristics of these rocks are used to constrain the depositional mechanisms and provide a reconstruction of their diagenetic evolution. These data allow a refinement of the paleoenvironmental picture inferred from previous paleobiological studies, (e.g. Rieber, 1973) and adds information to complete the paleogeographic model proposed by Zorn (1971) in his study of the Salvatore Dolomite.

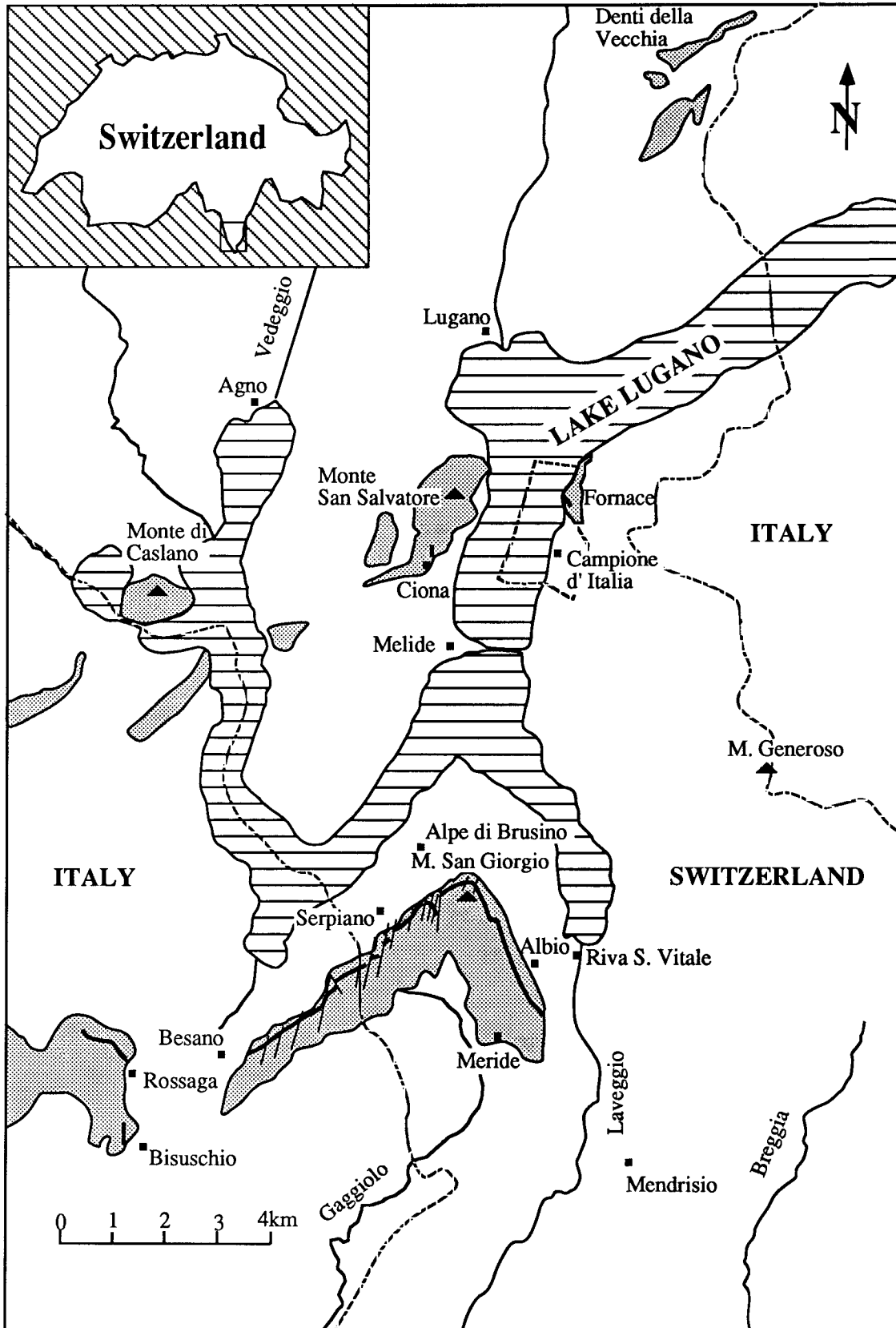


Fig. 1.1 Map of the study area. The dotted signature indicates outcrops of the Middle Triassic formations. The black line marks the outcrop of the Grenzbitumenzone.

Previous sedimentological observations (Müller, 1965; Rieber, 1973) have shown that dolomitization in the Grenzbitumenzone is of early diagenetic origin, but it was necessary to evaluate the extent of late diagenetic modification in order to determine the influence of late diagenetic processes on the early diagenetic geochemical signals.

In Chapter 4, major and trace element geochemistry of the sediments as well as their inorganic stable isotope signatures are presented. These data are used to constrain sedimentation rates and the Eh-pH conditions during sedimentation and allow a characterization of the timing and controls on dolomite, phosphate, pyrite and quartz formation. Chapter 5 combines modern organic geochemical techniques with organic carbon isotope studies in order to characterize the source of the organic matter in the Grenzbitumenzone and to determine the biological and environmental factors that promote the accumulation and preservation of organic matter in sediments. In addition, the organic carbon geochemical data allow an evaluation of the importance of bacterial activity and an estimate of the petroleum potential of the Grenzbitumenzone.

1.3 Methods

X-Ray diffractometry (XRD). Bulk samples and decarbonated samples were mineralogically analyzed by X-ray diffraction techniques on a Seifert diffractometer fitted with a Cu-K α radiation. Dolomite stoichiometry was determined by measuring the displacement of the (104) peak using quartz as an internal standard. No correction for the displacement of the (104) peak due to Fe-substitution (Al-Ashimi and Hemingway, 1974) was necessary because of the low iron content (generally < 0.2%) of the dolomites. Relative percentages of calcite and dolomite were calculated using relative peak height on bulk X-ray diffraction patterns.

Organic and inorganic carbon content Total carbon content was measured using a Carlo Erba CNS elemental analyzer at the Eidgenössische Anstalt für Wasserversorgung, Abwasserreinigung und Gewässerschutz (EAWAG), Dübendorf and with a LECO carbon analyzer at AGIP, Milano. Inorganic carbon was determined on a Coulometrics 5011 coulometer and organic carbon was calculated as the difference between total carbon and inorganic carbon.

Major element and trace element analyses. Major and trace elements were determined by X-ray fluorescence (XRF) on a Phillips PW 1450 spectrometer at the Eidgenössische Materialprüfungs- und Forschungsanstalt (EMPA), Dübendorf. For major elements, approximately 1 g of powder is placed in a ceramic vessel, heated at 1000°C for 2 hours and then weighed to determine the loss on ignition. The powder is then mixed in a proportion of 1 to 5 with lithium tetraborate, melted at 1150°C and then

fused into glass discs. Trace elements were determined on pressed powder discs. The method was calibrated against international rock standards.

Atomic absorption spectrometry. Atomic absorption spectrometry was used to determine trace element distribution in the dolomite. Approximately 100 mg of carbonate sediment were dissolved in dilute hydrochloric acid to minimize leaching from clays. The filtered solution was diluted to 10 ml in a volumetric flask and measured for Fe, Mn and Sr using a Perkin Elmer flame-ionization AAS.

Fluid inclusions. Fluid inclusions were measured on doubly polished rock slabs prepared with a cold technique (Reynolds, pers comm. 1988) to avoid fluid inclusion stretching due to overheating during sample preparation. Temperatures of homogenization and ice melting in the inclusions were determined by standard, calibrated microthermometric methods on a Reynolds-type, heating-cooling stage mounted on a Leitz microscope.

Carbon and oxygen isotopes in Carbonates. Carbonate samples for stable isotope analysis were drilled from polished blocks and then roasted in vacuum at 400 °C for one hour to remove reactive organic matter. The CO₂ gas from carbonates were prepared following the standard procedure (McCrea, 1950). Dolomites were reacted with 100% phosphoric acid for 72 hours at 25°C; calcites were reacted at 25°C for 12 hours. Oxygen isotope compositions of dolomite were corrected using the dolomite-phosphoric acid fractionation factor of 1.01090 (Sharma and Clayton, 1965).

Separation of calcite from dolomite in mixed samples was accomplished according to the method of Kastner et al. (1984). An aliquot of the mixture was dissolved by a pH 5-buffered solution of Na-acetate and acetic acid under continuous stirring until the reaction was complete. The residue was checked for complete removal of carbonates using XRD. The isotopic composition of the calcite coexisting with dolomite was obtained by mass-balance calculations based on calcite-dolomite percentages determined from XRD analysis.

Carbon isotopes in organic matter. Carbon isotope compositions of organic matter were measured on samples decarbonated by reaction with 1N HCl for 12-24 hours. The carbonate-free samples were checked by XRD to assure complete carbonate removal. The method used for organic carbon isotope analysis was described by Craig (1957). An aliquot of the sample (5-10 mg organic C) is placed in a pre-combusted ceramic vessel, introduced into a quartz glass furnace filled with 1.5 atm of oxygen, and burnt at 900 °C for 10 minutes. The gas produced is passed through a second furnace filled with CuO at 750 °C to completely oxidize carbon monoxide and any uncombusted hydrocarbons and then to a third furnace at 450 °C filled with MnO₂ and silver-wool to remove sulfur and nitrogen oxides. The CO₂ is then cryogenically purified with a mixture of methanol and

dry ice and collected for measurement. The extraction procedure was calibrated with the NBS-22 oil standard which has a $\delta^{13}\text{C}$ value of -29.81 (Schoell et al., 1983).

Oxygen isotopes in quartz. Oxygen was liberated from quartz by reacting 10 mg of sample with ClF_3 at 600 °C for 15 hours in nickel reaction vessels. Evolved oxygen was converted to CO_2 by high T combustion with carbon in the presence of a platinum catalyst. The CO_2 was then cryogenically purified through fractional distillation using liquid nitrogen and collected for analysis.

Carbon and oxygen isotopes in phosphate. Carbon and oxygen isotopic compositions of apatite were determined following a modified version of the procedure outlined by McRea (1950) and Kolodny and Kaplan (1970). All samples were drilled or broken out from polished slabs, finely ground by hand in an achate mortar, and checked for purity and CO_2 -content by XRD. CO_2 -content was determined with the (004)-(410) peak pair method of Gulbrandsen (1970). The samples determined to be free from carbonates were treated with 10 % H_2O_2 to remove organic matter and then reacted in 100% phosphoric acid for 72 hours at 25 °C. Samples containing dolomite were not measured because of the present inability to remove dolomite phases without altering the apatite crystal structure.

The CO_2 produced from the different extraction procedures were measured on a VG 903 triple collector mass spectrometer. Duplicate analysis of selected samples showed a reproducibility of better than 0.1 ‰ for carbon and 0.2 ‰ for oxygen for carbonates and phosphates, better than 0.3 ‰ for $\delta^{13}\text{C}$ of organic carbon and 0.2 for oxygen in silicates. All the data are reported in the standard delta notation with respect to the PDB-standard for carbonates, phosphates and organic matter and with respect to the V-SMOW standard for quartz.

Kerogen extraction for palynological analysis. Kerogen was extracted from crushed rocks using the standard HF/HCl technique (Durand, 1980), mounted on smear slides and studied under transmitted, reflected and UV-light. Organic petrological analyses and vitrinite reflectance measurements were made by AGIP, Milano.

Rock-Eval pyrolysis. Rock-Eval pyrolysis reproduces natural maturation of hydrocarbons in sediments by heating the samples in an inert atmosphere. Quantitative measurement of the free and potential hydrocarbons and the CO_2 -content of a sample gives an indication of the type and quality of the organic matter and of the degree of maturation reached by the sample (see Espitalié et al., 1977; 1986 for a description of the apparatus). Analyses were performed on unextracted crushed rock samples at AGIP, Milano. Under normal operating conditions reproducibility of the data is ± 1 °C for T_{max} , $\pm 8\%$ for S2 and $\pm 10\%$ for S3. A definition of the significance of the parameters measured by Rock Eval is given in Section 5.3.

Chloroform extraction of bitumen. The studied samples were chloroform-extracted in a beaker during one hour at 60 °C using 10 ml of solvent per g of sediment. The extract was concentrated at room temperature in a rotary evaporator and open-air dried. The relative proportion of bitumen to total organic carbon is expressed as EXT/TOC in mg bitumen per g of TOC.

Bitumen fractionation and characterization. The bitumens were fractionated by High Performance Liquid Chromatography (HPLC) into a saturated (SHC), an aromatic (AHC) and a non-hydrocarbon fraction composed of resins + asphaltenes (NSO). The saturated and aromatic fractions were studied on a GC/MS system consisting of a HP 5890 gaschromatograph with the capillary column directly connected to the ion source of a HP 5970 MSD-mass spectrometer. The data were collected in multiple ion acquisition mode and processed on a HP-UX computer system. The following operating conditions were used:

a) Saturated fraction:

column: HP ULTRA 1 (OV1)

carrier: H₂ at 16 psi, 2 ml/min

Injection: splitless (T injector at 275°C)

Temperature programming: 40°C for 1 min, 30°C/min to 100°C and then 4°C/min to 300°C.

For routine analyses the following masses were monitored: 71, 191, 217, 218, 253, 177, 231, 259.

b) Aromatic fraction

column: HP ULTRA 2 (SE 54)

carrier: He at 26 psi, 2 ml/min

Injection: splitless (T injector at 275°C)

Temperature programming: 40°C for 1 min, 30°C/min to 100°C and then 4°C/min. to 300°C.

For routine analyses the following masses were monitored: 128, 142, 156, 166, 170, 178, 180, 184, 191, 192, 198, 206, 212, 205, 190, 189, 154, 168, 182.

Compounds were identified by comparing their retention times and mass spectra with literature data and coinjected standards. Relative abundance of compounds was determined by peak area integration.

CHAPTER 2

STRATIGRAPHIC FRAMEWORK

2.1 Introduction

The stratigraphic nomenclature of the Triassic of the Southern Alps is complex and confusing because frequently several synonyms for the same formation have been created by geologists of different schools and countries. Moreover, the scarcity of fossils and the extreme lateral facies variations have led to contrasting interpretations and correlations because age assignments can often only be based on large-scale lithological correlations. Thus, the age boundaries of the formations in Fig. 2.1, which summarizes the Lower to Middle Triassic stratigraphy of the studied area, are in most cases approximate as only a few stratigraphically significant fossils have been found. The nomenclature used in this work is modified after Bernoulli et al. (1976, Geological Atlas of Switzerland, 1:25000, Sheet Lugano) for the San Giorgio area and taken from Zorn (1971) for the San Salvatore-Monte Caslano region. The sedimentology and petrography of the Salvatore Dolomite was thoroughly described by Zorn (1971), therefore, only a brief summary, with some additions based on observations made during the present study, is presented here. A more detailed description of the Meride Limestone lithologies can be found in Wirz (1945). The sedimentology and petrography of the GBZ and some observations on the petrography of the Salvatore and San Giorgio Dolomites, which are necessary to understand the presented dolomitization model and the isotope data, are presented in more detail in Chapter 3.

2.2 General Evolution of the Middle Triassic

The basement of the Southern Alps of the Lugano region consists mainly of gneisses and phyllites, metamorphosed during the Variscan orogeny, belonging to the Val Colla Zone and partly to the Ceneri zone (e.g. Reinhard, 1953, 1964, Bernoulli et al. 1976, Geological Atlas of Switzerland, 1:25000, Sheet Lugano; Zingg et al., 1990). Southeast of Lugano the basement is overlain by a complex of Permian conglomerates, lavas and pyroclastic rocks of basaltic to rhyolitic composition (e.g. Buletti, 1988 and references therein).

The oldest unmetamorphic sediments found in the western Southern Alps are slivers of conglomerates and sandstones of Westphalian age (Manno Conglomerate) which are exposed northwest and northeast of Lugano and are the products of erosion of the Variscan mountain chain (Lehner, 1952; Jongmans, 1960). Overlying the Permian volcanics are red sandstones, conglomerates and shales of the Servino Formation (Late Permian?-Late Anisian?) which represent sediments produced by the erosion of the basement and Permian volcanics. In contrast to the eastern shore of Lake Como, the

presence of the Late Anisian Bellano Formation (Gaetani, 1982; Farabegoli and De Zanche, 1984; Bertotti, 1991) in the study area cannot be demonstrated because evaporitic sediments correlatable with the Carniola di Bovegno (Gaetani, 1982; Bertotti, 1991) are missing and the lithological succession of the Bellano formation is quite similar to the Servino (Bertotti, 1991). The Servino sediments are associated with a progressive transgression of a shallow epicontinental sea from the east towards the west. With this Late Anisian transgression, carbonate platforms began to grow and shallow-water carbonate sedimentation became dominant throughout the Lombardian Alps. Extensional or transtensional tectonic activity associated with extensive volcanism during the Upper Anisian and Ladinian produced a first fragmentation of the continental margin and led to the formation of several subbasins with restricted circulation separated by carbonate platforms (e.g. Brusca et al., 1981; Jadoul and Rossi, 1982, Brack, 1984). In the Lugano region, shallow-water platform sedimentation continued unchanged in the north and west (Monte S. Salvatore, Monte Caslano, Val Ganna), where the Middle- and Upper Salvatore Dolomites were deposited. In the south (Monte San Giorgio-Besano-Bisuschio), a basin with restricted circulation and anoxic to disaerobic bottom waters developed in the latest Anisian. The sediments of the Grenzbitumenzone, San Giorgio Dolomite and Meride Limestones were deposited in this basin. The causes for the drowning of the Anisian carbonate platform in this region are unclear. A fragmentation of the crust which led to the formation of basins and swells as a result of extensional tectonics and differential subsidence was postulated by Zorn (1971). However, no positive evidence of tectonic activity or palaeofaults is recognizable in the Lugano area. A drowning due to environmental changes that led to the suppression of carbonate production on parts the Upper Anisian platform is also possible.

During the latest Ladinian the basins were filled and in the Early Carnian a similar facies again developed over the entire western Southern Alps. An abundant input of clastic material, probably derived from the erosion of a Southern Mobile Belt (Brusca et al., 1981; Garzanti, 1985; Gaetani et al. 1986), with local deposition of evaporites, characterized the Carnian. This phase of high detrital input corresponds to a major regressive phase which caused the emersion of the Esino Platform and can be observed across the entire Southern Alps (Jadoul and Rossi, 1982; P. Brack, personal communication, 1990).

2.3 Description of Individual Formations.

2.3.1 Servino (Upper Permian? - Late Anisian?)

The Servino Formation unconformably overlies the intensely weathered Permian Volcanics. It consists of alternating red and green sandstones, conglomerates, pelites and subordinate dolomites and is characterized by strong lateral variations in both lithology and thickness. Sedimentary structures are very scarce; only rarely cross stratifications

and current ripples can be observed. A correlation between different profiles is not possible because of fragmentary exposure and strong lithological variations over short distances. The large lateral facies variations suggest deposition on wide fluvial plains. The presence of a marine fauna of gastropods and bivalves of Scythian age (Frauenfelder, 1916) documents short-lived marine incursions. A detailed description of one profile at Monte San Giorgio can be found in Frauenfelder (1916). The age of the upper and lower limits of the Servino are unknown. Traditionally the transition from clastic to carbonate sedimentation was taken to represent the Skytian-Anisian boundary (Frauenfelder, 1916). However, based on lithological correlations with outcrops along the eastern shore of Lake Como, where terrigenous sedimentation can be shown to reach into the Anisian, De Zanche and Farabegoli (1988) postulate that the Servino sediments at Monte San Giorgio span from the Upper Permian to the Upper Middle Anisian. This interpretation is plausible but cannot be proven as no Permian or Anisian fossils were found.

The thickness of the Servino varies considerably; it reaches 100-120 m in the San Giorgio area (Frauenfelder, 1916), a few tens of meters in Val Ganna (Senn 1924), approximately 60 m northeast of Lugano (Lehner, 1952), and about 13 m at Monte Caslano (Hofmann, 1956). The variations in thickness, however, are not only due to primary depositional differences but, along the Monte Grona Line (Bertotti, 1991) and at Monte Caslano, also to tectonic reduction.

2.3.2 Lower Salvatore Dolomite

The Lower Salvatore Dolomite in the studied area can be divided in two members: (1) a lower member called "Plattendolomite" or "Mendola Dolomit" by the older authors and (2) an upper member called "Diplopora Dolomite".

2.3.2.1 "Plattendolomite"

The transition from the clastic sediments of the Servino to the shallow-water carbonates of the Plattendolomite is gradual. The transitional facies, mostly a few meters thick, is characterized by dolomitic sands and sandy dolomites which lead to the Plattendolomites s.s. The Plattendolomites are well-bedded, fine-grained grey to reddish dolomicrites with subordinate doloarenites (Zorn, 1971). Bed thickness ranges from 2 to 10 cm and rarely reaches up to 30 cm. The beds are mostly massive with planar surfaces, but occasionally algal laminations or nodular levels are observed. Although pervasive dolomitization and recrystallization have often destroyed the primary sedimentary structures, different microfacies types, such as micrites, pelmicrites, pelsparites and doloarenites, can be recognized (Zorn 1971). Macrofossils are completely absent and microfossils are very rare. Zorn (1971) reported the presence of *Diplopora annulata* SCHAFFHÄUTL and *Physioporella minutula* (GÜMBEL) as well as scarce undeterminable

bivalves and/or ostracod shell fragments. The thickness of the Plattendolomite unit varies between 55 m at Campione and 33 m at M. Caslano (Frauenfelder, 1916; Zorn, 1971). At Monte San Giorgio the thickness can not be determined because the transition to the massive dolomites is not exposed, but it must be less than about 40 m.

Based on their microfacies and the absence of stenohaline fossils, Zorn (1971) suggested that the "Plattendolomites" were deposited in a shallow-water, hypersaline environment protected from strong wave action. The stable isotopic compositions of the dolomites, however, are not consistent with the presence of highly evaporated waters (see Chapter 4).

2.3.2.2 Diplopora Dolomite

The Plattendolomites are overlain by a sequence of light gray, massive to thickly layered dolomites characterized by the presence of large quantities of skeletons of the dasycladacean alga *Diplopora annulata* SCHAFFHÄUTL and *Physioporella minutula* (GÜMBEL) (Zorn, 1971). Different microfacies types can be observed in areas where dolomitization and recrystallization have not completely obliterated the primary textures. The most common are biosparites and more rarely biomicrites, whereby all transitions between these two end-members can be found. Additional components are coated grains, peloids, oncolites and grapestone lumps (Zorn, 1971). Layers with planar algal laminations and birds-eyes occur at different levels; occasionally desiccation crusts and cavities partially or completely filled with a reddish silt-sized dolomite internal sediment can be observed. Moreover, previously unreported breccia layers and bodies are present at different localities. For example, above Albio, a stratiform breccia layer of about 50 cm thickness is observed. In the same profile and along the path that leads from Alpe di Brusino to the top of Monte San Giorgio (Fig. 2.2), breccia bodies at least 4-5 meters in thickness and up to 10 meters wide also occur. Unfortunately, because of poor outcrop exposure and the presence of a superficial weathering crust that at first give them the appearance of massive dolomites, it is impossible to determine their geometry and their lateral extension. The breccias are poorly sorted and have very little matrix; clasts are angular and range in size from a few mm to 15 cm. Dolomites of different microfacies types are represented in the clasts: pelsparites, featureless fine-grained mosaic dolomites, microbreccias and algal laminites. Models for the genesis of these breccias based on cathode luminescence cement stratigraphy, stable isotope geochemistry of the different dolomite phases and fluid inclusion data are discussed in Chapter 4. At the top of the formation, below the GBZ, the dolomites are generally well bedded, and sporadically planar algal laminations occur.

The microfacies, the abundant *Diplopora* and the presence of algal laminations and emersion surfaces indicate that the *Diplopora* Dolomites were deposited in a shallow subtidal to intertidal environment with well-oxygenated waters where calcareous algae could thrive. Because of the absence of stenohaline organisms, Zorn (1971) suggested that

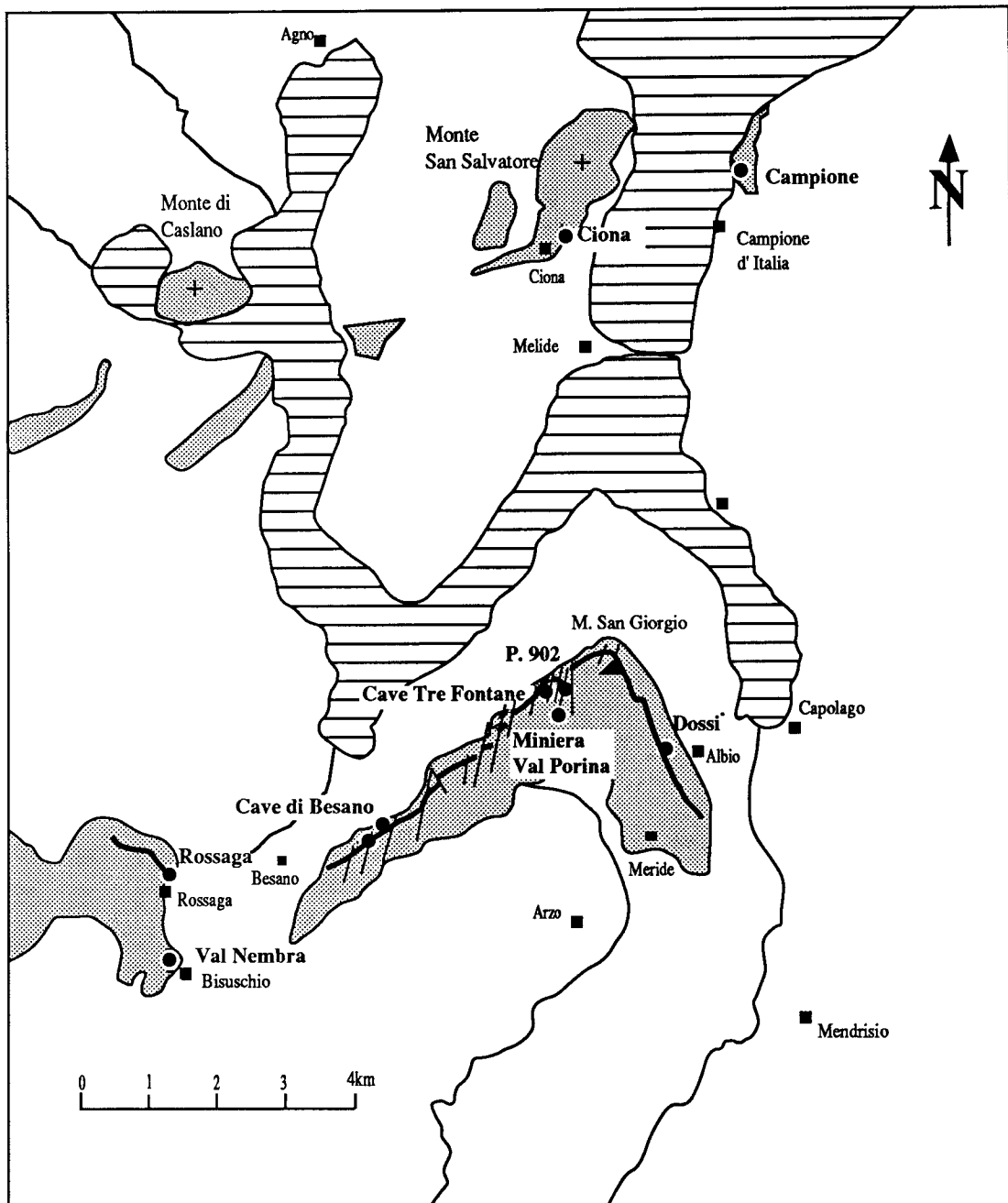


Fig. 2.2 Map of the Monte San Giorgio area. The outcrop localities of the GBZ are indicated by dots. Coordinates refer to Schweizerische Landeskarte 1:25'000, Sheets 1353 Lugano and 1373 Mendrisio.

Miriglioli (= P. 902) (716 512/085 525)

Val Porina Mine (716 580/085 300)

Dossi (717 800/085 162)

Campione (719 050/093 162)

Val Nembra/Bisuschio (710 775/082 025)

Cave Tre Fontane (716 000/085 325)

Rossaga/Pogliana (711.100/082.800)

Cave di Besano (714 050/084 525)

Ciona (716 400/092 375)

the Diplopora Dolomites were deposited under hypersaline conditions, however, this is not confirmed by stable isotope data (see Chapter 4).

2.3.3 Middle Salvatore Dolomite and Grenzbitumenzone

The Middle Salvatore dolomite and the Grenzbitumenzone can be considered roughly time-equivalent (Zorn, 1971, see also discussion in Section 3.3.3) and represent a shallow-water platform and a basinal sediment, respectively. The Middle Salvatore dolomite has only been recognized at Monte San Salvatore and at Monte Caslano (Fig. 1.1; Zorn, 1971). The extension of the GBZ is indicated in Fig. 2.2 by the heavy black line.

2.3.3.1 Middle Salvatore Dolomite

The Middle Salvatore Dolomite has the same shallow-water facies as the Diplopora Dolomite. It was distinguished from the Diplopora Dolomite by Zorn (1971) because of the occurrence of new facies types. He was able to distinguish eight microfacies types, which include algal biolithite-, grapestone-, oncolite-, peloid-, mud- and Diplopora-facies, and he developed a paleogeographic model (Fig. 2.3) for the carbonate platform complex which bounds the northern and western edge of the GBZ basin.

Unfortunately, because of tectonic disturbance and Quaternary cover and because the Salvatore Dolomite is extremely poor in age diagnostic fossils, it is not possible to precisely constrain the temporal and spatial relationship between the Middle Salvatore Dolomite and the GBZ. This would be important for a reconstruction of the paleobathymetry and for an estimation of the sedimentation rate of both the Salvatore dolomite and GBZ, as discussed in more detail in Chapter 3.

2.3.3.2 The Grenzbitumenzone

The Grenzbitumenzone (GBZ) was first formally defined by Frauenfelder (1916) as a sequence of interlayered dolomites, dolomitic marls and black shales with a thickness of 5 m overlying the massive Anisian dolomites of the San Giorgio-Besano region. Because it contains the Anisian-Ladinian boundary, he named it "Grenzbitumenzone", which can be translated in English as the "boundary bituminous zone". Various other names have been used in the literature for this formation including Scisti Bituminosi di Besano, Besano Formation, Serpiano Shales. The name Grenzbitumenzone will be used in this work, abbreviated as GBZ.

Paleontological excavations at Miriglioli (also often called P. 902) in the 1950's and 1960's organized by the Paleontological Institute of the University of Zürich provided a detailed and complete reference profile of the GBZ (Fig. 3.1). The layers were systematically removed one by one over an area of a few hundred square meters and numbered. The main purpose of these excavation was to get a detailed and complete picture of the faunal distribution in the GBZ. The outcrop from these excavations is now

almost completely covered, whereby only layers above approximately bed 180 can still be observed. Outcrops showing the complete section are no longer visible.

The base of the GBZ is defined by the first organic matter-rich layer (layer number 3 of the standard profile); the top is defined by the base of layer 187, which at Mirigioli reaches a thickness of 1.2 m and marks the disappearance of organic carbon-rich layers. This definition proposed by Rieber (1973) will be used in this work. Layers 187 to 230 of the standard profile (Fig. 3.1) are, therefore, included in the San Giorgio Dolomite. The GBZ at Mirigioli (layers 3 to 186) is 15.8 m thick. Black shales account for 2.35 meters, volcanic ashes (Müller et al., 1964) are less than 40 cm and dolomites or dolomitic marls account for the remainder. The Anisian-Ladinian boundary has recently been redefined by Brack and Rieber, 1986; 1991) and is placed between the Reitzi Zone and the Curionii Zone. Based on this definition, in the GBZ the Anisian Ladinian boundary is located between bed 144 and 230 but cannot be defined more precisely because of the lack of ammonites in the upper part of the profile (Brack and Rieber, 1986). Radiometrically dated sanidines from the bentonitic levels give an absolute age of 232 ± 5 Ma for the GBZ (Hellmann and Lippolt, 1981).

2.3.3.2.1 Dimensions of the GBZ basin

All known outcrops of the GBZ are shown in Fig. 2.2. At these localities the GBZ show very similar facies, with low terrigenous- and very rare coarse-grained, platform-derived input. The lateral extension of the outcrops indicate that the minimum east-west extent of the basin was about 10 Km. No data are available on the continuation of the GBZ towards the south, below the Tertiary and Quaternary cover of the Po Plain. The only indication that the GBZ basin extended further towards the south is the presence of rocks similar to the Meride Limestones about 40 km NW of Milano, where this formation was encountered in the Gaggiano and Villafortuna oil wells at depths of 4.6 and 6.2 Km, respectively (Pieri and Mattavelli, 1986). This hypothesis is also in line with the organic geochemical characteristics of the oils of the Gaggiano Field, which bear a number of similarities with rock extracts of the Meride Limestones (Pieri and Mattavelli, 1986; Riva et al., 1986). The GBZ has not been recognized in these wells, which for the greater part have not been cored, but the organic geochemical characteristics of the rock extracts of the GBZ are also very similar to the Gaggiano oils (see Chapter 5) and, therefore, I suggest that the GBZ may be the source rock or at least a co-source of these oils. This would indicate that at the time of GBZ deposition, the basin had already a long southern extension. Alternatively, the basin in which the GBZ was deposited could also have been only one of a chain of small basins (a few kilometers in diameter) with similar characteristics, separated by carbonate platforms.

The westernmost outcrops of the GBZ with its typical appearance are found in Val Nembra on the slope of Monte Minisfreddo and at Rossaga (Fig 2.2). The present outcrop conditions at this locality prevent a detailed observation of the GBZ, however, Müller

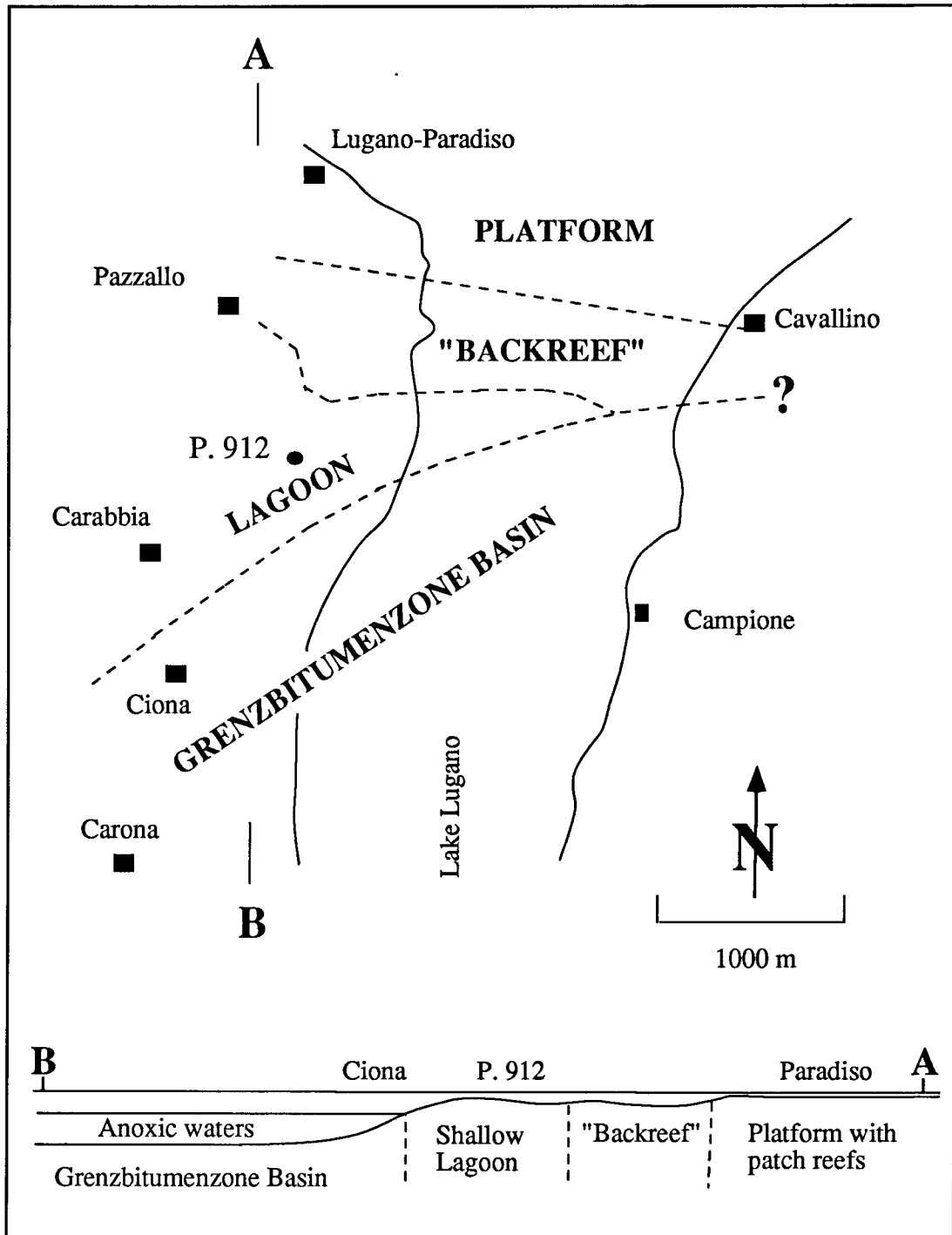


Fig. 2.3 Paleogeographic reconstruction of the Lugano area at the Anisian-Ladinian boundary showing the northern margin of the GBZ (modified from Zorn, 1971). Towards the north, the basin is characterized by a transition to a shallow-water lagoon and finally to a carbonate platform. The presence of tectonic slivers of Salvatore Dolomite along the Monte Grona Line suggest that Monte San salvatore was not a small isolated reef-complex as suggested by Zorn (1971), but more likely, the southern margin of a larger carbonate platform.

reported in 1965 that its overall organic matter content is reduced and the dolomite beds tend to be thicker and homogenized into thick bundles devoid of intercalated black shales. This may indicate that this part of the GBZ was possibly deposited at shallower depths close to the oxic-anoxic interface of the water column, and therefore organic matter was not always preserved. Further west, on Poncione di Ganna and Monte Chiusarella, only thin organic matter-rich layers are found in otherwise massive dolomites (Senn, 1924; Leuzinger, 1926). These observations indicate that the basin became progressively shallower towards the west, and that the sediments were deposited above the limit of the anoxic bottom waters. As there is no evidence of synsedimentary faults or fault scarp deposits and because the transition from the anoxic basinal sediments to the shallow-water platform dolomites is gradual, it is likely that the western margin of the basin had a low angle slope.

Towards the north, the GBZ-basin is limited by the San Salvatore Platform. The small outcrop of GBZ east of Ciona (Fig. 2.2) is also completely devoid of coarse detritus, although it presently lies very close to the platform. This was considered to be evidence for a shallow-water depth of the GBZ (Zorn, 1971). However, this may not be the case. The GBZ outcrop is separated from the main body of the Salvatore platform by a south-vergent Alpine thrust fault of unknown displacement (Bernoulli et al., 1976). An important thrust along this fault is indicated by the presence of a slice of Raibl Beds between the northern and southern blocks. Therefore, the northernmost GBZ outcrop could not have been as close to the platform as it is now, which would explain the lack of coarse detritus. Between the Lugano Line and Monte Grona only isolated slivers of Salvatore Dolomite and Cunardo Formation exist, however, north of Menaggio the Salvatore Dolomite reaches again a thickness of 500m (Bertotti, 1991). This suggests that the Salvatore carbonate platform extended far towards the northwest and that Monte San Salvatore cannot be considered an isolated reef, as suggested by Zorn (1971), but only represents a marginal part of a much larger carbonate platform.

Towards the east the GBZ-basin is presently limited by the Lugano Line, which is an Upper Triassic to Liassic normal fault that was reactivated during the Alpine orogeny (Bernoulli, 1964; Bertotti, 1991). No eastern basin margin between Monte S. Giorgio and the eastern shore of Lake Como can be recognized as no outcrops of Middle Triassic rocks exist. Although an exact estimate of the east-west extension of the basin cannot be made, it is possible to confidently constrain its maximum width if it is assumed that the GBZ and the Meride Limestones were deposited in the same basin as the Perledo-Varenna Limestone, as has been suggested by Gianotti and Tannoia (1988). The base of the Perledo-Varenna Limestone is characterized by the presence of platform-derived, coarse detritus and abundant slump structures and is interpreted as a sediment deposited on a low angle slope approximately 1 km away from the platform (Galbiati and Vanossi, 1986; Gianotti and Tannoia, 1988). If the Late Triassic and Early Liassic extensional movements along the Lugano normal fault are considered, the Middle Triassic sediments exposed along the

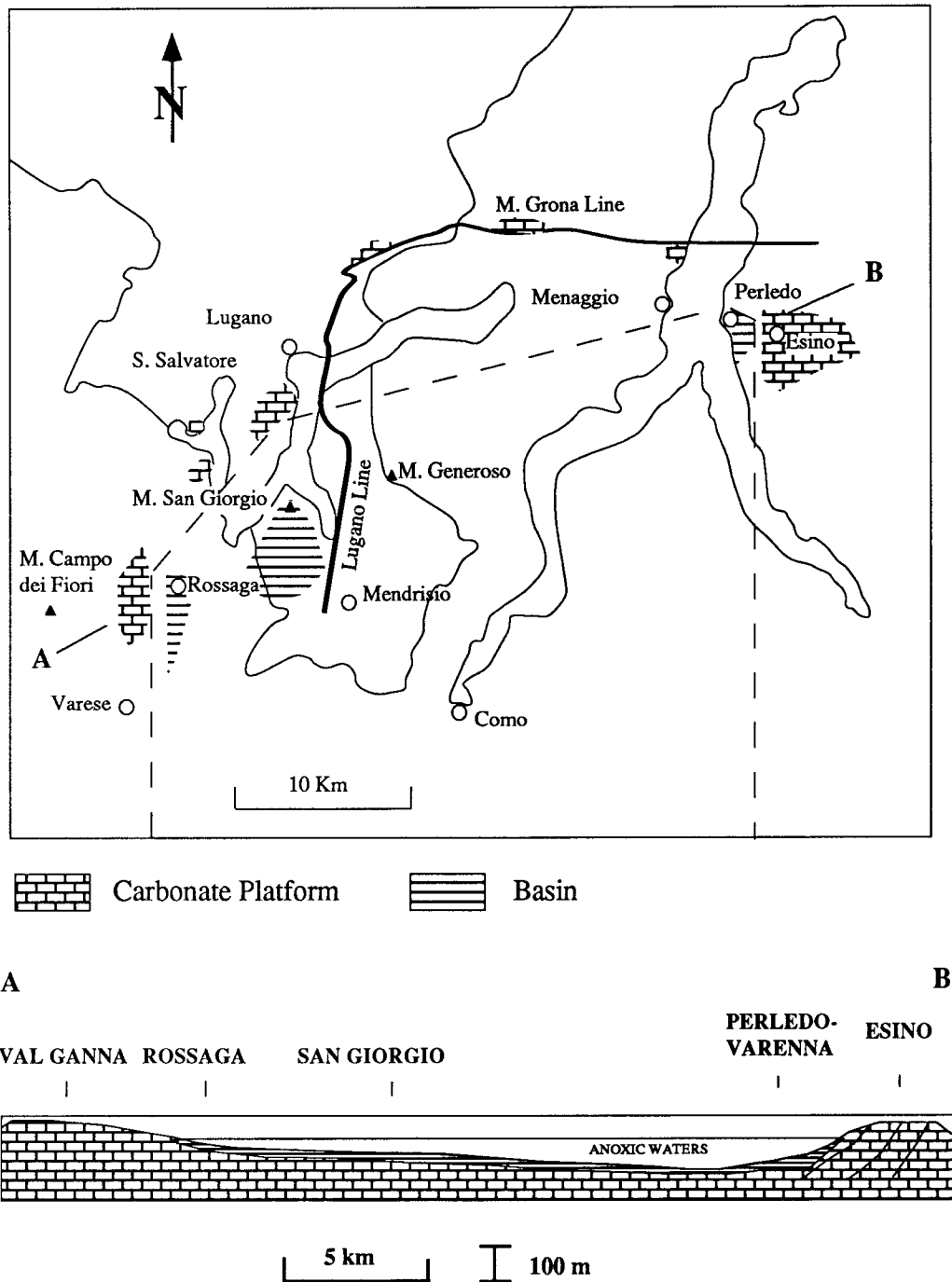


Fig. 2.4 Schematic map of the studied region. The dashed line indicates the maximum extension of the Grenzbitumenzone basin (not corrected for the displacement along the Lugano Line). In the paleogeographic east-west cross section the dimensions of the basin are corrected for the Late Triassic- Early Liassic extension along the Lugano Line.

eastern shore of Lake Como have to be moved westwards by approximately 13 kilometers (Bertotti, 1991). Considering these extensional movements, the E-W extension of the basin where the Perledo-Varenna Limestone, the GBZ and the Meride Limestones were deposited can be estimated to have been about 20 kilometers.

I suggest that the Perledo-Varenna Limestone may represent the more proximal part of the basin slope, whereas the GBZ may represent a more distal part of a slope or the basin floor of the same basin. Some evidence of Middle Triassic faulting is present in the Anisian-Ladinian Esino platform (Assereto et al., 1977; M. Mutti, pers. comm., 1991). The subsidence and the geometry of the basin could have been controlled by the presence of synsedimentary faults at its eastern margin, which led to the formation of an asymmetric basin with stronger subsidence in the east and a moderate slope in the west (Fig. 2.4).

2.3.4 Upper Salvatore Dolomite and San Giorgio Dolomites

2.3.4.1 Upper Salvatore Dolomite

The Upper Salvatore Dolomite was distinguished from the Middle Salvatore Dolomite by Zorn (1971) on the basis of a horizon which he called, following Frauenfelder (1916), "Gervillienhorizont". This horizon is characterized by an abundant fauna of small bivalves of the family Bakevella and undeterminable gastropods. The thickness of this horizon varies at different locations between 17 m and a few centimeters (Zorn, 1971). The Upper Salvatore Dolomite can only be distinguished from the Middle Salvatore Dolomite where the "Gervillienhorizont" is present, as both have exactly the same shallow-water intertidal to shallow subtidal facies. The "Gervillienhorizont" was reported by Frauenfelder (1916) at Monte San Giorgio above the GBZ. Zorn (1971) suggested that layer 187 of the standard GBZ-profile is the time-equivalent of the "Gervillienhorizont" because of the presence of a few, undeterminable bivalve and gastropod fragments. Although this time-equivalence cannot be proven, it can be used to constrain the maximum water-depth of the GBZ (see Chapter 3).

2.3.4.2 San Giorgio Dolomite

The base of the San Giorgio Dolomite is defined by layer 187 of the standard GBZ-profile at P. 902 (Fig 3.1). The transition from the GBZ to the San Giorgio Dolomite is characterized by the disappearance of black shales, by a reduction of the abundance of laminated dolomites, by a significant decrease of the amount of accumulated organic matter and by the presence of abundant silicifications. The dolomites are generally light grey to brown and are well bedded, although dolomitization has locally produced a homogenization of the layers to massive dolomite beds. Sedimentary structures have been completely obliterated by the dolomitization and/or recrystallization and, as a result, the depositional environment is difficult to reconstruct. Chert layers up to 1.5 cm

thick, derived from concentrations of radiolarians of the order Spumellaria (Wirz, 1945) and monaxone and tetraxone sponge spicules, occur at the base of some beds. The radiolarians are generally preserved as chalcedony-filled pseudomorphs in a microcrystalline quartz matrix. The chert-bearing beds are often slumped whereby the chert layers are broken and form angular clasts. The dolomite itself shows no evidence of deformation, indicating that dolomitization and lithification occurred after chert induration and slumping (cf. Bernoulli, 1972, p.814).

Macrofossils are rare; only bivalve shell fragments, often silicified, were observed. *Daonella*, rare ammonites, plant fragments and fish remains are reported by Wirz (1945). In addition, echinoderm fragments are reported by Frauenfelder (1916). Microfossils are dominated by abundant radiolarians. Sponge spicules and foraminifera are less commonly present. At the outcrop Dossi, on the eastern slope of Monte San Giorgio, a calcareous zone about 12 m thick is intercalated with the San Giorgio Dolomites. Mudstones, sometimes laminated but generally homogeneous, alternating with thin shale layers are the dominant lithology. Occasionally wackestones with well-developed graded bedding are interbedded with the mudstones. These lithologies are essentially identical to the Meride Limestone. The presence of turbidite beds and the abundance of radiolarians suggest that the San Giorgio dolomites are a subtidal deposit and may mark the transition to a basin with more open-marine conditions and more intensive circulation than the GBZ-basin. The petrography of the dolomites and cherts are discussed in more detail in Chapter 3. Results of stable isotope analysis of the dolomites are presented in Chapter 4.

2.3.5 Lower Meride Limestone

The transition from the San Giorgio Dolomite to the Lower Meride Limestone occurs over a vertical distance of a few tens of centimeters and is characterized by a rapid decrease in dolomite content. The Lower Meride Limestone consists of well bedded, dark grey to grey limestones, partially dolomitized limestones and marls intercalated with thin shale partings. Less common lithologies include finely laminated limestones, nodular early diagenetic cherts ("Scherzi" of Wirz, 1945) and volcanic ash tuffs. Bed thickness ranges from 1 to 30 centimeters; bed surfaces are mostly planar and continuous. Mudstones are the dominant lithology, but locally wackestones with fine platform-derived debris are observed. Calciturbidites with well-developed graded bedding occur sporadically. Organic carbon contents can reach up to 20% in thin black shale layers but on the average are below 1%. Bioturbation structures are very rare. Massive ash fall tuffs and fine volcanic ashes occur at different levels (Wirz, 1945). The presence of graded beds point to a sediment-gravity flow origin for the Lower Meride Limestone. Although most beds lack recognizable graded bedding, they are probably of turbiditic origin as well (see e.g. Cook and Mullins, 1983). The early Ladinian age of the

Lower Meride Limestone is indicated by the presence of *Protrachyceras archelaus* (Laube) (Wirz, 1945)

The Lower Meride Limestones can be interpreted as a sequence of lime mud turbidites deposited on the basin slope under disaerobic to anoxic conditions. The absence of reworking structures indicates deposition below the wave base. The limited occurrence of slump structures points to a low slope angle. The paleobathymetry of the basin is difficult to assess. The only indication of water depth is given by the preservation of vertebrate fossils with intact rib cages in the Cava Superiore Beds and Cava Inferiore Beds (Sander, 1989). After the animal carcass reaches the bottom of the basin, the microbial decay produces gases in the body cavities that can produce an explosion of the rib cage if the hydrostatic pressure is lower than the internal pressure. In contrast to the saurids found in the Meride Limestones, those preserved in the GBZ often have disrupted ribcages suggesting that the depth of the basin during the deposition of the Lower Meride Limestone was greater than during deposition of the GBZ. These formations may therefore represent a deepening-upward sequence.

2.3.6 "Dolomitband"

The top of the Lower Meride Limestone is defined by the appearance of an approximately 30 m thick dolomite zone known as "Dolomitband" (Frauenfelder, 1918, Wirz, 1945). It is composed of bituminous dolomitic marls and layered, laminated and massive dolomites. The organic matter-rich layers often contain abundant quartz silt detritus. Massive dolomite layers contain intraclasts and evidence for reworking. The dolomite is generally coarse-grained. The central part of the "Dolomitband" is massive, grey to reddish and is often cut by late diagenetic veins filled by coarse-grained saddle dolomite cements and partly by a reddish dolomite silt. The veins with saddle dolomite indicate a possible late diagenetic, high temperature dolomitization.

2.3.7 Upper Meride Limestone

The Upper Meride Limestone is a monotonous sequence of alternating well-bedded bituminous limestones, marls and shales similar to the Lower Meride Limestone. Thickness of the layers ranges from a few mm to 40 centimeters. Breccias and volcanic layers occur at different levels (Wirz, 1945). In the profile of Val Nembra, thin breccia levels and coarser-grained lithologies are more common than at Monte San Giorgio reflecting the closer proximity of the platform compared to Monte San Giorgio. The total thickness of the Upper Meride Limestone reaches about 400-500 m. In analogy to the Lower Meride Limestone, the Upper Meride Limestone is interpreted as a basinal deposit of lime mud turbidites.

2.3.8 "Kalkschieferzone"

The Kalkschieferzone is characterized by very finely laminated calcareous shales, marls and bituminous shales and shows an upward increasing evaporitic character. The fauna is much poorer than in the underlying Upper Meride Limestones, indicating a closure of the basin and an isolation from the open sea (Wirz, 1945). Towards the top, the clay input increases leading to a gradual transition to shales and ultimately to the evaporites of the Raibl Formation. The transition to the Raibl formation is now covered by a small artificial lake which was formed in an old quarry where gypsum of the Raibl Formation was extracted. The top of the "Kalkschieferzone" was dated as Late Ladinian with palynomorphs (Scheuring 1978).

2.3.9 Raibl Beds

The Raibl Beds in western Lombardy are characterized by rapid facies changes and are generally poor in fossils. The Raibl beds represent a period of high terrigenous input derived from erosion of a Southern Mobile Belt (Brusca et al., 1981) with local development of evaporitic conditions. In the Monte San Giorgio area the Raibl beds consist mainly of marls, shales and evaporites (gypsum) (Frauenfelder, 1916). The age of the base of the formation has long been a matter of debate. In the Lake Como region it is considered to be Middle Carnian (Gaetani et al., 1986). In the San Giorgio region, however, palynological data by Scheuring (1978) indicate that the base of the Raibl Beds is probably Late Ladinian.

CHAPTER 3

SEDIMENTOLOGY AND PETROGRAPHY

3.1 Introduction

The reference profile of the GBZ presented in Fig. 3.1 is a compilation of data from the paleontological excavations at Miriglioli by Müller (1965), unpublished data of Rieber and observations made during this investigation. The GBZ corresponds to beds 3 to 186 of the reference profile, whereas beds 187 to 230 belong to the overlying San Giorgio Dolomite. Although it does not belong to the GBZ, the basal part of the San Giorgio Dolomite is included in Fig. 3.1, because the reference profile represents all beds quarried during the paleontological excavations at Miriglioli and references to this part of the profile are often found in the paleontological literature. The discussion in the following paragraphs concentrates on the GBZ, whereas layers 187 to 230 are briefly discussed in Section 3.6. Because the GBZ is presently poorly exposed, samples from the paleontological excavations at Miriglioli samples collected by Müller (1965) and some of his observations are included in this study to complement my field observations.

3.1.1 The Grenzbitumenzone: General Description

The GBZ is characterized by a well-developed cyclic sedimentation (Figs. 3.1 & 3.2). The sedimentation pattern, summarized in Fig. 3.3, clearly shows that the alternation of different types of sediments is produced by the superimposition of two orders of cyclicity. The first order of cyclicity is characterized by an alternation of dolomite beds and black shales on a cm- to dm-scale. The second order of cyclicity is characterized by fine lamination due to grain-size and compositional variations within the beds on a millimetric- or sub-millimetric scale. This rhythmic pattern is sporadically interrupted by short-lived events which are represented by layers of pure dolomite ranging in thickness from a few millimeters to 10 centimeters and interpreted as mud turbidites. In addition, intercalations of volcanic ash layers occur. Bioturbation structures and other indications for benthic life are completely absent, as evidenced by the well-preserved lamination.

Bed thicknesses range from a few millimeters to several centimeters; bedding planes are generally continuous and planar unless deformed by synsedimentary slumps. Some beds, which have a characteristic lamination pattern persisting across the entire basin, enable the correlation of outcrops located kilometers apart. Figs. 3.4 a-c, displaying three samples of layer 144u collected at outcrops separated by approximately 5 kilometers, show the extreme constancy of the fine structure of this bed to the smallest detail. Although parts and individual beds of the GBZ can be correlated relatively well

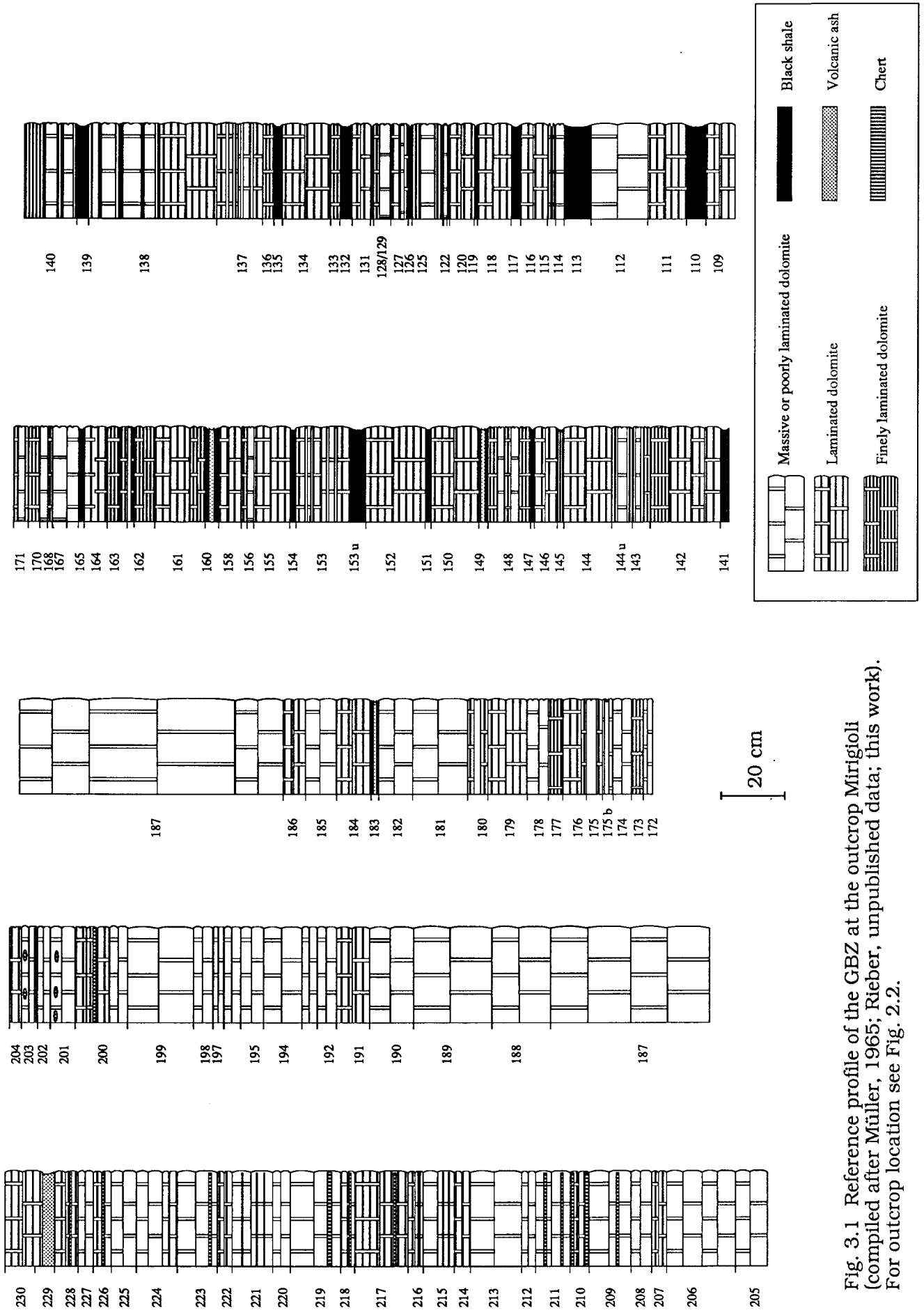


Fig. 3.1 Reference profile of the GBZ at the outcrop Mirigioli (compiled after Müller, 1965; Rieber, unpublished data; this work). For outcrop location see Fig. 2.2.

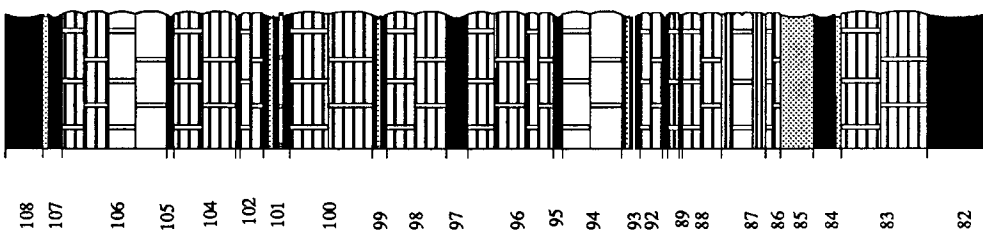
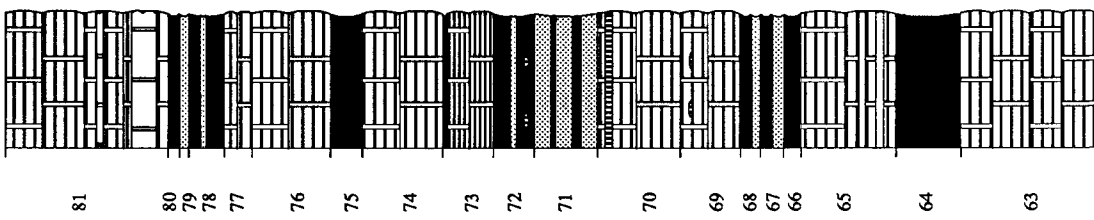
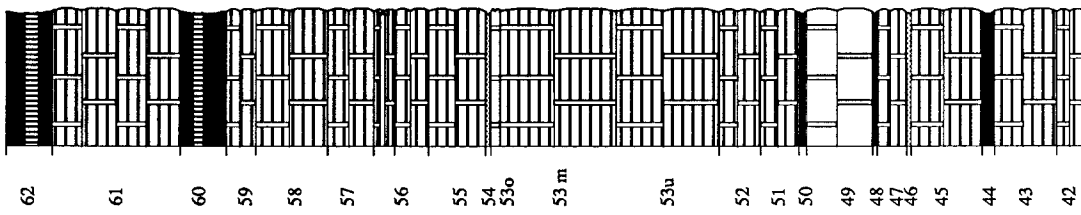
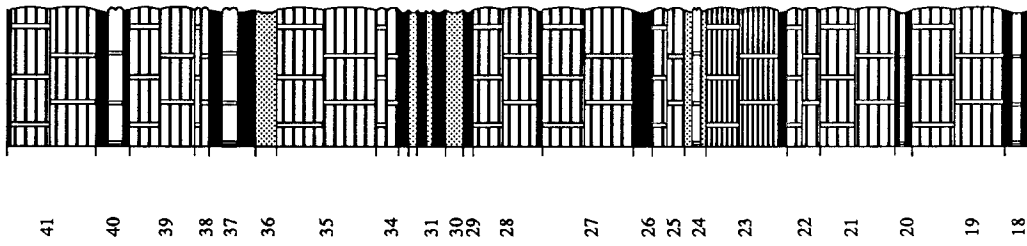
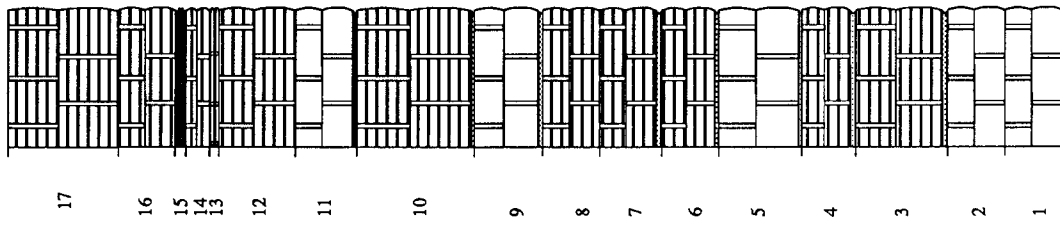
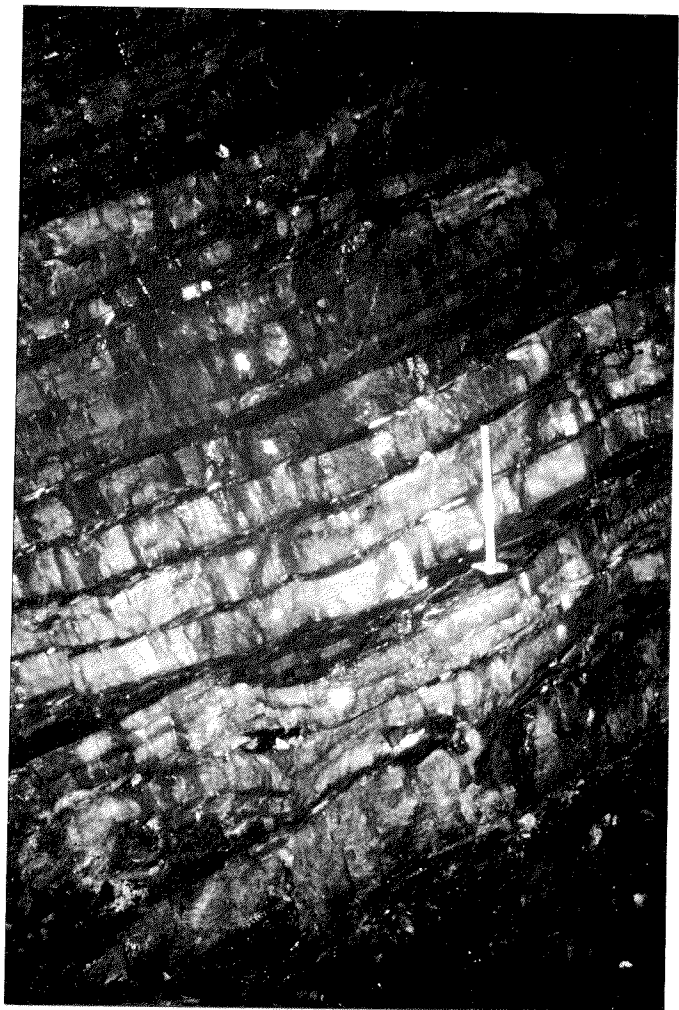


Fig. 3.1 continued

over the entire basin (Fig. 3.5), a bed-by-bed correlation of the whole formation is not always possible, even between outcrops located a few hundreds meters apart (see e.g. Rieber, 1973). The facies differences between the outcrops, however, are only minor. For example the outcrop Dossi is characterized by a slightly greater thickness which is correlated with an overall reduction in organic matter content due to a higher carbonate dilution. The outcrop at Ciona shows a very similar facies as Mirigioli with the only difference being a slightly higher abundance of biogenic debris and the presence of thick slumped sediment packages (Zorn, 1971; for outcrop localities see Fig. 2.3). This is probably a consequence of the closer vicinity of the Salvatore carbonate platform and a slightly steeper slope of the basin than at Monte San Giorgio.

Fig. 3.2

Outcrop photograph of the GBZ at the mine Val Porina showing the well-developed rhythmic bedding characterized by alternating black shale and dolomite layers.



At Mirigioli, dolomite beds represent approximately 80 % of the total formation thickness and vary in color from white to dark brown or black, depending on the organic carbon content, which can reach up to 12 wt%. Dolomitization was pervasive and complete, as no other carbonate phases have been found in the sediments. Black shales (55 layers) represent a total thickness of 2.35 meters out of 15.8 m. The thickness of individual layers ranges from a few mm to 15 cm; they are finely laminated and when

weathered split into mm-thick laminae. Organic carbon contents range from approximately 10 to 41.4 wt%. Thirty-six volcanic layers are recognized in the reference profile (Fig. 3.1). They range in thickness from a few mm to 10 cm and consist of tuffs without any detrital admixture altered to bentonites with relatively small amounts of coarse crystals (Müller et al., 1964; Hellmann and Lippolt, 1981). They are generally gray and are easily recognized in outcrop as they weather to a brown-ocre color.

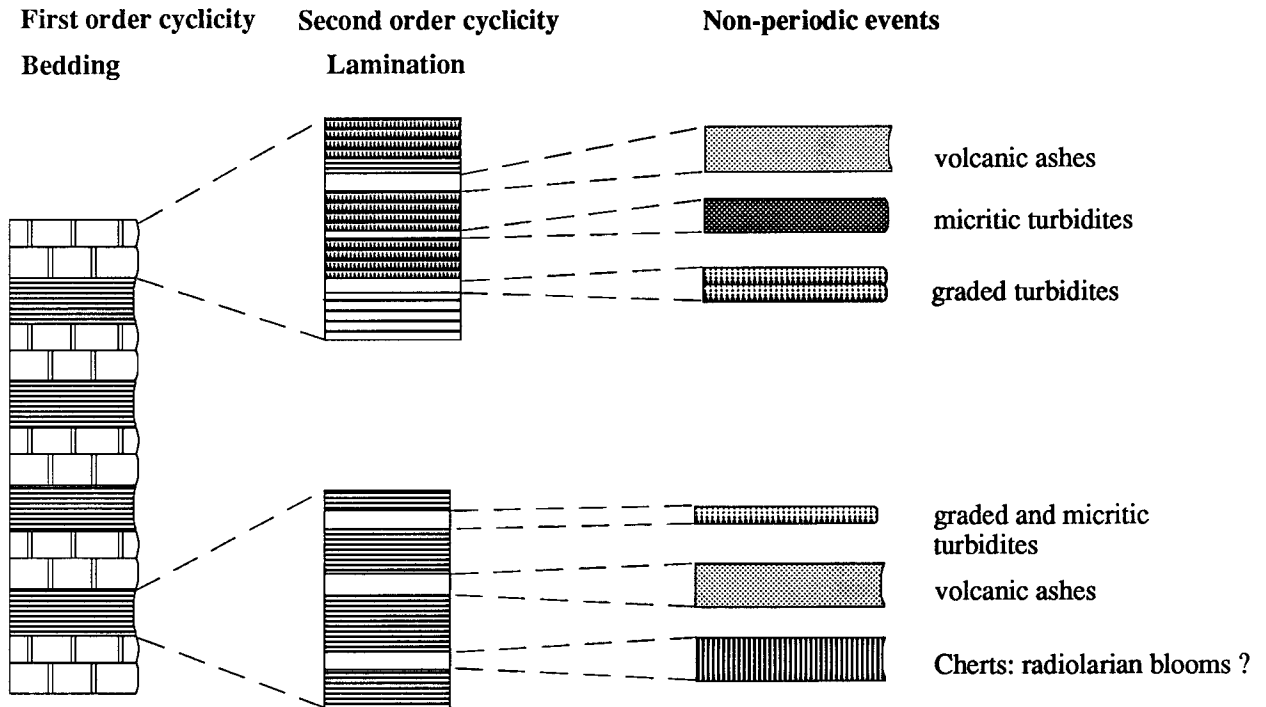


Fig. 3.3. Schematic representation of the cyclic sedimentary pattern of the GBZ. The two superimposed rhythmic cycles, bedding and lamination, are irregularly interrupted by short-lived depositional events, such as volcanic ash falls and mud turbidites.

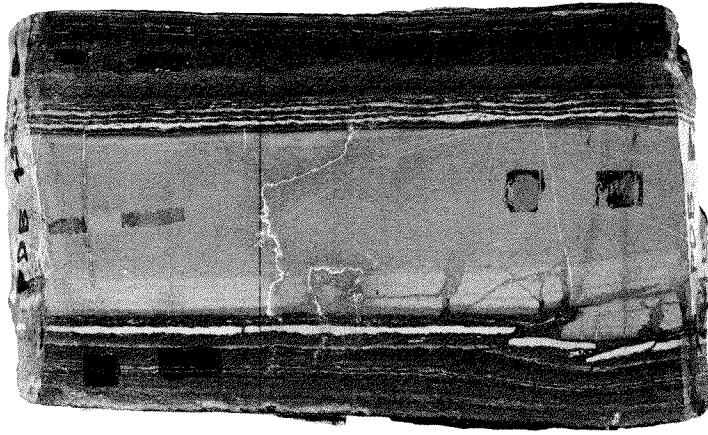
3.2 Description of Lithologies

3.2.1 Rhythmic sediments

3.2.1.1 Laminated dolomites

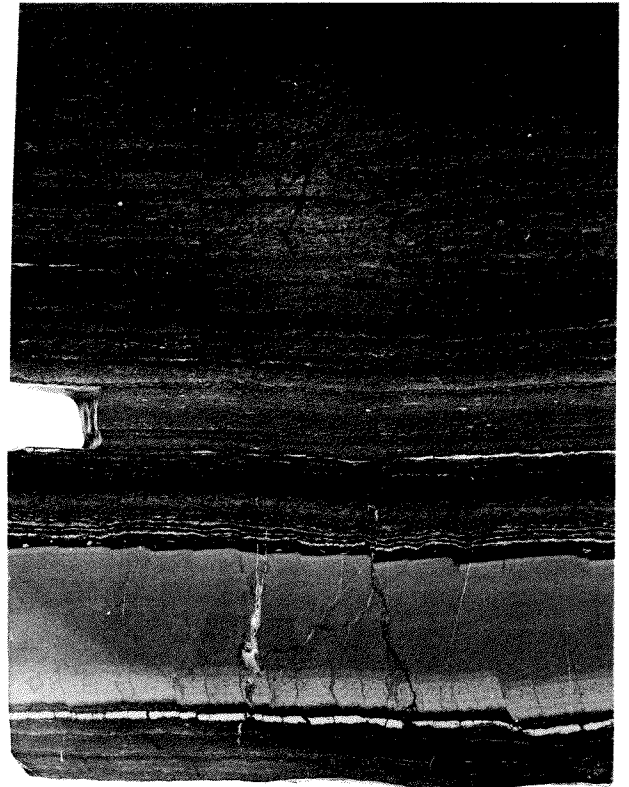
Some characteristic examples of laminated dolomites are presented in Figs. 3.6 a-c. Macroscopically, laminations appear to be mostly planar and continuous, but, when the carbonate laminae are very thin, they can merge and the rock assumes a lenticular texture. This texture is produced either by differential compaction or by displacive dolomite growth in the sediment after deposition. The laminae vary in thickness from 0.01 to 5 mm. The number of laminae per bed or per centimeter is strongly variable and ranges from a few (Fig. 3.6a) to tens of laminae per cm (Fig. 3.6c). Laminations can be

a



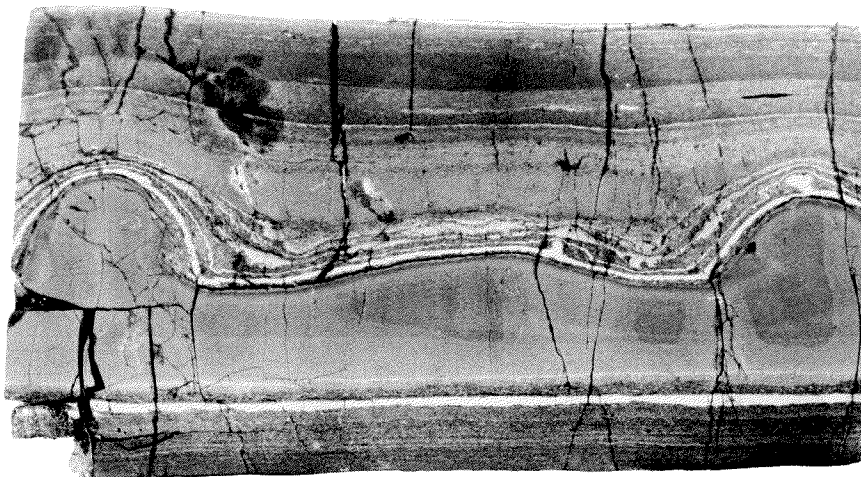
10 cm

b



10 cm

c



10 cm

Fig. 3.4 Samples of layer 144u collected at outcrops Miriglioli (3.4 a), Dossi (3.4b) and Besano (3.4c), encompassing a distance of over 5 km, demonstrate an extensive lateral continuity of the resedimented dolomites. This continuity is particularly evident by the constant thickness of the central thicker dolomite layer and the thin white laminae above and below it.

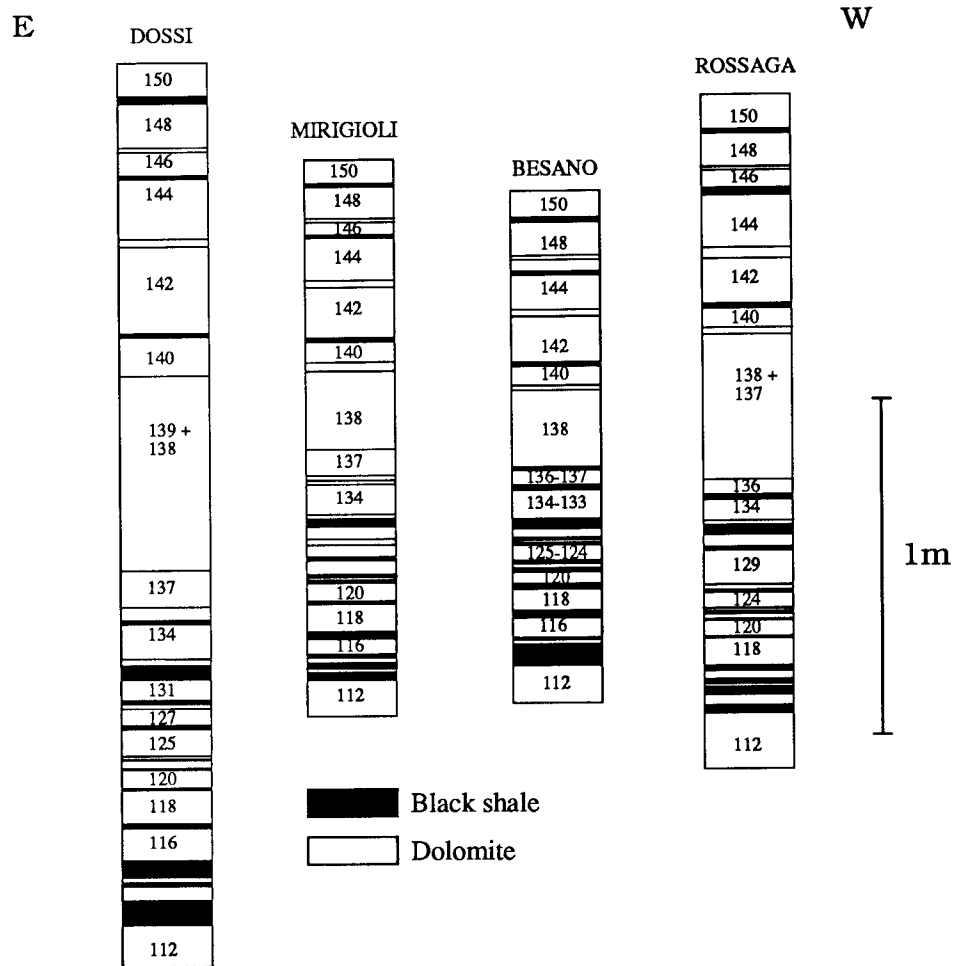
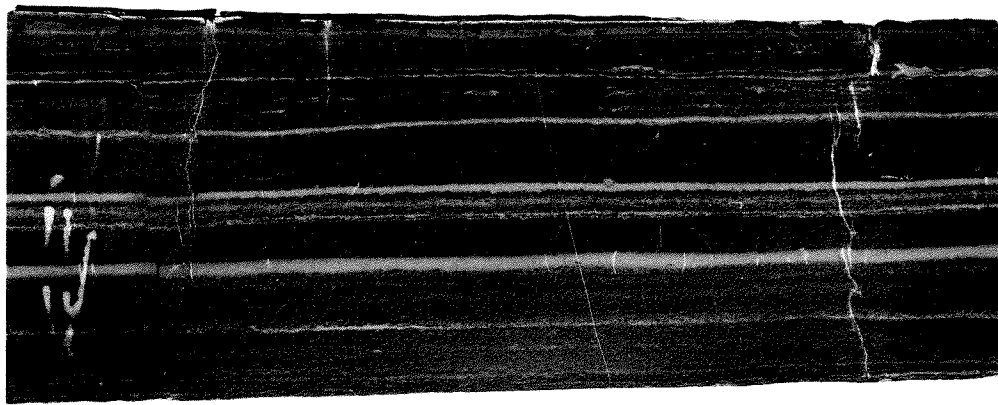


Fig. 3.5. Schematic profiles of the central part of the GBZ from different profiles (modified from Müller, 1965) showing the constancy of bedding across the basin. The variations in thickness of the dolomite layers may represent local variations in carbonate supply due to the different position of the localities relative to the platform.

produced by various mechanisms which together contribute to the formation of a single bed. The microscopic characteristics of the different types of laminites are presented in Figs. 3.7a-f.

In most cases, the lamination is a result of rhythmic variations in the relative proportions of dolomite, organic matter and clay minerals (Figs. 3.7a & b). Quartz is a minor component, mostly occurring as scattered angular grains, and is more enriched in organic matter-rich layers. The angular shape and the absence of chalcedony could suggest a detrital origin of the quartz, but some of the crystals contain framboidal pyrite inclusions which indicate an authigenic origin. Radiolarian tests filled by fibrous chalcedony occur sporadically. However, radiolarians more commonly occur as molds

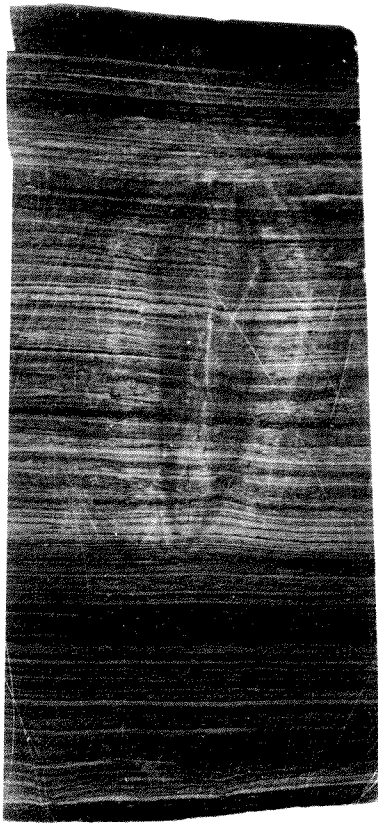


a

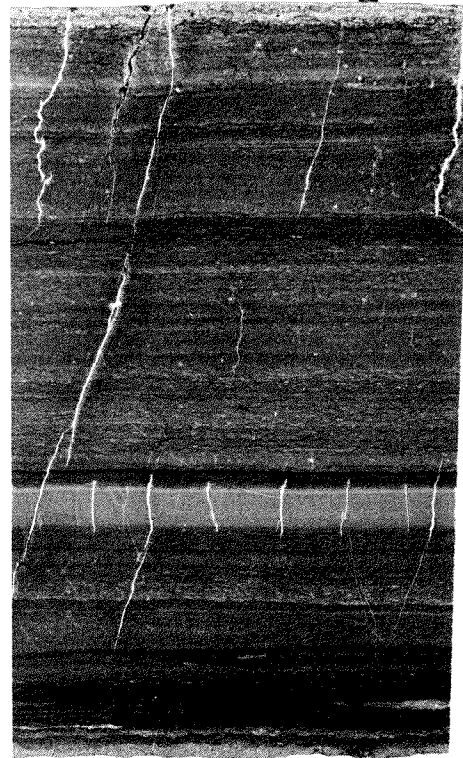


10 cm

b



c



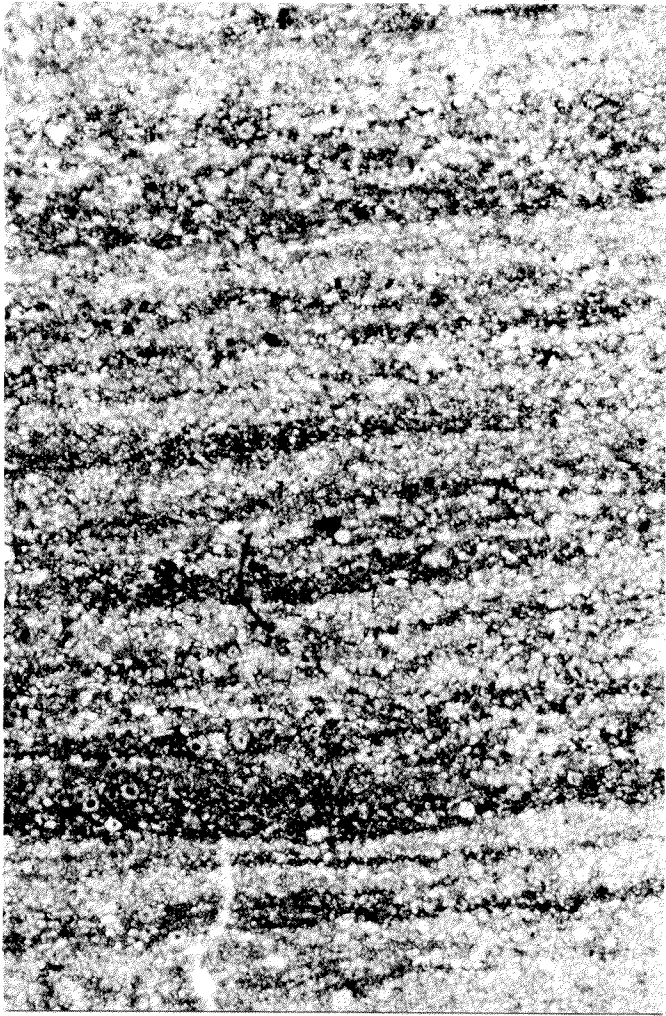
Figs. 3.6a-c Examples of variations in type of laminated dolomites from the outcrop Mirigioli. a) layer 140 showing abundant dolomite resediment laminae (white) in thickly laminated organic carbon-rich dolomite. b) Layer 134, note the fine lamination interrupted by a thick dolomite resediment (white). c) Layer 23, showing millimeter to sub-millimeter lamination and lacking resediments.

filled by sparry dolomite. When the organic matter content is high, dolomite forms lenses and crystal aggregates elongated parallel to lamination. Primary depositional textures inside the laminae are not always visible because of recrystallization and diagenetic dolomite formation, however, a distinct graded bedding is occasionally observed in the dolomite-rich laminae (Fig. 3.7d). Dolomite grain-size decreases from 80-50 μm at the base to micritic at the top, where higher concentrations of organic matter are present. These laminae often show a slightly undulatory base, which is interpreted as evidence for erosion. Rare laminae, both of the graded and homogeneous types, contain shadows of fecal pellets and/or indeterminable fragments of biogenic debris. Some laminae are enriched in silt-sized angular quartz crystals at the base. These structures suggest that these laminae may represent diluted distal turbidites. The association of organic matter with detrital siliciclastic components and the presence of the re-sedimentation textures in the dolomite-rich laminae suggest that the organic matter content of the sediments was controlled by the dilution of a more or less constant organic matter and siliciclastic input through sporadic carbonate sedimentation.

A second type of lamination in layers with low organic matter content is produced mainly by changes in dolomite grain-size (Fig. 3.7c) with no variations in mineralogical composition. In these laminites, thick microsparitic dolomite layers alternate with dolomicrites. Fig. 3.7e shows another type of lamination which is characterized by intercalated pure dolomite layers and thin (0.1-0.01 mm) organic matter laminae. A close up view of this type of lamination (Fig. 3.7f) shows that the organic matter laminae contain abundant pyrite framboids with almost no associated clay minerals. Organic matter generally forms thin continuous films between the dolomite layers, but when the overall organic matter content of the layer is low, the organic matter forms only discontinuous flakes oriented parallel to bedding.

3.2.1.2 Black shales

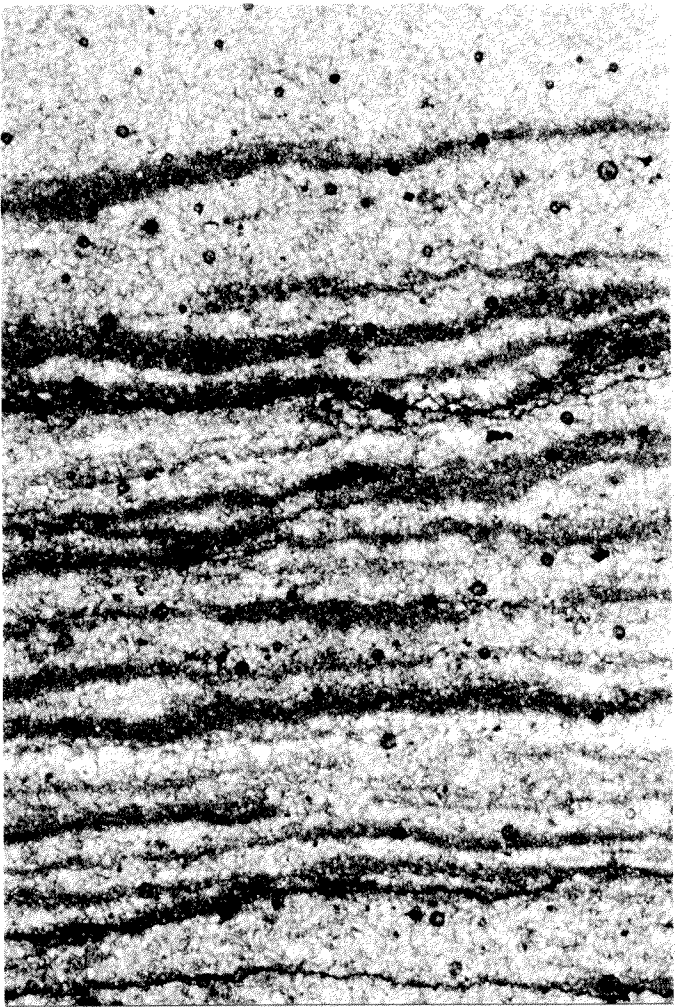
Black shales in the GBZ are fissile and characterized by carbonate contents lower than a few wt% and organic carbon contents mostly exceeding 10%. They are finely laminated (Fig. 3.8) and in polarizing microscope show a bed parallel extinction due to the preferential orientation of clay minerals. The fine lamination becomes more apparent when the black shales are weathered, as they split into mm to sub-millimetre thick layers. Lamination in the black shales is formed by changes in abundance of organic matter, clay minerals and quartz. Petrographic observations indicate that quartz is primarily of biogenic origin. Radiolarians can be very abundant and form chert layers within the black shales (Fig. 3.8a) and are preserved as molds filled by fibrous chalcedony. Detrital quartz grains are more rarely observed in thin section as it is generally very fine-grained and is covered by the organic matter.



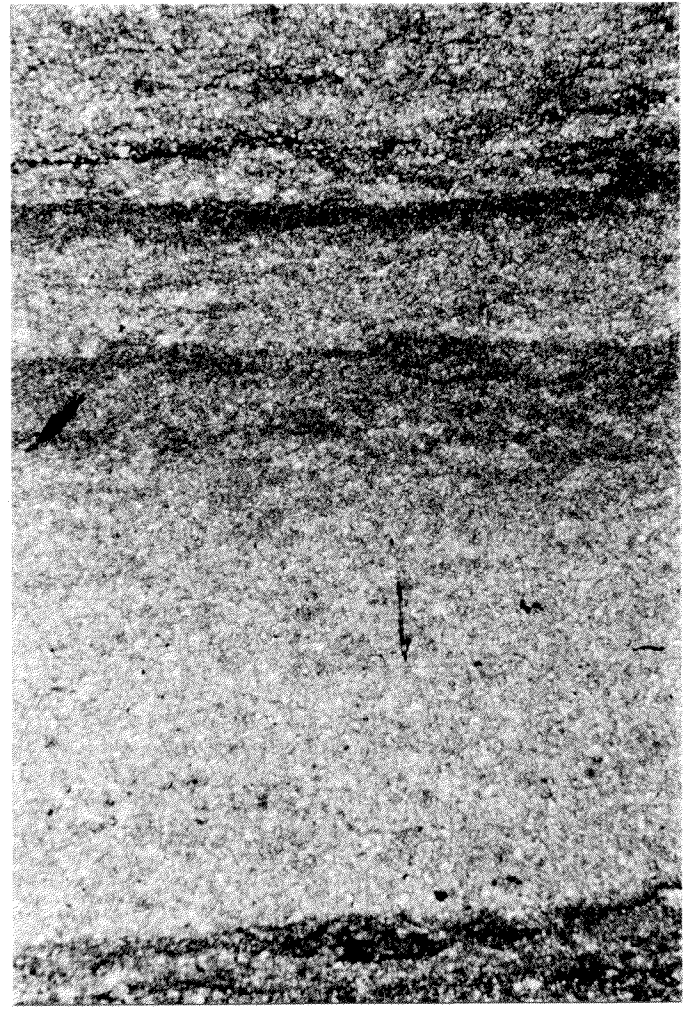
a



b



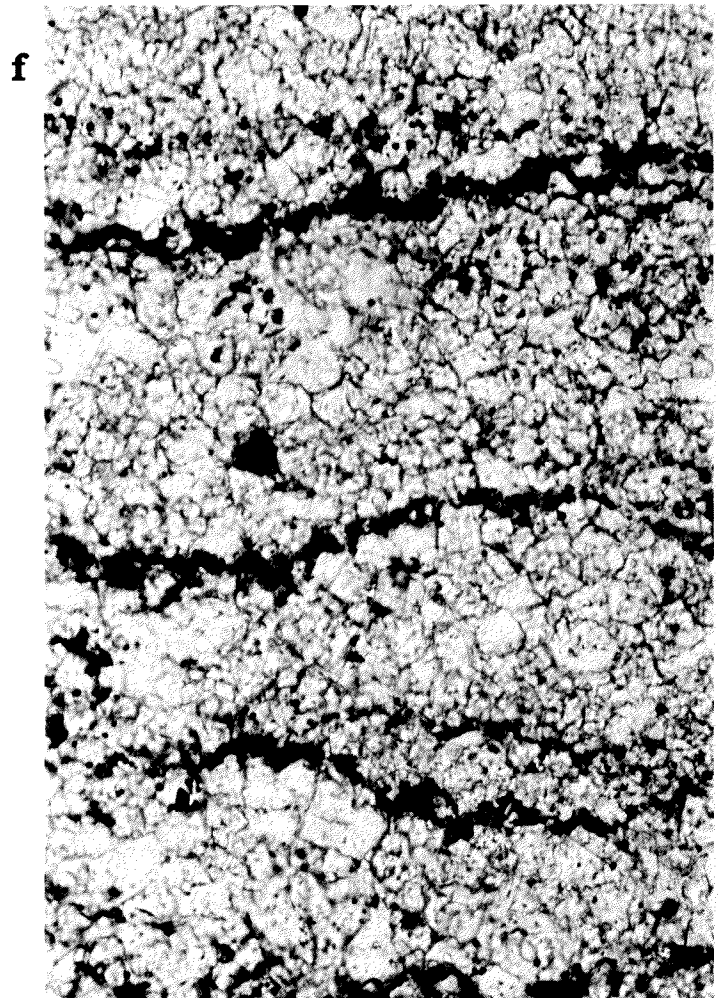
c



d



e



f

Fig 3.7 a-f Thin section micrographs of different types of lamination in samples from outcrop Mirigioli. Field of view 1.1 mm wide except (f) which is 1.5 mm. **a)** Layer 120. Lamination defined by variations in dolomite and organic matter abundance. **b)** Layer 72. Organic matter rich layer in laminated dolomite. The thin layer at the center is a volcanic layer showing graded bedding. **c)** Layer 112. Lamination defined by grain size variations in organic matter-poor dolomite. **d)** Graded lamina in layer 171 showing turbiditic origin of the lamina. **e)** Lamination defined by thin organic matter films. **f)** Close up view of Fig 3.7e showing sparry dolomite laminations alternating with organic-matter films containing pyrite framboids.

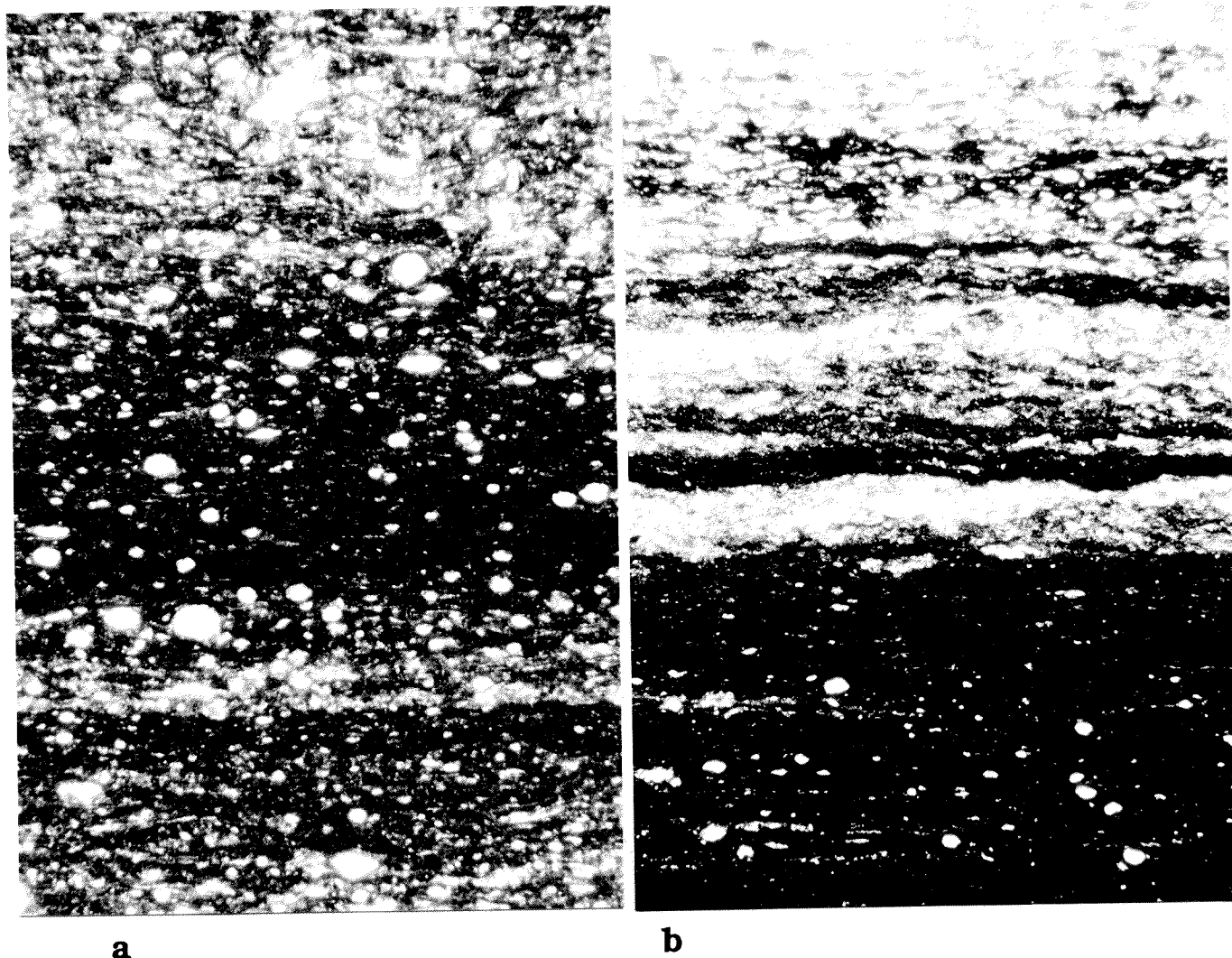


Fig. 3.8 Examples of laminations in the black shales. a) Layer 60, showing quartz and organic matter rich laminae and radiolarian molds filled by chalcedony. b) laminae composed of almost pure quartz alternating with organic matter rich laminae. Field of view is 1.1 cm wide

Dolomite occurs only in low proportions, as dispersed rhombs which generally have dissolved or inclusion-rich centers and clear rims. More rarely dolomite layers occur as thin, primarily micritic layers, which can be easily recognized in the field as white bands. These layers in analogy with those found in the dolomites are interpreted as resediments (see Section 3.2.2.1).

The low carbonate content of the black shales probably reflects a combination of low carbonate input and carbonate dissolution during early diagenesis. Invertebrate calcareous fossil remains are completely absent in the black shales, whereby only rare imprints of mollusks have been observed (Kuhn-Schnyder 1974). In contrast, vertebrate fossils are abundant, which suggests that the lack of calcareous shells does not reflect an absence of life in the water column, but rather is a result of dissolution due to calcite and aragonite undersaturation during early diagenesis. The mineral matrix of the black shales is formed by well-crystallized illite (2m-type dioctahedral), chlorite (illite:

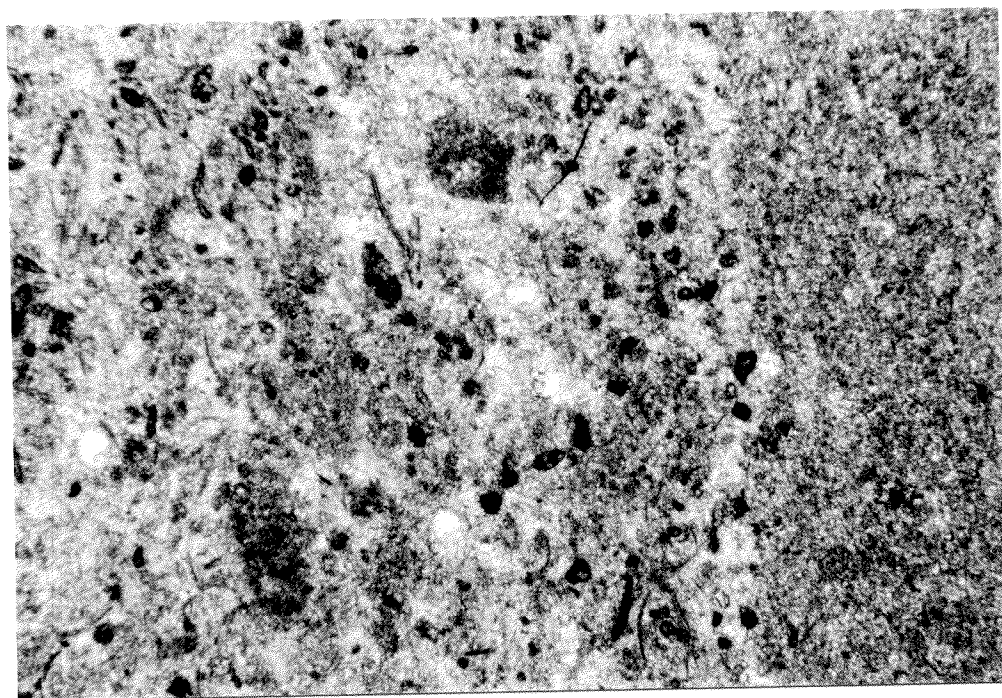
chlorite = 8:1, quartz (2,5-5%), trace amounts of feldspar and pyrite (Müller, 1965). The pyrite is mainly framboidal but rare larger euhedral crystals are also observed.

Carbonate fluorapatite is present as a minor phase in all lithologic types of the GBZ but is especially enriched in the black shales layers, P_2O_5 contents are lower than 0.1% in dolomites but reach up to 0.5% in the black shales. Various types of phosphate occurrences can be distinguished: conodonts, fish and reptile bones and teeth, phosphatized soft tissues of vertebrates and coproliths and/or early diagenetic nodules. Phosphate concretions and coproliths form elongated bodies of 1 to 3 cm in diameter and up to 10 cm long, are mostly composed of pure carbonate fluorapatite and are only rarely replaced by dolomite or quartz. Apatite nodules formed in situ during early diagenesis prior to significant compaction: this is evidenced by differential compaction of laminae of the enclosing sediment around the nodules and indicates a minimum vertical shortening of the black shales by a factor of 10. This is also confirmed by the compression of vertebrate bones in black shales to approximately 1/10 of the original thickness (Kuhn-Schnyder, 1974)

3.2.2 Non-periodic events

3.2.2.1 White dolomite layers

The rhythmic millimetric lamination is often interrupted by layers of pure dolomite with thicknesses ranging from 1 mm to several centimeters (Fig. 3.9, see also Fig. 3.3). These layers and laminae are white in hand specimen and are often very fine-grained and mainly free of organic matter. They are characterized by a high concentration of pellets, occasional biogenic debris (bivalves and/or ? ostracod fragments, fecal pellets and more rarely gastropods) (Fig. 3.9a) and are commonly graded (Fig. 3.9b). Their base is sometimes wavy, which may indicate erosion but could also be a result of differential compaction. Locally the layers show a high lateral continuity over many kilometers, e.g. layer 144u (Figs. 3.3 a-c). Thicker beds are generally composed of more than one resedimentation event; for example, the thick layer at the center of layer 144u is formed by 4 resedimentation events. Other evidence for the allochthonous origin of the sedimented carbonate and of resedimentation is the presence of mollusc molds containing randomly oriented geopetal infillings (Fig. 3.9c). This is indicative of reworking of sediment which had already undergone some cementation. It should be noted that not all of the white dolomite layers show graded bedding or evidence for resedimentation. However, since homogeneous laminae are very fine-grained and macroscopically very similar to those which show positive evidence of resedimentation, all the white dolomite laminae and layers are interpreted as turbidites.



a



b



c

Fig. 3.9. Thin section micrographs of thin dolomite laminae showing evidence of resedimentation (see Section 3.2.2.1). **a)** bioclast-rich lamina with undulatory base and partially filled biomolds, layer 175. **b)** thin dolomite layer showing well developed graded bedding and erosive base, layer 155. **c)** Rotated geopetal fabric in micritic resedimented lamina, layer 155. Field of view is 1.1 cm wide.

3.2.2.2 Bentonites.

The bentonites are composed of a groundmass of illite-montmorillonite with a small amount of phenocrysts, generally smaller than 1 mm, of K-feldspar (sanidine; Or₆₉₋₆₈ Ab₃₂₋₃₁) with diagenetic overgrowths of an adularia-like K-feldspar (Or₉₆₋₉₈ Ab₄₋₂), quartz, biotite and accessory euhedral zircon and apatite (Hellmann and Lippolt, 1981). The complete absence of plagioclase may be primary or be due to diagenetic conversion to montmorillonite (Müller et al. 1964; Hellmann and Lippolt, 1981). The volcanic layers often show a clear graded bedding produced by the enrichment of crystals at the base of the layers. This can be attributed to differential settling velocities of the crystals and glass shards in the atmosphere and in the water column.

The volcanic ashes in the GBZ are similar to bentonite levels found in the Meride Limestones (Wirz, 1945) and in the Salvatore Dolomite at Monte Caslano (Hofmann, 1956), but, because of the lack of plagioclase, are different from all other time-equivalent volcanoclastic rocks of the Eastern Southern Alps (Müller et al., 1964; Callegari and De Pieri, 1967; Jadoul and Rossi, 1982). The difference in plagioclase content and the similarity with volcanic layers in the Middle Triassic of the Briançonnais (Caby and Galli, 1964) has been interpreted as an indication for the presence of other volcanic eruption centers, distinct from those of the Pietra Verde-type in the Eastern Southern Alps (Müller et al, 1964). Only a detailed geochemical study of the ashes would allow a distinction in origin to be determined.

3.2.2.3 Cherts

Although cherts are not very abundant in the GBZ, a few layers up to 1.5 centimeters in thickness are found in some black shales (e.g layers 60, 62). These layers are formed by high concentrations of radiolarian tests and are interpreted as products of sporadic population blooms. Silicifications in the dolomites are rare, although radiolarians occur throughout the section in low abundance in almost all of the beds. In the dolomites, the radiolarians are often replaced by dolomite, but their outlines are still clearly recognizable. The cherts are composed of microquartz and/or chalcedony, with the latter commonly filling the radiolarian molds. Both the length-slow and length-fast variety of chalcedony (Folk and Pittman, 1971) coexist in the same sample. However, length-slow chalcedony is more abundant in organic matter-rich layers, whereas, when dolomite is the predominant host lithology, the length-fast variety prevails. This may reflect differences in Eh-pH conditions or in silica concentration between the different layers (Folk and Pittman, 1971). Inside radiolarian tests relict spheroidal textures, which may represent pseudomorphs after opal-CT lepispheres, are observed. Megaquartz grains are comparatively rare and occur as clear crystals of up to a few mm in length which cement pore space in ammonite molds.

3.2.2.4 Massive dolomites

Massive dolomites are relatively rare in the GBZ. They are characterized by a mosaic dolomite which often shows a patchy texture with domains of coarse sparry dolomite and domains with fine-grained dolomite. Massive dolomites are generally organic matter-poor and are often characterized by a high porosity due to the presence of fossil molds. Occasionally a poorly developed lamination marked by organic matter layers is present in parts of the beds. The complete absence of sedimentary structures due to recrystallization does not allow a characterization of the origin of these layers. The lack of lamination could be interpreted as the result of bioturbation during periods of oxygenation of the bottom waters. However, this is considered unlikely because no unequivocal structures indicative of bioturbation were found. In analogy to the micritic layers, the massive dolomites can be interpreted as mud turbidites or alternatively as a product of reworking of the bottom sediment through strong bottom currents.

3.2.2.5 Coarse resediments

Coarse resediments are very rare in the GBZ; only a few thin layers with intraclasts have been observed (Fig. 3.10). The reworked fragments are mostly derived from the underlying sediment layer. For example, Fig. 3.11 shows a thin breccia layer composed of angular dolomite clasts with a similar texture as the underlying layer in a fine dolomite and organic-matter matrix. The base of the layer is wavy. These layers indicate reworking through bottom currents of previously indurated dolomitic layers and short transport distances.

3.2.3 Fossil content and preservation

As the paleontology of the GBZ has been extensively studied (for extensive reviews see Rieber, 1973; Kuhn-Schnyder, 1974), only the major results necessary for a paleoenvironmental reconstruction are summarized here. The vertebrate fauna found in the GBZ is very diverse and is dominated by marine fish and reptiles which were adapted to a reefal habitat with only a limited amount of truly pelagic fish (Schwarz, 1970; Bürgin et al., 1989; Bürgin, pers. comm., 1991). The reptiles were all marine, and most of them were adapted to a life close to the coast, with the exception of *Ticinosuchus ferox* KREBS which was a land animal (Krebs, 1965; Kuhn-Schnyder, 1974). Vertebrate fossils are more abundant in the black shale layers than in the dolomite beds. For example, in an area of approximately 240 square meters about 220 complete skeletons of vertebrates (saurids and fish) were found in layer 113 (Kuhn-Schnyder, 1974). Close observation of the black shale layers, however, reveals that these skeletons were deposited on different laminae and thus were not embedded at the same time (Sander, 1989). Moreover, the

Fig. 3.10.

Coarse resediments of layer 102 from outcrop Mirigioli. The darker spots on the lower part of the specimen are intraclasts

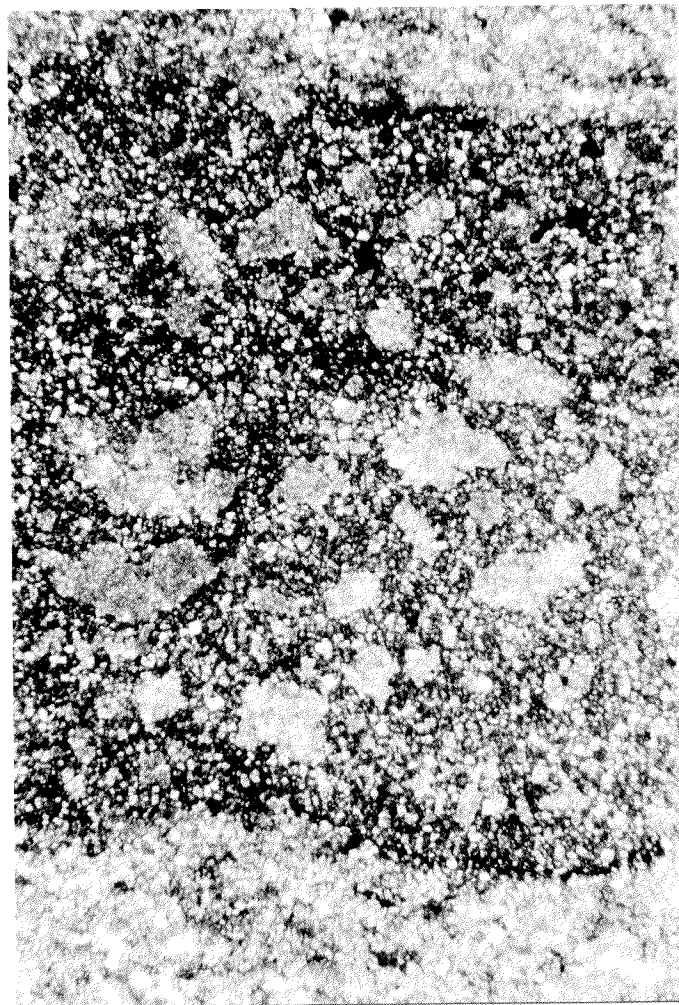
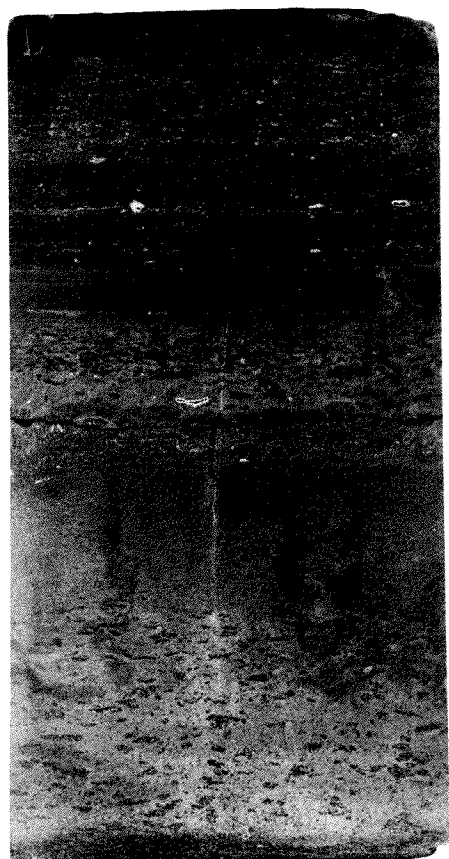


Fig 3.11 Thin section micrograph showing a thin microbreccia layer with reworked dolomite clasts. Field of view is 1.1 cm wide.

presence of individuals of different age suggest a normal attritional mortality for varying reasons and not a catastrophic event. The great concentrations of well-preserved vertebrates in the black shales is, therefore, considered to be the result of a combination of slow sedimentation rates, a high preservation potential in the anoxic bottom waters and additional concentration by compaction (Rieber, 1973; Sander, 1989). On the other hand, the lower content of vertebrate fossils in the dolomite beds suggests that the time represented by one dolomite bed is much shorter than the time encompassed in a black shale layer of comparable thickness.

Invertebrate macrofossils are found only in dolomitic layers and are completely missing in the black shales. *Daonellas* and ammonoids are the most common invertebrate species found in the GBZ. *Daonellas*, which are very thin shelled, are mostly preserved as "steinkerne" or imprints. They can be completely absent or appear in high concentrations as lumachellas in a few layers (e.g layers 38, 58). No size sorting is

observed, and most of the shells are embedded in a convex-upward position (Rieber 1968). Their good preservation indicates no or little transport by currents. *Daonella* and *Posidonia* are the only bivalve species found in the GBZ. The exclusive presence of these species, together with the complete absence of benthos, is a proof of a pseudo-planktonic mode of life of *Daonella* and *Posidonia* (probably attached to driftwood or seaweed) (Rieber, 1968). The presence of layers with concentrations of thousands of specimens is difficult to explain if a pseudo-planktonic life is assumed, because these layers should also be very rich in organic matter or at least contain recognizable remains of driftwood. An alternative explanation would be that *Daonella* were adapted to live on top of the sediments even at low concentrations of oxygen. The mass accumulations in layers could represent population blooms during short-lived periods of partial oxygenation of the bottom waters.

The *Daonella* are commonly flattened and the elements of the sculpture are slightly thrust one over the other. This indicates that they were first compacted and crushed and, only later, were dissolved during the lithification process. On the other hand, ammonites coexisting with the *Daonella* are often uncrushed, indicating that the lithostatic pressure was not strong enough to crush their thicker shells before compaction was interrupted by the lithification process (Rieber, 1973). Therefore, the pressure of compaction before lithification must have been relatively low and only sufficient to crush the very thin shells of the *Daonella* but not the thicker ammonoids. These observations indicate that dolomitization was an early process and that compaction in the dolomitic layers was limited by the relatively rapid lithification.

Cephalopods are preserved as uncompacted molds in the more massive dolomitic layers and become progressively more flattened with increasing organic-matter and/or clay-content of the rock (Fig. 3.12; from Rieber, 1973). Only the living chambers are occasionally filled with sediment, whereas the rest of the shells are partially or, more rarely, completely filled with sparry dolomite and/or quartz cement. When no late cementation occurred the molds perfectly reflect the external morphology of the shell. The shell itself is completely missing and cements grew on the matrix dolomite and generally increase in size towards the center of the mold. When the living chamber is filled with sediment the shell is marked by a dolospar slightly coarser-grained than the enclosing sediment. Petrographic, fluid inclusion and isotopic evidence indicate that pore-filling cements belong to a late, relatively high temperature, phase of dolomitization (dolomite IV, see section 3.5). The mode of preservation of the cephalopods indicates that dolomitization and lithification of the enclosing sediment took place before dissolution of the aragonitic shell. Because the cephalopod shells are aragonitic, it is surprising that they survived dolomitization and recrystallization longer than the enclosing carbonate. This behavior is probably a consequence of the presence of the organic coating on the shell, the periostracum, which under the reducing

conditions in the GBZ was very stable and protected the shell from dissolution. Additionally, the original sediment, which probably consisted of aragonite or high magnesium calcite, was very fine-grained, had a large reactive surface and provided a large number of nucleation centers for dolomite. Although most of the ammonites are preserved in a horizontal position, occasionally vertically embedded specimens are found. Rieber (1973) interpreted this as evidence for fast deposition of the dolomitic layers.

Microfossils are rare and generally poorly preserved. As previously mentioned, radiolarians are the only clearly recognizable microfossils and occur in most of the dolomite layers throughout the section, although they are commonly present as molds filled by a few crystals of sparitic dolomite cement. They are present in higher concentrations in the black shales where they often form chert layers and occur in greater abundance in layers 180-230, at the base of the San Giorgio Dolomites.

Macroscopic land plant remains are rare. Only *voltzia*, a conifera, is sporadically found and rare bisaccate pollen grains can be seen in thin section and in palynological slides. This, together with the presence of *Ticinosuchus*, suggests that land must have been in the vicinity.

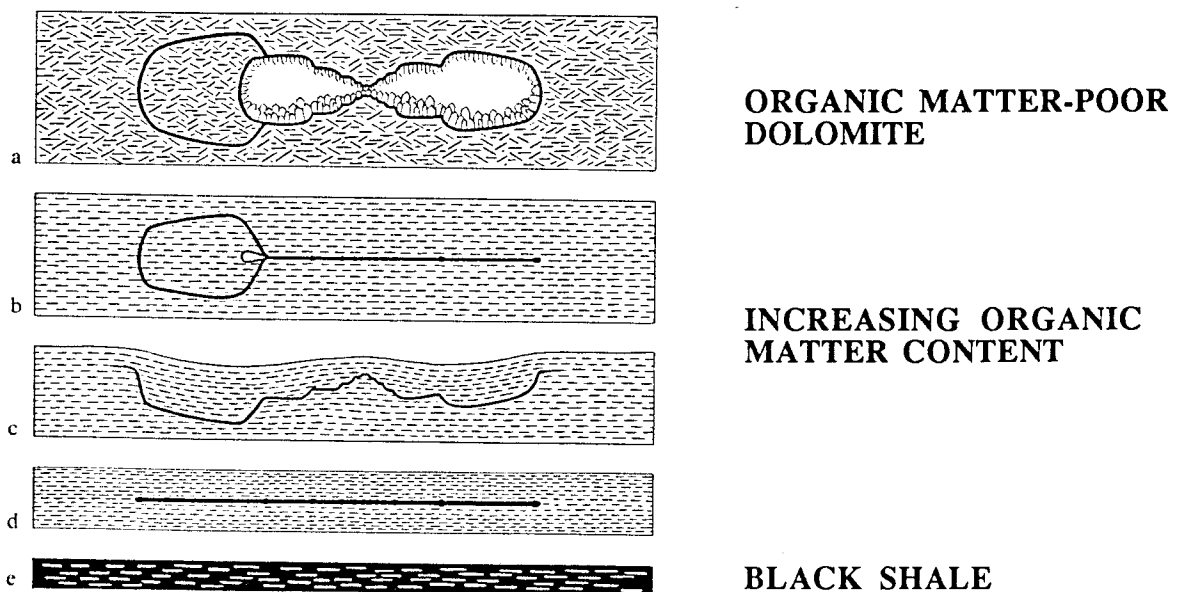


Fig 3.12. Preservation style of ammonoids in the GBZ. The compaction of the shells increase with increasing organic matter content (from Rieber, 1973).

3.3 Discussion: Depositional Environment

3.3.1 Origin of dolomite laminations

Laminated sediments are formed in a variety of marine, estuarine and lacustrine settings and can have widely different origins. Preservation of laminated sediments requires that no or only weak disturbance of the sediment by bioturbation, wave or current activity and gas production in the sediment through organic matter decay takes place. The presence of anoxic bottom waters with oxygen concentrations lower than 0.1 ml/l is, therefore, necessary to eliminate burrowing and bottom feeding fauna (Hallam, 1987). A low angle slope and flat-bottomed basin also reduces creep and/or reworking of the freshly deposited sediments and enhances the preservation potential of the laminations. In addition, sufficient depth is necessary to limit deep water circulation due to storms and wave action, whereby a permanent or at least periodic water column stratification contributes to the reduction of wave-induced turbulence and currents in the lower part of the water column.

The presence of undisturbed lamination and the lack of autochthonous benthic organisms and bioturbation structures indicate that the GBZ basin was characterized by a very stable water column stratification. The bottom waters in the GBZ basin were, therefore, either permanently anoxic, or at least the duration of periods of bottom-water oxygenation were too short to enable colonization by benthic organisms. Sedimentary structures indicating current activity are absent; however, based on limited data on reptile skeletons orientation, Sander (1989) suggested a possible presence of weak oscillating bottom currents during the deposition of the black shales. In any case, the excellent preservation of laminations indicates that the sediments were deposited below storm wave base.

The abundant marine fauna indicate that the basin had surface waters of normal marine salinity which supported an abundant and varied population. Some of the species found in the GBZ are described only from this locality and could be endemic, however, many ammonite forms are recognized across the Southern Alps and elsewhere in the Middle Triassic Paleotethys (Brack and Rieber, 1986; Brack and Rieber, in prep) and are similar to forms recognized in Canada. This, together with the presence of pelagic fish species and ichthyosaurs, indicate that the GBZ may have been deposited in an isolated basin which was at least periodically connected with the open ocean.

Mechanisms which produce laminated sediments as well as the duration of the event forming a single lamina can vary considerably (e.g. Wetzel, 1982). The mechanism leading to the formation of lamination is always difficult to determine, especially in older sediments where compaction and extensive diagenesis may have altered the primary textural characteristics of the sediments. In the GBZ, the laminations are composite in character (Fig. 3.3) and cannot have been produced by a single process. The

principal type of lamination is characterized by changes in the relative proportion of dolomite, organic matter and clay minerals. Not all of the laminae show evidence for re-sedimentation, however, it is likely that most dolomite-rich laminae have a detrital origin. Periodic blooms of carbonate-producing planktonic microorganisms could be an alternative hypothesis for the origin of the laminations. However, carbonate-producing planktonic organisms from Triassic time have been recognized only in Australia on the Wombat Plateau (ODP Leg 122) from Carnian-Rhaetian sediments and therefore, they are probably not important and widespread in the Triassic oceans. This suggests that most likely the carbonate present in the GBZ was not produced in the water column overlying the basin, but rather on the carbonate platform, and was subsequently carried into the basin. I, therefore, propose that the laminations are primarily deposits of carbonate mud which was eroded off the platform and brought into suspension by wave activity during storms and transported into the basin by diluted turbidity currents. This process is considered particularly viable for the origin of the rhythmic laminations in the dolomites and the sporadically occurring white dolomite layers (see Section 3.2.2.2).

The extreme constancy of the lamination pattern in some of the layers (e.g. layer 144u; see Fig. 3.4) is rather surprising if a turbiditic transport mechanism is envisaged, because distribution of the sediment over a large area is required. This apparent inconsistency can be explained by the "detached turbid layer model" of Stanley (1983). The presence of a strong density stratification can hinder the descent of downward currents which are less dense than the waters below the pycnocline. This process, depicted in Fig. 3.13, can lead to the transport and distribution of the fine sediment fraction of a turbidite over the pycnocline and far out into the basin. When the current comes to a rest, the particles sink to the bottom and produce fine laminations, whereby graded bedding can form as a consequence of differential settling of particles of different grain-size. This process is considered viable for the formation of the rhythmic laminations in the dolomites rich in organic matter. Thus, it can be concluded that the organic matter content of the GBZ was controlled by dilution of a more or less constant organic matter-siliciclastic detrital input with periodic carbonate sedimentation.

3.3.2 Origin of pure organic matter laminae.

The origin of the laminae which consist of pure organic matter alternating with dolomite requires a different mechanism of formation. Schieber (1986, 1989) proposed processes involving benthic bacterial mats to explain such laminations in the mid-Proterozoic Newland Formation, Montana. However, structures similar to those observed by the above author were not found in this study. As an alternative, a process analogous to that observed in the Black Sea by Dickmann and Artuz (1979) is considered here. These authors proposed that periodic oxygenation of the water below the

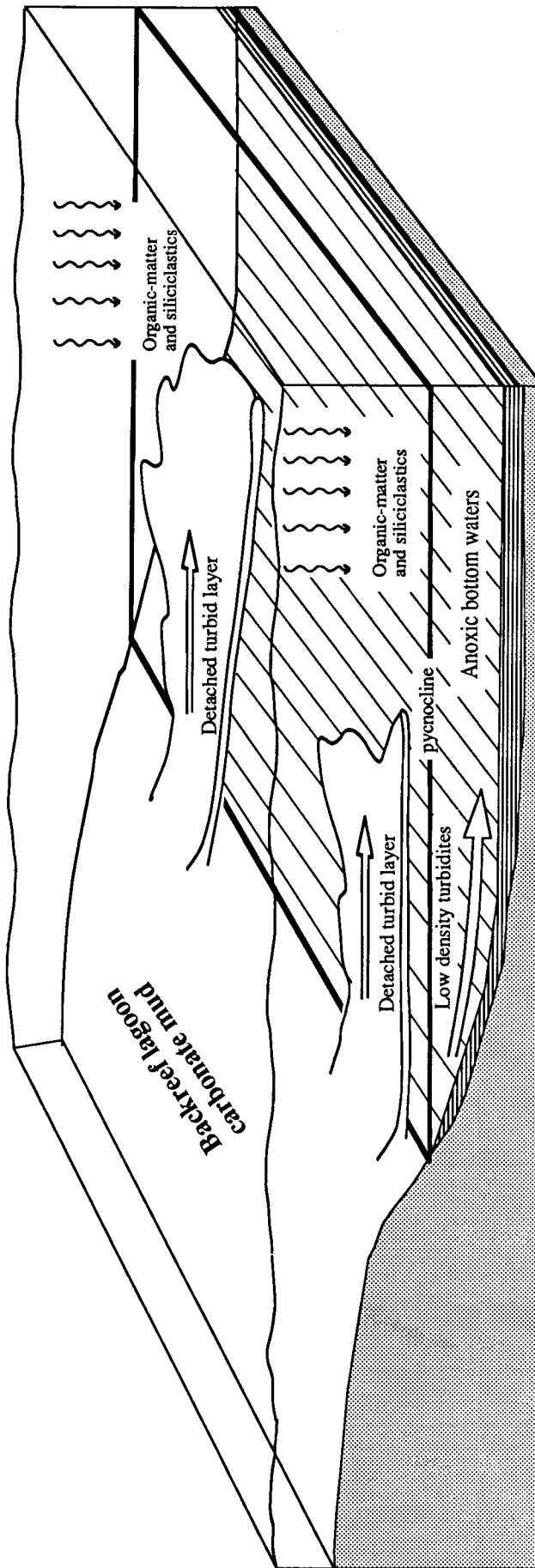


Fig. 3.13 Schematic model of the sedimentary environment and sedimentation processes in the Grenzbitumenzone. The presence of a density stratification in the water column produced the detachment of turbidites favouring the transport of sediment basinward and the spreading of carbonate mud over large areas of the basin. This process, together with "normal" turbidites is responsible for the formation of thin laminations and thicker dolomite beds containing no organic matter.

chemocline leads to mass mortality of the strictly anaerobic photosynthetic (sulfate-reducing) bacteria which live in the anoxic water column, resulting in the deposition of laminae of pure organic matter. It was noted that in the water column during descent of the bacteria, the sulfur contained in the bodies of the bacteria is released and reacts to form iron monosulfides. The strong relationship and intergrowth between pyrite (Figs. 3.6e,f) and organic matter strongly supports a similar process for the formation of the sub-millimeter scale, organic matter-rich laminations in the GBZ sediments.

Although the laminae in the beds were not systematically counted, the variability in the number of laminae per bed (see Fig. 3.6) suggests that each bed reflects varying lengths of time. In addition, the duration of the event forming one lamina is difficult to evaluate. Climatic models for the Triassic (Parrish et al., 1986) suggest a seasonal climate with strong monsoons at these latitudes. The laminae could therefore be annual or, if the monsoonal activity had a cyclicity of more than one year, could represent a few years. The timing of the cyclic sedimentation and the significance of bedding cyclicity is discussed in more detail in Chapter 6.

3.3.3 Bathymetry

The bathymetry of the GBZ basin remains a difficult problem to solve. Relatively shallow waters are indicated by the close proximity of the Grenzbitumenzone to the carbonate platform at Ciona and Rossaga, together with the lack of coarse detritus at the margin of the basin. This is also supported by the palaeoecological interpretation of the life style of the abundant fauna found in the GBZ (Kuhn-Schnyder, 1974; Bürgin, pers. comm.; Rieber, pers. comm. 1990) and by the common occurrence of ichthyosaurs with disrupted abdominal cavities (Sander 1989; see also Section 2.3.5). The lack of evidence for strong currents, the rare occurrence of coarse resediments and the undisturbed lamination, however, imply deposition below wave-base.

Considering the GBZ as a closed basin, a quantitative estimate of the minimum depth of the basin can be made, assuming that the sediments were deposited below the storm wave base, with wind as the sole source of water turbulence and ignoring the effect of tides and tidal currents. The location of the wave base in modern lakes and completely closed basins is controlled solely by wind-induced wave action within the lake body (Beadle, 1981; Duncan and Hamilton, 1988). Treating the GBZ basin as a first approximation as a lake, the depth of the wave base for wind-induced water circulation can be estimated by applying the empirically derived formula of Smith and Sinclair (1972) as modified by Duncan and Hamilton (1988). This formula relates wave base (WB), wind speed (w) and fetch (L_f) for non-hypersaline lakes:

$$WB = 0.00616 L_f^{0.56} w^{0.88}$$

The relationship between these parameters is illustrated in Fig. 3.14.

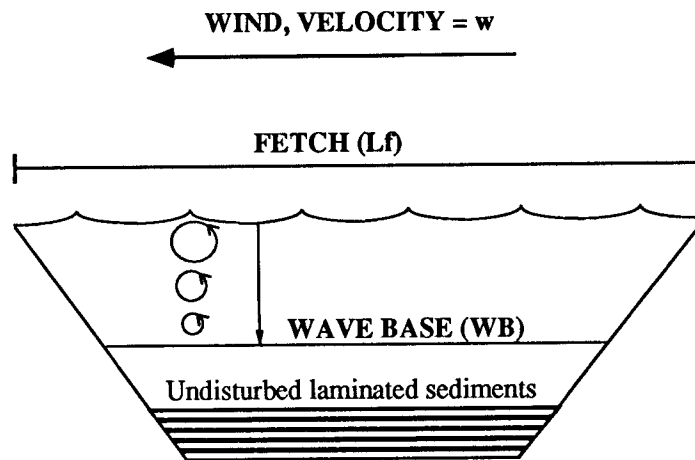


Fig. 3.14. Schematic model illustrating the physical parameters fetch (L_f), wave base (WB) and wind velocity (W), used in the determination of the depth of the wave base in the GBZ (modified from Duncan and Hamilton, 1988).

Paleoclimatic modeling by Parrish et al. (1986) suggests that the climate in the Middle Triassic was characterized by strong monsoonal activity and a predominant wind direction of approximately east-west at the latitude estimated for the GBZ region. Based on the observed lateral extent of undisturbed microlaminated layers, the minimum east-west extension of the GBZ is approximately 10 km. This width serves as a bracket for the fetch and results in a minimal estimated wave base of 21 m for a storm wind speeds of 30 m/s (108 km/h) or 40 m for a wind speed of 60 m/s (216 km/h). With a maximum width of the basin of about 20 km, assuming a single depositional basin for the GBZ and Perledo-Varenna limestone (see Chapter 2), maximum values for the wave base are 31 and 57 m, respectively. Although other influencing, but indeterminable factors, such as turbulent inflows or tidally-induced waves which could increase the depth of the wave base have been ignored, these estimates are considered maximum values. This is because the density stratification in the GBZ basin would have had an attenuating effect on the energy propagation through the water column, lifting the wave base to shallower depths even if the salinity difference between bottom and surface waters was only a few ‰ (e.g. Kullenberg, 1983).

A more precise constraint on the maximum depth of the basin could only be obtained if the geometry of the basin and sedimentation rates of the Salvatore platform were more accurately known. The only useful data to constrain the maximum depth are those of Zorn (1971). On the basis of mollusc remains belonging to the *Daonella sturti-lommeli* group and *Paraceratites Luganensis* (Merlan), Zorn suggested that 160 m of Middle Salvatore Dolomite are the time-equivalent of the GBZ. If a factor of 10 for the

compaction of the GBZ black shales is assumed and compaction in the dolomite layers is neglected and assuming that both sedimentary environments were on a single subsiding tectonic block, the maximum depth of the GBZ would be approximately 130 m. This large difference in depth is difficult to explain because the GBZ sediments lack coarse detritus and slope sediments which would indicate a steep basin margin. However, a maximum depth of over 100 m is possible if one considers that the GBZ basin graded into a muddy back-reef lagoon (Fig. 2.2, modified from Zorn, 1971) without reef-building corals which could sustain a steep slope.

To explain the strong differences in thickness without creating a steep slope between basin and platform, Zorn postulated that the Salvatore platform and the GBZ basin were located on two different tectonic blocks with different subsidence - a high subsidence in the S. Salvatore block and a slow subsidence in the GBZ basin. This would explain the large difference in sediments thickness without creating a high relief and, therefore, a steep slope at the margin of the basin. Zorn's model, however, requires first the formation of a basin, and thus a higher subsidence in the San Giorgio area, and then an inversion of this trend, with the basin staying more or less stable and the platform subsiding rapidly. This inversion of trend appears mechanically difficult to explain in an extensional regime because it requires an inversion of the movement on a normal fault plane. In conclusion, the depth of the GBZ can be confidently estimated to be between 40 and 100 m.

3.4 Synsedimentary Deformation Structures

3.4.1 General characteristics

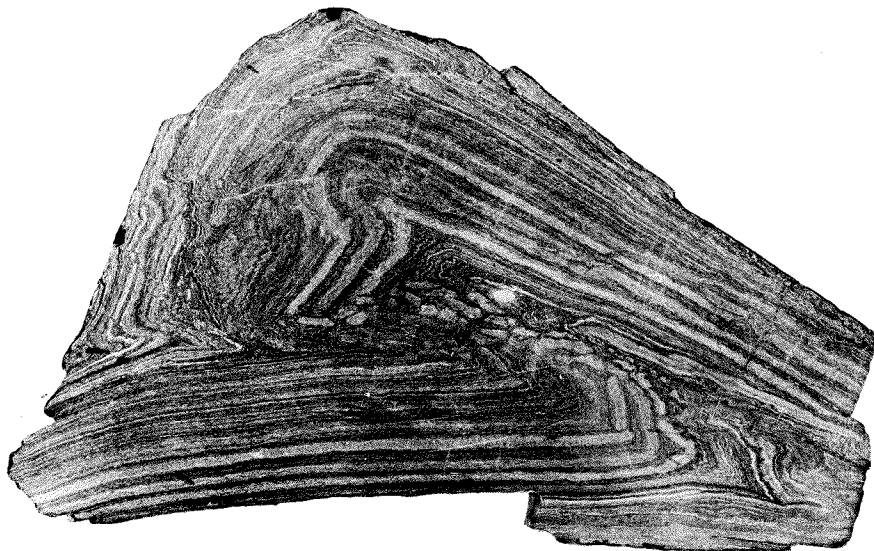
Several layers of the GBZ were affected by slumping very early after deposition. Many of the examples discussed in this chapter are from samples collected during the paleontological excavation at Mirigioli (Müller, 1965), and, because this outcrop is presently covered up to layer 185, none of the deformational features are still observable in the field. However, corresponding deformations can be observed in other outcrops, although not in all of the layers described here and not with the same variety of structures. The slump structures are mostly on a dm-scale and rarely exceed a meter in thickness. The layers overlying and underlying the deformations are generally completely unaffected by the slump movements, except for the compensation of thickness variations of the deformed layers. Deformation structures observed in some layers, although only a few centimeters in extent at each outcrop, are present in the same layer at different localities which can be a kilometer apart (e.g. layer 144u). Orientations of the slumps were not systematically measured during the excavations, but the dominant direction of the movements is generally approximately N-S, suggesting that at Mirigioli the basin floor had a slight north-south inclination (Müller, 1965). The most

striking characteristic of the slumps is the contrasting rheological behavior between the pure dolomite beds and the dolomites rich in organic matter. The pure dolomite beds mainly show brittle fracturing, whereas the organic matter-rich layers are plastically deformed.

3.4.2 Semi-ductile deformation features

A relatively large slump deformed layers 175 to 186 at Mirigioli, affecting approximately a 1m package of sediment with a lateral extension of approximately 6 m (Müller, 1965). The hump formed by these layers is flattened by variations in thickness of layer 187 so that the overlying layers are again planar. Layers 176 to 178 show a pinch and swell morphology. Müller (1965) suggested that the overlying beds were deformed at the surface and the deposition of layer 179 directly onto 175 or 176 is a primary sedimentary contact. Towards the source area the layers show partly a pinch and swell morphology and partly pull-apart cracks. In the direction of the movements they are overthrust and folded.

Where undisturbed, layer 175b has a thickness of 3.4 to 4 cm and is characterized by a well-defined lamination marked by the presence of abundant white layers of pure dolomite. The white layers contain abundant ghosts of pellets and indeterminable biogenic fragments and are interpreted as turbidites (see section 3.2.2.1). Three folded samples of layer 175b from the Mirigioli outcrop are shown in Fig. 3.15. The decollement surfaces of the folds are located in an organic matter-rich lamina. The folding and fragmentation of the white layers indicate that the dolomite layers were in a semi-lithified state when the deformation occurred, whereas the organic matter-rich laminae were still in a plastic state. The competence contrast between the different layers promoted the development of disharmonic folds. It is also important to note that the folds are well preserved and that the thickness of the white dolomite layers is constant and independent of orientation relative to bedding. This indicates that compaction after deformation was minor and the lithification process in the dolomites was rapid, occurring close to the sediment-water interface before substantial burial. The phosphate nodule (arrow in Fig. 3.15) was also clearly formed prior to deformation and behaved as a solid inclusion. This documents that phosphate formation also occurred soon after sediment deposition.

**a**

10 cm

b

Fig. 3.15. Synsedimentary deformation structures in layer 178 at Mirigioli, characterized by semi-ductile to brittle behaviour of the pure white dolomite layers and fluidal behaviour of the dark organic matter-rich dolomites. Note constant layer thickness suggesting minor post-deformation compaction. The arrow points to phosphate nodule which behaves as a solid inclusion.

3.4.3 Brittle deformation (Layers 140, 144u, 88)

The deformational behavior of the dolomite laminae in the following examples is much more brittle than the behavior in those previously discussed, indicating that lithification was more advanced when deformation occurred.

Layer 140

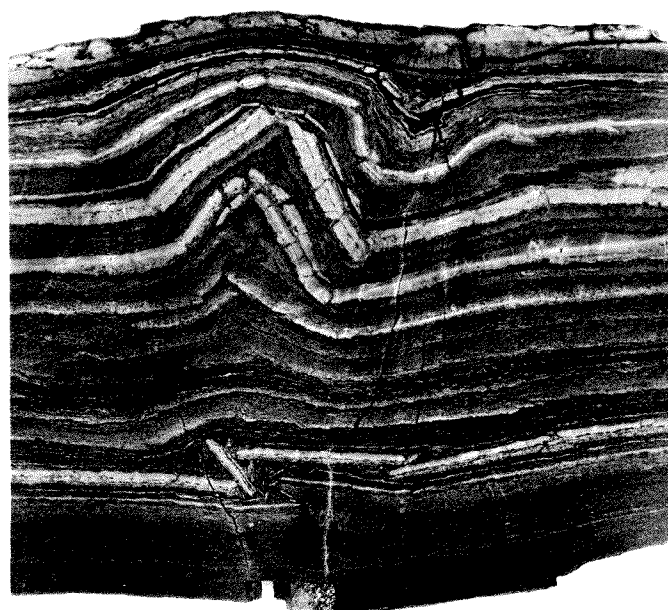
Layer 140 is well laminated and contains 8 layers of pure dolomite. The folded specimens (Figs. 3.16a&b) show a clear competence contrast between the white, dolomite-rich layers and the dark organic matter-rich layers. The white dolomite layers are broken into fragments with sharp edges and occur in an almost vertical orientation and displace the more plastic matrix rich in organic matter. These movements have produced an irregular orientation of the clay minerals and a chaotic texture in the matrix. In addition, the thicknesses of the dolomite layers in samples of layer 140 remain approximately constant. These observations indicate that complete lithification of the matrix occurred soon after deformation without substantial post-deformational compaction.

Layer 144u

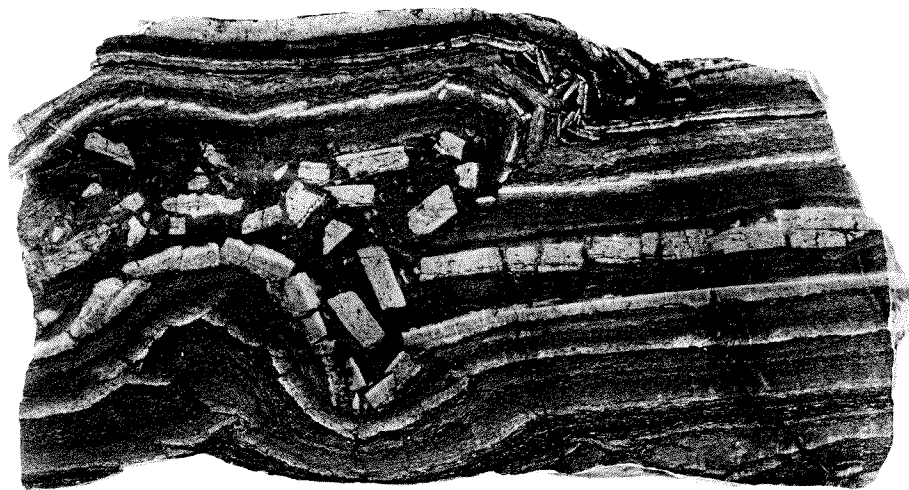
Deformation structures in layer 144u have been observed at the outcrops Mirigioli, Val Porina, Tre Fontane and Dossi. In many samples both compressional and extensional features are present, indicating a complex interplay of different deformation phases during the movement of the sediment package (Figs. 3.17 a-h). The three upper laminae a1, a2 and a3 are often disrupted and the fragments are rotated, whereas only minimal deformation is seen in the underlying or overlying layers (Fig. 3.17a). A slight overthrusting of layer b is seen in the center of the figure, but the amount of shortening in this layer can not account for the shortening in the three layers a1, a2 and a3. This deformation could have been produced by a bottom current that had enough energy to rework a few millimeters of the sediment and would indicate that dolomitization of some of these laminae was very rapid and occurred only a few millimeters to centimeters below the sediment-water interface.

Fig. 3.17b shows the central part of layer 144 cut by cracks. The cracks are filled with material coming from above (intruding downwards) indicating that only the white dolomite layer was lithified when these cracks formed. The intrusion of sediment from the top suggests that deformation took place close to the sediment-water interface before substantial compaction occurred. If they had been formed at depth, the movement of matter would probably have pushed sediment upwards as a result of the pressure gradient due to the sediment overload.

The samples shown in Figs. 3.17 c, d & e were collected only a few meters from those previously discussed. The structures in these samples are a consequence of extensional movements within a sediment package during gliding followed by compressive



10 cm



10 cm

Fig. 3.16 a, b Slump folds in layer 140 showing the rheological contrast between different lithologies. Note the absence of compaction of the vertical layer fragments and the lack of features indicating post-deformational compaction which suggest rapid lithification of the sediment prior to significant burial.

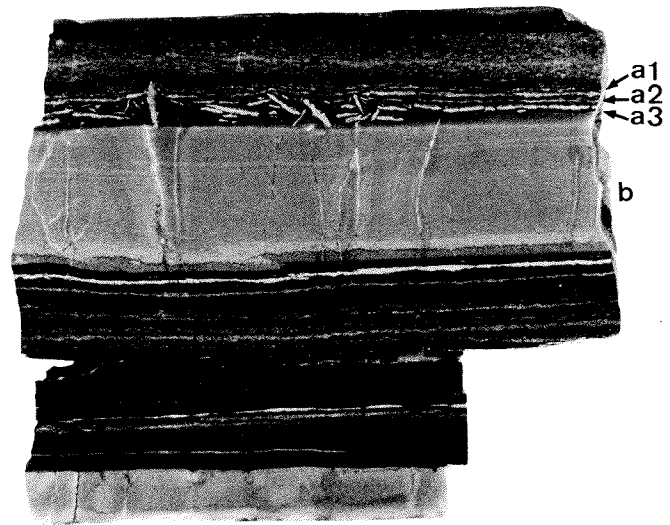
movements after the sliding sediment came to a rest. The angularity of the broken dolomite layers and the absence of deformation features in the clasts indicates that the dolomite layers were already lithified before deformation. The underlying organic matter-rich laminites also show some cohesion and are broken into clasts with dark material from above filling the voids (Fig. 3.17c). This may reflect partial lithification of the underlying dark layers at the time of deformation, or alternatively, the organic matter in these layers may have acted as a cohesive agent essentially gluing the sediment particles together. The uppermost layer of the samples illustrated in Figs. 3.17 c, d & e show no evidence of deformation. This indicates that deformation occurred before its deposition and therefore only a few cm below the sediment-water interface. The lack of major differential compaction around the thickened segments indicates that none of the lithologies were substantially compacted after deformation.

In contrast to other occurrences, deformation of layer 144u at outcrop Dossi is plastic rather than brittle (Fig. 3.17h). The thick dolomite layer at the center of the layer show a diapiric ascension of the mud. This behavior is observed over a distance of many meters. The observed features can be interpreted as load structures, which induced regularly spaced, diapiric ascension of dolomitic mud when the sediment was still unconsolidated. In contrast to the preceding examples, layers a1, a2 and a3 also show completely fluid behavior. Comparison of oxygen isotope compositions of the layers deformed brittly and those deformed plastically show no significant variations. This suggests that the dolomitization process, was relatively rapid and led to a complete lithification of the sediments soon after deposition. This is also supported by the petrographic observations, which indicate a limited compaction after deformation.

Figs. 3.17a-f Examples of brittle deformation structures in layer 144u at outcrop Mirigioli.

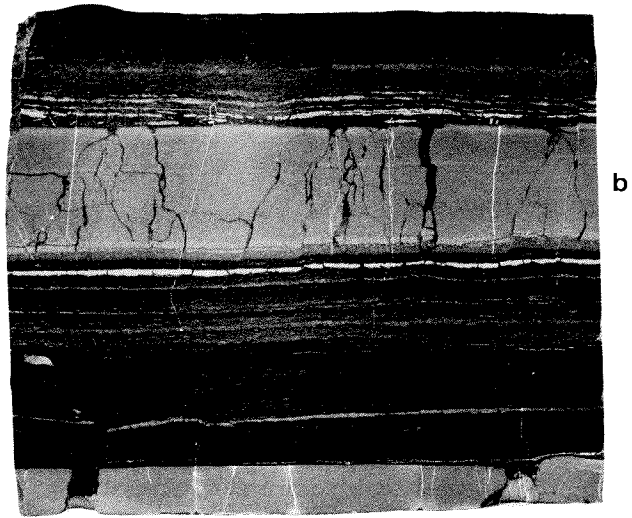
a)

Disrupted and rotated layers a1, a2, a3 showing that deformation took place at an advanced stage of lithification of the thin dolomite layers



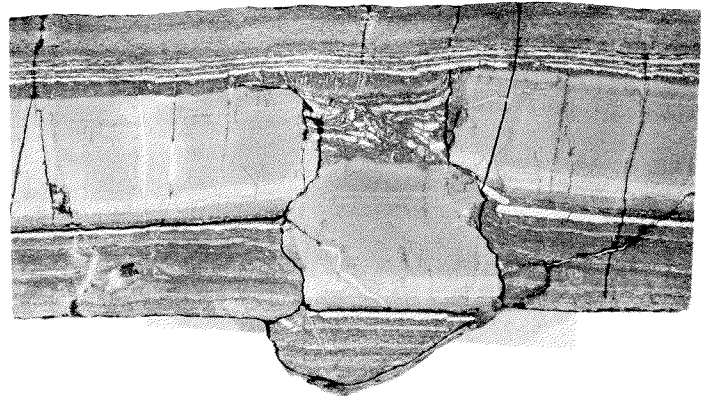
b)

Extensional cracks in layer b with sediment infilling from the directly overlying organic-rich layer.

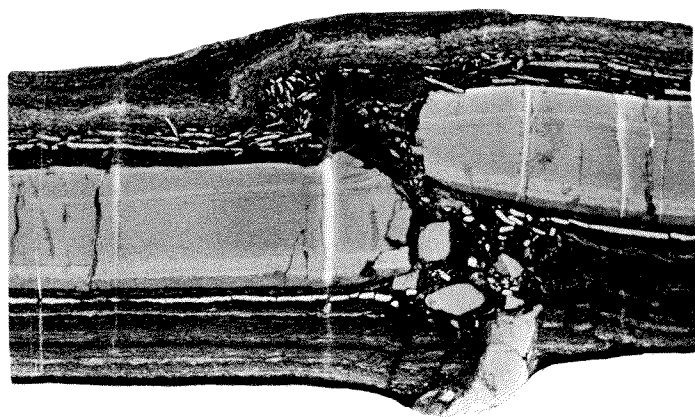


c, d, e)

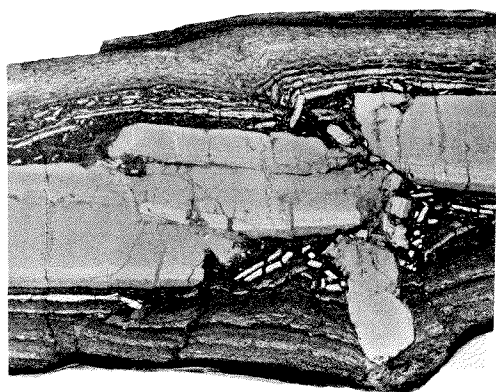
Compressive deformations showing the advanced state of lithification of the white dolomite resediment layers at the time of deformation.



d)



e)



10 cm

f)

Example of plastic deformation of layer 144 at the outcrop Dossi.



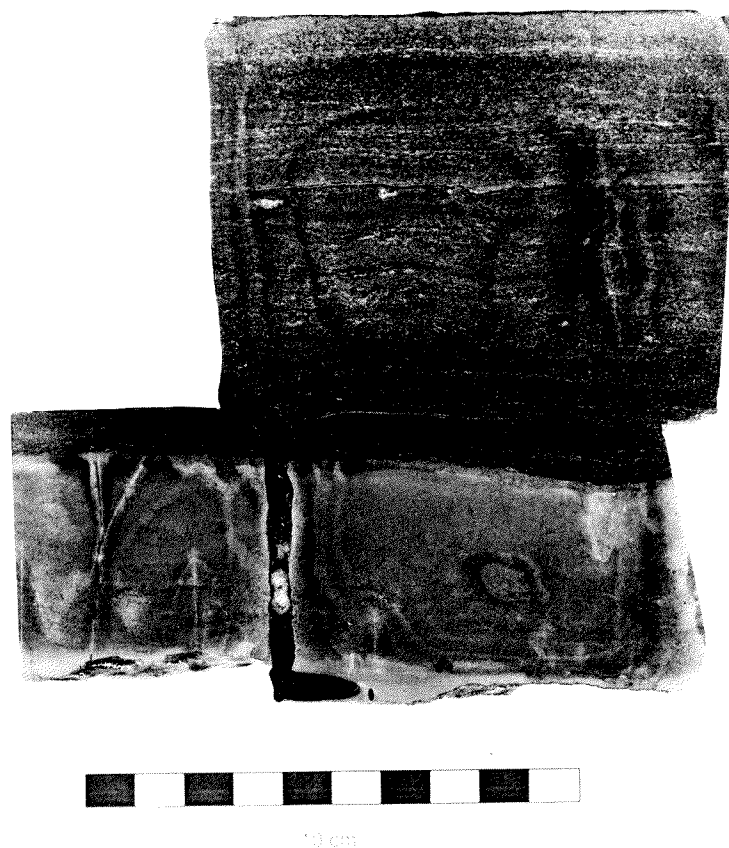
10 cm

Layer 87

Layer 87 consists of a basal non-laminated dolomite layer overlain by an organic matter-rich laminite (Fig. 3.18). The crack in the basal layer, which had approximately a E-W strike, could be followed for many meters at the outcrop Mirigioli (Müller, 1965). The angular margins of the crack and the fluidal behavior of the laminated sediment infilling the crack, again demonstrate the different degree of lithification of the lithologies when deformation took place. This sample also clearly indicates that deformation took place when only about 2 centimeters of laminated dolomite were deposited on top of the cracked layer as the lamination above these 2 centimeters is completely undisturbed.

Fig. 3.18

Example of brittle deformation of layer 87, at Mirigioli. Note the sharp edges of the already lithified dolomite layer and the fluidal behavior of the organic rich material filling the crack from above. This suggests that deformation took place close to the sediment-water interface.

**3.4.4 Interpretation**

The deformation structures discussed above allow the timing of lithification relative to deposition to be constrained and have implications for the geometry of the GBZ basin. The presence of undisturbed layers overlying the deformed layers as well as the downward-infilling of the organic-rich sediments indicate that deformation occurred close to the sediment-water interface. The brittle or slightly viscose deformation of the

dolomite layers indicates that slumping occurred at a stage of advanced lithification of the dolomites. In contrast, at the time of deformation the organic matter-rich laminated dolomites were probably still water-rich and unconsolidated. The excellent preservation of the structures and the limited compactional features provide evidence for minimal compaction after deformation and indicates that the lithification process throughout the formation was fast, whereby the dolomite layers were lithified slightly faster than the organic matter-rich layers. The black shales in contrast are strongly compacted indicating that their lithification happened much later.

Isotopic analyses of beds with different lithologies and rheological behavior were carried out to determine whether a correlation exists between the timing of dolomitization and carbon and oxygen isotope composition. The variations in isotopic signatures are minimal and below the resolution power of oxygen isotope thermometry. Thus, dolomitization of the white and the organic matter-rich layers can be considered nearly simultaneous. The consistency in carbon isotope composition between deformed and undeformed layers indicates that both the white dolomite layers and the organic matter-rich layers were formed in the sulfate reduction zone. Results of isotopic analyses will be discussed further in Chapter 4.

Mechanisms proposed for the initiation of submarine mass movements are varied but no means are available to distinguish the different processes. Sudden variations in water depth, earthquakes, storm surges associated with hurricanes, sea level changes and other mechanisms have been postulated as causes for destabilization of sediment packages (for a comprehensive review see Schwarz, 1982). Further instability could be caused by the production of gas by anaerobic bacteria, as postulated by Nelson and Lindsey-Griffin (1987). Bacterial activity was probably intense in the sediments and gas buildup at the base of more impermeable layers is a viable possibility to create instability in the sediment column. The small scale of the displacements and the short transport distance of the disturbed layers suggest that the slope of the basin bottom was very small, probably only a half to one degree. This is consistent with observations in modern environments where small scale slumping occurs on slopes with angles as low as 0.5° (Schwarz, 1982).

3.5 Dolomite Petrography and Cathodoluminescence (CL) Cement Stratigraphy

3.5.1 Grenzbitumenzone

Dolomite in the GBZ is generally fine-grained and anhedral to subhedral. Grain-size ranges from below microscope resolution to 200 μm . Porosity is low in the laminites but can be significant in massive dolomite beds. Staining of thin sections with potassium ferricyanide, shows that all dolomite in the GBZ is Fe-poor. With cathodoluminescence petrography four dolomite generations can be distinguished. The earliest recognizable

generation, *Dolomite I*, is characterized by 20-50 μm rhombs, with inclusion-rich or dissolved centers and clear rims. Inclusions in *Dolomite I* are indeterminable opaque material (organic matter?) and pyrite framboids. The dolomite rhombs are generally only present in organic matter-rich laminae with a relatively low dolomite content. Their absence in dolomite-rich layers is due to subsequent recrystallization, as evidenced by recognizable ghosts. This type of dolomite represents a maximum of 1% of the total dolomite volume and has a dull red homogeneous color in cathodoluminescence. Cathodoluminescence microscopy failed to show any chemical zoning or evidence for a precursor carbonate. The texture suggests direct precipitation of *Dolomite I* rather than replacement of precursor carbonate grains. Physical separation of these grains is impossible and prevents a more definite chemical characterization. The presence of pyrite inclusions in the cores of the *Dolomite I* crystals indicates that pyrite formation at least partly predates the earliest formation of dolomite. The presence of dissolved centers can be interpreted as a result of dissolution of an early precipitated dolomite phase which became unstable in the pore waters at some time after its formation (e.g. Randazzo and Cook, 1987).

Dolomite II is the most common dolomite type and forms 85 to 100% of the total dolomite volume. Crystals are generally anhedral to subhedral and clear but inclusion-rich varieties also occur. In cathodoluminescence *Dolomite II* is red and shows no chemical zoning. *Dolomite II* is interpreted as a replacement of a fine-grained carbonate mud. The third generation of dolomite, *Dolomite III*, is easily recognized in cathodoluminescence as it shows a bright orange color (Fig. 3.19a,b) but is indistinguishable from *Dolomite II* under the petrographic microscope. This dolomite is a pore-filling cement and is only abundant in dolomite layers with low organic matter contents and relatively coarse grain-sizes. The cathodoluminescence microtextures demonstrate that the fluid responsible for the precipitation of *Dolomite III* infiltrated into the rock either through interconnected pores or through hair-thin microcracks. This phase of dolomite precipitation is responsible for an important porosity reduction. The dispersed nature of dolomite III prevents its separation from dolomite II for isotopic analysis, however, a correlation between its abundance and a decreasing $\delta^{18}\text{O}$ -composition of the bulk samples indicates that it is a late diagenetic higher temperature cement (see also Chapter 4). The last phase of dolomite observed in the GBZ, *Dolomite IV*, is only present in larger pores or in fossil molds. It is characterized by a well-defined chemical zonation parallel to crystal growth faces (Fig. 3.20) and shows an increase in crystal size towards the center of the cavities. This is a strong indication that *Dolomite IV* is a true cement which did not suffer any recrystallization. This phase of dolomite contains abundant primary fluid inclusions which are used to constrain its temperature of formation (see Section 3.6).

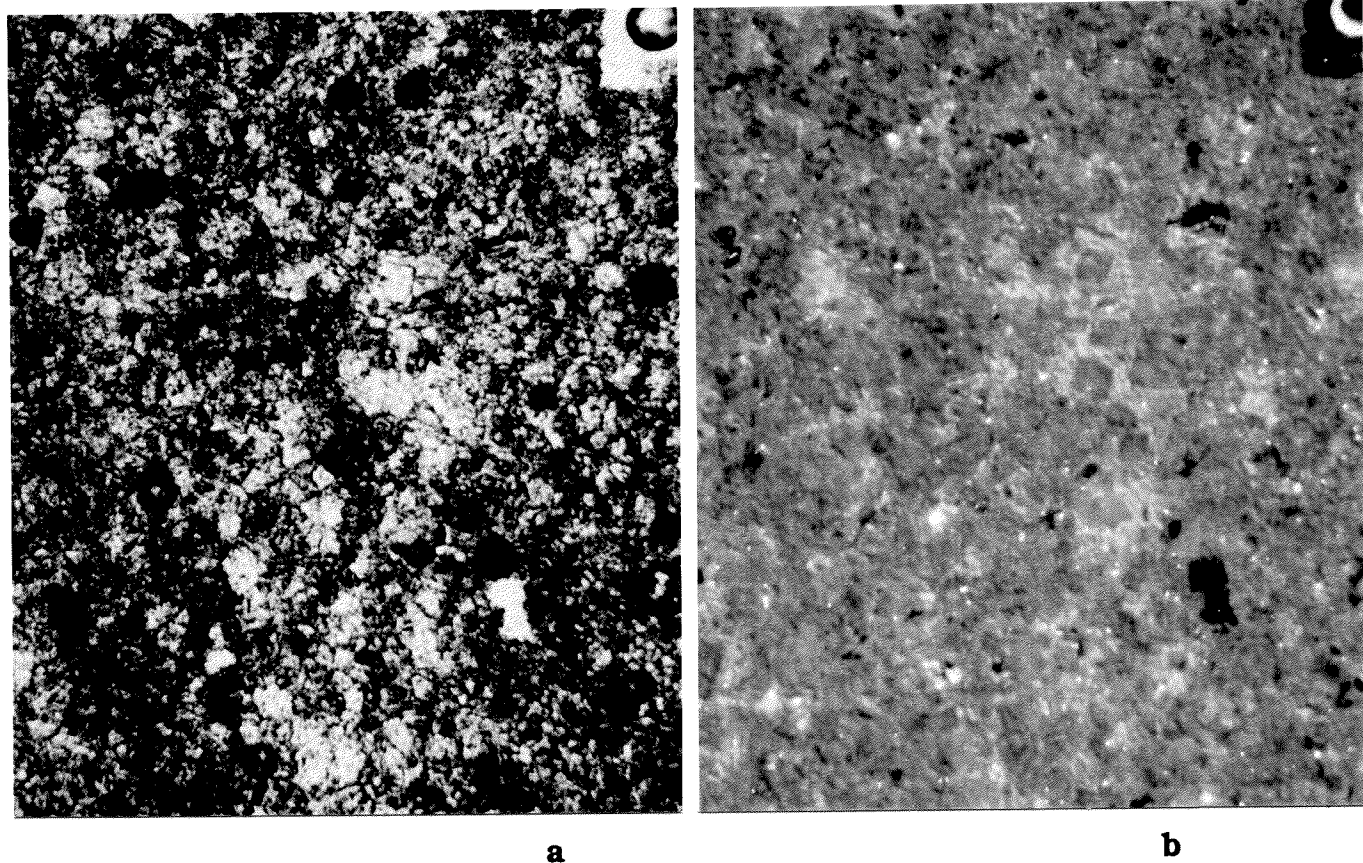


Fig. 3.19 Plane polarized light (a) and cathodoluminescence micrographs (b) allow the distinction of different generations of dolomite in the GBZ. Dolomite II is characterized by a red luminescence, whereas dolomite III shows bright yellow luminescence. Field of view is 8 mm wide.

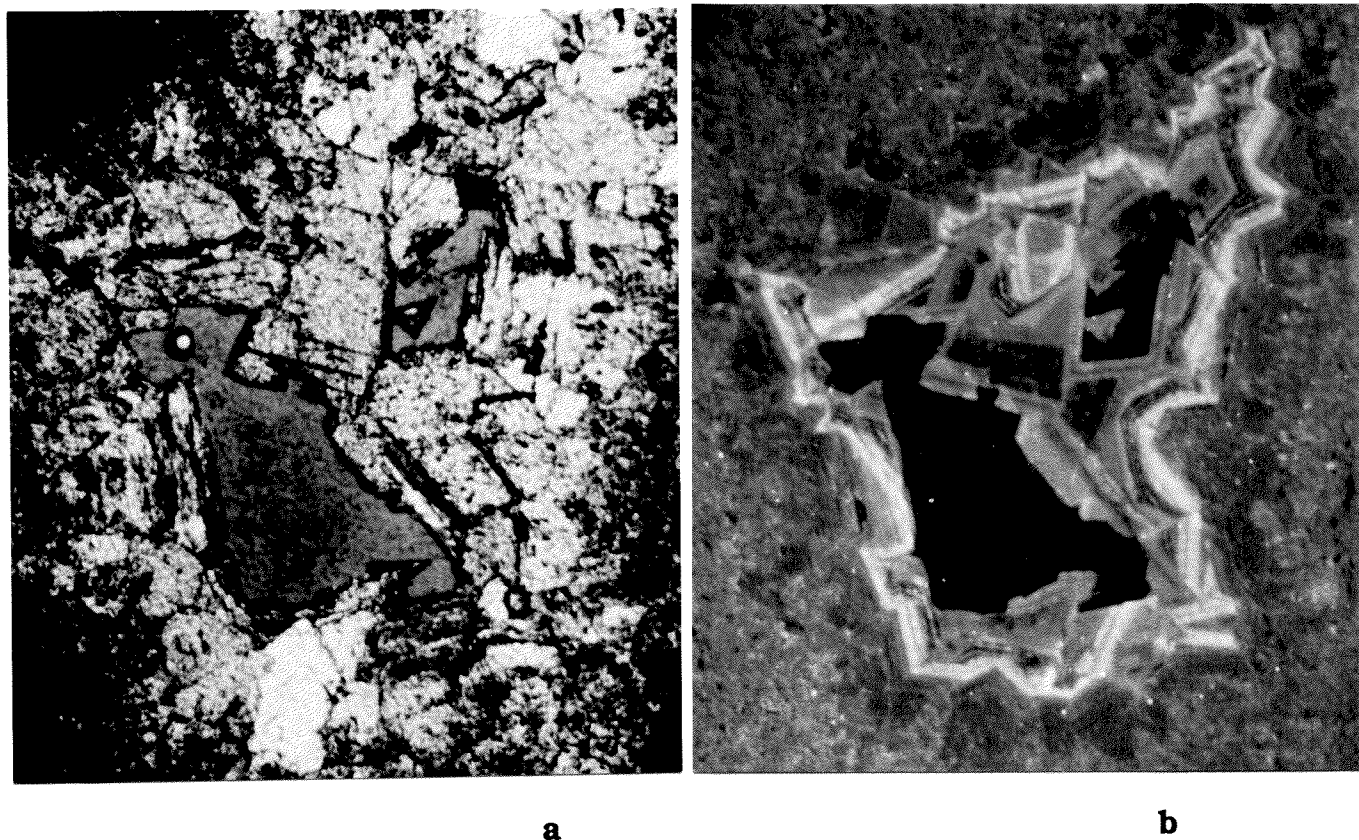


Fig. 3.20 Plane polarized light (a) and cathodoluminescence micrographs (b) of dolomite IV showing chemical zonation and growth structure. The increasing grain size towards the center of the pore and the chemical zonation parallel to the growth faces of the crystals indicate that it is a primary cement. Field of view is 8mm wide.

3.5.2 San Giorgio Dolomites and Lower Salvatore Dolomite

Only a few diagenetic features of the Salvatore and San Giorgio dolomites which are necessary to constrain the late diagenetic history of the Grenzbitumenzone are discussed here. For a general discussion of the petrography and sedimentology of these formations see Chapter 2 and Zorn (1971).

3.5.2.1 Salvatore Dolomite

In the Monte S. Giorgio region, the thickly layered to massive Diplopora Dolomite is interlayered with sedimentary breccias (Figs. 3.21a & b). These breccias form bodies of indeterminable geometry which are at least a few meters in thickness and width and more rarely form bedding parallel layers up to 30 cm thick (Fig. 3.21a). The breccias are characterized by angular clasts of fine-grained grey dolomite, up to 5 cm in diameter, and are cemented by two generations of dolomite cements and late diagenetic calcite (Fig. 3.22). Cathodoluminescence petrography (Fig. 3.22b) allows a correlation of these cements with those observed in the GBZ, with the exception of the late phase calcite which occurs only in the Salvatore Dolomite. The cements depicted in Fig. 3.22b correspond to *Dolomite III* and *Dolomite IV* of the GBZ. The dark lines in the idiomorphic *Dolomite III* crystals (Fig. 3.22a) are stringers of one and two-phase primary fluid inclusions similar to those seen in the cements in the GBZ dolomites (discussed further in Section 3.5.3).

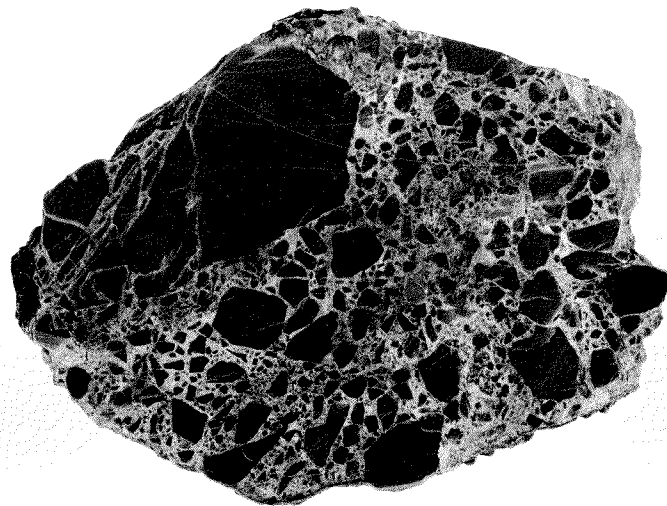
3.5.2.2 San Giorgio Dolomite

The base of the San Giorgio Dolomite is characterized by abundant silicifications (Fig. 3.1, layers 187-230) which form layers and/or nodules (Fig. 3.23a) in numerous beds. The cherts, composed of microcrystalline quartz and chalcedony, are characterized by the presence of abundant radiolarian molds filled by chalcedony and always show sharp contacts to the enclosing dolomite. The dolomite crystals are generally xenomorphic, Fe-poor and range in size from 50 to 200 microns. In general, only one phase of dolomite is observed, although rarely brightly luminescent dolomite with growth zones of alternating luminescence colors occurs in open pores associated with late subvertical dolomite veins. In cathodoluminescence, the dolomite displays a dull red color and shows no evidence of chemical zoning. Dolomite beds are often affected by slumping, whereby the chert layers are broken into small angular clasts (Fig. 3.23b). In contrast, dolomite never shows evidence of deformation indicating that dolomitization is later than chert induration. This is substantiated by the presence of mollusk shell fragments replaced by quartz. In contrast to shells replaced by dolomite, the silicified shells show a good preservation of the internal layering of the shell, which indicates that they were silicified prior to recrystallization of the original shell. In partially dolomitized beds, a

**a**

Fig. 3.21 a,b

Outcrop (a) and hand specimen photograph (b) of a breccia layer in the Lower Salvatore Dolomites above Albio showing angular clasts of dolomite in a sparry dolomite cement (Dolomite III and IV). Coin is 2 cm in diameter.



10 cm

b

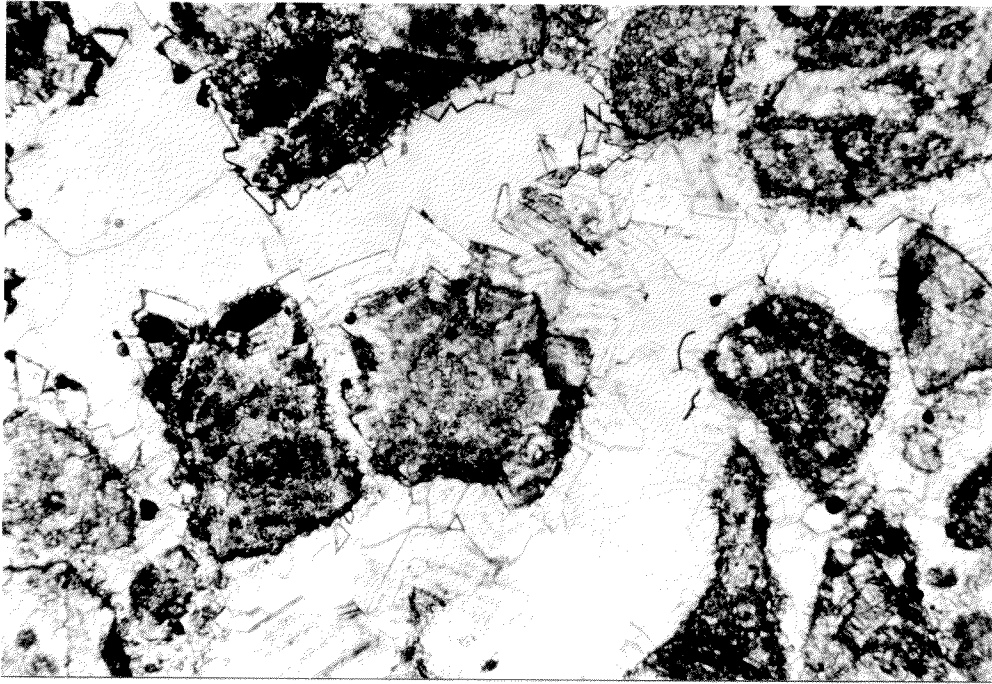


Fig. 3.22a

Photomicrograph of the cements in the breccia of Fig. 3.21 in plane polarized light showing the different dolomite-cement generations. Pores are completely occluded by a late calcite cement. Note the clearly developed growth bands in the rhombic dolomite cement. The dark bands are defined by solid and one- and two-phase fluid inclusions. Field of view is 1.1 cm wide.



Fig. 3.22b

Cathodoluminescence detail of the cements in the breccia of Fig 3.21. The different cements exhibit the same sequence of cementation as in the GBZ. (compare Fig. 3.20). The black spots are pores. Field of view is 3 mm wide.



Fig. 3.23a Chert layers (arrow) at the base of the San Giorgio Dolomite at outcrop Dossi.



Fig. 3.23b Slump in the San Giorgio Dolomite showing brittle deformation of the cherts. Outcrop Dossi. Coin is 2 cm in diameter.

preferential replacement of the mud, leaving intact coarse calcite bioclasts, is observed. The lack of different generations of cements prevents a direct correlation of the timing of dolomitization with the GBZ and Salvatore dolomites, however, the rapid transition to the Meride Limestone and the presence of discordant dolomite-limestone transitions suggest a relatively late origin of these dolomites.

3.5.3 Fluid inclusions

Fluid inclusions occur only in *Dolomite IV* and are always aligned along the growth faces of the crystals (Fig. 3.22a). This can be taken as a proof for their primary origin (Roedder, 1984). The presence of chemical zonation parallel to the growth faces of the crystals (seen in cathodoluminescence) exclude a recrystallization or a neomorphic origin of the crystals, therefore, the fluid inclusions should reflect primary conditions of dolomite precipitation. The fluid inclusions are in general only a few micrometers long. Only a few of them are two-phase liquid-gas inclusions, whereas the majority consist of one phase (fluid) only. Daughter minerals in the inclusions were never observed. Temperatures of homogenization (to liquid) range between 57 and 94°C, and the majority are between 70 and 80°C (Fig. 3. 24). Salinities could be measured only in a few inclusions because, on cooling, most of the inclusions crack due to the volume increase produced by the formation of ice. The five salinities that could be determined indicate a fluid composition close to that of seawater.

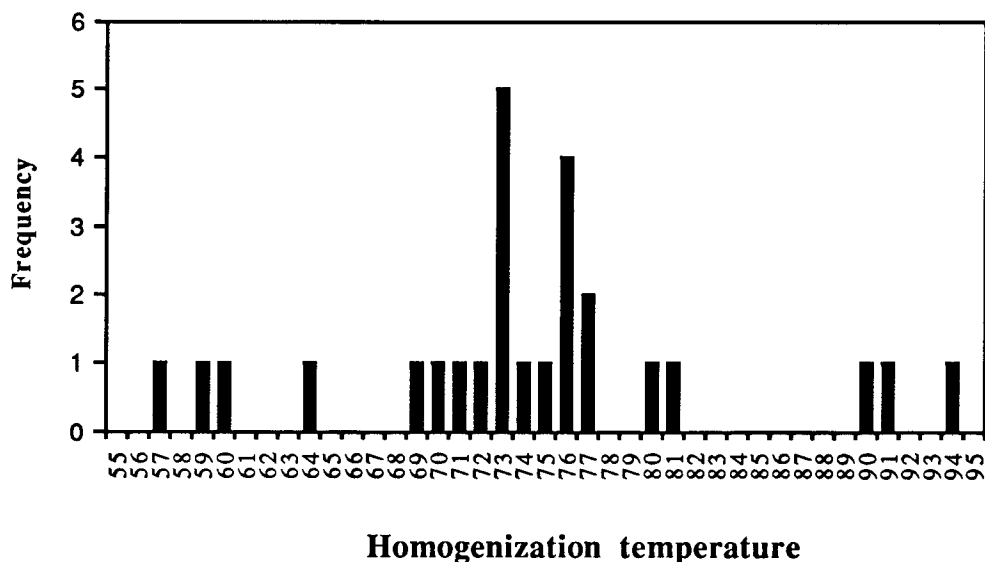


Fig. 3.24 Histogram of homogenization temperatures of fluid inclusions from Dolomite IV (samples from GBZ and Salvatore Dolomite).

The homogenization temperatures of the fluid inclusions give the minimum temperature of trapping of the fluid during crystal growth (Roedder, 1984) and, therefore, give an estimate of the minimum temperature of formation of the crystal. The

coexistence of one-phase and two phase fluid inclusions in low-temperature diagenetic settings, however, is generally attributed to the metastability of the fluid in the inclusions. In fact, in fluid inclusions formed at temperatures below approximately 60°C, the nucleation of a gas bubble can be hindered by kinetic factors, and the fluid inclusion can persist in a metastable state as one phase (Roedder, 1984). The common coexistence of one and two-phase fluid inclusions in the GBZ *Dolomite IV* cements is therefore interpreted as evidence for a maximum temperature of precipitation of 70°C. The anomalous high temperatures, reaching 90°C, of some of the inclusions are probably due to stretching during sample preparation or during sample heating (Roedder, 1984).

3.5.4 Summary

The petrographic observations show that, in the GBZ and Salvatore Dolomite, dolomitization was a multi-stage process. The main percentage of dolomite is of early diagenetic origin in both formations. The intercrystalline porosity left by the first stage of dolomite formation (Dolomite I and II) controlled the extent of the late dolomitization (Dolomite III and IV). These late dolomite phases are present only in beds which were permeable enough to support fluid circulation during burial diagenesis. Fluid inclusion data indicate that the late diagenetic cements were precipitated from fluids with salinities close to seawater at temperatures of approximately 70°C.

CHAPTER 4

INORGANIC GEOCHEMISTRY

4.1 Major and Minor Element Geochemistry

4.1.1 Introduction

Black shales are often enriched in certain trace elements, particularly V, Zn, U, Mo, Ni, Co and Cr (e.g. Vine and Turtelot, 1970; Brumsack, 1980, 1986; Coveney and Glascock, 1989). Although these high metal concentrations are generally associated with the presence of high quantities of organic matter, the timing and mechanisms of enrichment and especially the source of the metals are still poorly understood. Scavenging of metals through inorganic sulfide (co-)precipitation and organic complexation at the oxic-anoxic interface in the water column and/or in the sediment have been proposed as mechanisms for syngenetic trace metal enrichment in black shales (e.g. Vine and Turtelot, 1970). Direct metal contribution from marine organisms, which can be highly enriched in some trace elements, may also be a source for the high trace metal content of black shales (e.g. Brongersma-Sanders, 1965). Moreover, epigenetic and supergene processes may play a role as concentrating or leaching agents (e.g. Coveney and Glascock, 1989).

If late diagenetic or weathering processes can be ruled out as sources of metal enrichment, trace metal geochemical signatures can be used as indicators for variations in redox conditions during sedimentation and early diagenesis. The solubility and the fixation in the sediment of some metals, such as Ni, U, V and Mo, are controlled by the pH-Eh conditions, therefore, their enrichment reflects variations in redox conditions. In addition, calculation of the amount of trace metals added during early diagenesis can be used to constrain sedimentation rates. If excess trace metals are enriched in the sediment by diffusion from seawater along chemical gradients, the pore-waters must remain connected to the bottom waters through open porosity. The preservation of an open system in the sediments is dependent on the sediment accumulation rate. Therefore, the magnitude of trace metal enrichment should be inversely proportional to the bulk sedimentation rate.

Major and trace element geochemical analyses (for complete analyses see Appendix A) have been made in order to determine the origin of the metals and the timing of enrichment, to estimate the sedimentation rate and to test for possible variations in sediment input characteristics and anoxic conditions.

4.1.2 Results

4.1.2.1 Major Elements

A plot of aluminium concentrations in black shales and dolomitic beds and silica show a good positive correlation ($R^2 = 0.94$, Fig. 4.1a). $\text{SiO}_2/\text{Al}_2\text{O}_3$ ratios clustering around 3.5 are typical for average terrigenous shales (Wedepohl, 1970). A few samples show a higher $\text{SiO}_2/\text{Al}_2\text{O}_3$ ratio, indicating a higher input of biogenic and/or detrital silica. Due to diagenetic remobilization of silica, however, this ratio cannot be used as a direct indicator for variations of siliceous microorganism productivity or for variations in detrital input. Potassium and titanium concentrations also show a good positive correlation with Al_2O_3 ; ($R^2 = 0.97$ and 0.99 respectively, Figs. 4.1b, 4.1c) and may indicate a detrital origin and a dominance of illitic clays over chlorites. Iron contents correlate positively with Al_2O_3 (Fig. 4.1d) indicating that iron is mostly of detrital origin. However, Fe is not incorporated to aluminosilicates, as 53 to 82 % of total iron is now bound to pyrite (see section 4.2.).

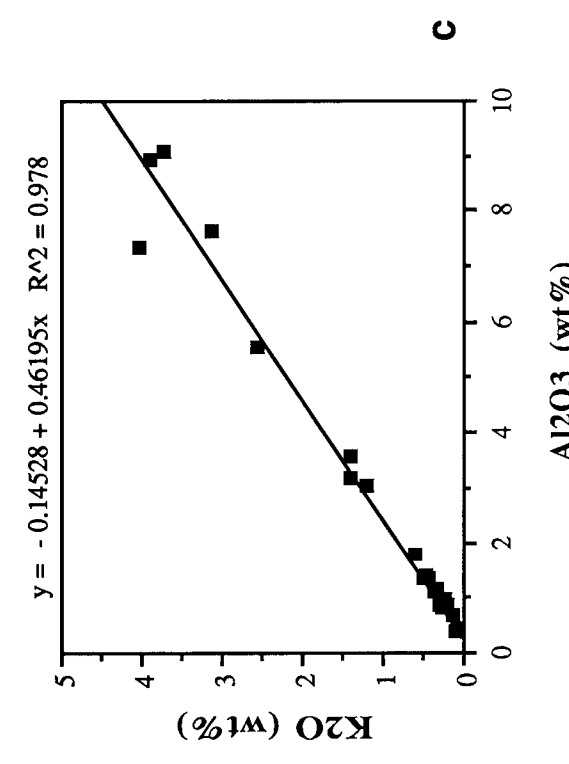
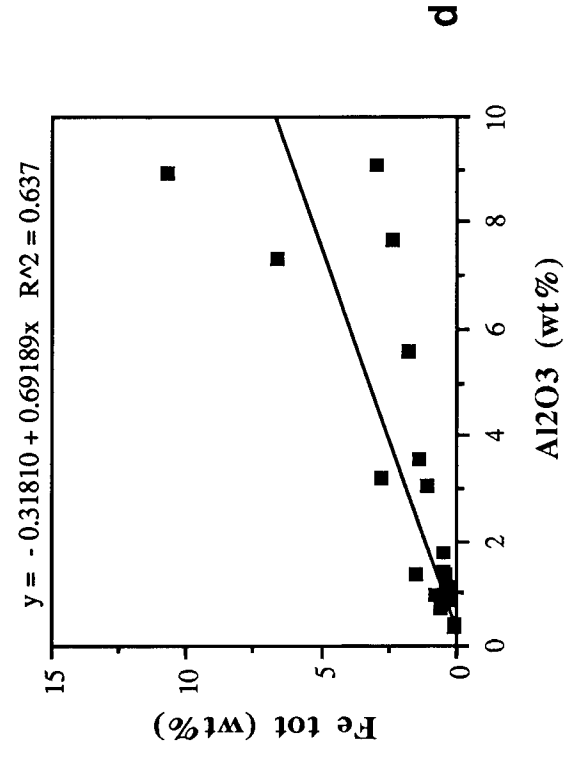
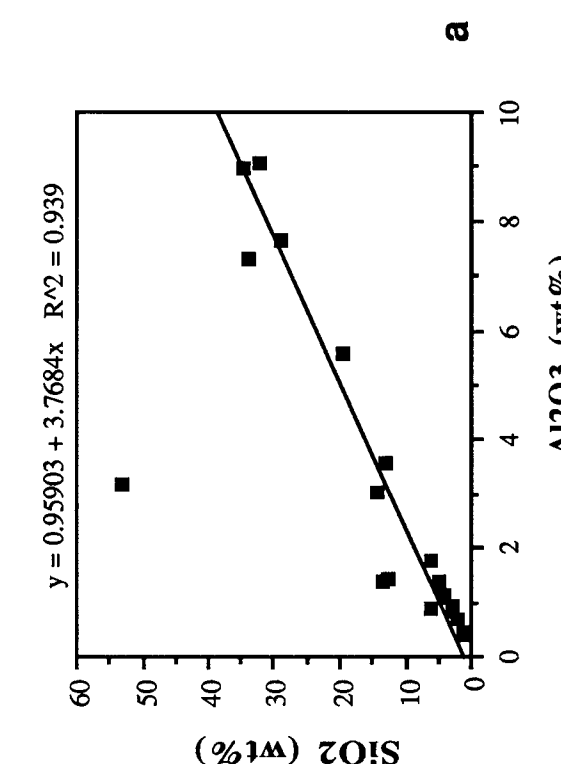
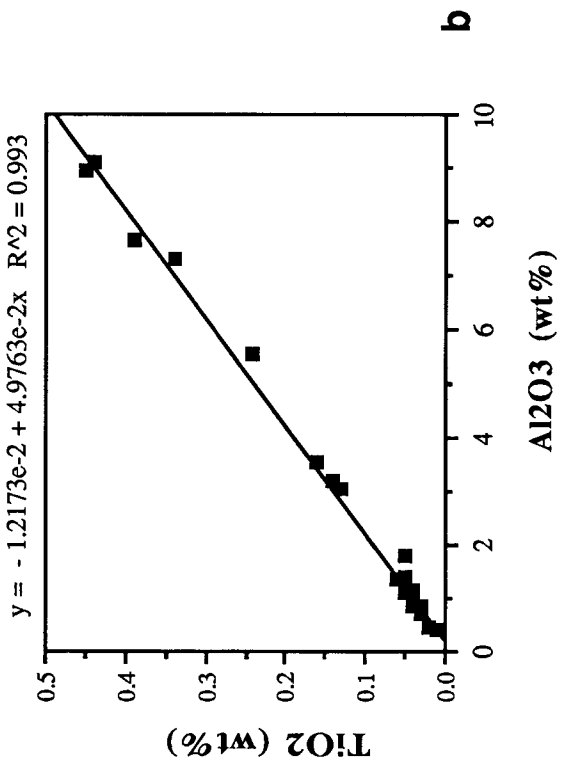
The low manganese contents (< 0.02 % in black shales) are typical of sediments deposited under reducing conditions. Both manganese and iron are highly insoluble in oxic environments but are mobilized as Mn^{2+} and Fe^{2+} under reducing conditions. In the presence of sulfide ions, Mn can diffuse out of the sediment along concentration gradients because it does not form a stable sulfide mineral, whereas Fe is immobilized by precipitation as pyrite or as a monosulfide. Thus, high Fe/Mn ratios indicate deposition of sediments (both black shales and dolomite beds) in a sulfidic environment.

4.1.2.2 Trace elements

Concentrations of selected trace elements in average GBZ black shales are listed in Table 4.1 together with values for average shales (Wedepohl, 1970), modern sea water and living plankton. Complete analyses of the GBZ sediments can be found in Appendix A.

Vanadium contents range from 1537 to 3600 ppm and show an excellent positive correlation with TOC (Fig. 4.2a). The maximum V content of 3600 ppm corresponds to an enrichment of up to 1.4×10^6 times compared to modern sea water (2.5 ppb) and 28 times compared to the average shale. Nickel contents range from 97 to 260 ppm, an enrichment of approximately 3 times relative to average shale and approximately 1.1×10^5 times that of modern sea water. Ni also correlates positively with TOC (Fig. 4.2b.). Both vanadium and nickel enrichment are apparently strongly associated with organic matter concentration. The $\text{V}/(\text{V} + \text{Ni})$ ratios range from 0.7 to 1. (Fig. 4.3) indicating deposition under highly sulfidic conditions (see section 4.1.3.2. for discussion).

Mo concentrations range from 110 to 350 ppm, which correspond to an enrichment of up to 135 times relative to the average shale and 2.6×10^4 times relative to modern sea water. U contents range between 17 and 54 ppm (enrichment up to 15 times), whereas Zn



Figs. 4.1a-d. Whole rock geochemical distribution diagrams of selected major elements versus Al₂O₃.

contents vary considerably between 32 and 999 ppm which corresponds to concentrations ranging from lower than those of the average shale to enrichments of 9 times. Cu contents range from 30 to 936 ppm, and Pb contents from below detection limit to 234 ppm.

Table 4.1 Selected trace element concentrations in average Grenzbitumenzone black shale, average shale (Wedepohl, 1970), sea water and plankton (from Arthur et al., 1990 and references therein). All values in ppm.

Element	Average GBZ Black Shale	Average Shale	Seawater	Plankton
Ba	1283	580	14×10^{-3}	80
Ni	191	68	1.7×10^{-3}	9
V	2875	130	2.5×10^{-3}	3.5
Zn	314	110	5×10^{-4}	165
Cu	328	39	1×10^{-4}	18
Mn	148	600	8×10^{-5}	11
Pb	104	23	5×10^{-7}	5
Mo*	271	2.6	10.6×10^{-3}	2
U*	28	3.7	--	--

* Grenzbitumenzone data from Blumer (1950).

4.1.3 Discussion

4.1.3.1 Source of trace metals.

Trace metals may have been added to the GBZ sediments with the circulation of different types of fluids (e.g. brines or meteoric waters) at various stages after their deposition ~230 M.y. ago until the present. However, the good preservation of early diagenetic signals, such as carbon and oxygen isotopic compositions of the dolomites, the presence of only minor late diagenetic, higher temperature cements, and the low degree of thermal maturation inferred from the organic geochemical studies indicate that probably no pervasive fluid circulation occurred during the burial history of the GBZ. Based on these observations, a late diagenetic metal enrichment or remobilization is considered unlikely.

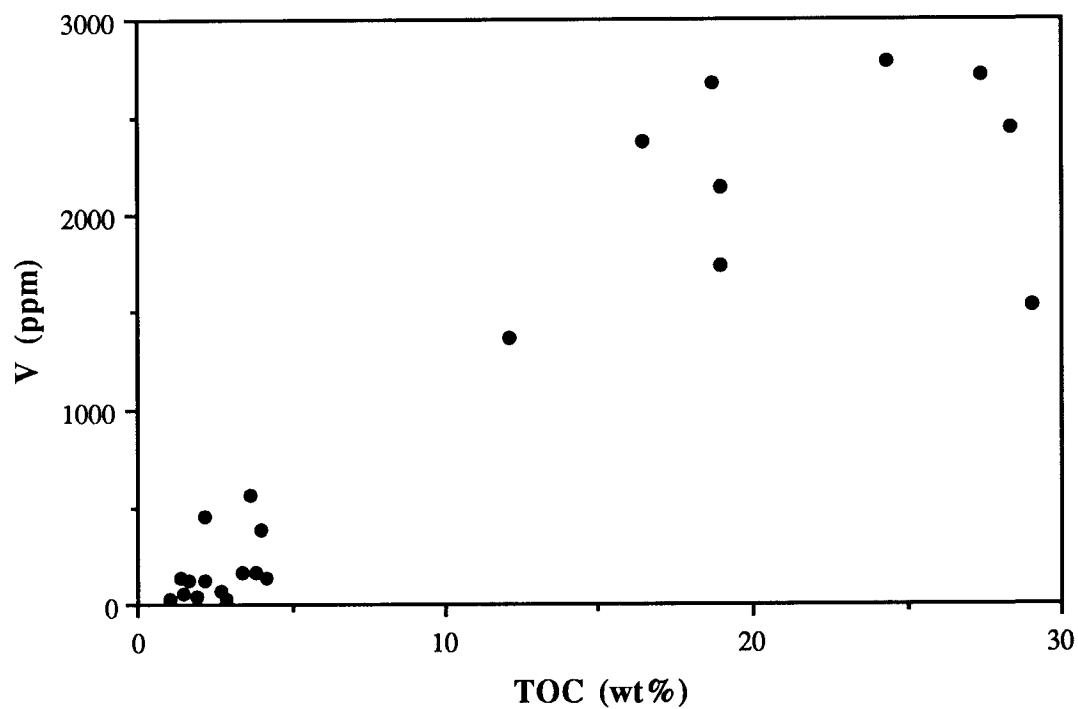


Fig. 4.2a Whole rock geochemical distribution diagram of vanadium concentrations versus total organic carbon contents in the dolomites and black shales of the GBZ.

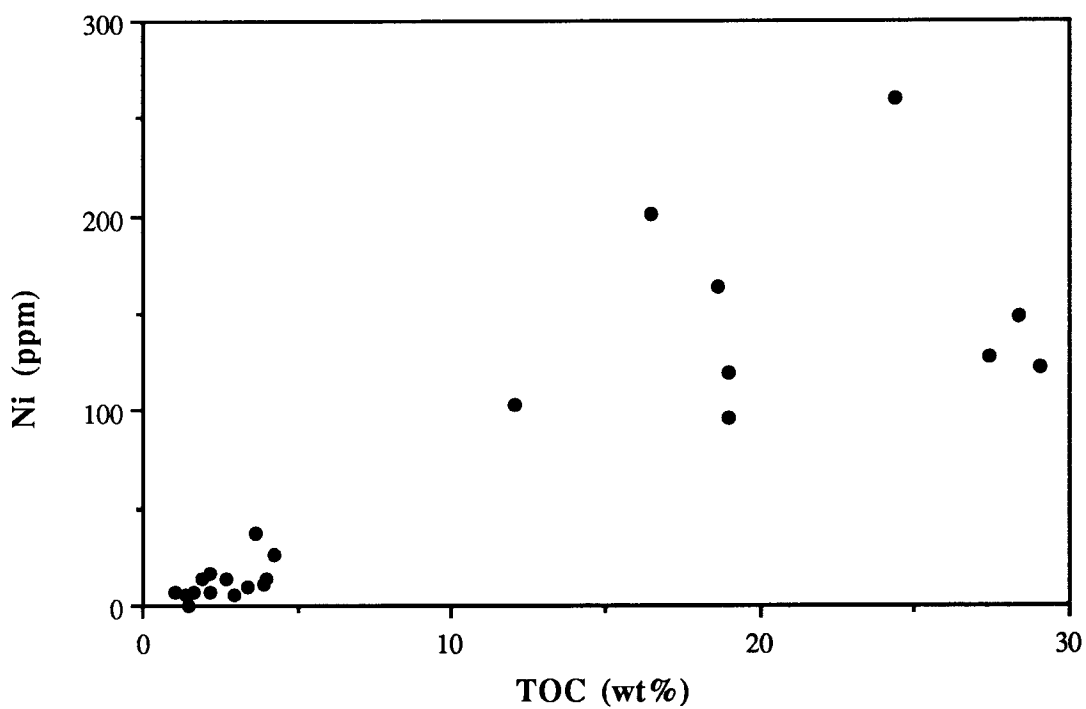


Fig. 4.2b Whole rock geochemical distribution diagram of nickel concentrations versus total organic carbon contents in the dolomites and black shales of the GBZ.

Recent to sub-recent interactions with meteoric fluids is also a plausible mechanism for trace metal enrichment or leaching. For example, supergene processes have been shown to be responsible for Mo and V enrichment of the black shales of the Gibellini deposit in Nevada (Bohlke et al., 1981). Moreover, Coveney et al. (1987) have shown that Mecca Shales from Indiana retain the capacity to fix Mo from dilute aqueous solutions, although the fixation mechanism is unknown. In the case of the GBZ, the impermeability of the shales, the lack of evidence for oxidation of the organic matter and the selection of unweathered samples for analysis indicate that an enrichment due to recent to sub-recent interaction with meteoric fluids is unlikely.

Bioturbation structures are absent and fine lamination is well preserved in all of the analyzed samples. Therefore, possible synsedimentary remobilization and homogenization of the geochemical signature by burrowing fauna can be excluded. Some remobilization during early diagenesis due to moving redox fronts could also be a cause of enrichments or depletions in particular layers, as shown by Jarvis and Higgs (1987) in turbidites deposited in a basin with intermittently anoxic conditions in the water column. In their case oxidation fronts migrating through the sediment due to intermittent anoxia cause metal remobilization and preferential enrichment in some layers. Although it cannot be excluded that similar processes were active during deposition of the GBZ, their effect was probably minor, as the pervasive laminations in almost all of the layers are indicative of persistent bottom-water oxygen deficiency with minor variations in the intensity of reducing conditions. Moreover, the dolomitic layers show metal enrichments relative to average carbonate sediments and are therefore a sink and not a source for metals for the black shales.

Based on these considerations, I conclude that the concentration processes of trace metals were purely synsedimentary and that the geochemical signatures were solely controlled by the depositional environment (intensity of anoxia, presence of sulfide ions, sedimentation rate) and variations in organic matter and detrital input.

4.1.3.2 Controls on V and Ni enrichment

In a recent paper, Lipiner et al. (1987) have shown experimentally that the metallation of porphyrins by V is strongly accelerated by the presence of organic sulfur compounds and dissolved polysulfides. This observation explains why vanadium dominates over Ni in sediments deposited under sulfidic conditions, even though it is not the thermodynamically preferred cation for porphyrin metallation. Thus, the $V/(V + Ni)$ ratio is a good paleo-redox indicator especially for distinguishing sediments deposited under sulfidic bottom waters. Most of the samples have a $V/(V+Ni)$ ratio close to unity (Fig. 4.3), which indicates that the bottom waters of the GBZ basin were anoxic and

sulfidic throughout deposition or that after a water-column turnover anoxic conditions were quickly reestablished.

Although the metallation of porphyrins is thermodynamically possible over the entire range of diagenetic conditions from early diagenesis to catagenesis (Lipiner et al., 1987), the lack of a source, other than sea water, for high quantities of V implies an early diagenetic or syndepositional origin for the vanadium enrichment. High V concentrations and a V/(V+Ni) ratio close to unity require highly anoxic, sulfidic bottom waters and extremely slow sedimentation rates. The slightly lower ratio in some of the organic poor samples may indicate less sulfidic conditions.

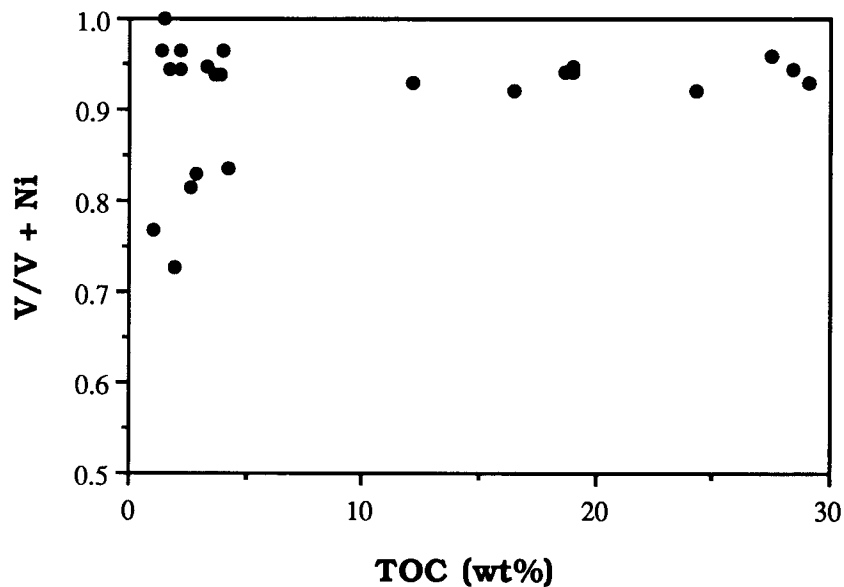


Fig. 4.3. Plot of V/(V +Ni) ratios versus total organic carbon content in the dolomites and black shales of the GBZ. In general, the ratios are close to 1 and reflect relatively constant V-concentrations, independent of TOC-content.

4.1.3.3 Calculations of excess trace metals

On the basis of the preceding discussion, the trace metal geochemical signatures found in the GBZ sediments are the sum of three main components:

- 1) a detrital component related to the accumulation of aluminosilicates,
- 2) a biogenic component related to the accumulation of organic matter, and
- 3) a early diagenetic-synsedimentary component produced by metal scavenging from sea water at the sediment-water interface through organic complexation and/or sulfide (co-)precipitation.

Excess metal concentration, defined as total concentration minus the primary detrital and biogenic input, is dependent on the time available for sediment-water interaction

during sedimentation and, therefore, reflects sedimentation rates. At high sedimentation rates, the sediment-pore water system is likely to quickly become a closed system because of fast burial, whereas with low sedimentation rates, diffusion along chemical gradients and exchange with sea water can continue for a longer time. Thus, calculations of early diagenetic trace metal enrichments can be used to estimate sedimentation rates either through comparison with trace metal accumulation rates in modern sediments or through estimation of the volume of water that must be stripped free of metals to produce the observed enrichment.

The contribution of the detrital and the biogenic component to the trace metal signature can be determined as follow:

1) *Detrital trace metal input*

The Al content of the sediment can be a proxy for the detrital content of the sediment, as Al is an immobile element and is present as aluminosilicates only. Assuming that the trace element composition of the detrital component in the black shale is the same as that of the average detrital shale of Wedepohl, (1970), the detrital input of any trace metal (Me) of interest can be estimated and subtracted from the total concentration using the formula given by Bralower and Thierstein (1987):

$$\text{Excess Metal} = \text{Me}_{\text{ samp.}} - (\text{Al}_{\text{ samp.}} \times [\text{Me/Al}]_{\text{ avg. shale}})$$

Where: $\text{Me}_{\text{ samp.}}$ = concentration of the metal in the sample; and
 $[\text{Me/Al}]_{\text{ avg. shale}}$ = Me/Al ratio in the average shale

The contribution from carbonate and silica skeletal material is neglected because various authors (e.g. Collier and Edmond, 1983, and references therein) have shown that skeletal material is an insignificant carrier of trace elements, such as V and Ni, into the sediment.

2) *Direct biological input:*

Living organic matter is greatly enriched in some trace metals compared to sea water. (Martin and Knauer, 1973; Collier and Edmond, 1984). Accumulation of organic matter can be responsible for a significant trace metal input into the sediment. The direct contribution from marine organisms can be estimated from TOC concentrations and published data on trace element contents of recent marine plankton.

For a correct estimate, however, potential trace element enrichments due to organic carbon losses during particle sinking in the water column and early diagenetic organic matter degradation have to be considered. Broecker and Peng (1982) and Collier and Edmond (1984) have shown that particulate organic matter can be an important carrier of trace elements into the deep ocean but also noted that the residual particulate organic carbon (POC) leaving the photic zone is not enriched in trace metals compared to the living matter, i.e. the organic carbon/trace metal ratio is essentially the same for

undegraded organic matter and POC. Therefore, the organic matter reaching the sediment can be assumed to have the same composition as that of living organisms. Organic carbon losses during early diagenesis are difficult to estimate. In anoxic and particularly in euxinic (H₂S-bearing) bottom waters, bacterial degradation of organic matter is less efficient and more incomplete than in oxic environments (Tissot and Welte, 1984); diagenetic organic carbon losses generally do not exceed 20 to 30% of the organic matter reaching the sediment surface (Bernier, 1982). The high hydrogen indices (Tab. 5.2) of the organic matter of the GBZ indicate good preservation. Therefore, it is assumed that early diagenetic carbon losses did not exceed 30%. Thus, the trace element enrichment through diagenetic organic carbon losses of the final organic rich sediments compared to the original biomass should not exceed a factor of 1.42 (30% loss). The exact calculation procedure can be found in Appendix B.

Excess trace metal concentrations in GBZ black shales obtained from detrital and direct biological input calculations are reported in Table 4.2. The excess metal concentrations in different layers can vary widely, indicating changing conditions during the various events of black shale deposition. In some layers, the concentration of some metals can be explained by a purely biogenic and detrital input and do not require further enrichment. The high excess concentrations of trace metals found in most of the samples, however, indicate that the major contribution to the trace metal geochemical signature of the black shales is derived from early diagenetic and/or syndepositional interaction between sea water and the sediment.

4.1.3.4 Calculation of sedimentation rates and water residence times.

An estimate of sedimentation rate and residence time of the water in the basin can be obtained by calculating the volume of seawater that must be stripped free of a specific element to account for the mass of this element in a particular layer. In the following calculations, vanadium is used because it shows the highest excess concentration of all the elements measured and therefore gives an estimate of the minimum volume of water required.

Assuming a 10 cm thick black shale layer with a V excess concentration of 2500 ppm, a shale density of 1.7 g/cm³ (Rickenbach, 1947) and a mean seawater vanadium concentration of 2.5 ppb, approximately 170,000 m³ of water would have to be stripped free of V to account for the V stored in the sediment during the deposition of the 10 centimeters of black shale over a area of 1 m². If basin dimensions of 10 x 10 km and a constant thickness of the layer are assumed, the total vanadium content of the layer is 4.25 x 10¹⁰ g. This corresponds to the vanadium contained in 1.7 x 10¹³ m³ of seawater. The depth of the GBZ can be estimated to lie between 40 and 100 m (see Section 3.3.3). Thus, for a mean basin depth of 50 m approximately 3400 basin volumes, are required to

Table 4.2 Excess trace metal concentrations in the GBZ (ppm).

Sample	Total Metal Concentration					Excess Metal Concentration *				
	Ni	V	Zn	Cu	Pb	Ni	V	Zn	Cu	Pb
60	164	2666	124	452	51	146	2639	28	438	43
75	260	2785	140	936	148	217	2725	--	909	133
82	201	2368	98	206	188	134	2242	--	163	164
97	148	2441	999	338	234	103	2367	829	306	215
108	128	2709	190	457	--	97	2663	46	434	--
115	97	1734	181	136	6	78	1704	83	120	--
132	123	1537	118	30	25	84	1474	45	--	8
average	160	2320	264	365	93	127	2266	131	341	79

* excess metal = Total metal - detrital input - primary biogenic input

account for the vanadium contained in this layer, whereas, if a depth of 100 m is assumed, 1700 basin volumes are necessary.

On the basis of evolution rates of daonella species, Rieber (1973) estimated the compacted sedimentation rate of the GBZ to be between 1 to 10 m/m.y.. Taking these values as a bracket, the 10 cm of layer 97 represent 10^5 or 10^4 years, respectively. Assuming a 50 m water depth, the residence time of the water in the basin would be between 29 and 3 years, whereas if a depth of 100 m is assumed, residence times between 58 and 6 years can be estimated. These estimates of residence time are independent of basin size as the volume of the black shale and water volume increase proportionally if a larger basin is assumed. The calculated residence time can be considered as maximum estimates because the calculations are based on 100% extraction of vanadium from seawater and a complete renewal of the water column is assumed. However, the presence of a stable density stratification and of H_2S in the water column, indicate that probably only part of the water column was periodically changed. Thus, the actual sedimentation rate for the black shales was probably close to 1 m/m.y., and the residence time of the water in the basin was between 30 and 60 years.

Parameters controlling the residence time of the water mass in a closed basin are size, shape and slope of the basin, size and depth of the channels which ensure the connection to the open sea and relative amounts and densities of the inflowing and outflowing waters (e.g. Deuser, 1975). Because these parameters cannot be constrained for the GBZ, it is difficult to compare the calculated values for the GBZ with modern analogues. Only very limited data are available on the residence time of water masses in recent enclosed lagoons and basins. For example, the residence time of water in the Kahu Bay (Indonesia), which is an anoxic to disaerobic basin covering an area of 30 by 60 km, is between 27 and 55 years (Middelburg, 1990).

The question arises whether such short residence times of water in the basin are long enough to efficiently scavenge trace metals from the water column. No data are available for scavenging rates of vanadium in sea water, but Jacobs et al. (1985) showed that other trace metals, such as Cu and Zn, have a residence time on the order of a few months in a permanently anoxic Norwegian fjord where surface water has a residence time of approximately 1 year. Broecker and Peng (1982) indicate that the scavenging time for Th can be on the order of days in estuarine environments associated with high productivity. Therefore, it is possible that V, which has a lowered solubility in reducing environments and easily forms stable organic complexes under sulfidic conditions (Lipiner et al., 1987), could be efficiently removed at the rates necessary to explain its enrichment in the GBZ shales.

Premovic et al. (1986) suggested that a special input of V was necessary to explain its high concentration in the GBZ and that the volcanic layers could be a source. They assumed a basaltic composition for the volcanic products because basalts have higher

vanadium contents. However, the ashes in the GBZ are the product of an intermediate to acidic volcanism which generally has V levels comparable to the average shale. The above calculations, however, show the feasibility of the enrichment process from sea water without a need for unusual sources of trace metals.

4.1.3.5 Calculation of primary productivity

Based on estimates of sedimentation rates and TOC-contents, primary productivity was calculated for degrees of preservation ranging from 2 to 30% (Tab. 4.3). This range includes the entire spectrum of preservation factors calculated for modern environments ranging from open marine anoxic to disaerobic (2%; e.g. Pratt, 1984) to restricted environments, such as the Black Sea (4 to 9%) and the Saanich Inlet, British Columbia or the Bornholm basin in the Baltic Sea, where preservation factors reach 17% and 29%, respectively (Bralower and Thierstein, 1987). The results are summarized in Table 4.3.

Recent shallow-water lagoons can be environments of high productivity, exceptionally reaching $1000 \text{ gC/m}^2/\text{yr}$ (Barnes, 1980). That is partly because the shallow water enable rapid recycling of nutrients from decaying organic matter at the bottom (Kelly and Naguib, 1984). However, primary productivities are generally around 200-300 $\text{gC/m}^2/\text{yr}$ or less. Productivities can reach up to $500 \text{ gC/m}^2/\text{yr}$ in upwelling regions, where nutrients are abundant and are continuously replenished. In comparison, calculated primary productivities for the GBZ range from 1440 to $21600 \text{ gC/m}^2/\text{yr}$ for a sedimentation rate of 10 m/m.y. and from 161 to $482 \text{ gC/m}^2/\text{yr}$ for 1 m/m.y. These calculated primary productivities greatly exceed the values observed in recent environments except where very low sedimentation rates are assumed.

In conclusion, the more reasonable lower primary productivities calculated for the GBZ black shales agree with trace metal calculations and indicate that the sedimentation rate was probably closer to 1 m/m.y. than 10 m/m.y.. Even considering a very high preservation factor of 30% of the primary productivity, the primary productivities calculated for a sedimentation rate of 10 m/m.y. largely exceed the value of $1000 \text{ gC/m}^2/\text{yr}$ which can be considered a maximum. This indicates that only a combination of very low sedimentation rates with high productivity and/or a high preservation factor can produce the observed enrichments in organic carbon. The productivities calculated for the laminated dolomites under the same assumptions are very low, which suggests that they were rapidly deposited with high dilution of organic matter and detrital input by carbonate.

Table 4.3 Data used to estimate primary productivity and constrain sedimentation rates.

Layer	Sed. rate (m/My)	Density ¹ (g/cm ³)	TOC (Wt%)	Accumulation Rates ² (g/cm ² /1000 yr)		Primary Productivity ⁴ (gC/m ² /yr)			
				R _{bulk}	R _{TOC}	R _{P2%}	R _{P10%}	R _{P20%}	R _{P30%}
97	1	1700	28.4	0.17	4.828	2414	482	241	161
	10	1700	28.4	1.7	48.28	24140	4828	2414	1610
Average black shale	1	1700	25.4	0.17	4.320	2160	432	216	144
	10	1700	25.4	1.7	43.20	21600	4320	2160	1440
dolomite	1	2500	3.55	0.25	0.009	4.438	0.9	0.438	0.30
	10	2500	3.55	2.5	0.09	44.38	9.0	4.438	3.0

1. Average bulk densities (From Rickenbach, 1947)

2. $R_{\text{bulk}} = \text{Sedimentation rate} \times \text{bulk density}$

$R_{\text{TOC}} = R_{\text{bulk}} \times \text{TOC}$

3. $R_p = \text{Primary productivity} \times \text{Preservation factor}$.

The different values are calculated using preservation factors of 2%, 10%, 20% and 30%, respectively.

4.1.4 Summary

The relatively homogeneous chemical compositions of the shales suggest a constant detrital input occasionally diluted by increased carbonate deposition and introduction of mainly biogenic silica. The trace element distribution in both the black shales and the dolomites indicate deposition under permanently sulphidic conditions. The excess trace metal mass balance and source calculations indicate that the trace element enrichments in the black shales are mainly controlled by early diagenetic redox reactions at the sediment-water interface or at the redoxcline and that these enrichments are only possible with extremely slow sedimentation rates. Estimations of primary productivities indicate that the sedimentation rates (compacted) for the black shales were probably close to 1m/m.y., whereas the carbonate layers were deposited faster. These results are compatible with sedimentological observations which indicate a sporadic, discontinuous carbonate sedimentation as the mechanism for bedding formation. The high organic matter content of the black shales is the result of a combination of high productivity and low sedimentation rate associated with high preservation rates.

4.2 Sulfur Geochemistry

4.2.1 Introduction

Sulfur is widely distributed in the lithosphere biosphere and hydrosphere. The presence of reduced sulfur in sediments is generally associated with the activity of sulfate reducing bacteria in the water column and /or in the sediment. Bacterial reduction of sulfate produces hydrogen sulfide enriched in ^{32}S by 14 to 46‰ relative to the initial sulfate. The magnitude of the fractionation depends on the bacterial species and is generally inversely proportional to the rate of sulfate reduction (Kaplan, 1983). The sulfur isotopic composition of pyrite in sediments is dependent on bacterial activity (both on bacterial species and rate of reduction) and isotopic composition and availability of the starting sulfate, and is therefore a good indicator for bacterial activity in sediments. Moreover, it constrains the time and depth of sulfide precipitation as it allows a distinction between pyrite formation under open-system conditions from formation at depth in the sediment, where pore-waters are within a closed system. In the latter case, pore-water sulfate cannot be replenished fast enough by diffusion from the overlying bottom water forcing the bacteria to use the residual sulfate which becomes progressively enriched in ^{34}S as sulfate reduction continues (this process is called the reservoir effect). For this reason, pyrite formed in closed-system environments generally show highly variable isotopic compositions with up to 40‰ variations (e.g. Dinur et al., 1980) whereas, if

Table 4.4

Organic carbon and sulfur isotope data of selected samples. (from A. Apin and J.D. Hudson, unpublished)

Layer No	(Weight %)										
	56m	82	88	97 o	99 o	108	115	132			
Total C	18.30	15.80	13.21	28.20	25.50	29.33	32.70	35.40			
Carbonate C	6.20	0.00	11.30	0.10	0.00	0.32	0.20	0.50			
TOC	12.09	15.80	2.20	28.10	25.50	27.43	32.50	34.90			
Organic S	--	1.80	--	3.20	2.90	--	4.40	4.50			
Total S	2.10	10.44	0.30	5.51	5.61	3.10	5.85	6.28			
Total Fe	1.48	9.80	0.50	2.60	2.90	1.80	2.40	2.50			
Pyrite S	--	8.64	--	2.31	2.71	--	1.45	1.78			
Pyrite Fe	--	7.56	--	2.02	2.37	--	1.27	1.56			
Reactive Fe	--	1.20	--	0.17	0.09	--	0.08	0.08			
S/C organic	--	0.115	--	0.113	0.114	--	0.135	0.128			
DOP total	0.87	0.770	0.83	0.78	0.82	0.91	0.53	0.62			
DOP reactive	--	0.86	--	0.92	0.96	--	0.94	0.95			
$\delta^{34}\text{S}_{\text{pyr}}(\text{CDT})$	--	-29.20	--	-28.20	-27.60	--	-26.40	-26.40			
$\delta^{34}\text{S}_{\text{org}}(\text{CDT})$	--	-15.90	--	-18.00	-19.50	--	-17.70	-18.30			
$\delta^{34}\text{S}_{\text{tot}}(\text{CDT})$	--	-26.00	--	-23.50	-23.10	--	-19.90	-20.00			
$\Delta^{34}\text{S}_{\text{pyr-org}}$	--	13.30	--	10.20	8.10	--	8.70	8.10			
Sorg/Stot	--	0.172	--	0.581	0.517	--	0.752	0.717			

pyrite is formed under open-system conditions, very negative compositions with little variations are observed.

The combination of analysis of sulfur isotope composition of pyrite with the determination of the degree of pyritization (Berner, 1970) and the analysis of the relations between Fe, S and organic carbon concentrations are used in the next sections to determine the controls on pyrite formation and sulfur incorporation in organic matter.

4.2.2 Results

Total sulfur contents range between 2.1 and 10.4% in GBZ black shales and are generally below 0.5% in the carbonate-rich samples (App. A, Tab. 4.4). Pyrite is the only sulphide mineral phase detectable by XRD and is mainly present in the form of framboids or more rarely as larger euhedral cubes. Other sulfides (sphalerite and galena) were observed in some samples but they occur in minor amounts only. Sulfate minerals are absent. Organic matter is the other dominant sulfur carrier in the GBZ rocks.

Pyrite sulfur contents range from 1.4 to 8.6 wt%. Sulfur isotope compositions of the pyrite range between -26.4‰ and -29.2‰ (CDT) (Tab. 4.4). This range corresponds to a fractionation of 40 to 43‰ relative to Middle Triassic sea water sulfate (approximately 14‰ (CDT), Claypool et al., 1980) and is within the normal fractionation range of (33-46‰) observed in marine sediments undergoing sulfate reduction (Goldhaber and Kaplan, 1974).

Organic sulfur contents range from 1.8 to 4.5 wt% and account for 17 - 75% of the total sulfur content of the sediment. The OS/OC ratios vary between 0.113 and 0.135 and are very high compared to the ratio of 0.01 found in living organisms, but lower than the value of 0.17-0.20 which is considered the saturation value (i.e. maximum S/C ratio) of marine organic matter (Bein et al. 1990). The isotopic compositions of the organic sulfur range between -15.9‰ and -19.5‰, which is 8.1 to 13.2‰ heavier than the co-existing pyrite.

The degree of pyritization (DOP_{tot}), defined by Berner (1970) as the ratio of pyrite-Fe to total-Fe (Py_{Fe}/T_{Fe}), ranges from 0.53 to 0.85. Fe in sediments can be distinguished into two categories: reactive Fe and non-reactive Fe. The former is less strongly bound in minerals and can readily react with H_2S to form sulfides, whereas non-reactive Fe is strongly bound in detrital minerals and is not available for sulfide formation. The degree of pyritization of the reactive iron (DOP_{react}), defined as the ratio of pyrite-Fe to reactive-Fe, range from 0.86 to 0.96 (Tab. 4.4) in the GBZ black shales. This indicates that some of the Fe is present as non-reactive iron

A cross-plot of TOC vs total S (Fig. 4.4) shows a positive correlation, whereby most of the samples have a S/OC-ratio lower than 0.4 corresponding to ratios found in Holocene

normal marine sediments (Berner and Raiswell, 1984; Raiswell and Berner, 1986). This relationship is rather unusual as generally sediments deposited under euxinic conditions plot above this regression line and do not show a definite correlation between organic carbon and sulfur (e.g. Leventhal, 1979). The total Fe vs total S cross-plot in Fig. 4.5 shows a generally positive correlation. The scatter around the stoichiometric pyrite line indicate that some of the samples have excess sulfur bound to organic matter while others have excess iron (non-reactive iron and/or low degree of pyritization).

4.2.3 Discussion

4.2.3.1 Controls on pyrite formation

Among the many factors known to influence pyrite formation in sediments, the presence of sulfate and metabolizable organic matter, the availability of reactive (reducible) iron and the presence of anaerobic conditions in the water column are most important (e.g. Berner, 1984; Berner and Raiswell, 1986). The limiting factors for pyrite formation are best illustrated by plotting the relative concentrations of total S, TOC and total Fe in a ternary diagram (Fig. 4.6; Dean and Arthur, 1989). Organic matter limitation on pyrite formation in the GBZ is unlikely in view of the high TOC and the high hydrogen indices, which suggest that enough reactive organic matter was available to support sulfate reducing bacterial activity. In Fig. 4.6, the GBZ samples scatter along the stoichiometric pyrite line, indicating that Fe availability was probably the limiting factor for pyrite formation. Thus, only a small fraction of the sulfide produced by bacterial activity could be fixed in the sediment as pyrite. Although organic matter was also a sink, most of the reduced sulfur must have diffused out of the sediments into the overlying water column. The low total sulfur content of the GBZ sediments (Fig. 4.4) is a consequence of the extreme Fe limitation. This observation is also supported by the high DOP_{react} (Table 4.4), which indicates almost total incorporation of Fe into pyrite. The highest excess iron (Fig. 4.6) occurs in samples from layers with high carbonate contents and is probably incorporated in dolomite.

4.2.3.2 Timing of pyrite formation

The $\delta^{34}S$ values of pyrite in the GBZ black shales (-26 to -29 ‰, Tab. 4.4) do not show much variations and their composition indicate a fractionation between sulfate and sulfide close to the maximum biologically-induced fractionations observed in nature (Claypool and Kaplan, 1974). This indicates that pyrite formed under open system conditions, where sulfate could be replenished by diffusion during pyrite formation.

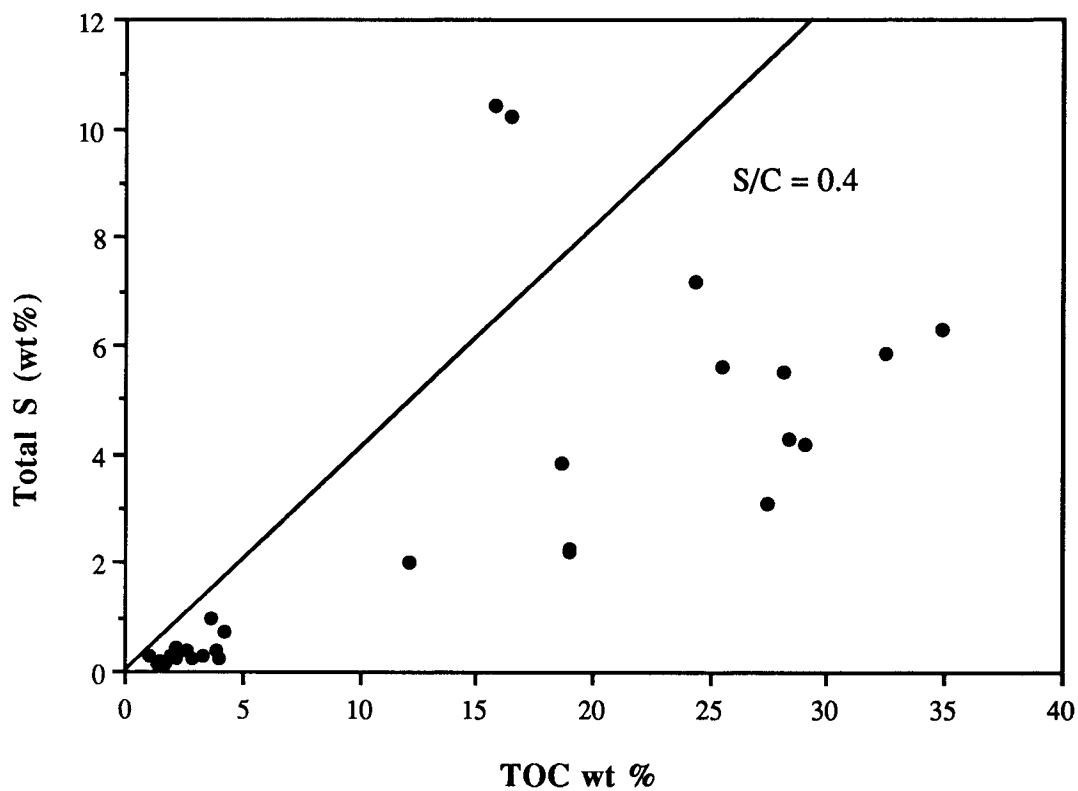


Fig. 4.4. Scatter diagram of total sulfur concentration versus total organic carbon content in the dolomites and black shales of the GBZ. The S/C ratio of 0.4 is the best fit regression line determined for Holocene normal marine shales by Berner and Raiswell (1984).

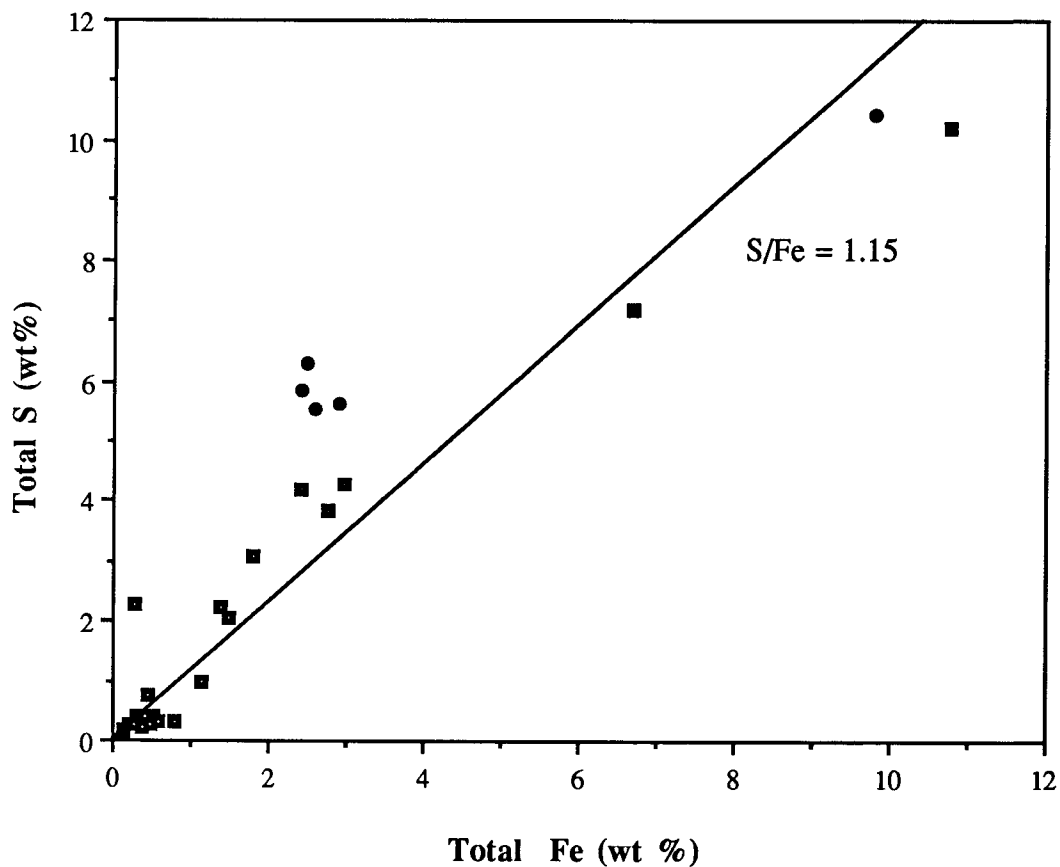


Fig. 4.5. Scatter diagram of total sulfur concentration versus total Fe-content in the dolomites and black shales of the GBZ. The line with $S/Fe = 1.15$ reflects pyrite stoichiometry.

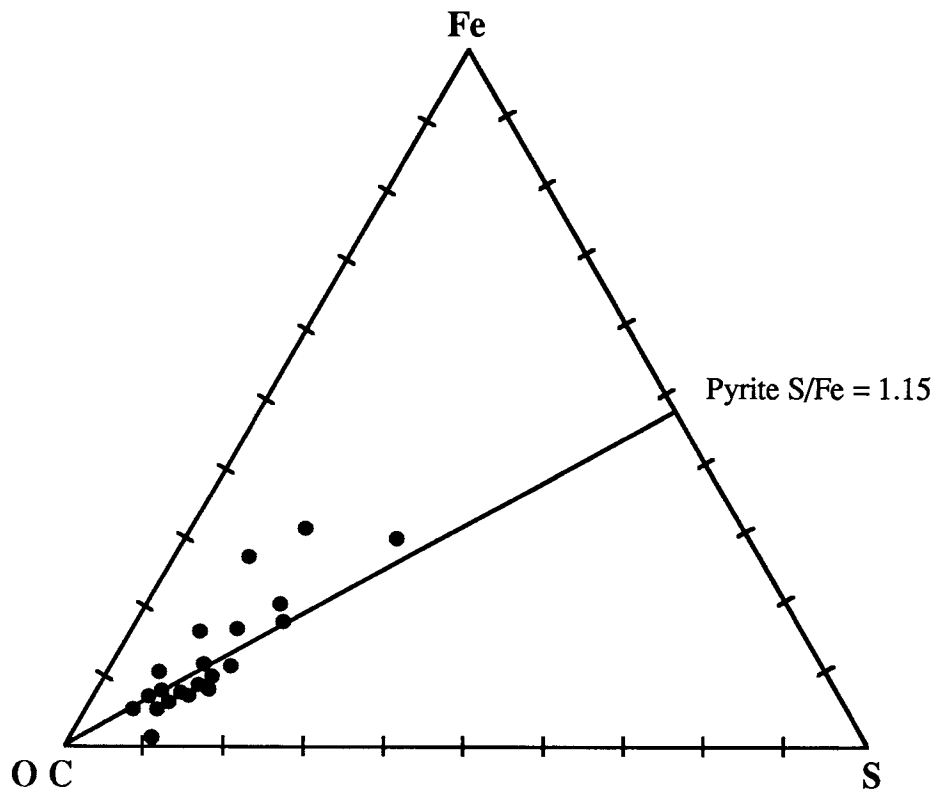


Fig. 4.6 Iron-sulfur-organic carbon ternary diagram. Pyrite stoichiometry is indicated by the line at $S/Fe = 1.15$. Note the scatter of the points along the stoichiometric pyrite line, indicating iron limited pyrite formation. The two samples showing the highest excess Fe are dolomite-rich lithologies. The excess Fe in these samples is probably incorporated in the dolomite lattice.

Possible scenarios accounting for the observed isotopic signatures are: (1) significant pyrite was formed in the water column and/or at the sediment-water interface as is observed in some recent euxinic environments (e.g. Leventhal, 1983), (2) Pyrite was formed in the sediment but due to the low sedimentation rate, marine sulfate could be continuously resupplied to the pore-waters through diffusion, and (3) the available reactive iron available was rapidly converted to pyrite during the initial stages of diagenesis, and the later evolution of the system is not recorded in the sulfur isotopes because pyrite did not continue to form due to the lack of a reactant. The observed isotopic signal only reflects a limited time-slice of the evolution of the pore-water system. In this latter case, the isotopic composition of the pyrite may have been ultimately controlled by the availability of Fe.

It is impossible to distinguish between these three options, but the presence of fine organic matter laminae containing high amounts of pyrite framboids (see section 3.2.1.1) and the presence of pyrite inclusions in the earliest formed dolomite rhombs indicate that at least part of the pyrite formed very early, possibly in the water column and /or at the sediment-water interface. In general, when pyrite forms in the water column, no correlation exist between total S and TOC because pyrite formation is decoupled from organic matter degradation. H₂S is present in the water column and there is no dependence of pyrite formation on organic matter availability. The positive TOC-total S correlation (Fig. 4.4), together with the progressive enrichment in ³⁴S with increasing DOP_{react} (Fig. 4.7a), may indicate that as pyrite formation continued in the sediment it incorporated a small amount of heavier sulfide produced in the pore-waters. The facts that $\delta^{34}\text{S}_{\text{Om}}$ negatively correlates with the DOP_{react} (Fig. 4.7 b) and that the fractionation between organic- and pyrite-sulfur substantially decrease with increasing degree of pyritization (Fig. 4.8) indicate that Fe availability not only can influence the sulfur isotopic composition of the pyrite but also that of the organic matter.

4.2.3.3 Sulfur incorporation in GBZ organic matter

The sulfur content of phyto- and zooplankton vary from 0.3 to 3.3% dry weight (Goldhaber and Kaplan, 1974). Sulfur is mainly present in the reduced form incorporated in sulfur-bearing aminoacids (Goldhaber and Kaplan, 1974; Mekhthyeva et al. ,1976). The increased organic sulfur content of sedimentary organic matter cannot be explained simply by preservation of biochemical organic sulfur compounds. Concentration of these compounds by preferential preservation is rather unlikely because biochemical sulfur compounds are readily degraded during diagenesis due a lower stability relative to lipids or aliphatic biopolymers. In addition, the organic sulfur compounds found in oils and rock extracts are different from those found in the biosphere (Sinninghe-Damste, 1988). Moreover, assimilative organic sulfur has an isotopic composition similar to that

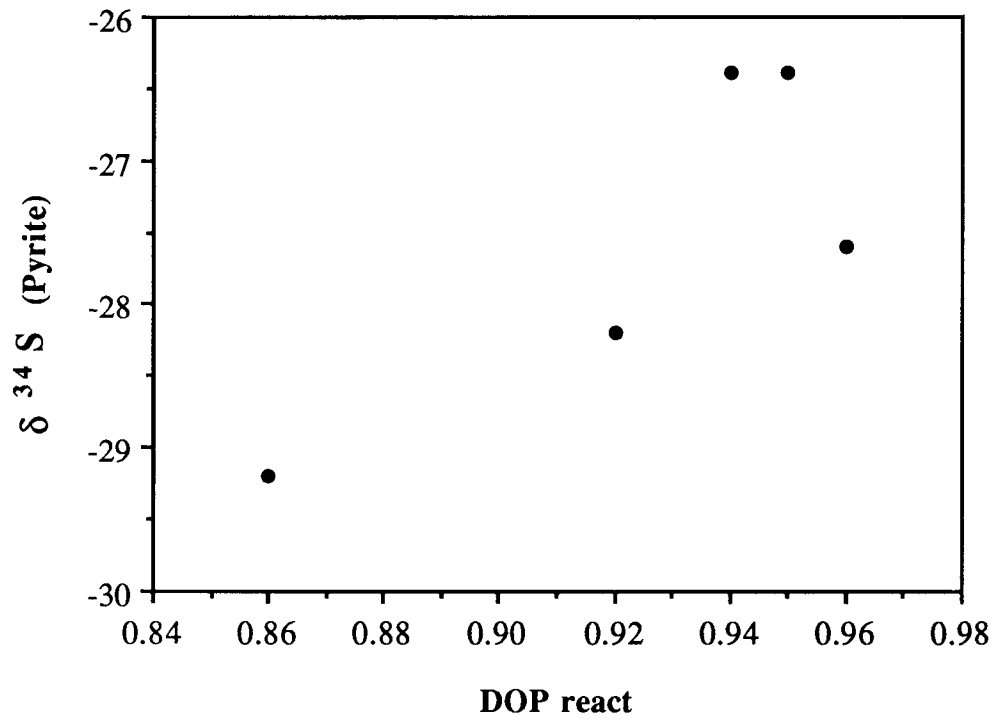


Fig. 4.7a. Relationship between degree of pyritization of reactive iron (DOP_{react}) and sulfur isotope composition of pyrite.

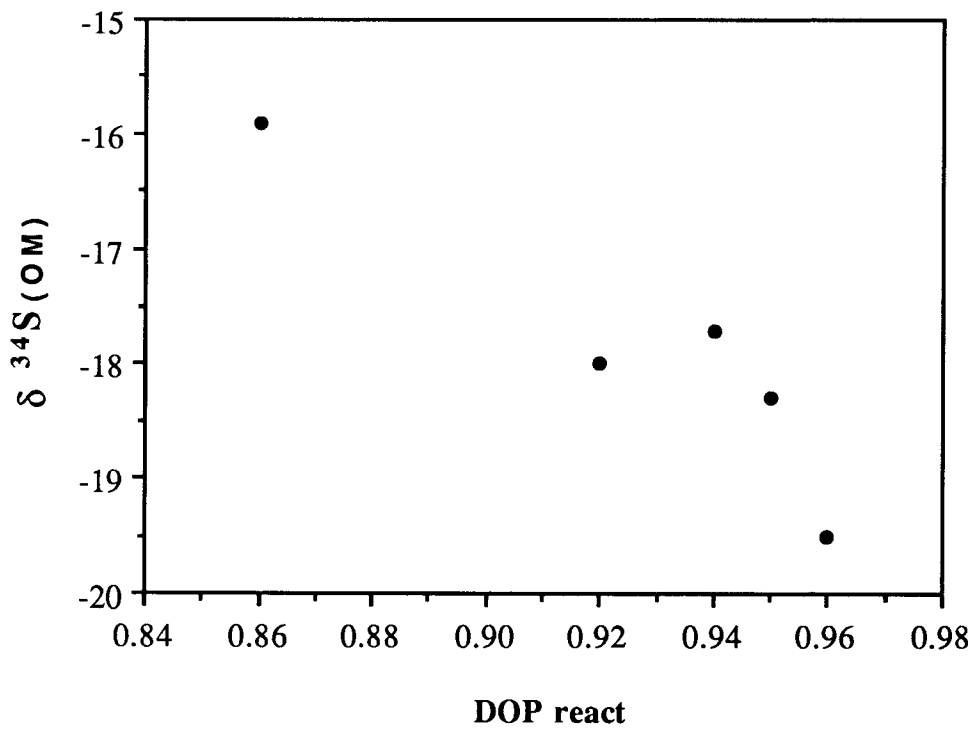


Fig. 4.7b Relationship between degree of pyritization of reactive iron and sulfur isotope composition of organic matter (OM)

of marine sulfate because biological sulfur assimilation occurs without significant isotopic fractionation (Orr, 1974; Aizenshtat et al. 1984), whereas sulfur present in sedimentary organic matter often has an isotopic composition which is much more negative than the coeval marine sulfate. Thus, the presence of high amounts of sulfur in sedimentary organic matter is due to early diagenetic reactions of the freshly deposited organic matter with H_2S , elemental sulfur and/or polysulfides, which are produced by the biological activity of sulfate reducing bacteria in the water column and/or in the sediment (Tissot and Welte, 1984; Orr, 1978). The key condition for the formation of high sulfur kerogens in marine settings is the lack of reactive iron compounds which would successfully compete with the organic matter for the incorporation of sulfur.

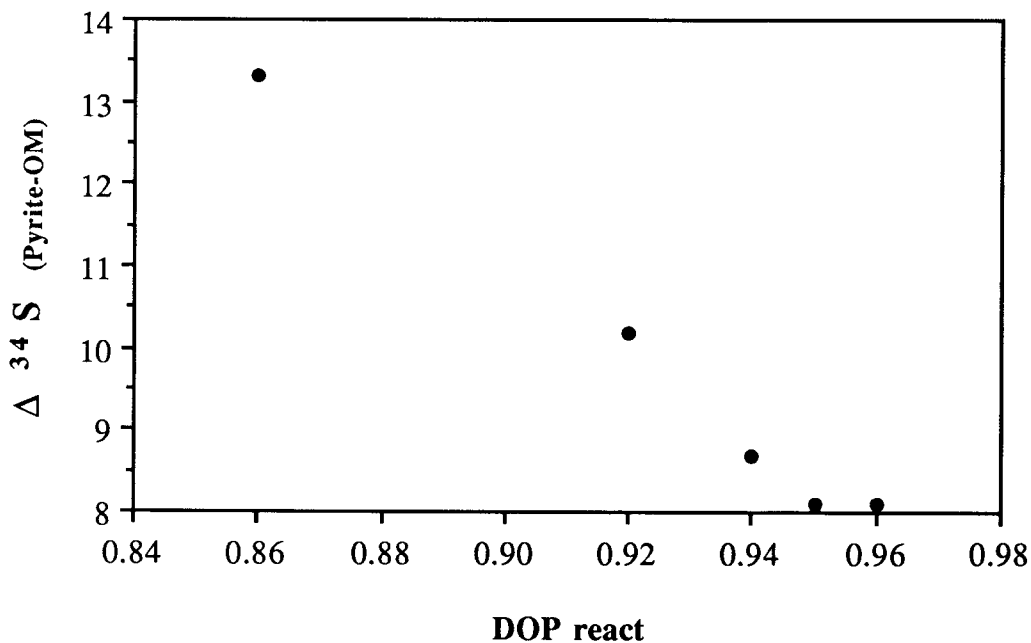


Fig. 4.8. Relationship between the degree of pyritization of reactive iron and the sulfur isotope fractionation between pyrite and organic matter. Note the substantial decrease in $\Delta^{34}S$ with increasing degree of pyritization.

The high organic sulfur content in the GBZ organic matter is a consequence of the low reactive iron availability in the sediments, which probably led to high concentrations of reduced sulfur species (H_2S , polysulphides) in the pore-waters during diagenesis. The relatively low $\delta^{34}S$ of the organic matter indicate a high contribution of light sulfur produced by sulfate reducers. The heavier isotopic composition of the organic matter compared to the associated pyrite can be attributed to incorporation of assimilative sulfur with a composition equivalent to the marine sulfate or to incorporation of polysulfides which could have had a different isotopic composition than the H_2S (Dinur

et al., 1980). The lack of even less negative organic sulfur $\delta^{34}\text{S}$ values could also indicate that organic matter sulfur incorporation ceased before the system became closed to the infiltration of fresh sulfate. During early diagenesis of the GBZ, the activity of methanogenic bacteria was probably limited by the competing activity of sulfate reducing bacteria fed by the constant presence of diffused sulfate in the pore-waters.

4.2.4 Summary

The S-Fe-TOC relationships and the high DOP indicate that the limiting factor for pyrite formation in the GBZ was reactive-Fe availability. The absence of isotopically heavy pyrite indicate that sulfide formation occurred within an open system in the presence of abundant sulfate. This may result from pyrite formation in the water column or in the sediment prior to significant reduction of sulfate concentrations in the pore waters. The high organic sulfur content of the GBZ black shales is a consequence of the Fe limitation, because excess sulfide was available for incorporation in organic matter. The light sulfur isotopic composition of both organic matter and pyrite is a consequence of Fe-limitation and low sedimentation rates. Although iron availability limited pyrite formation, making the interpretation of its sulfur isotopic composition ambiguous in terms of open-system diagenesis, the high sulfur concentrations in organic matter and its light isotopic composition indicate that sulfate was long available in the pore waters. This suggests that sulfate reducing bacteria were the most important organisms responsible for organic matter remineralization in the sediments whereas methanogens were probably absent. Thus, although iron availability probably limited pyrite formation, there is no indication of a closure of the system to interaction with the water column.

4.3 Oxygen and Carbon Isotope Geochemistry of Dolomite

4.3.1 Introduction

Ideal dolomite contains cation planes composed entirely of Ca alternating with planes composed entirely of Mg with a Ca:Mg molar ratio of 1. Ideal dolomite is the thermodynamically most stable form of dolomite, but is extremely rare in nature. Most natural dolomites deviate both in composition and crystal structure from the ideal form and are therefore thermodynamically less stable. Although Holocene dolomites may have a Mg:Ca ratio close to 1, they often have only weak and poorly developed x-ray superstructure reflections. Dolomites with varying degrees of structure disorder (Reeder, 1983) and are commonly called "Protodolomites". Structural disorder causes changes in enthalpy and entropy and thus alters the thermodynamic properties of dolomite. For example, the solubility constant of dolomite can vary by orders of magnitude, depending on the degree of ordering (Carpenter, 1980; Hardie, 1987). In addition to structure

distortions, deviations from ideal stoichiometry further enhance the solubility of protodolomites. The instability of the protodolomites formed during early diagenesis results in a large thermodynamic drive to undergo spontaneous ordering and to recrystallize to a more stable form during burial diagenesis. With these considerations in mind, it is evident that any geochemical and isotopic method used to determine the origin of dolomite must be used with caution and the effects of reequilibration during recrystallization of early-formed dolomite must be taken into account.

Trace element distributions in dolomites have been often used to constrain their origin. However, because of the inability to precipitate dolomite in the laboratory at temperatures below 100°C, the partition coefficients for the various trace elements at low temperatures are poorly known. Moreover, recent studies have shown that partitioning coefficients of trace elements into carbonates are not only dependent on temperature but also on crystal growth rate (Land, 1985) and dominant crystal faces where growth occurs (Reeder and Grahms, 1987). In this work, trace element distributions are used only for a rough estimate of the depositional environment.

Stable isotopes of oxygen and carbon have also been commonly used to elucidate the origin of dolomite. Although late diagenetic recrystallization and reequilibration during burial may alter the original signature, stable isotope geochemistry has proven to be a reliable tool to characterize the environment of dolomite precipitation. Carbon isotopes are especially useful in organic carbon-rich sediments because biochemical degradation of organic matter through different bacterial species produces large variations in the carbon isotopic composition of dissolved bicarbonate in the pore-waters and leads to the precipitation of dolomites with widely varying isotopic compositions (e.g. Irwin et al. 1977; Pisciotta and Mahoney, 1981; Kelts and McKenzie, 1984; Burns et al., 1988). After oxygen is consumed from the bottom or pore-waters, anoxic sulfate-reducing bacteria are the main agents of remineralization of organic matter in marine sediments. The decomposition of organic matter through sulfate reducers produces bicarbonate that is greatly depleted in ^{13}C , i.e. the bicarbonate carbon isotope composition is similar to that of the precursor organic matter. After sulfate is depleted from the pore-waters, methanogenic bacteria become the dominant organic matter decomposers. The end products of their metabolism are methane ($\delta^{13}\text{C}$ -40 to -60‰) and bicarbonate with compositions of up to + 20 ‰. The sequence of diagenetic zones and the expected carbon isotopic composition of dissolved bicarbonate in the pore-waters of an organic matter-rich sediment is schematically depicted in Fig. 4.9.

Because the size of the carbon pool in carbonate sediments is orders of magnitude greater than the carbon pool of diagenetic fluids, the carbon isotopic composition of a carbonate is less sensitive to resetting or alteration during burial diagenesis than any other geochemical signature. On the other hand, oxygen isotopes are very sensitive to recrystallization and early diagenetic signatures are often modified during diagenesis

because oxygen is much more abundant in the fluids than in the rock. For these reasons, a wide spread in oxygen isotope compositions are often observed in diagenetically altered rocks, whereby ^{18}O -rich compositions are indicative of low precipitation temperatures and are likely to represent early diagenetic signals. Only by combining petrographic observations with isotopic studies is it possible to evaluate the effects of late diagenesis on the isotopic signatures and to constrain temperatures and fluid composition of the dolomitizing fluids.

In this section, carbon and oxygen isotope geochemistry of dolomite, apatite and quartz in the GBZ are presented. These data are used to constrain the environment, temperature and timing of dolomitization and, together with the petrographic observations, allow the effects of burial diagenesis on the primary geochemical signature of the dolomites to be evaluated. Data on the isotope geochemistry of the Salvatore and San Giorgio dolomites are included for comparison. The petrographic investigations (Chapter 3) have shown that there is a correlation between the various cement generations in the three formations and, therefore, for a complete dolomitization model to be developed a comparison is necessary.

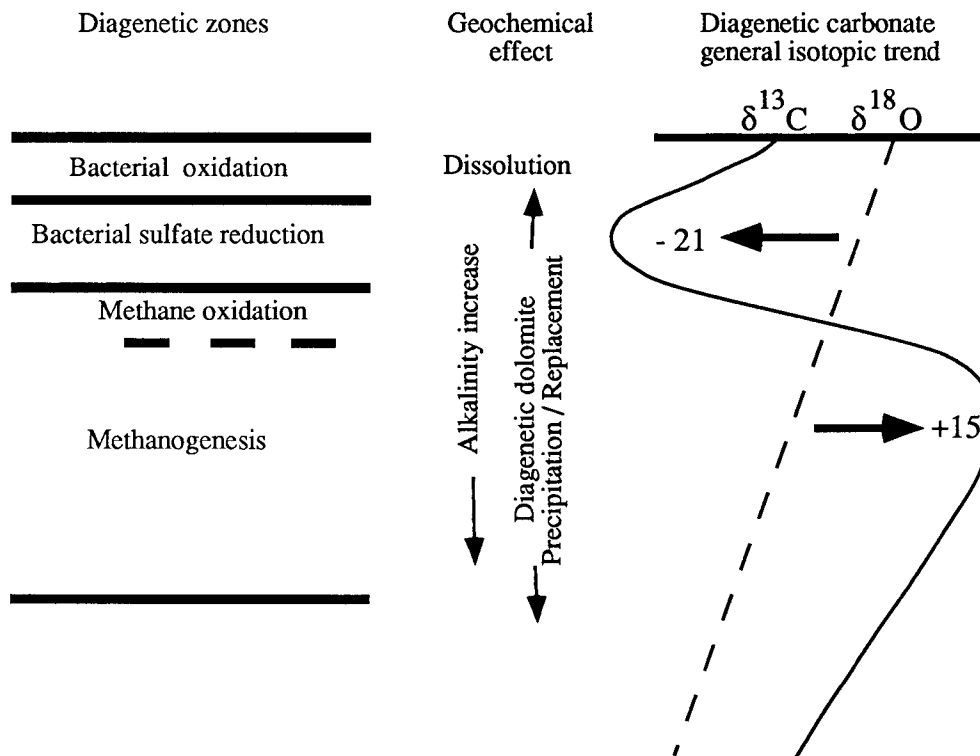


Fig. 4.9 Schematic representation of expected variations in $\delta^{13}\text{C}$ of diagenetic carbonates in zones of progressive organic matter decay (from Kelts and McKenzie, 1984).

4.3.2 Results

4.3.2.1 Dolomite crystallography and crystal chemistry

All of the GBZ, San Giorgio and Salvatore dolomites show superstructure reflections with varying degrees of definition. The degree of ordering, based on the relative intensities of peak (015) to (110) (Hardy and Tucker, 1988), ranges from 0.6 to 1.0. Although the late dolomite cements are generally better ordered than the early matrix dolomite, no clear correlation of degree of ordering with carbon and oxygen isotope composition is observed. The displacement of the (104) peak indicates a spectrum of stoichiometries ranging from 48.7 to 54.8 mol% CaCO₃. Stoichiometry shows no correlation with either oxygen or carbon isotopic composition.

Non-stoichiometry and lattice imperfections are generally attributed to the fact that the dolomites are precipitated as Ca-rich protodolomites and incompletely recrystallize to well ordered dolomites (e.g. Burns and Baker, 1987). However, if the dolomites were primarily precipitated as ordered dolomites and not as protodolomites, this could also indicate that not only the original crystallographic characteristics but also the early diagenetic geochemical signatures have been preserved and are relatively unaffected by later large scale dissolution-reprecipitation processes. Early diagenetic precipitation of ordered dolomites has been reported in sediments off Baja California (Shimmield and Price, 1984), in Kahu Bay Indonesia (Middelburg et al., 1990) and in the Gulf of Mexico (Batz et al., 1988).

Trace elements in selected samples of different dolomite generations were measured by AAS. Analysis of single phases by electron microprobe were attempted, but, as the concentrations of the trace elements measured are close to the detection limits, no significant variations could be observed. Ca and Mg concentrations estimated by XRD indicate a smaller range in stoichiometries than those determined by electron microprobe analysis where concentrations of up to 57 mol% CaCO₃ were found. The reason for this difference is unknown.

The average iron content of GBZ dolomites is 0.17 wt%. These low Fe-contents are typical for dolomites formed in the sulfate reduction zone, where available Fe is more readily precipitated as sulfides, leaving the pore-waters depleted with Fe (e.g. Irwin, 1980; Pisciotto, 1981). The low Fe-content of the dolomites is consistent with the conclusion that Fe-limited pyrite formation occurred in the GBZ sediments. Only the late cements showing dark non-luminescing bands in cathodoluminescence have Fe-concentrations up to 0.4 wt%.

Manganese contents are low, in the range of 199-445 ppm, compared with other organogenic dolomites (e.g. Burns et al., 1988; Burns and Baker, 1987). This is probably due to the low detrital input and thus a low primary Mn availability in the sediment. Mn is highly soluble in anoxic pore-waters and if available should be readily incorporated

into the dolomite lattice. Mn is present in higher concentrations in the late cements. Sr-contents range from 51 to 171 ppm.

4.3.2.2 Isotope geochemistry of Grenzbitumenzone Dolomites

The carbon and oxygen isotope compositions of the dolomites of the GBZ are shown in Fig. 4.10 and are compared with the isotopic compositions of carbonates in the Salvatore and San Giorgio dolomites and the Meride Limestones in Fig. 4.11. The complete data are tabulated in Appendix C.

Carbon isotope compositions of the dolomites of the GBZ range from -1.4 to to -5.7 ‰ and averages -3.4‰ (Figs. 4.10 & 4.11). Although profiles across beds show minor random variations, no consistent trends in carbon isotope composition could be observed. Multiple measurements along and across individual beds show maximum variations of 1‰. The presence of consistent carbon isotope trends across beds would be proof for a concretionary origin of a bed (e.g. Kelts and McKenzie, 1984; Irwin, 1981). No correlation is seen between carbon and oxygen isotopic composition (Fig..4.11) and no regional variations or trends across the basin occur. Comparison of the GBZ dolomites with calcites of the Meride Limestone are shown in Fig. 4.10. The carbon isotope ratios of the calcites in the Meride Limestones, which may retain an isotopic ratio representative of the precursor carbonate in the GBZ, indicate that the contribution of isotopically lighter carbonate from organic matter diagenesis has produced a maximum depletion of 8.5 ‰ relative to the precursor carbonate.

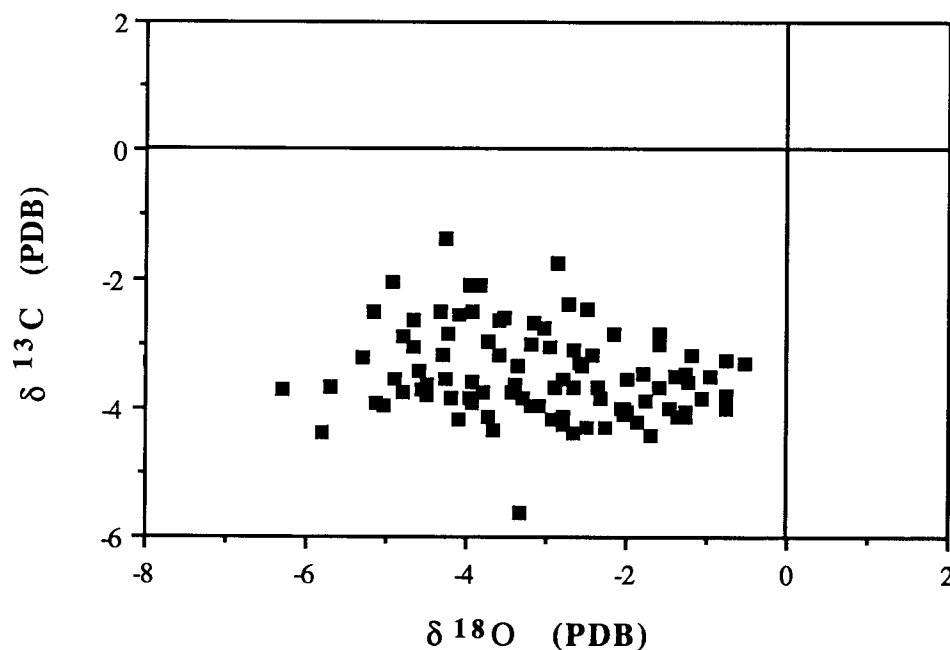


Fig. 4.10 Carbon versus oxygen isotope compositions of dolomites from the Grenzbitumenzone.

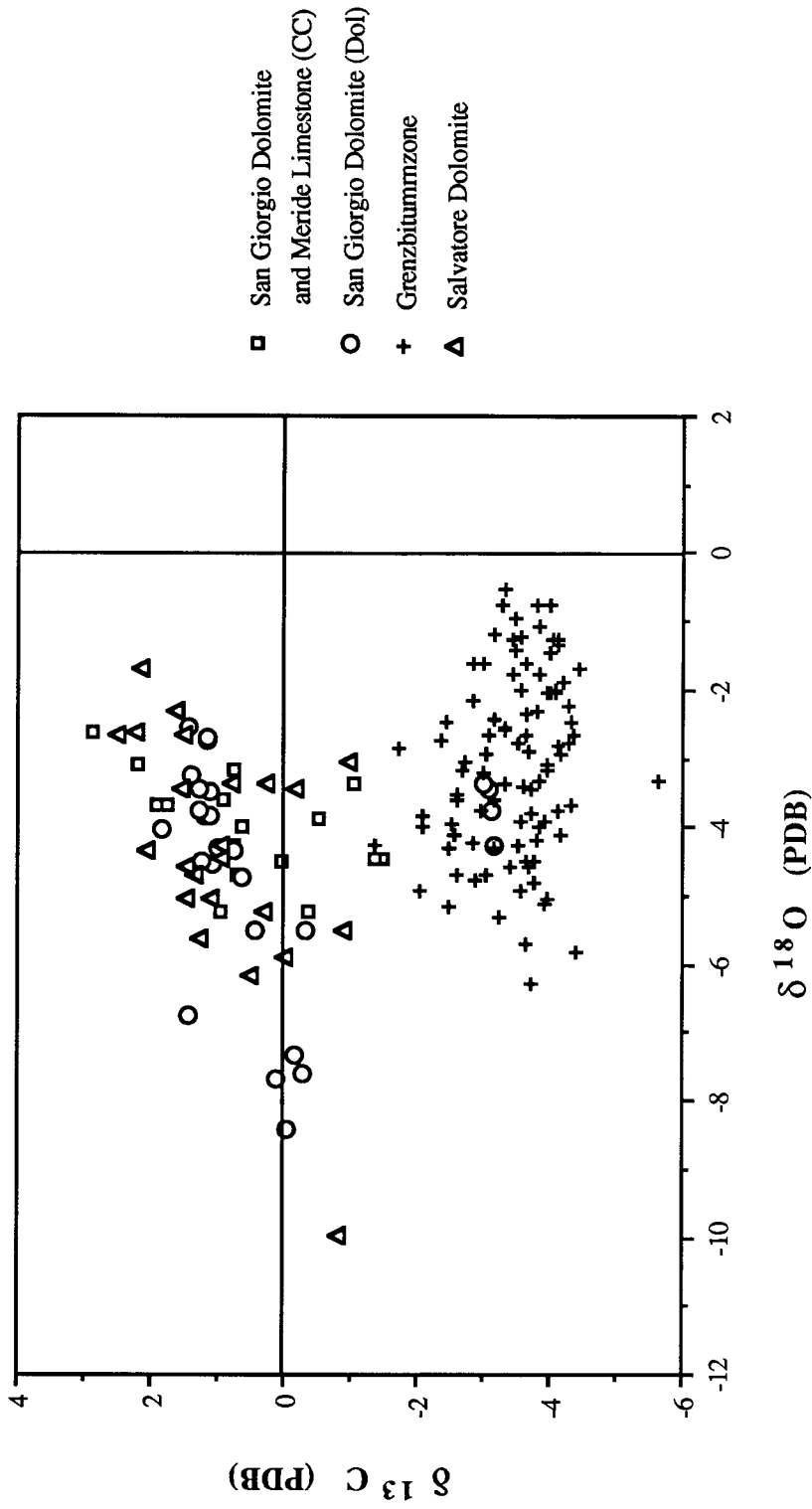


Fig. 4.11 Carbon versus oxygen isotope compositions of dolomites from the Anisian dolomites (Plattendolomite, Diplopora Dolomite and Middle Salvatore Dolomite).

Oxygen isotopic compositions of the dolomites range from -0.73‰ to -6.53 ‰ and average -3.2‰. The most positive samples correspond to micritic dolomite laminae and fine grained dolomites, whereas the most negative sample with a value of -6.5‰ is a idiomorphic dolomite cement (Dolomite IV; see Section 3.5.1) partially filling an ammonite mold. This value can be considered the end-member high temperature composition of late diagenetic dolomite in the GBZ. The oxygen isotopic compositions of the dolomites generally become more negative with increasing grain-size and with increasing amount of dolomite III cement present in the sample (estimated by observation in cathodoluminescence microscopy).

4.3.2.3 Isotope geochemistry of Salvatore dolomite

Carbon isotope composition of the dolomites vary between +2.51 and -0.98‰. (Fig. 4.12). The matrix dolomites have a mean value of + 1.13‰, the most negative values are from cements (Dolomite IV). Oxygen isotope composition show a wide scatter ranging from -2.31 to -9.98 ‰, whereby the matrix dolomites range between -2‰ and -4‰ and the lighter values are from cements. Fig. 4.13 shows stable isotope trends in dissolution cavities of the Anisian dolomites from the locality Rossaga. The different dolomite generations show a consistent depletion in ^{16}O from matrix dolomite to the internal sediments to the late cements, indicating a progressive temperature increase and/or an increasing contribution from meteoric waters. With the exception of one sample, the oxygen isotope compositions of the Salvatore Dolomite are in the same range as those from the GBZ. These generally negative isotopic compositions are inconsistent with the presence of hypersaline conditions as postulated by Zorn (1971).

4.3.2.4 Isotope geochemistry of San Giorgio Dolomite and Meride Limestone

The carbon and oxygen isotope compositions of dolomites and calcites from the San Giorgio Dolomite and of calcites from the Meride Limestone are presented in Fig. 4.14. Carbon isotope compositions of the calcites vary between +2.86‰ and -1.5‰. The negative values are found in samples rich in organic matter, whereas the positive values are from samples with no organic matter. This suggests that the negative compositions are the result of the addition of light organic carbon-derived carbonate during diagenesis and that the compositions around 2‰ reflect the primary carbon isotopic composition of the calcite.

The oxygen isotope compositions of the calcites vary between -2.64‰ and -5.2‰. The highest values are in the range inferred for Middle Triassic marine carbonates (Frisia-Bruni et al., 1989), whereas the lower values probably represent reequilibration of the original carbonate with late diagenetic fluids. The carbon isotope composition of the dolomites vary between 1.8 and -3‰, whereby the values of -3‰ are from dolomites

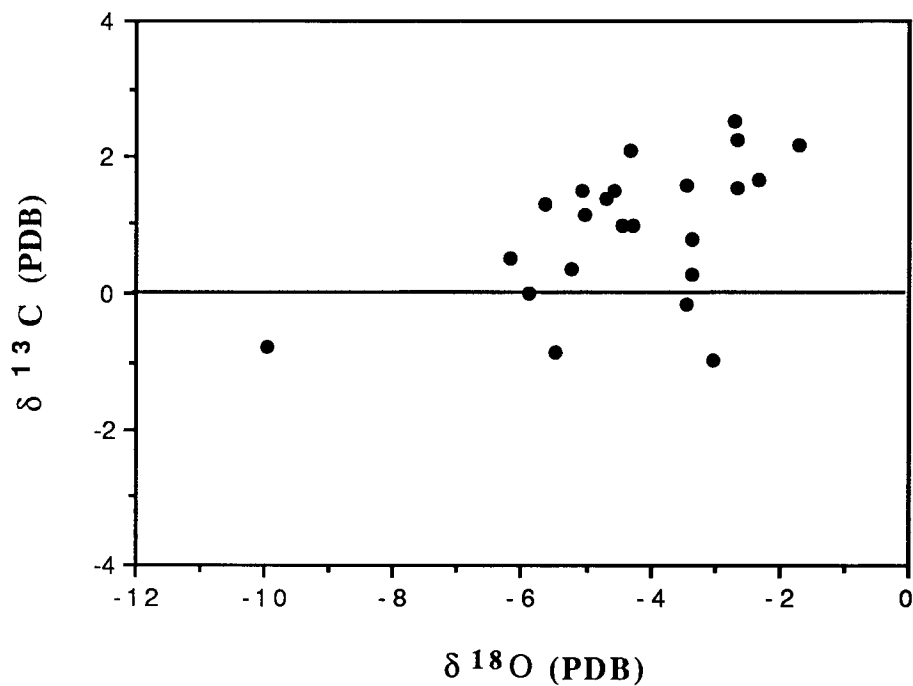


Fig. 4.12 Carbon versus oxygen isotope compositions of dolomites from the Anisian platform shallow water dolomites (Plattendolomite, Diplopora Dolomite and Middle Salvatore Dolomite).

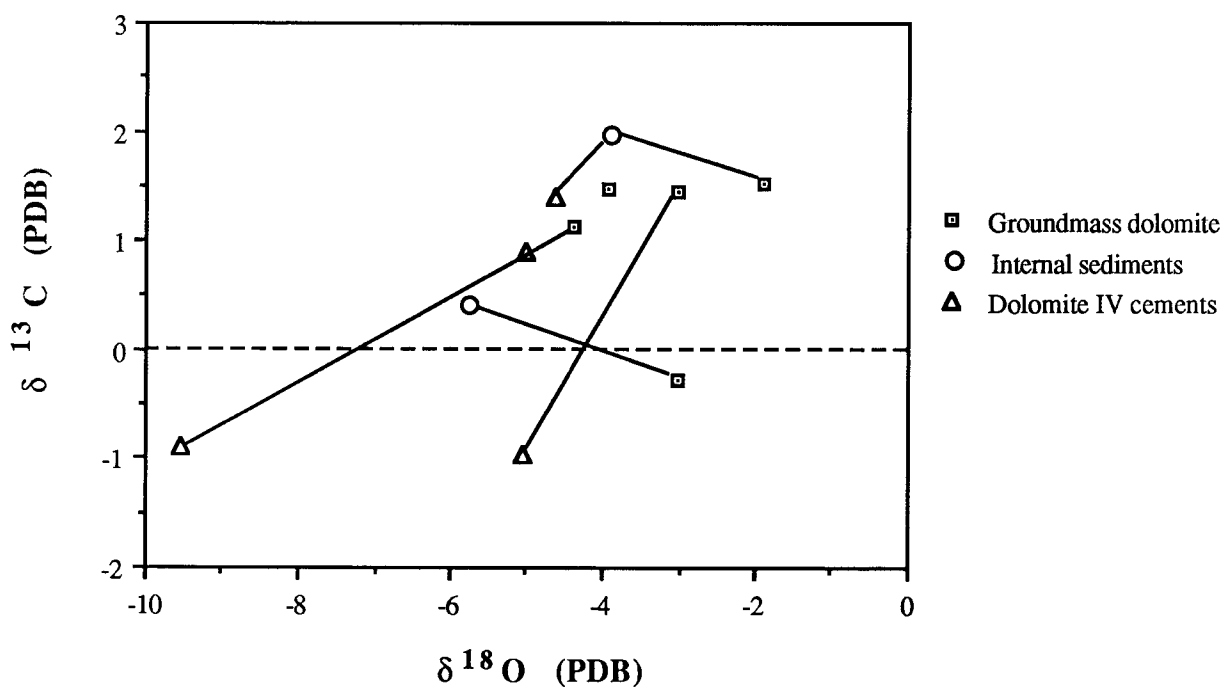


Fig. 4.13. Stable isotope trends in different generations of dolomites in the Anisian dolomites (samples from Rossaga).

from organic matter-rich lithologies. The oxygen isotopic compositions of the dolomites are more variable (-2.2 to -8.5‰) than the calcites and show a wider range than the GBZ and Salvatore dolomites. The most negative values are all idiomorphic cements or saddle dolomite crystals from late cross-cutting veins and represent the latest diagenetic event recorded in these rocks. All of the dolomite and calcites from partially dolomitized rocks have very similar oxygen and carbon isotope compositions. This is an indication that these two minerals are not in isotopic equilibrium because dolomite should be enriched in ^{18}O by approximately 3‰ with respect to coexisting calcite (Clayton et al. 1968, McKenzie, 1981).

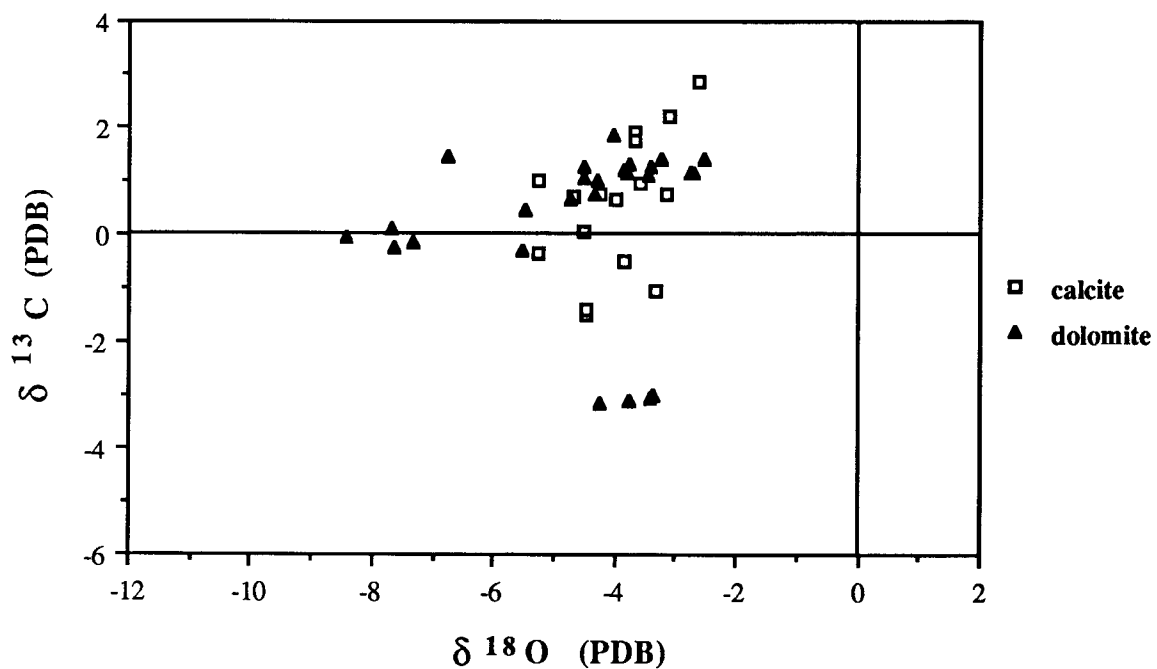


Fig. 4.14 Carbon versus oxygen isotope compositions of dolomites and calcites from the San Giorgio Dolomite and the Meride Limestone.

4.3.3 Discussion: Origin of GBZ dolomites

4.3.3.1 Controls on the carbon isotope composition.

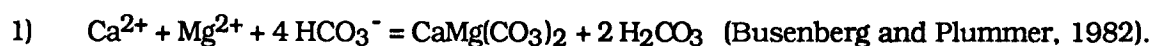
The oxygen content of the bottom waters in a basin is the result of a balance between advective and diffusive oxygen supply and consumption through organic matter oxidation. In organic carbon-rich settings with limited circulation, organic matter oxidation quickly removes oxygen from the pore-waters and/or the bottom waters, providing ideal conditions for anaerobic bacterial activity. The ecologic succession of bacteria found in marine anaerobic settings is controlled by the thermodynamic efficiency of the microorganisms to liberate energy from the same organic substrate and by the presence of electron acceptors (e.g. Claypool and Kaplan, 1974). The large variations in carbon isotopic composition of dissolved bicarbonate observe in organic

matter-rich sediments (Fig. 4.9) potentially make carbon isotopes a good tool to define the diagenetic zone in which carbonate precipitation occurred (e.g. Irwin, 1980; Kelts and McKenzie, 1984; Pisciotta and Mahoney, 1981). The carbon isotope composition of diagenetic carbonates, however, is not only dependent on the composition of the dissolved bicarbonate in the pore-waters but is also influenced by the carbon isotope composition and amount of precursor carbonate present in the sediment prior to lithification and cementation. The bulk isotopic composition of the final product is, therefore, the result of mixing of different pools of carbon with potentially extremely different isotopic compositions.

Three explanations for the small range (-1.4 to -5.6‰) in carbon isotope values of the GBZ dolomites can be considered. (1) The precursor sediment had a high carbonate content and the amount of precursor carbonate with a normal marine isotopic composition in the sediments was large relative to the amount of isotopically light bicarbonate derived from sulfate reduction, added during diagenesis. In this case the carbon pool would be dominated by the composition of the precursor carbonate and, therefore, the range of the end product would not be expected to vary greatly. Dolomite would principally have a replacement origin. (2) Alternatively, the dolomite could have formed predominantly as a primary precipitate at the boundary between the sulfate reduction and methanogenesis zones. In this case, the $\delta^{13}\text{C}$ -values of the diagenetic carbonate would be the result of mixing an isotopically light bicarbonate produced by sulfate reducing bacteria and an isotopically heavy bicarbonate produced by methanogenesis. (3) A third hypothesis is that the dolomite formed by direct precipitation close to the sediment-water interface where light carbonate derived from organic matter degradation is mixed with marine bicarbonate with a composition of approximately 0‰.

The first hypothesis is favoured because the petrographic evidence of depositional sedimentary structures, such as graded beddings and the presence of layers and laminae with high lateral continuity (Section 3.2), indicate the presence of high quantities of precursor carbonate. Moreover, the lack of indicators of methanogenesis, as concluded from sulfur isotope geochemistry (see Section 4.2) and organic geochemistry (see Chapter 5) indicate that the dolomite precipitated very early within the sulfate reduction zone. Moreover, if a methanogenesis contribution were present, one would expect to find at least some samples with positive $\delta^{13}\text{C}$ -values. Based on these considerations the stoichiometry of the dolomitization reaction is tentatively modelled. Chemical reactions commonly used to represent dolomitization are listed below.

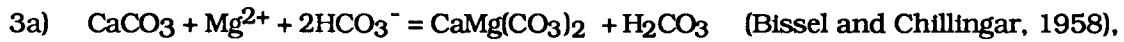
For direct precipitation without precursor carbonate:



For simple replacement dolomitization:



For combined precipitation-replacement dolomitization:



or



Because the studied dolomites primarily have a replacement origin, reaction 1 is not considered further here. Reaction 3b is considered the more appropriate because the carbon isotopes indicate that a contribution of externally derived bicarbonate is present. The stoichiometry of the dolomitization reaction (3b) can be established with a simple mass-balance calculation using carbon isotope values of the contributing carbon pools:

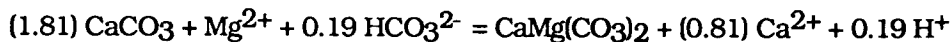
$$\delta^{13}\text{C}_{\text{Dolomite}} = x (\delta^{13}\text{C}_{\text{PC}}) + (1-x) \delta^{13}\text{C}_{\text{OM}},$$

where:

$$\delta^{13}\text{C}_{\text{PC}} = +2\text{‰} \quad (= \text{isotopic composition of the precursor carbonate}),$$

$$\delta^{13}\text{C}_{\text{OM}} = -27 \text{‰} \quad (= \text{isotopic composition of CO}_2 \text{ derived from organic matter degradation}).$$

The ranges of contributions of precursor carbonate calculated with the isotopically lightest and heaviest samples are 74 to 88 %. The stoichiometry of dolomitization using the average dolomite carbon isotopic composition of -3.4‰ would be:



This stoichiometry indicates that the production of 1 mole of dolomite (184 g) requires at least 0.22 moles (2.6 g) of organic carbon to be oxidized. On the other hand, the calculated stoichiometry indicates that dolomitization required a net Ca-removal.

4.3.3.2 Possible temperature and composition of dolomitizing fluids

The determination of temperature, timing and burial depth of dolomite formation and origin of dolomitizing fluids from oxygen isotope values is always a major problem in dolomite studies because the oxygen isotopic composition of the water from which dolomite precipitated is unknown. The slump structures and the petrographic features described in Chapter 3 clearly indicate a very early diagenetic dolomitization within the first centimeters to decimeters of uncompact sediment. Therefore, the oxygen isotopic compositions of the dolomites should reflect formation at temperatures near the sediment-water interface. As no evidence for anomalous salinities has been found in the GBZ, it is assumed that the water in the basin had the same composition as average Triassic seawater (-1.0 ‰ (SMOW)), the value for an ice-free earth (Shackleton and Kennett, 1977). Scherrer (1977) determined the oxygen isotopic composition of an Upper

Triassic aragonite shell to be -2.5‰ (PDB). Using these parameters, the ocean temperature calculated using the aragonite-water paleotemperature equation of Grossman and Ku (1981) is 24.7 °C . The data from the calcites from the Meride Limestone are consistent with this calculation if only the heaviest values, which are probably the least altered by late diagenesis, are considered. The least negative value determined is -2.64 ‰ and corresponds to a temperature of 24.1 °C . A $\delta^{18}\text{O}$ of -2.59 was also obtained for the carbonate in the apatite lattice of a phosphate nodule from the GBZ (Table 4.5). Assuming a water-carbonate fractionation factor similar to that of calcite (e.g. Shemesh et al., 1988) this corresponds to a temperature of 25 °C . All of these independent lines of evidence support the assumption that water in the GBZ basin had a normal marine oxygen isotopic composition of approximately -1‰ (SMOW) and that the temperature was around 25 °C . The oxygen isotopic composition of a dolomite in equilibrium with sea water with a $\delta^{18}\text{O} = -1\text{ ‰}$ (SMOW) and 25 °C temperature would be -0.62 ‰ (PDB) using the calibration curve of Matthews and Katz (1977).

The least negative oxygen isotopic composition found in the GBZ is -0.76 ‰ which corresponds to a temperature of approximately 25 °C and, therefore, supports the hypothesis of penecontemporaneous dolomitization for at least part of the samples. However, the range of oxygen isotope compositions of the GBZ dolomites is quite large and needs to be explained. Two possible scenarios are:

- 1) Because variations in oxygen isotopic composition in one bed are at the most 2‰ and generally smaller than 1‰ , the variations seen in the GBZ can be due to fluctuations in seawater composition through time. These variations could be a consequence of variations in input of freshwater, changes in the hydrological balance of the basin (evaporation vs. precipitation) or fluctuations in the water connection with the open ocean.
- 2) The variations in oxygen isotope composition are related to late diagenetic reequilibration with fluids at higher temperature and/or with mixed seawater-fresh water fluids whereby the extent of reequilibration was controlled by the porosity left after the formation of the early diagenetic dolomite II .

The most negative value of -6.5 ‰ , a dolomite cement (dolomite IV) partially filling an ammonite mold, gives a calculated temperature of 57 °C using a seawater oxygen isotopic composition of -1‰ (SMOW) and using the temperature equation of Matthews and Katz (1977). This temperature is in agreement with the fluid inclusion data of these cements, which indicate a precipitation below approximately $60\text{-}70\text{ °C}$ (see Chapter 3). Dolomite IV occurs only in large pores and represents the last phase of cement observed in the GBZ, therefore, its isotopic composition is probably representative of the highest temperature reached by the diagenetic fluids. Dolomite III unfortunately cannot be separated from dolomite II, therefore, its isotopic composition is unknown. However, the observation of varying proportions of dolomite III in different layers support the hypothesis that the bulk oxygen isotopic composition of the dolomite is controlled by

variations in proportions of these two dolomite types and selective recrystallization. This suggests that the preservation of the early diagenetic isotopic signals is controlled by the porosity of the individual layers after the formation of dolomite II. The circulation of late diagenetic fluids was controlled by primary porosity and probably also influenced by the presence of the rather impermeable black shale layers.

4.4 Carbonate fluorapatite isotope geochemistry

4.4.1 Results and Discussion

4.4.1.1 Carbon isotopes

All of the carbonate fluorapatite (CFA) samples analyzed are nodules from within dolomite beds, except for sample SB 31 which is from a black shale. Carbon isotopic compositions range from -4.99 to -9.0 ‰ (PDB), which is comparable or slightly lower than the values found for the associated dolomites. These values suggest a very early formation close to the sediment-water interface where light carbonate of biogenic origin is mixed with normal marine carbonate. This is in agreement with the petrographic observation of differential compaction around the nodule in the black shale and with the presence of hard phosphate nodules in soft sediment deformations. The nodular shape and the lack of evidence for precursor carbonate indicate that their carbon isotope composition is controlled solely by the pore-water carbonate composition and not by the presence of a precursor carbonate. These interpretations are based on the assumption that there is little or no carbon isotope fractionation between total dissolved carbonate and the carbonate ion in the apatite during its incorporation.

Pore water $\delta^{13}\text{C}$ -profiles in anoxic marine pore-waters show that dissolved carbonate $\delta^{13}\text{C}$ range from 0 to -10 ‰ at depths of less than one meter. Along the Peru Margin carbon isotope compositions of dissolved carbonate in anoxic sediments reach values of -10‰ at a depth less than 10 cm below the sediment water interface (Glenn et al. 1988). By analogy, a precipitation almost at the water-sediment interface can be envisioned for the GBZ samples.

4.4.1.2 Oxygen isotopes

All GBZ CFA samples range from -5.86 to -9.24 ‰ (PDB) with the exception of sample SB 131, which has an isotopic composition of -2.6 PDB (Tab. 4.5). Due to the lack of experimental data, the interpretation of oxygen isotope data of carbonate substitution in apatite is very difficult. Glenn et al. (1988) considered the oxygen isotope data unreliable for any interpretation, but, in an extensive study of isotopic composition of carbonate substitution in apatite, Shemesh et al. (1988) noted a good agreement between carbonate and phosphate oxygen isotope composition and suggested that these ratios can be used for a

paleotemperature calculation. The value of -2.6‰ in one sample, which is in agreement with the data from some of the calcites and dolomites, support their conclusion. However, the wide scatter in $\delta^{18}\text{O}$ -compositions in the other samples indicate that carbonate in apatite is sensitive to later reequilibration with either warmer waters during diagenesis or to weathering.

Sample	% CO ₂	$\delta^{13}\text{C}$ ‰ (PDB)	$\delta^{18}\text{O}$ ‰(PDB)
102P	4.5	-7.89	-8.42
88P	3.7	-6.38	-7.15
131	n.d.	-9.50	-2.59
SB 70	3.7	-5.02	-5.89
SB 70 P	4.2	-4.99	-5.81
102	n.d.	-6.75	-5.70
SB 31 p	n.d.	-6.95	-9.24

n.d.= not determinable because of poor peak definition

Table 4.5 Stable isotopic composition of the carbonate substitution in carbonate fluorapatite nodules.

4.4.1.3 Carbonate substitution in the apatite lattice

Carbonate has been shown to substitute for PO_4^- in the apatite lattice at concentrations of up to 6 % (Glenn et al. 1988, and references therein). The controls on the amount of CO_3^{2-} incorporated by the apatite lattice are still poorly understood. Variations in CO_3^{2-} -substitution have been attributed to temperature variations (Gulbrandsen, 1970) or to variable pH buffering of the pore-waters due to the presence or absence of carbonate (McArthur, 1989). On the other hand, Glenn et al. (1988) suggest that CO_3^{2-} -substitution in apatite is proportional to the in situ carbonate concentrations of the pore-waters at the time of precipitation and increases with depth of formation as a response to carbonate production through suboxic to anoxic organic matter decomposition. The homogeneous CO_3^- -concentration in the studied GBZ samples could, therefore, indicate a common depth of formation.

4.5 Oxygen isotope geochemistry of cherts

4.5.1 Introduction

The formation of a microcrystalline quartz chert from accumulations of siliceous biogenic opal-A is a diagenetic process involving multiple dissolution-reprecipitation steps which can take place over a range of depths and temperatures (Murata and Randall, 1975; Kastner et al., 1977; Murata et al., 1977). Oxygen isotope compositions of cherts, therefore, is determined by the isotopic composition and the temperature of the fluid in which they formed. Despite these limitations, it has been shown that oxygen isotope studies in cherts have some potential for the determination of environmental paleotemperatures (Kolodny and Epstein, 1976; Knauth and Epstein, 1976; Karhu and Epstein, 1986). The first aim of the measurements in the GBZ was to check if the isotopic composition of the cherts could give an indication of the water temperatures in the basin in order to confirm the temperatures inferred from the analyses of the carbonates. Moreover, the presence of idiomorphic quartz crystals in ammonite molds offers the possibility of an independent estimation of the temperatures and composition of the burial diagenetic fluids and to compare these with the temperatures determined from dolomite cements.

Petrographic observations in the San Giorgio dolomite indicate that chert lithification predated dolomitization (see Section 3.5.2.2). The oxygen isotope composition of the cherts should therefore constrain the minimal temperature of dolomitization and help interpret the diagenetic history of this formation.

4.5.2 Results and discussion

Oxygen isotopic compositions and a short description of each sample measured are compiled in Table 4.6. All samples are composed of microcrystalline quartz, with only minor chalcedony. The only exception is sample SB 72 which consists of idiomorphic quartz crystals of up to 1mm length grown by direct precipitation from a fluid in an ammonite mold. The fine-grained samples were chosen because microcrystallinity of chert is generally taken as an evidence for limited recrystallization and therefore it is considered likely that the primary oxygen isotopic composition is better preserved (Karhu and Epstein, 1986).

Temperatures of formation can be calculated with the formula of Karhu and Epstein (1986):

$$\delta^{18}\text{O}(\text{SiO}_2\text{-H}_2\text{O}) = 3.24 \times 10^6 / T^2 - 2.26.$$

Assuming a water composition of -1‰ (SMOW), a temperature range between 56 and 60°C is determined for the GBZ samples, whereas for the San Giorgio dolomites a temperature range of 46 to 54°C is found. The high calculated temperatures indicate that the isotopic

composition of the cherts do not reflect depositional temperatures but are purely diagenetic signals. The temperatures calculated for the GBZ samples are in agreement with the maximum temperatures determined on the dolomite IV cements if a water composition of -1‰ is assumed. This may indicate that the chert layers in the black shales were reequilibrated and possibly recrystallized at temperatures of around 60°C, approximately contemporaneous with the precipitation of the idiomorphic quartz crystals in the ammonite mold.

Tab. 4.6 Oxygen isotope composition of cherts from the GBZ and San Giorgio Dolomite.

Sample	$\delta^{18}\text{O}\text{‰}$ (SMOW)	Observations
SB94	26.4	Biogenic chert layer in black shale, layer 62, GBZ
SB 96	26.6	Biogenic chert layer in black shale, layer 56, GBZ
SB 72	25.9	Idiomorphic quartz in ammonite mold, layer 146, GBZ
SB 75	26.6	Chert layer in bed 200, San Giorgio Dolomite.
SB 4	27.1	Chert layer, brittily deformed, San Giorgio Dolomite.
SB 6	27.7	Chert layer, brittily deformed, San Giorgio Dolomite.
QN1	28.6	Quartz nodule, San Giorgio Dolomite.

The temperatures calculated for the cherts in the San Giorgio dolomite are also consistent with precipitation and/or reequilibration at relatively high temperatures and/or from a fluid with a meteoric component. Surprisingly, lower temperatures (36 to 40°C, calculated for samples SB4 and SB6) were determined from the oxygen isotopic composition of the dolomites coexisting with these cherts if the same fluid composition is assumed. This contradicts petrographic observations which indicate that chert induration predates dolomitization. A possible explanation for this inconsistency is that the cherts were transformed to opal-CT then slumped (opal-CT cherts are brittle) and later recrystallized to microcrystalline quartz in equilibrium with late diagenetic fluids. Alternatively, the difference in composition between the cherts and the dolomites may reflect equilibration with different diagenetic fluids.

4.6 Summary

Early diagenetic geochemical signals are well preserved in the GBZ. Stable isotope compositions of the dolomites in the GBZ confirm the petrographic observations indicating an early diagenetic dolomitization and lithification. The main amount of dolomite probably formed close to the sediment-water interface in the sulfate reduction

zone of organic matter diagenesis. Dolomite is mainly of replacement origin. The variations observed in oxygen isotope compositions of the dolomites are produced by burial diagenetic recrystallization and/or precipitation of minor quantities of cements from diagenetic fluids at approximately 60-70°C. The circulation of the burial fluids and the extent of reequilibration was controlled by the porosity left by the early diagenetic dolomite formation.

The presence of breccias with angular dolomite clasts together with other petrographic evidence discussed by Zorn (1971) indicate that dolomitization in the Salvatore Dolomite can be considered to be early diagenetic. The stable isotope composition of the dolomites confirm this hypothesis and indicate that the dolomites were produced by fluids of normal marine salinity or fluids with a small meteoric water component. The correlation of cement cathodoluminescence stratigraphy in the GBZ and Salvatore dolomite indicate that both these formations were partially reequilibrated at higher temperatures during late diagenesis by the same fluids.

CHAPTER 5

ORGANIC GEOCHEMISTRY

5.1 Introduction

With organic geochemical and petrological studies, the type and amount of organic matter, the petroleum potential and the maturity level of a source rock can be characterized. In addition, with help of molecular markers, information pertaining to depositional environment, early diagenetic conditions and organic matter input can be evaluated. Several recent studies involving petroleum source rocks have shown that variations in both bulk and molecular parameters are very sensitive to changes in depositional environment (e.g. Eh, pH conditions) and/or organic matter input (Curiale and Odermatt, 1989; Moldowan et al., 1986). The integration of organic geochemical tracers with inorganic geochemical parameters (Chapter 4) can, therefore, improve our understanding of the depositional conditions and diagenetic evolution of a source rock.

Although the GBZ has interested organic geochemists for over 40 years, no systematic organic geochemical study has previously been carried out. Most of the work has concentrated on the isolation and characterization of the porphyrins (Blumer, 1950; Thomas and Blumer, 1964; Blumer and Omenn, 1961; Blumer and Snyder, 1966; Chicarelli and Maxwell, 1984; Chicarelli et al., 1984, 1990; Wolff et al., 1983, 1984). These studies show that bitumens of the black shales contain between 0.15 and 0.58% VO-porphyrin complexes (Blumer 1950), mostly as VO^{2+} -DPEP (=deoxophylloerythroetioporphyrin), with a ratio DPEP/ETIO-porphyrins of 4.9. (Thomas and Blumer, 1964). Most of the porphyrins were derived from chlorophyll a, with a 3 to 5% contribution of derivatives from chlorophyll b, but porphyrins with no known biologic precursor have also been recognized. Chlorophyll, the main precursor of porphyrins in sedimentary organic matter, is readily decomposed in oxygenated waters (Baker and Louda, 1986). The presence of high concentrations of porphyrins in the GBZ is, therefore, indicative of a short residence time of the dead plant material in oxygenated waters. The distribution of hopanoids in one GBZ sample was studied by McEvoy and Giger (1986). They observed that the organic matter in the GBZ contains extremely high concentrations of hopanes and methylhopanes and concluded that the organic matter of the GBZ contains a high bacterial contribution, specifically, from cyanobacteria and/or methylotrophs.

The first objective of this organic geochemical study is to characterize the source of the organic matter, the petroleum potential of the GBZ and, with the analysis of maturity-sensitive biomarkers, to constrain the maximum burial temperature reached by the GBZ. By using samples from different lithologies and TOC-content from a closely spaced profile, we exclude maturation as a cause for the variations observed. This gives us the possibility to evaluate the changes in biomarker parameters in terms of primary

input or environmental variations. This, moreover, allows the reliability of different molecular maturity parameters to be assessed. Furthermore, to determine lateral variations in the organic facies, samples from Monte S. Giorgio (Miriglioli; samples MI of the standard profile, Fig. 3.1) and Besano (sample BE) were studied.

5.2 Organic Petrology

5.2.1 Results

The composition and distribution of organic matter in the GBZ sediments was studied using smear slides prepared from kerogen isolated from the rock with the standard HCl-HF dissolution technique (Durand, 1980). Using transmitted light the optical determination of the kerogen in smear slides is difficult because the presence of organic matter as thick opaque aggregates often hinders the recognition of organic structures. The kerogen is dominated by amorphous organic matter (AOM) and herbaceous fragments with subordinate pollen and spores (CHF) (Fig. 5.1, Tab. 5.1). Woody fragments (CWF) are minor. Tasmanites and other undetermined algae are relatively common. No significant variations in the palynofacies among samples from different lithologies and outcrops within the basin exist.

Vitrinite reflectance is in the range $R_0 = 0.23 - 0.35\%$ (Tab. 5.1) and liptinitic organic matter has a yellow fluorescence color (Fig. 5.1), which indicate a low degree of thermal maturation. The organic matter is often non-fluorescent or becomes fluorescent only after prolonged exposure (20-30 minutes) to UV-light. The only notable difference in organic matter character among the different lithologies is a stronger fluorescence seen in the carbonate-rich lithologies. The black shales are mostly non-fluorescent except for sporadic algal remains. The upper part of the section shows a decrease in woody material input and the amorphous organic matter shows a better fluorescence than in the lower part.

5.2.2 Discussion

The vitrinite reflectance values are probably underestimated because they are too low compared to the other maturity parameters (See below). Moreover, vitrinite-reflectance measurements in these ranges of maturity are considered unreliable (Kalkreuth, pers. comm. 1989). The causes for the non-fluorescence of the amorphous organic matter in the lower part of the section (samples 48 to 115) remain puzzling. The fact that fluorescence is generally better developed in the organic carbon-poor dolomitic lithologies than in the black shales, which were deposited much slower than the dolomites, could suggest that the non-fluorescence may have been caused by extensive syndepositional alteration due to bacterial activity. Based on the organic geochemical data, e.g. high hydrogen index, low oxygen index and n-alkane distribution, this amor-

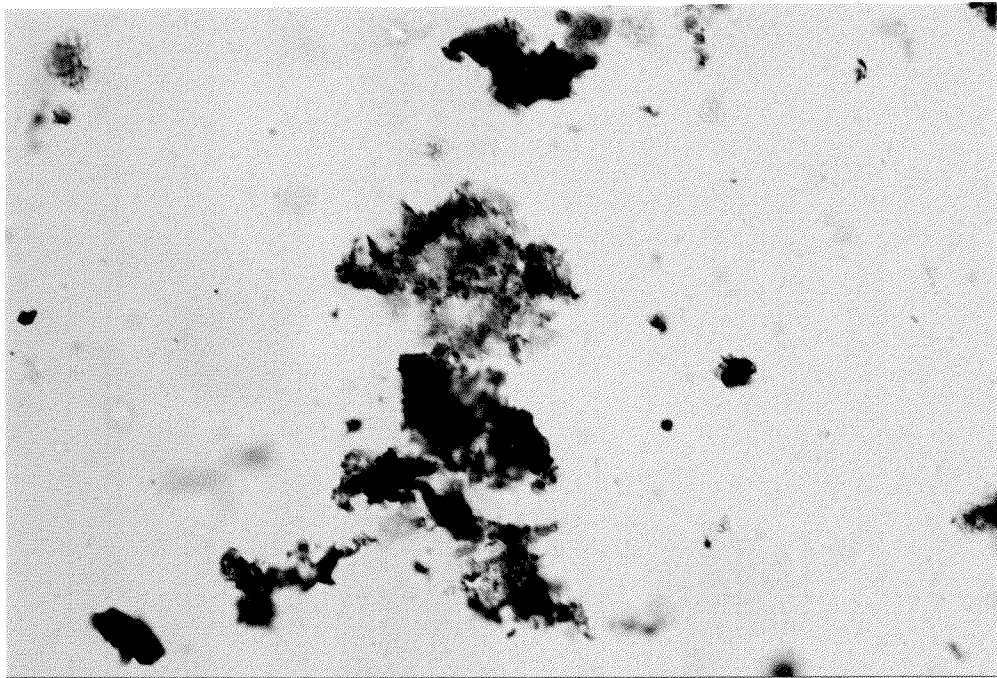
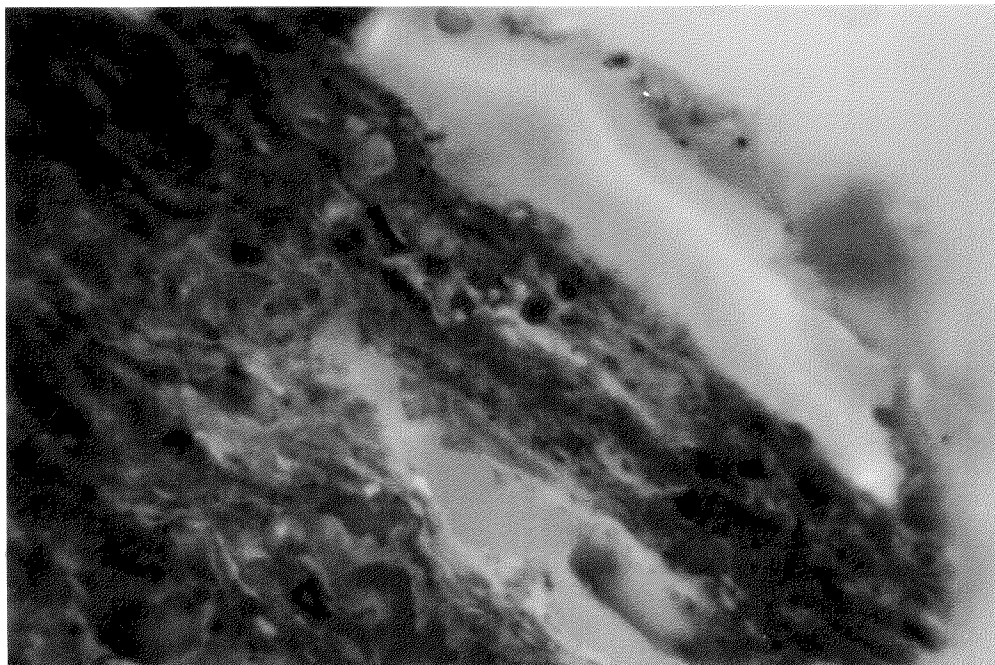
a**b**

Fig 5.1 Photomicrographs of the organic matter in the GBZ. (a) Amorphous organic matter in transmitted light. Layer 132, c.a. 250 x. (b) Fluorescent tasmanite in UV-light. Layer 132, c.a. 410 x

Table 5.1 Kerogen composition and maturity

Layer No.	AOM	CHF	CWF	R _o %	n
48	40	40	20	0.331	9
56	55	30	15	--	--
80	60	20	20	0.270	20
84	50	30	20	--	--
95	45	30	25	0.237	13
97	50	25	25	0.341	22
101	50	30	20	0.305	22
110	55	30	15	0.292	18
113	50	30	20	0.323	20
115	55	30	15	0.325	18
122	55	35	10	--	--
132	60	30	10	0.333	20
135	60	30	10	0.350	10

AOM = amorphous organic matter

CHF = continental herbaceous fragments

CWF = continental woody fragments

R_o % = vitrinite reflectance in oil

n = number of reflectance measurements

phous organic matter cannot be derived from either sapropelized higher plant debris or extensive oxidation of marine organic matter unless bacterial activity has completely destroyed the biomarkers indicative of higher plant input.

The fluorescence of organic materials is controlled by the presence of double bonds C=C (Stach, 1969). Bertrand et al. (1986) attribute the phenomenon of fluorescence to aromatic molecules of unknown structure which they called chromophores. In an experimental study, they demonstrated that fluorescence is controlled not only by the presence of chromophores but also by their concentration. If their concentration is too high a quenching effect can occur. Fluorescence normally disappears only at coalification ranks corresponding to a vitrinite reflectance of 1.3 to 1.5% (Stach, 1969). Therefore, the absence of fluorescence in these samples is not due to a high degree of maturity, but may be caused by the lack of chromophores, as suggested by the predominantly aliphatic character of the bonds in the kerogen seen in infrared spectra (Premovic et al., 1986), or by a quenching effect due to some unknown factor.

5.3 Rock-Eval Pyrolysis

5.3.1 Definition of parameters

Before discussing the results of the Rock-Eval pyrolysis studies, compiled in Table 5.2, a short definition of each parameter are briefly summarized here:

S1: The amount of free hydrocarbons volatilized during 3.5 minutes at 300°C, expressed in mg HC/g of rock.

S2: The amount of hydrocarbons released by cracking of the kerogen between 300° and 550°C, expressed in mg HC/g of rock.

S3: amount of CO₂ released by the cracking of kerogen at temperatures between 300 and 390°C, expressed in mg CO₂/g of rock.

T_{max}: Pyrolysis temperature where maximum hydrocarbon production takes place. This temperature is dependent on the maturation level of the kerogen.

Hydrogen index (HI): An approximation of the hydrogen content of the kerogen (Espitalié, 1977), defined as the value of S2 normalized to TOC content and expressed in mg HC/g of TOC.

Oxygen index (OI): An approximation of the oxygen content of the kerogen (Espitalié, 1977), defined as the value of S3 normalized to TOC content and expressed in mg CO₂/g of TOC.

Production index (PI): The ratio S1/S1+S2 and represents the proportion of free hydrocarbons in relation to the total amount of hydrocarbons produced. It is dependent on the maturation and can be used as an indication of migration (Espitalié, 1977).

5.3.2 Results

The GBZ samples can be divided into two groups (Fig. 5.2, Tab. 5.2). One group is characterized by TOC < 1% with hydrogen indices (HI) which vary between 36 and 400 and oxygen indices (OI) scattering between 20 and 250. The second group is characterized by TOC > 1% with HI varying between 400 and 600, and in a few cases higher than 700, and a small range of OI between 7 and 50. Samples with low TOC contents always correspond to dolomite beds.

All samples are immature as indicated by a T_{max} < 430°C. In a T_{max}/HI diagram (Fig. 5.3) the samples plot below the empirically determined R₀ = 0.5, which is generally considered to represent the beginning of the oil window (Tissot and Welte, 1984). The low production index (range 0.02-0.1) confirm the low maturation and indicate that the hydrocarbons present in the rocks are indigenous. Comparison of samples from the different locations in the basin (P.902, Cave di Besano, Val Nembra) show that preservation of the organic matter was excellent, even at the margins of the basin, and that there are no significant lateral variations in organic matter type or quality across the basin.

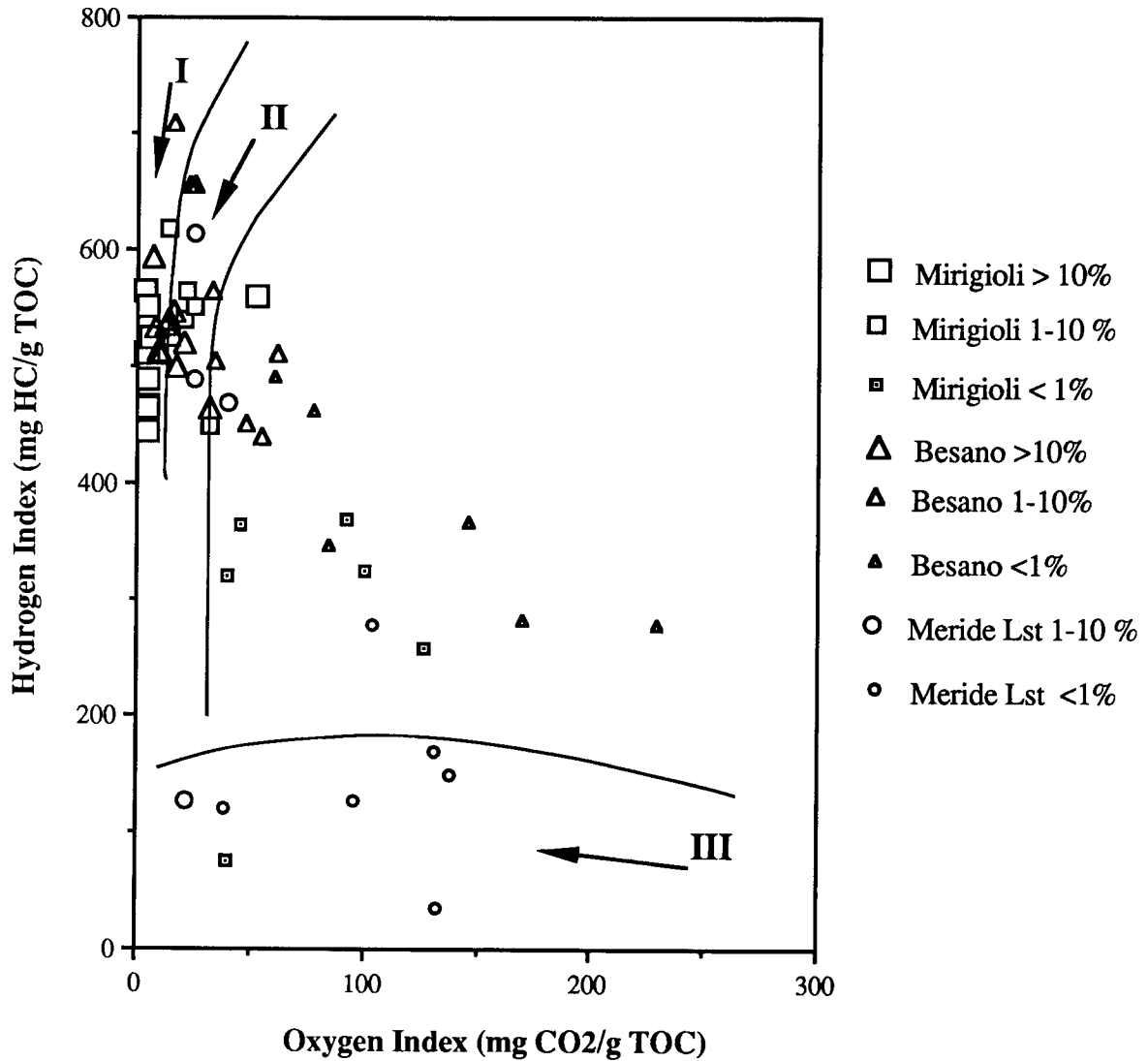


Fig. 5.2 Modified Van Krevelen-diagram from whole rocks of the Grenzbitumenzone and Meride Limestones from different outcrops. The samples from each locality are divided into three groups according to TOC-contents: TOC > 10%, TOC = 1-10% and TOC < 1%. The lines indicate the maturation paths for organic matter of type I, II, and III respectively.

Table 5.2 Rock-Eval pyrolysis results. For an exact definition and units of each parameter see Section 5.3 Samples MI: Grenzbitumenzone from outcrop Mirgioli (P.902). Samples BE: Grenzbitumenzone from Besano. Samples ME: Meride limestone.

SAMPLE	T max	SI	S2	S3	TOC	HI	OI	PI	S2/S3
MI 32	427	0.09	3.09	0.39	0.97	319	40	0.03	7.9
MI 52	418	1.29	27.91	1.07	4.95	564	22	0.04	26.1
MI 56M	422	3.06	43.31	1.22	8.25	525	15	0.07	35.5
MI 75	418	6.13	118.66	0.98	26.70	444	4	0.05	111.0
MI 82	420	3.15	82.12	0.91	17.70	464	5	0.04	90.0
MI 84	401	0.01	0.19	0.10	0.25	76	40	0.05	1.9
MI 86	423	0.14	5.31	0.38	1.10	450	32	0.03	14.0
MI 97	418	5.90	145.17	1.27	28.40	511	4	0.04	127.7
MI 108	419	3.50	68.16	0.80	13.00	524	6	0.05	85.2
MI 110	420	6.71	162.82	1.55	34.90	467	4	0.04	116.7
MI 115	417	6.63	122.10	1.10	24.90	490	4	0.05	122.5
MI 120	421	0.27	6.41	0.24	1.19	539	20	0.04	26.7
MI 125	413	1.34	34.99	1.61	6.36	550	25	0.04	21.7
MI 130	414	6.00	149.13	1.00	29.20	511	3	0.04	170.3
MI 132	424	4.94	157.37	1.15	28.50	552	4	0.03	138.0
MI 132	422	5.76	162.59	0.76	28.80	565	3	0.03	188.3
MI 136	418	1.04	20.08	0.44	3.25	618	14	0.05	45.6
MI 138	424	0.05	2.17	0.54	0.59	368	92	0.02	4.0

Table 5.2 Rock-Eval pyrolysis results (continued)

SAMPLE	T max	S1	S2	S3	TOC	HI	OI	PI	S2/S3
MI142U	414	0.12	3.07	0.39	0.84	365	46	0.04	7.9
MI153B	430	7.48	68.34	6.52	12.20	560	53	0.10	10.5
MI 155	428	0.48	16.73	0.94	2.22	754	42	0.03	17.8
MI 162	427	0.07	1.69	0.52	0.52	325	100	0.04	3.3
MI 226	420	0.42	19.28	1.13	3.65	527	31	0.02	17.1
MI 230	427	0.06	1.44	0.71	0.56	257	127	0.04	2.0
BE 89/0	421	2.41	87.66	3.30	16.90	519	20	0.03	26.6
BE89/1A	421	0.10	5.69	0.71	1.29	441	55	0.02	8.0
BE 89/1B	424	0.13	7.53	0.80	1.67	451	48	0.02	9.4
BE 89/2	420	5.49	157.74	5.49	31.60	499	17	0.03	28.7
BE 89/3	416	2.74	116.61	7.95	25.10	465	32	0.02	14.7
BE 89/4	420	4.32	129.37	3.23	23.90	541	14	0.03	40.1
BE 89/5	419	0.30	10.58	0.71	2.10	504	34	0.03	14.9
BE 89/6	421	3.72	116.46	3.31	21.30	547	16	0.03	35.2
BE 89/7	425	0.03	1.91	0.76	0.52	367	146	0.02	2.5
BE 89/8	422	5.83	162.82	2.98	31.70	514	9	0.03	54.6
BE 89/9	420	2.98	83.42	1.80	15.60	535	12	0.03	46.3
BE 89/10	421	5.73	142.42	2.78	27.90	510	10	0.04	51.2
BE 89/11	418	0.08	4.17	0.69	0.90	463	77	0.02	6.0
BE 89/12	421	8.11	214.17	3.21	40.10	534	8	0.04	66.7
BE 89/13	417	0.05	4.52	0.56	0.92	491	61	0.01	8.1

Table 5.2 Rock-Eval pyrolysis results (continued)

SAMPLE	T max	S1	S2	S3	TOC	HI	OI	PI	S2/S3
BE 89/14	424	4.54	167.18	1.96	28.20	593	7	0.03	85.3
BE 89/15	430	0.01	0.86	0.71	0.31	277	229	0.01	1.2
BE 89/16	423	0.05	3.37	0.81	0.97	347	84	0.01	4.2
BE 89/17	422	0.10	8.86	1.07	1.73	512	62	0.01	8.3
BE 89/18	426	0.48	30.64	1.17	4.67	656	25	0.02	26.2
BE 89/20	429	0.56	37.31	1.31	5.69	656	23	0.01	28.5
BE 89/21	421	0.38	12.29	0.72	2.18	564	33	0.03	17.1
BE 89/22	428	1.06	47.64	1.06	6.72	709	16	0.02	44.9
BE 89/23					0.09				
BE 89/24	421	0.01	0.85	0.51	0.30	283	170	0.01	1.7
ME 89/1	412	0.02	0.54	0.42	0.32	169	131	0.04	1.3
ME 89/2	413	1.62	26.07	1.06	4.25	613	25	0.06	24.6
ME 89/3A	419	0.05	1.18	0.38	0.98	120	39	0.04	3.1
ME 89/3B	403	0.01	0.08	0.29	0.22	36	132	0.11	0.3
ME 89/4	423	0.01	0.31	0.29	0.21	148	138	0.03	1.1
ME 89/4C	431	0.01	0.29	0.22	0.23	126	96	0.03	1.3
ME 89/5	420	0.04	1.31	0.23	1.03	127	22	0.03	5.7
ME 89/6	405	0.45	8.16	0.69	1.74	469	40	0.05	11.8
ME 89/7	404	0.08	1.30	0.49	0.47	277	104	0.06	2.7
ME 89/8	416	1.32	38.70	2.00	7.89	490	25	0.03	19.3

Two alternative explanations for the variation in HI can be considered. The generally lower HI of the TOC-poor samples, together with the higher oxygen indices, could indicate that the depositional or early diagenetic conditions were less reducing during the deposition of the dolomite-rich layers, leading to a relatively greater degree of oxidation of the deposited organic matter and thus to higher OM consumption and degradation in the oxic zone. As a result, the variations observed could represent variations in oxygen content of the bottom waters or shifts in the location of the oxic-anoxic interface in the water column and/or in the sediments.

On the other hand, the mineral matrix, especially in organic matter-poor rocks, can have an important effect on the parameters measured during pyrolysis (e.g. Espitalié et al., 1985). Particularly clays, due to their highly reactive surface, can retain the hydrocarbons produced from the cracking of the kerogen through absorption depressing the S₂-value. This leads to the determination of anomalously low hydrogen indices. This is especially the case for sample MI 84 which is a volcanic ash composed principally of clay minerals. Other matrix effects, such as thermal decomposition of carbonates which produces CO₂, can result in anomalously high oxygen indices (Espitalié et al., 1985) and could account for the high OI in the carbonate-rich, organic carbon-poor samples. The effect of the mineral matrix as a cause for the variations in HI and OI is also supported by the higher y-intercept of the regression curve on a S₂ vs TOC diagram for samples with TOC < 2% (Fig. 5.5), compared with samples with higher TOC contents (Fig. 5.4) (see discussion below).

5.3.3 Discussion kerogen type and organic matter preservation

Van Krevelen-type HI vs. OI diagrams, such as Fig. 5.2, are commonly used to determine organic matter type and to draw conclusions about variations in preservation of organic matter, but often the possible influence of the mineral matrix on HI- and OI-determination are ignored. As indicated above, problems with the measurement of Rock Eval parameters can produce an artificial scatter in HI vs. OI diagrams. Moreover, at maturity levels above about $R_0 = 0.5$, the evolution paths for organic matter of type I and II converge, making their distinction on such diagrams impossible. The classification of organic matter based on a S₂ vs. TOC diagrams recently introduced by Langford and Blanc-Valleron (1990) helps to eliminate these problems and is applied in this study (Figs. 5.4 and 5.5).

In the HI vs. OI diagram (Fig.5.2), the samples show considerable scatter, whereas in the S₂ vs. TOC diagram (Figs. 5.4 and 5.5) a linear regression line with a high degree of correlation is seen. This indicates a very coherent, similar organic matter source for all samples, which is independent of the location in the basin or organic matter content. The regression line has a slope close to that of the boundary between type I and type II

organic matter, indicating either a mixing of kerogen type I and II or a hydrocarbon-rich variety of kerogen type II. The slope of the regression line gives a mean HI of 536 mg HC/g of rock, which is defined as ten times the slope of the regression line (Langford and Blanc-Valleron, 1990), and shows that about 54% of the organic matter is formed by pyrolyzable hydrocarbons.

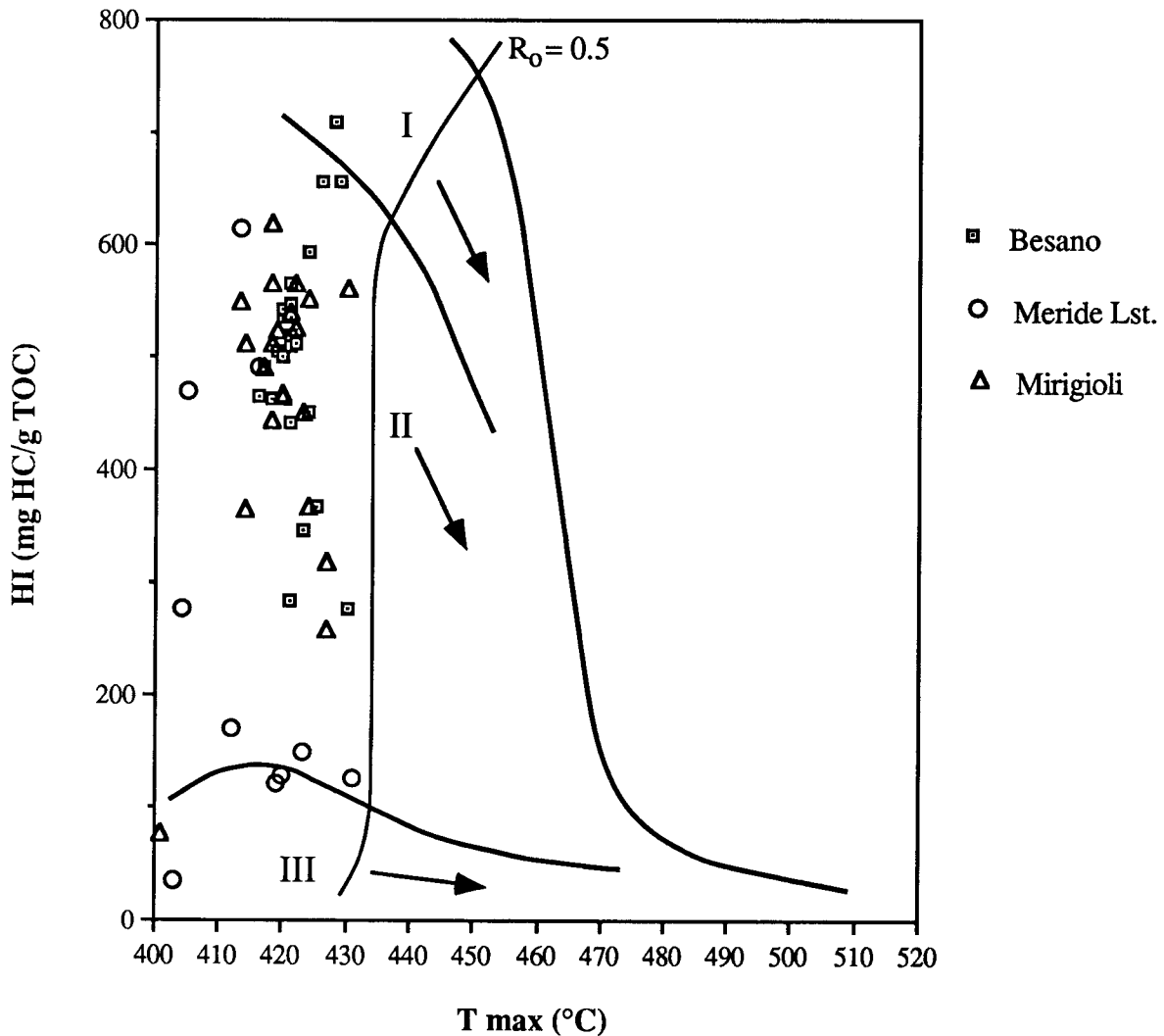


Fig. 5.3 T_{max}/HI diagram. Lines delimit the fields of organic matter of type I, II, and III respectively, arrows indicate maturation paths. The line marked $R_o = 0.5$ is the vitrinite iso-reflectance of 0.5 and marks the onset of the oil window.

The y-intercept of the regression line on a TOC vs. S₂ diagram is a measure of the adsorption potential of the rock matrix. Theoretically, the intercept should be zero because even the smallest amount of kerogen should produce some hydrocarbons. The organic carbon poor rocks have a y-intercept of -1.23 (Fig. 5.5) in contrast to -0.2 (which considering the experimental error can be considered equal to 0) in organic carbon rich

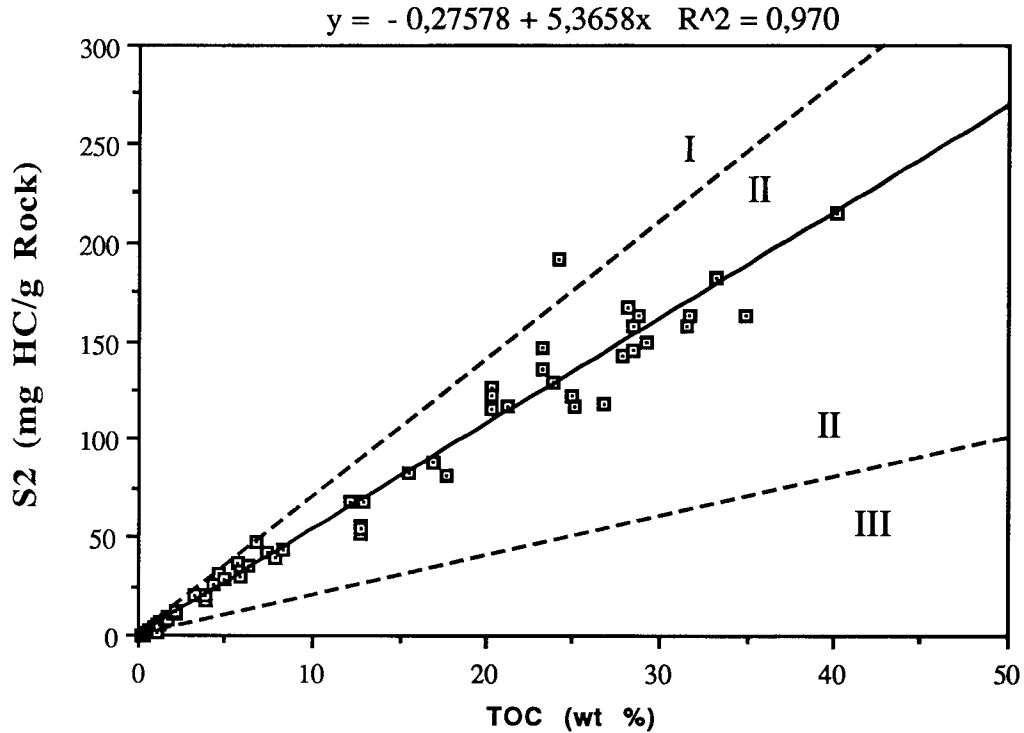


Fig. 5.4 TOC vs S2 scatter diagram of all the samples from the Grenzbitumenzone. Dashed lines indicate the boundaries for type I/II and type II/III kerogen. They correspond to an HI of 700 and 200, respectively. The average HI given by the slope of the regression line, is 536 mgHC/g TOC. The y-intercept at -0.27 indicates a very limited matrix effect on the hydrogen index of the organic-rich samples.

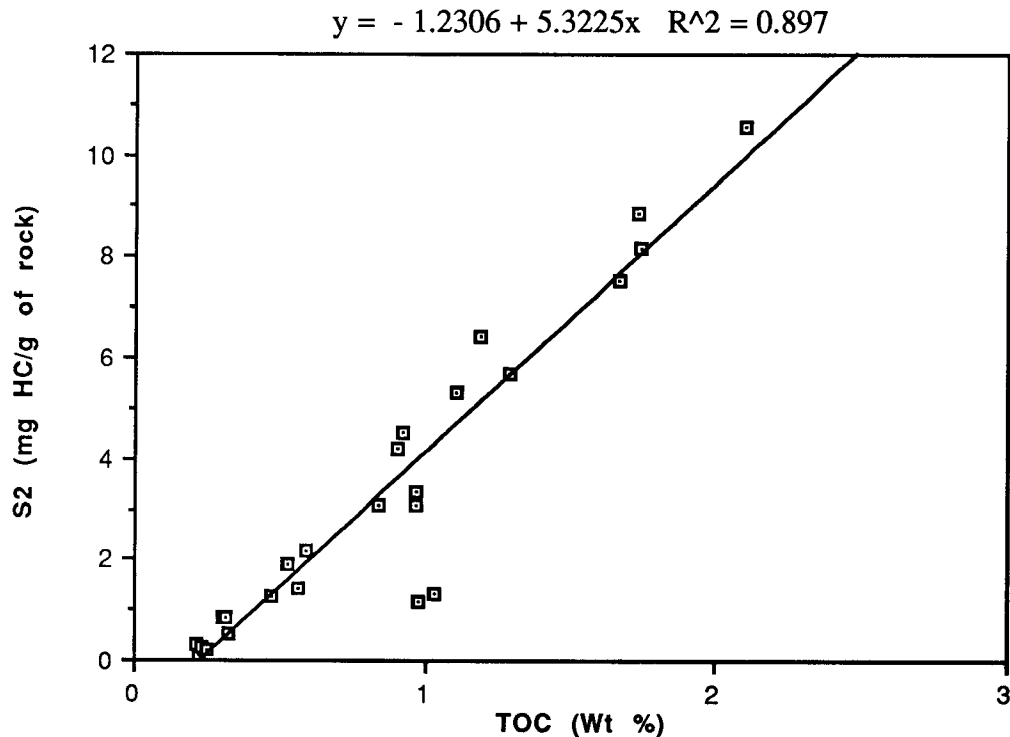


Fig. 5.5 TOC vs S2 plot for samples with less than 2% TOC. The lower y-intercept of the regression line compared to Figure 5.4 indicates that the organic-poor rocks have a higher hydrocarbon retention potential than the organic-rich samples. This produces an artificial lowering of the HI if this matrix effect is not taken into account.

samples (Fig. 5.4), corresponding to adsorption potentials of 1.23 and 0.2 mg HC/ g of rock, respectively. This indicates that the lower hydrogen index measured in the organic carbon poor samples is mainly due to a matrix effect and not to the poorer quality of the organic matter. If a correction for the matrix absorption effect is applied, an average HI of 536 is found for all the samples. The corrected hydrogen indexes are thus constant for all of the samples and indicate that the concentration of organic matter does not reflect variations in degree of preservation, but rather is controlled by differing amounts of carbonate which diluted a constant organic matter input.

5.3.4 Petroleum potential

Petroleum potential, defined as the sum of free plus pyrolyzable hydrocarbons, ranges between 2 kg HC/ton of rock for dolomites with TOC of 0.5% to 220 kg HC/ton of rock for some of the black shales (Tab. 5.2). Espitalié et al. (1985) recommend that rocks having more than 5 to 10 mg HC/g of rock be considered as good to very good source rocks, respectively. Most of the GBZ samples can thus be considered very good source rocks.

The total source potential of the GBZ can be estimated assuming that it contains 2.3 m of black shales, with an average hydrocarbon potential of 130 kg HC/ton of rock and a mean specific weight of 1.7 tons/m³ (Rickenbach, 1947), and 10 m of dolomites with an average potential of 13 kg HC/ton rock and a mean specific weight of 2.5 tons/m³. The calculated total potential of 330 000 tons HC km⁻² which is equivalent to about 2.4x10⁶ barrels of oil /km² is good. If the extension of the GBZ towards the south were comparable with that inferred for the Meride Limestones (Pieri and Mattavelli, 1984), the GBZ may have been the source rock or a least a co-source for the Gaggiano oil in the northern Po Plain. This possibility is also supported by the geochemical characteristics of the Gaggiano oils (Riva et al, 1986) which are very similar to those of the rock extracts of the GBZ.

5.4 Gas Chromatography - Mass Spectrometry Studies

5.4.1 Introduction

In the previous sections bulk parameters of the total organic matter were discussed. In this section only the composition of the rock extracts, which represent only a small fraction of the total organic matter, is considered. The discussion will first concentrate on the significance of the distribution of the different extractable hydrocarbon families (saturated and aromatic hydrocarbons and polar NSO compounds). The following section then presents and discusses a set of biomarker-parameter ratios which are used to characterize the source and the maturity level of the organic matter. These ratios were chosen because they are widely used in organic geochemistry and allow a comparison with literature data to be made. Biomarkers are geopolymers which are formed during

diagenesis of organic matter from biological compounds. For many biomarkers the precursor molecules and the diagenetic pathways of formation are fairly well known, however, because the precursor molecules for each biomarker are often found in many different organisms, the significance of each individual parameter is often ambiguous. Only the study of multiple parameters enables a correct interpretation. Because of this, each biomarker ratio will first be discussed individually and then the possible interpretations are considered in detail. Because many of these ratios are seen to correlate with stable isotopic composition of organic carbon a comprehensive interpretation will be given after the isotope geochemistry of the organic matter is discussed.

The distribution of the different hydrocarbon families together with some molecular parameters of the n-alkanes and the isoprenoid hydrocarbons are summarized in Table 5.3. Total ion current chromatograms and chromatograms for hopanes (m/z 191.2) and steranes (m/z 217.2 and 218.2) of two representative samples are presented in Fig. 5.6. The chromatograms of the entire sample set can be found in Appendix D. Biomarker parameter ratios are tabulated in Tab. 5.4. Samples labeled MI are from the outcrop Mirigioli. Unpublished data on samples from the Besano Mine (samples RC) were kindly provided by AGIP, Milano and are included for comparison.

5.4.2 Composition of the extracts

The extract/TOC ratio distinguishes samples MI153, RC 2057 and RC 2062 from all other samples because the former samples have a very low percent of extractables. The relatively low EXT/TOC ratio suggests an indigenous origin for the hydrocarbons, although a minor migration from nearby layers is suggested by the sporadic presence of bitumen staining in some layers with high porosity. The distribution of the fractions extracted is dominated by polar NSO compounds (resins and asphaltenes), which is typical for low maturity carbonate source rocks. The samples from the upper part of the profile (MI 155, 162, 226) have a lower percentage of NSO compounds. This may be the result of a lower bacterial contribution (Williams, 1984).

5.4.3 Saturated Hydrocarbons

Saturated hydrocarbons represent between 2.3 and 36 % of the extractables. The analyzed samples can be divided into two groups. The first group, comprising layers 52 to 136, is characterized by a low proportion of saturate hydrocarbons relative to the total extracts (Tab. 5.3) and by a high abundance of sterane and terpane biomarkers (Fig. 5.6 b & App. D). The second group (layers 153 to 226) in the higher part of the section is characterized by a high proportion of saturated hydrocarbons relative to the the total extracts and by a lower relative concentration of steranes and hopanes. All samples from the lower part of the section, independent of lithology or TOC content, show a

Table 5.3 Results of chloroform extraction of bitumen from bulk rocks and isoprenoids and n-alkane distributions.

SAMPLE	TOC (Wt%)	EXT/TOC	% SAT	% ARO	% NSO	n-alkane maximum	Pr/Ph	pr/n-C17	Ph/n-C18	R 22
KK52	4.95	10.92	4.6	8.70	86.7	20	0.76	1.93	2.24	1.10
MI 82	17.70	12.64	3.6	7.60	88.8	20	0.91	1.83	1.94	1.10
MI 110	34.90	7.36	5.8	9.80	84.4	16-20	1.09	1.18	1.39	1.05
MI 132	28.50	9.02	4.1	10.40	85.5	16	1.08	1.97	2.30	1.10
136-137	3.25	10.26	8.7	12.30	79.0	17	1.00	0.96	0.96	1.10
MU 153	12.20	0.08	2.3	0.80	96.9	20-21	1.25	0.63	0.49	0.94
MU 155	2.22	5.55	13.5	11.20	75.3	20-21	0.94	0.76	0.72	1.01
MU 162	0.52	5.96	36.0	14.00	50.0	21-22	0.87	1.07	1.01	1.04
SB57(226)	3.66	3.27	18.9	25.20	55.9	16-20	0.79	0.88	1.30	1.32
RC 2062	32.70	0.07	6.9	12.40	80.6	16-18	1.26	1.83	1.60	1.10
RC 2057	41.40	0.09	5.9	16.30	77.9	16-18	1.17	1.68	1.73	1.10

TOC = total organic carbon (wt %)

EXT/TOC = extractable organic matter normalized to total organic carbon

Pr/n-C17 = abundance of pristane relative to the C17 normal alkane

Ph/n-C18 = abundance of phytane relative to the C18 normal alkane

R22 = abundance of the C22 normal alkane relative to the abundance of the C23 and C 21 normal alkanes. See text for explanation.

SAT = Saturated hydrocarbons

ARO = aromatic hydrocarbons

NSO = nitrogen, sulfur and oxygen polar compounds

Pr/Ph = pristane/phytane ratio

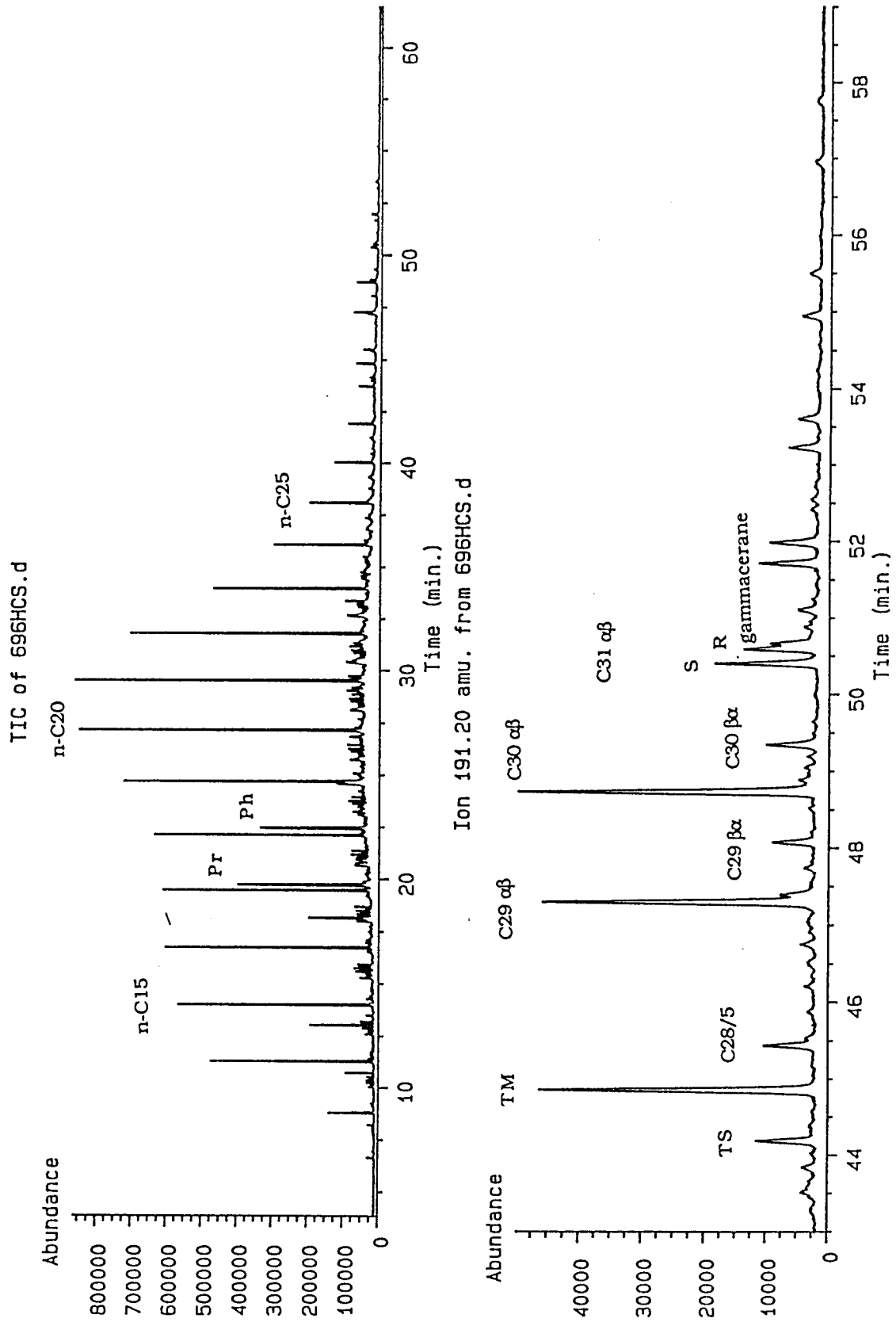


Fig. 5.6 a. Total ion current (TIC) chromatogram of the saturated hydrocarbon fraction and mass fragmentogram of hopanes (m/z 191) . Layer 153.

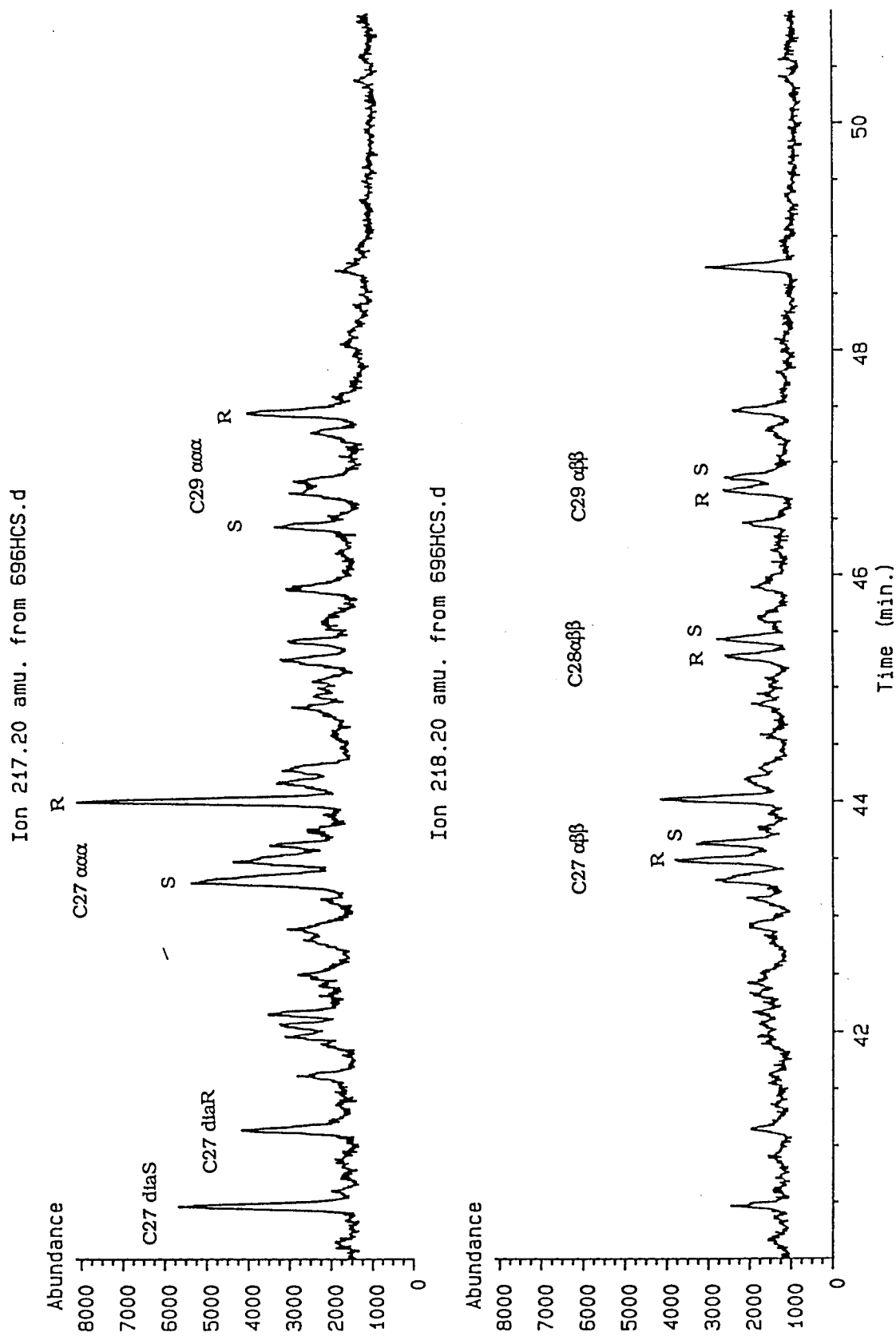


Fig. 5.6 a contd. Mass fragmentograms of steranes (m/z 217) and diasteranes (m/z 218).

Layer 153.

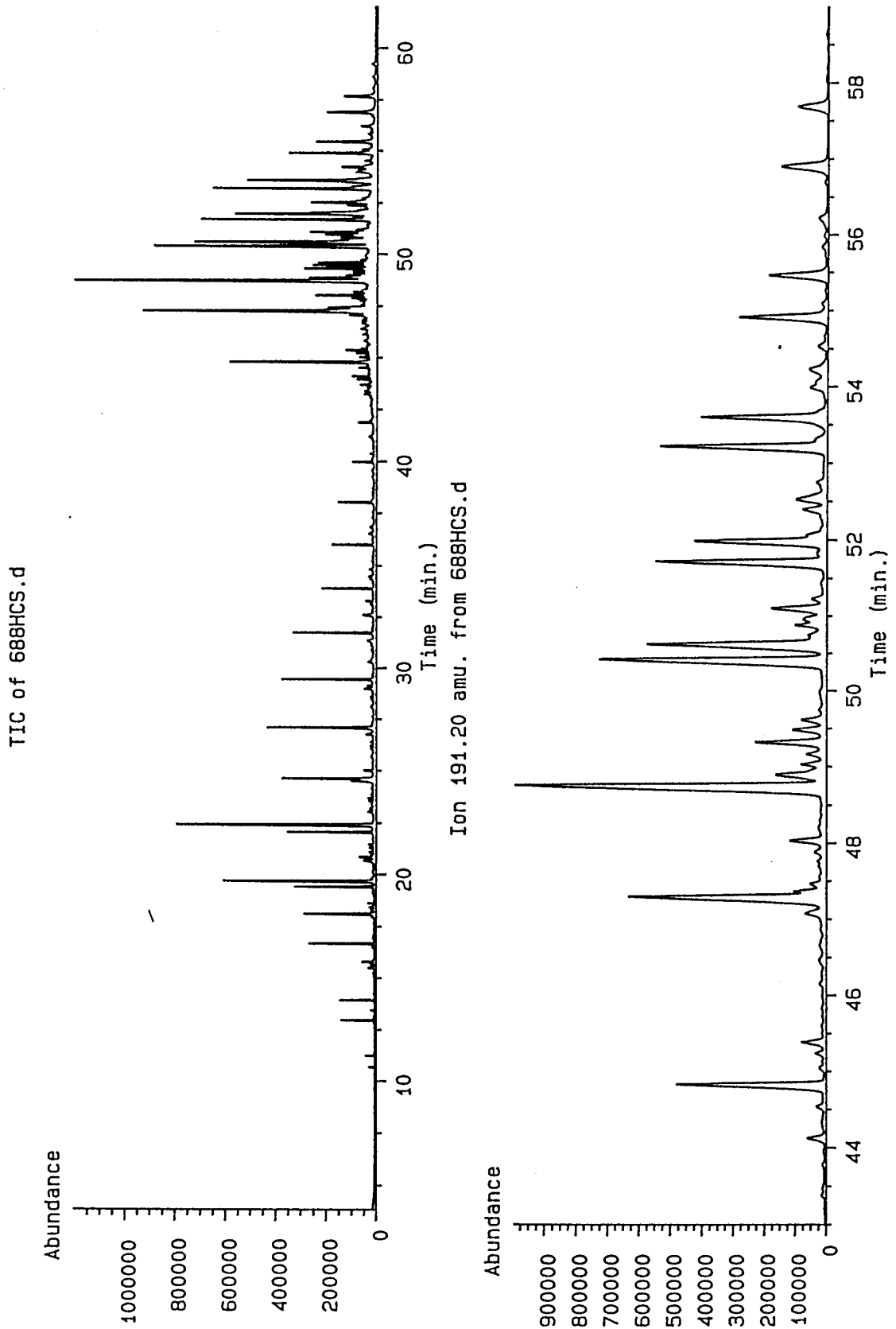


Fig. 5.6 b. Total ion current (TIC) chromatogram of the saturated hydrocarbon fraction and mass fragmentogram of hopanes (m/z 191). Layer 52. For peak assignments see Fig. 5.6.a

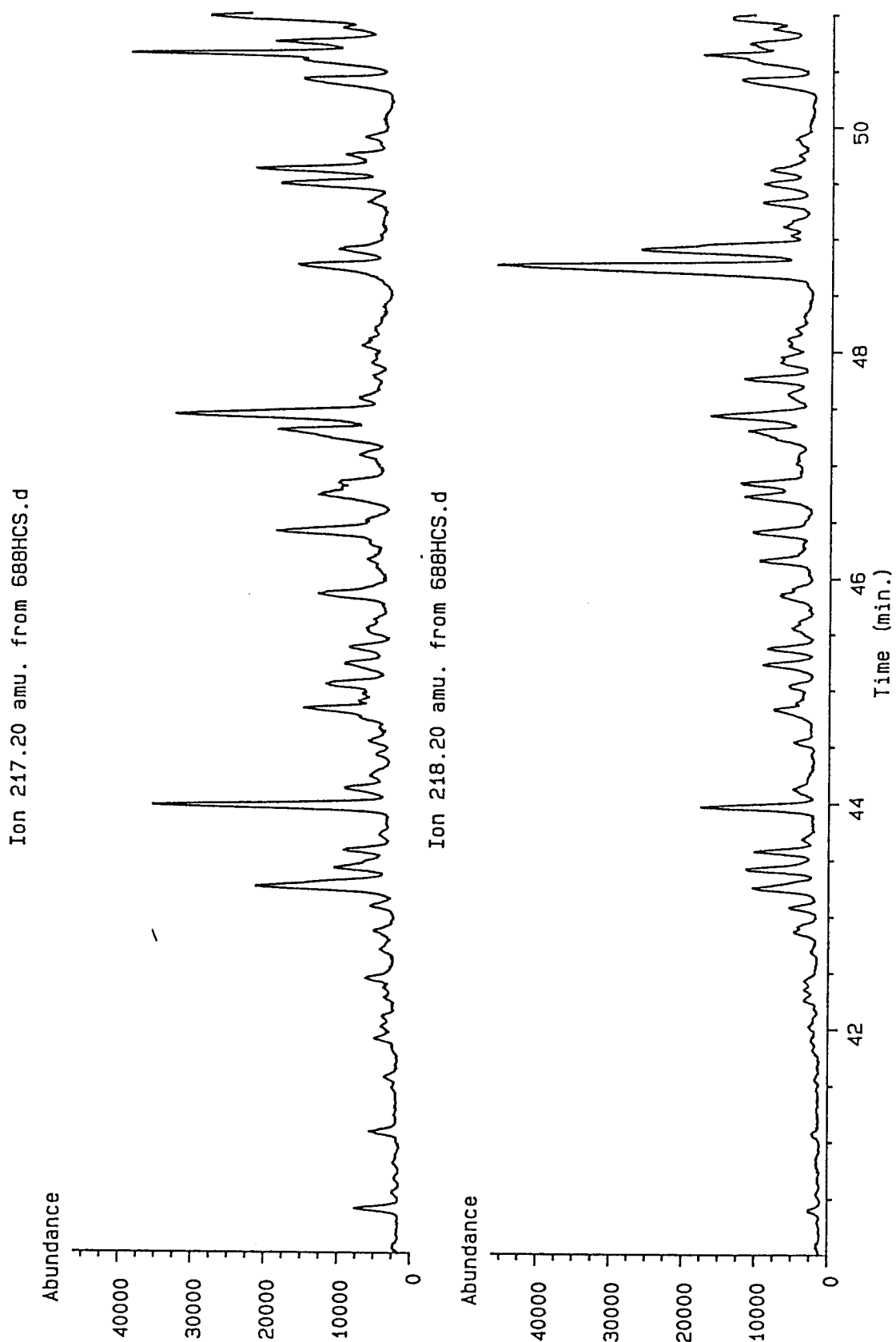


Fig. 5.6 b contd. Mass fragmentograms of steranes (m/z 217) and diasteranes (m/z 218).
Layer 52. For peak assignments see Fig. 5.6.a

similar distribution of the different families of saturated hydrocarbons (Fig. 5.6 & App. D) with only relatively minor variations. The high content of hopanes (bacterial input) relative to steranes (algal input) is a characteristic common to most of the samples. Hopanes are present in some of the samples at up to an order of magnitude greater concentrations than steranes.

5.4.3.1 Normal alkanes and isoprenoid hydrocarbons

The *n*-alkanes show a flat distribution with no even/odd predominance and a low proportion of long chain *n*-alkanes (Fig. 5.6 & App. D). Samples overlying MI153 are different from those from the lower part of the section in that they have a better defined maximum at *n*-C20 to *n*-C21. This distribution is characteristic of autochthonous marine organic matter derived mainly from phytoplankton and bacteria (e.g Tissot and Welte, 1984). The low abundance of long chain *n*-alkanes with more than 25 C-atoms is indicative of very low terrigenous input. This contradicts palynological data which suggest a significant input of herbaceous material, however, palynological data are not as quantitative as GC-MS data.

Pristane/Phytane (Pr/Ph) ratios show a wide scatter between 0.76 and 1.26 (Tab. 5.3) and surprisingly correlate positively with TOC contents (Fig. 5.7). Brooks et al. (1969) suggested that this ratio could represent a measure of the intensity of reducing conditions during sedimentation and early diagenesis because these compounds were considered to be pure diagenetic products. Data from Dydick et al. (1978), a comparative study of black shale samples of different ages and from different locations, confirmed this interpretation. They found decreasing Pr/Ph ratios with the increasing preservation of OM, which is opposite to the relationship found in the GBZ. The rationale for their interpretation is that in reducing diagenetic environments, reducing diagenetic pathways will prevail over oxidative ones. The precursor isoprenoid phytol, which is presumed to be liberated by hydrolysis from chlorophyll during very early diagenesis, may be transformed through a series of defunctionalization reactions to phytane if the prevailing conditions are reducing. On the other hand, if conditions are oxidizing, it will be transformed to pristane via decarboxylation of an intermediate carboxylic acid (Dydick et al. 1978, and references therein).

The foundations of the above interpretation of the Pr/Ph ratios have been weakened by the recent discovery of an other possible pristane precursor, tocopherol in phytoplankton (Risatti et al., 1983; Volkmann and Maxwell, 1986), by the detection of pristane and pristenes in zooplankton (Blumer and Snyder, 1965), and by the discovery of phytane in some groups of archeobacteria, especially halophiles and methanogens. Based on these considerations, as pointed out by ten Haven et al. (1987), the use of the Pr/Ph ratio as an indicator of reducing conditions must be regarded with caution. In fact,

it is quite surprising that the GBZ samples do not show a lower Pr/Ph ratio (e.g the range for comparable highly anoxic sediments is 0.2-0.6; Dydick et al., 1978) considering the high content of oil prone OM, the high vanadium porphyrin content (Blumer, 1950) and the high sulfur content, all of which are indications of highly anoxic conditions. Moreover, in view of the very low sedimentation rate (on the order of a few meters per million years), the bottom waters must have been permanently highly anoxic in order to preserve the large amounts of OM (up to 41% TOC) found in the GBZ sediments. It is more likely that the observed Pr/Ph ratio in the GBZ was at least partly controlled by the OM input and, thus, does not reflect moderately anoxic conditions.

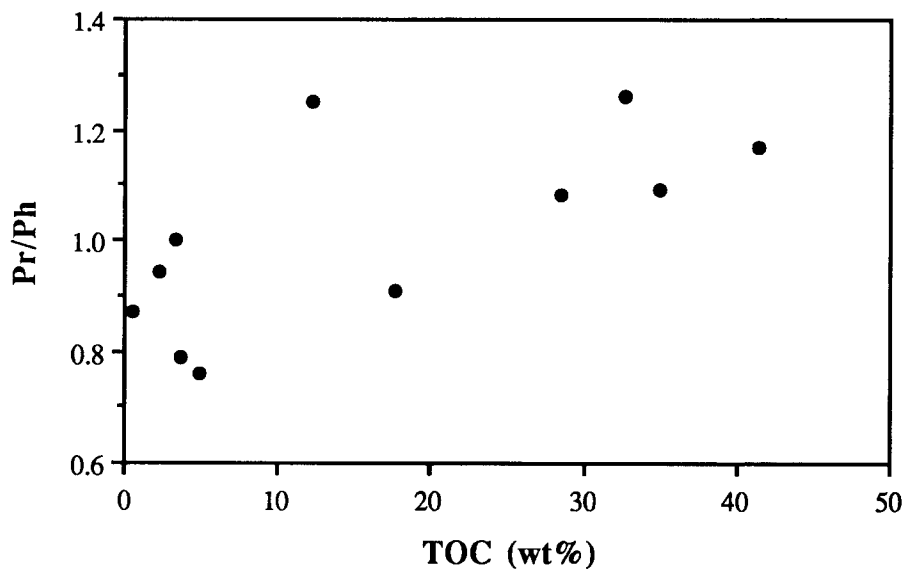


Fig. 5.7 Pr/Ph ratio vs. TOC (wt%). Note the increase in Pr/Ph ratio with increasing total organic carbon content.

If phytane can be derived from lipids of methanogenic and halophilic bacteria, the relatively high Pr/Ph ratios may be interpreted as a reduced input of phytane due to low activity of methanogens during early diagenesis or to the lack of hypersaline conditions. On the other hand, a high input of pristane from algae and/or zooplankton (Brassel et al., 1978) could also increase the ratio. Methanogens can compete effectively with the more energy efficient sulfate-reducing bacteria only when the sulfate content in the pore waters is completely depleted (e.g. Raiswell, 1988; Boudreau and Westrich, 1984). As mentioned previously, the carbon isotope compositions of the dolomites and the sulfur isotope compositions of pyrite in the black shales indicate that much of the diagenesis occurred close to the sediment-water interface in a relatively open system where sulfate ions had more or less free diffusional access to the pore waters. The presence of sulfate in the pore waters would have inhibited the activity of methanogenic bacteria in the early diagenetic stage producing a relatively high Pr/Ph ratio. In addition, squalane and

2,6,10,15,19-pentamethyleicosane are considered good indicators of methanogenic activity as they are abundant in sediments where high concentrations of methane or methanogenic bacteria have been found (Brassel et al., 1981). The absence of these components in all samples is further indication of a lack of methanogenesis in the GBZ sediments.

Pristane/n-C17 (Pr/n-C17) ratios vary between 1.97 and 0.73. The use of this ratio as a paleoenvironmental indicator was first proposed by Lijmbach (1975) who suggested a subdivision of depositional environments in three main groups: peat-swamp ($Pr/n-C17 > 1.0$); fluviomarine, coastal swamp ($0.5 < Pr/n-C17 < 1.0$) and marine, freshwater or brackish aquatic ($Pr/n-C17 < 0.5$). More recent studies, however, have shown that this ratio, at least in type III kerogens, can be influenced by factors other than the depositional environment (e.g. Leythausser and Schwarzkopf, 1986). These influences are discussed separately below in light of the rather wide scatter and high Pr/n-C17 ratios measured in the GBZ sediments.

1) Maturity: Leythausser and Schwarzkopf (1986) have shown that maturity produces a decrease in both Pr/n-C17 and Ph/n-C18 ratios, and that these reach values below 1.0 over most of the oil window, which corresponds to the peak production time of liquid hydrocarbons during catagenesis. The high values found in most of the samples are thus a further indication of the low maturity degree of the GBZ rocks (Connan and Cassou, 1980). Considering the small vertical distance between the studied samples, it is impossible that the observed variations are due to different maturity levels, therefore, other factors must be taken into account to explain the scatter in the GBZ ratios .

2) Hydrocarbon expulsion: In source rocks intervals with homogeneous kerogen type and equivalent maturation level, the Pr/n-C17 ratio tends to increase with increasing hydrocarbon expulsion (Leythausser and Schwarzkopf, 1986). In the GBZ samples there is no correlation between amount of hydrocarbons produced (EXT/TOC ratio) and Pr/n-C17 ratio. This suggests that, in the GBZ, differences in HC production do not influence the ratio in different samples.

3) Depositional environment: Organic matter deposited under terrestrial oxidizing conditions tend to produce hydrocarbons with high Pr/n-C17 ratios, whereas marine source rocks, with predominantly planktonic material deposited under reducing conditions, yield hydrocarbons with low ratios (Leythausser and Schwarzkopf, 1986). Pratt et al. (1986) have shown that in alternating laminated and bioturbated layers of Cretaceous black shales, bioturbation produces a decrease in both the Pr/n-C17 and Ph/n-C18 ratios confirming their possible use as indicators of oxidizing conditions.

The complete lack of correlation between TOC and Pr/n-C17 ratio and the fact that all the GBZ samples are derived from non-bioturbated laminated rocks containing organic matter with a comparable degree of preservation (similar HI) suggest that the scatter of

this ratio is probably principally dependent on small variations in the organic matter source and/or on the extent of bacterial activity.

4) Organic matter source: In the study of modern lake sediments, Giger et al. (1980), and Hollander (1989) have used the Pr/n-C17 ratio as an indicator of the relative contribution of phytoplankton (n-C17) and archeobacteria (pristane) and found a good correlation between this ratio, TOC contents, and the historical record of productivity, where times of high algal productivity produce a decrease in the ratio. The high content of pristane relative to the n-alkane can therefore be an indication for a high bacterial contribution to the total organic matter in the GBZ sediments.

The *Phytane/n-C18 (Ph/n-C18)* ratios of the GBZ sediments range between 0.49 and 2.24 and show a very good correlation with Pr/n-C17 ratios, indicating similar controls on the relative proportion of all these compounds.

The *R22 parameter*, defined as $2 \times (n-C22)/(n-C23 + n-C21)$ (ten Haven et al. 1985) has a value of 1.1 or less in all GBZ samples. Ten Haven et al. (1988) have shown that the value of R22 is higher than 1.5 in source rock extracts or oils derived from hypersaline settings and therefore suggested that this parameter can be used as a evidence for hypersalinity. The low R22 values found in the GBZ samples are in agreement with other observations that hypersaline conditions did not occur in the GBZ basin.

5.4.3.2 Terpenoids (hopanes, steranes)

Steranes are geolipids derived from the biosynthetic precursors sterols and stanols through complex diagenetic reactions. An excellent review of the pathways of sterol diagenesis and their stereochemical evolution during catagenesis can be found in MacKenzie et al. (1982). Sterols are absent in prokaryotic organisms except for two bacterial species (Ourisson et al., 1987). Although their diagenetic evolution can be influenced by bacterial activity and by the mineral matrix present in the sediments (MacKenzie, 1984), their abundance is mainly controlled by the input of eukaryotic biomass. Hopanoids, on the other hand, are derivatives of hopane which is an important constituent of bacterial membranes, and are therefore good indicators of bacterial activity in the water column and/or in the sediment. Hopanoids in prokaryotes and sterols in eukaryotes represent only a small part of the total organism ($0.1-2 \text{ mg g}^{-1}$ dry weight, Ourisson et al., 1987). However, because of their cyclic and often branched structure, they are not easily biodegradable and have a high preservation potential in sediments. Hopanoids have been found in most cyanobacteria, methylotrophs and various gram-positive and gram-negative bacteria but have never been found in strict anaerobes, archeobacteria and purple sulfur bacteria (Ourisson et al., 1987). The presence and distribution of hopanes in sediments and oils deposited in basins under permanently anoxic conditions (as in the Grenzbitumenzone) reflect the microbial

Table 5.4 Biomarker parameters calculated for the saturated hydrocarbons.

Sample	A	B	C	D	E	F	G	H	I	L	M	N	O
KK52	0.11	0.56	0.34	0.02	0.02	0.63	--	0.15	0.15	0.91	0.18	37:25:38	21.11
MI82	0.22	0.59	0.40	0.06	0.05	0.60	--	0.09	0.20	0.71	0.29	33:24:43	2.63
MI110	0.18	0.58	0.33	0.07	0.08	0.72	--	0.14	0.14	0.80	0.13	34:27:39	3.46
MI132	0.14	0.58	0.33	0.02	0.03	0.54	--	0.13	0.12	0.95	0.18	35:29:36	20.00
MI136	0.14	0.55	0.29	0.03	0.03	0.58	--	0.13	0.20	0.67	0.27	32:24:44	19.43
MU 153	0.22	0.58	0.42	0.62	0.23	0.92	0.17	--	0.12	1.42	0.67	43:29:28	6.25
MU 155	0.23	0.58	0.40	0.45	0.16	0.55	0.19	0.11	0.15	1.7	0.20	47:25:28	5.2
MU 162	0.28	0.58	0.43	0.53	0.11	0.50	0.21	0.03	0.23	0.9	0.70	37:21:42	5.5
MI226	0.27	0.57	0.33	0.09	0.11	0.70	?	0.05	0.13	0.8	0.32	32:26:42	1.0
BE89/2	0.08	0.57	0.23	0.14	0.20	0.87	--	0.90	0.50	n.m.	0.13	n.m.	n.d.
BE89/6	0.08	0.61	0.28	0.12	0.11	0.69	--	0.09	0.07	n.m.	0.19	n.m.	n.d.
BE89/12	0.06	0.55	0.25	0.10	0.15	0.81	--	0.13	0.08	n.m.	0.12	n.m.	3.2
BE89/11	0.11	0.61	0.21	0.10	0.06	0.64	--	0.07	0.07	n.m.	0.20	n.m.	4.2
BE89/22	0.15	0.61	0.38	0.09	0.66	0.57	--	0.06	0.17	1.12	0.20	38:28:34	11.9
RC2057	0.12	0.55	0.24	0.04	0.08	0.70	--	0.13	n.d.	n.m.	0.09	n.m.	4.18
RC 2062	0.10	0.56	0.20	0.05	0.08	0.73	--	0.12	n.d.	n.m.	0.13	n.m.	3.75

Explanation:

A = Ts/Tm (Ts = 18 α (H)- trisnorhopane, Tm = 17 α (H)- trisnorhopane)C = C29 5,14,17 $\alpha\alpha\alpha$ (20S)/(20S+20R) Steranes

E = C24-4/C30 hopane (tetracyclic/pentacyclic triterpanes)

G = Gammacerane/C30 hopane

I = C29-5/C29 norhopane (C29-5 =unnamed pentacyclic terpene with 29 C atoms)

M = C27 (R) diastereane/C27 $\alpha\alpha\alpha$ (R)

O = T/S (Terpane/ Sterane ratio)

n.d.= Non determined, n.m.=non measurable due to poor peak definition

B = C31 $\alpha\beta$ (S)/ (S + R) hopanes (Equilibrium value = 0.6)

D = C23-3/C30 hopane (tricyclic/pentacyclic triterpanes)

F = C29 hopane/C30 hopane

H = C30 lin/C30 hopane

L = C27 $\alpha\beta\beta$ (S + R)/C29 $\alpha\beta\beta$ (S + R)

N = C27 : C28 : C29 steranes

-- = compound absent

? = possible presence in low concentrations

processes that were active in the water column at the oxic-anoxic interface rather than processes occurring in the sediment after deposition.

In this study we will concentrate on the most abundant hopanes; the reader is referred to McEvoy and Giger (1986) for a full description of the hopane distribution of a sample from layer 117. A number of conventional biomarker ratios which reflect maturation and source differences have been calculated from the sterane and hopane mass fragmentograms. These parameters are listed in Table 5.4 and discussed below.

5.4.3.2.1 Maturity parameters

The T_s/T_m ratios of the GBZ samples range from 0.06 to 0.28 and are characteristic for immature rocks which have not reached the oil window (Seifert and Moldowan, 1978). T_s (= 18 α (H)-trisnorhopane) is a source parameter and is not affected by maturity changes. Although its mode of formation is unknown, its structure requires formation during the earliest stages of diagenesis rather than through maturation (Seifert and Moldowan, 1978). In contrast, T_m (= 17 α (H)-trisnorhopane) is formed in the same way as the other regular hopanes and its concentration in oils or extracts is dependent on maturation. Thus, for source rocks derived from similar organic matter, the T_s/T_m ratio is a maturity parameter. However, Seifert and Moldowan (1977, 1986) point out that the generation of T_s may be dependant on acid catalysis and, therefore, the presence of clays in the mineral matrix could play a role in overprinting the maturity-induced value of the T_s/T_m parameter. In the GBZ samples, the covariance of the T_s/T_m ratios with Pr/Ph ratios (Fig. 5.8), isotopic compositions of the saturated hydrocarbons (see Section 5.5.2) and sterane isomerization ratios (Fig. 5.9) indicate that organic matter input and/or varying redox conditions during early stages of diagenesis could have had an influence on both these maturity parameters. This explains the wide variation, which cannot be attributed to differences in maturity as the selected samples are only a few meters apart.

The range of the maturity parameter $C_{31} \alpha\beta (S)/(S+R)$ (Hopanes) in the GBZ samples is 0.55-0.61. The values of this ratio ranges from 0 to an end point of 0.6 (equilibrium value) with increasing maturity (Seifert and Moldowan, 1980). The complete isomerization of the hopanes is commonly reached before the onset of intense hydrocarbon generation (MacKenzie and Maxwell, 1981). Therefore, the GBZ values are consistent with the other maturation parameters, such as vitrinite reflectance and Rock-Eval T_{max} , which indicate that the GBZ sediments are only marginally mature.

The GBZ range for the ratio $C_{29} 5,14,17 \alpha\alpha\alpha(20S)/(20S+20R)$ (Steranes) is 0.21 to 0.42. It is lower than the equilibrium value of 0.5-0.6 which is reached when the organic matter is well into the zone of oil generation (MacKenzie, 1984). However, the variations are rather high and cannot be attributed to maturity changes because of the close vertical

spacing of the samples. Comparisons with literature data (e.g. MacKenzie et al., 1980) suggest that only the lowest value can be considered representative of the maturity level of the GBZ at these locations. The higher values and the wide variability in the data indicate that primary input and/or early diagenetic processes influence the isomerization of steranes.

A detailed study of two samples has shown the presence of low concentrations of diasterenes (unsaturated precursors of diasteranes) and the complete absence of sterenes. McEvoy and Giger (1986) also reported the minor presence of low amounts of hopenes and methylhopenes. These unsaturated compounds are found only in immature sediments, before the onset of the oil window (MacKenzie et al., 1982).

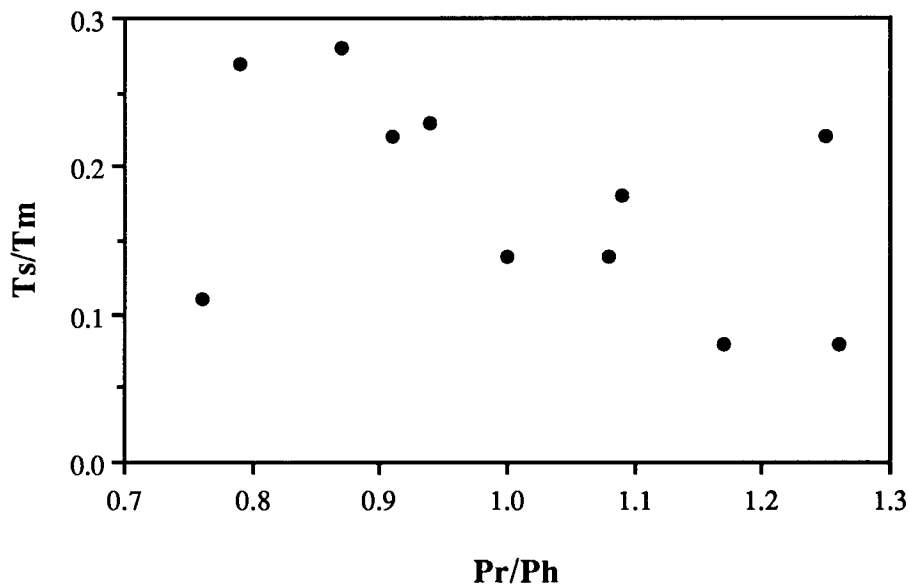


Fig. 5.8 Scatter plot of Ts/Tm- vs. Pr/Ph-ratios. The correlation indicates a source control on the Ts/Tm ratio.

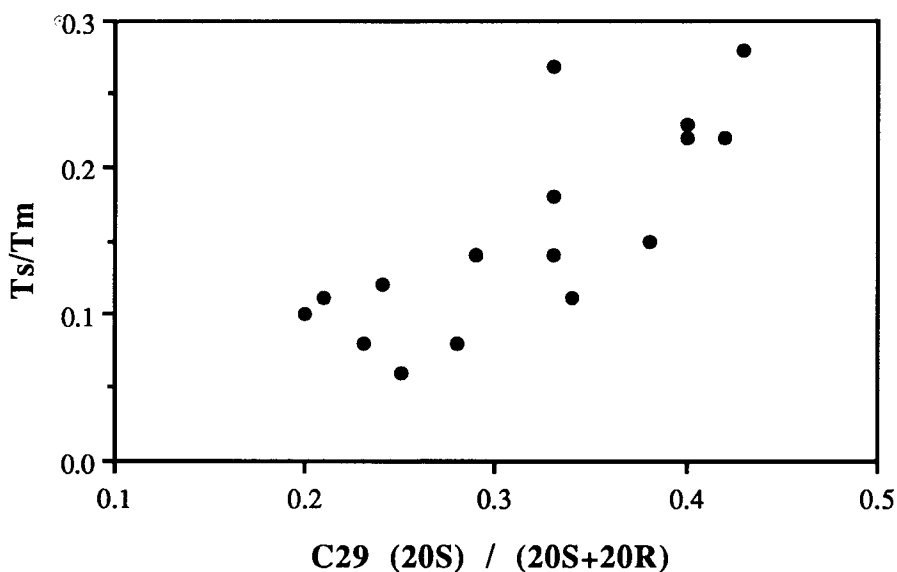


Fig. 5.9 Scatter plot of Ts/Tm vs C29 sterane isomerization parameter. The strong variance and the good correlation of these maturity parameters indicate a significant source and/or syndepositional bacterial activity control.

5.4.3.2.2 Source parameters

The *C23-3/C30 hopane ratio* is a measure of the relative abundance of tricyclic (C23-3) over pentacyclic triterpanes (hopanes). Tricyclic terpanes are widely distributed in most oils and source rock extracts of marine origin, whereas they are absent in oils derived from purely terrestrial source rocks (Aquino Neto et al., 1983; Philp, 1985; Moldowan et al., 1983). Although their precursors are not well known, their ubiquitous presence in oil and source rocks suggest a bacterial (Ourisson et al., 1982) or algal origin (Aquino Neto et al., 1983). This ratio gives a good indication of input variations. As evidenced by their C23-3/C30 ratio, samples 153, 155 and 162, from the upper part of the section, show a clear difference in input compared to all other samples. The fact that the highest relative concentrations of tricyclic terpanes are found in the samples with low abundance of hopanes compared to the n-alkanes, suggests that tricyclic terpanes probably originate from algal precursor (Aquino Neto et al., 1983).

The ratios of *tetracyclic/pentacyclic terpanes* (C24-4/ C30 hopane) range from 0.02 to 0.66 in the GBZ samples. Aquino Neto et al. (1983) proposed that tetracyclic terpanes are derived from degradation of the pentacyclic hopane-type triterpanes, either through bacterial activity during early diagenesis or through maturation. However, Philp (1985) observed an abundance of C24 tetracyclic terpane in Australian oils, which are mostly derived from terrestrial source material, and concluded that this compound could be taken as an indicator of terrestrial input. In analogy, the change in tetracyclic/pentacyclic terpanes ratios in samples MI153, 155, 162, BE89/2 and BE89/22

could indicate higher terrestrial input or alternatively a higher or different type of bacterial activity during early stages of diagenesis.

Variations in bacterial population should be reflected in the parameter *C29/C30 hopane*. Its constancy in all GBZ samples indicates a relatively homogeneous bacterial population for the entire formation.

Gammacerane was detected only in samples 153, 155 and 162. *Gammacerane* is thought to be derived from tetrahymanol, which occurs in a protozoan (Mallory et al., 1963) and in ferns (Zander et al., 1969). Tetrahymanol is rather common in sediments deposited under hypersaline conditions (ten Haven et al., 1988) but has also recently been recognized in a variety of open marine deposits (Venkatesan, 1989). Therefore, the geochemical significance of *gammacerane* is rather uncertain. However, the association of higher concentrations of tetracyclic terpanes in the samples containing *gammacerane* may suggest a terrestrial source for the *gammacerane* in these samples.

The *C30-lin compound* is a hopane with a straight rather than of branched side chain. Its presence is characteristic for carbonate source rocks and can be used for oil-source rock correlation. Its presence in the GBZ is in agreement with the high carbonate contents. The *C29-5 compound* is a pentacyclic terpane of unknown structure whose formation appears to be enhanced by the presence of clays. The variations of this parameter reflect variations in clay content of the source rock but can be used as a correlation tool.

The ratio $C27 \alpha\beta\beta(S+R)/C29 \alpha\beta\beta(S+R)$ (*Steranes*) reflects variations in organic matter source. The C27-steranes are commonly thought to represent phytoplankton and the C29-steranes higher plant input. However, Volkman (1988) has challenged this rather simplistic interpretation showing that some species of phytoplankton can also contain appreciable amounts of C29-steranes. Therefore, the high amounts of C29-steranes found in the majority of the GBZ samples from the lower part of the section compared to samples 153 and 155 do not necessarily imply a higher terrigenous input for the lower part of the formation but probably reflect changes in plankton population.

Diasteranes are principally formed in argillaceous lithologies through catalysis in acid sites of the clay crystals (MacKenzie et al., 1982, Palacas et al., 1985). The ratio $C27 \text{diasteranes}/C27 \alpha\alpha\alpha \text{steranes}$ can be used as a source parameter but has more significance in the characterization of the inorganic matrix accompanying the organic matter (presence of clays, pH of associated pore fluids) than for the organic matter itself. The absence of diasteranes is usually indicative of carbonate-rich lithologies. The observed variations in the GBZ are probably due to lithological variations.

The relative proportion of *C27 to C28 to C29 steranes* could not be calculated for all the samples because of the poor definition of the S and R isomer peaks due to the low maturity. All the GBZ samples, with the exception of MI153 and MI 155, plot in the field for estuarine or bay environments indicating a homogeneous organic matter input and a

restricted environment for the lower part of the GBZ (Fig. 5.10). Samples MI153 and MI155 plot in the marine field suggesting a transition to more open marine conditions towards the top of the formation.

The GBZ *terpane/sterane (T/S) ratios* show a strong scatter from 2.6 to 21.1. Two groups can be distinguished; one with values between 2.6 and 6.2 and one with a value of around 20. This means that hopanes can be present in concentrations of up to one order of magnitude higher than steranes (Fig. 5.6, Tab. 5.5). The sterane concentration is a measure of the autochthonous eukaryotic algal production in the water column, whereas the hopane concentration reflects both the bacterial input into the sediment (from chemolithotrophic and chemiolithoautotrophic bacteria) and the degree of bacterial reworking of the organic matter sinking in the water column (heterotrophic bacteria). The latter is therefore a measure of both primary and secondary biochemical activity. The variation in the terpane/sterane ratio is very high, in contrast to the rather constant C29 hop/C30 hop ratio. This indicates a qualitatively homogeneous bacterial population with a strongly varying quantitative input of algal and/or bacterial material.

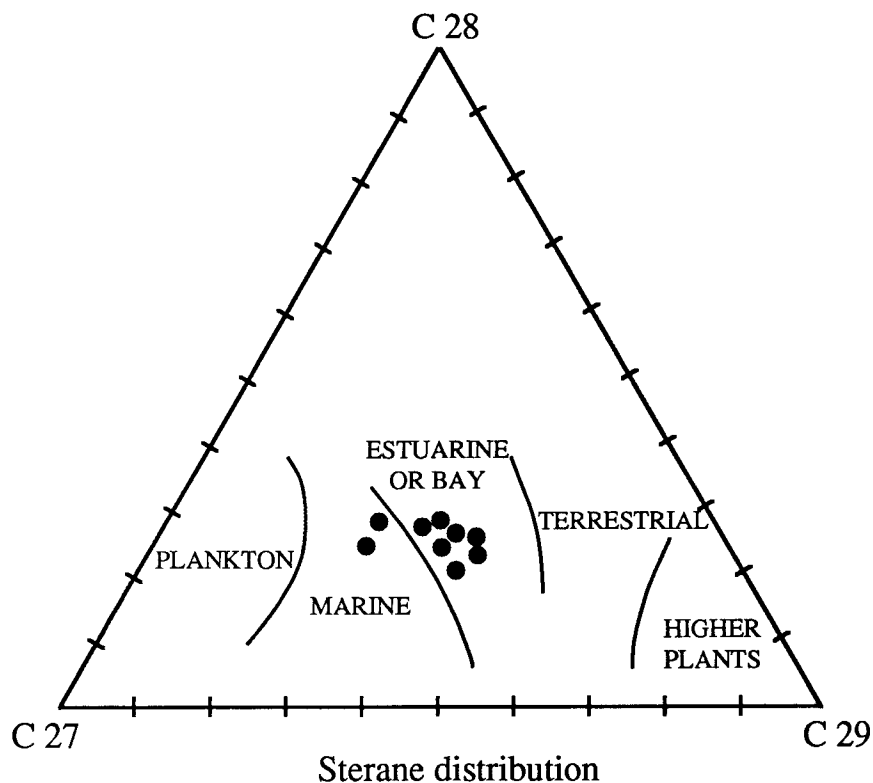


Fig. 5.10 Triangular diagram of the relative abundance of C27, C28 and C29 5 α (H), 14 α (H), 17 α (H) steranes (R + S isomers). This diagram (based on that of Huang and Meinschein, 1979) shows the homogeneity of the organic matter input. The samples falling into the marine field are MI153 and 155 from the upper Grenzbitumenzone.

5.4.4 Aromatic hydrocarbons

The results of GC-MS studies on GBZ aromatic hydrocarbons are summarized in Tab. 5.5. Aromatic hydrocarbons represent between 0.8% and 25.2% of the extractable fraction (Tab. 5.3). It must be noted that only sample MI153 shows a very small aromatic fraction; all other samples show concentrations higher than 7.6%. Sample MI153 is also characterized by the presence of 4-5 methylenphenantrene and dibenzothiophenes, which are absent or present only in very low concentrations in the other samples (see Tab. 5.5.)

Table 5.5 Aromatic hydrocarbons

Sample	4-5 MeP (1)	DBT's (2)	Benzohopanes (3)	4 MA (4)	T/M+T (5)	MPI1 (6)
KK52	?	?	C34>C35>C33>C32	+	<1	0.50
MI82	?	?	C34>C35>C33>C32	+	<1	0.74
MI110	?	?	C34>C35>C33>C32	+	<1	1.04
MI132	?	?	C34>C35>C33>C32	+	<1	0.82
MI 136	?	?	C34>C35>C33>C32	+	<1	0.62
MU 153	+	+	C34>C35>C33>C32	+	<1	0.37
RC2062	nd.	nd.	nd	nd.	0.44	0.80
RC2057	nd.	nd.	nd	nd.	0.33	0.47
BE 89/2	nd.	nd.	C34>C35>C33>C32	nd.	0.49	nd.
BE 89/6	nd.	nd.	C34>C35>C33>C32	nd.	0.50	nd.
BE 89/12	nd.	nd.	C34>C35>C33>C32	nd.	0.49	nd.
BE 89/11	nd.	nd.	C34>C35>C33>C32	nd.	0.52	nd.
BE89/22	nd.	nd.	C34>C35>C33>C32	nd.	0.33	nd.

(+) = present (?) = dubious (n.d.) = not determined

(1) 4-5 Methyleneanthracene present

(2) Dibenzothiophenes

(3) Benzohopanes, relative intensity of
C32, C33, C34, C35

(4) 4 MA (Methylantracene)*

(5) Triaromatic/(monoaromatic+triaromatic) steranes

(6) Methyleneanthracene index 1

MPI 1 =
$$\frac{1.5 (2\text{-methyleneanthracene} + 3\text{-methyleneanthracene})}{\text{phenanthrene} + 1\text{-methyleneanthracene} + 9\text{-methyleneanthracene}}$$

5.4.4.1 Maturity parameters

The *methylenphenantrene index* was first introduced as a maturity index by Radke et al. (1982), and is based on studies of extracts of type III kerogens. More recent studies have shown that this parameter is not very useful in rocks containing type II kerogens (Radke et al., 1986; Cassani et al., 1988). In particular, Cassani et al. (1988) found that the methylphenantrene index correlates positively with the carbonate content and does not correlate at all with other maturity parameters such as T_{max} , atomic H/C ratios or steroid isomerization parameters. The range of 0.37 to 1.04 found in the GBZ samples, corresponding to maturities ranging from immature to overmature, demonstrate that this parameter is highly influenced by variations in organic facies and possibly by mineral matrix effects and is therefore not very meaningful.

The abundance of triaromatic steranes over mono- and triaromatics (T/M+T) is maturity dependent (MacKenzie et al., 1981) and the value of this ratio increases from 0 in immature rocks to 1 (the equilibrium value) at the peak of oil generation. The GBZ values of 0.33 to 0.52 are consistent with the lowest values found for the isomerization of the steranes.

5.5 Organic Carbon Isotope Geochemistry

5.5.1 Total organic carbon

Total organic carbon isotope compositions in the GBZ samples range between -27.5 and -31.8 ‰ (PDB) (Tab. 5.6, Fig. 5.11). Stratigraphic variations are depicted in Fig. 5.12. No clear correlation between TOC-content and isotopic composition exists (Fig. 5.11), as samples with lower organic carbon content show a wide variability. A trend towards less negative values (avg. ~ -28‰) is seen at above 13 m from the base of the profile, corresponding to layer 136 (Fig. 5.12), whereby layer 155 at 15.1 m is an exception in this trend. The $\delta^{13}C_{TOC}$ in the San Giorgio Dolomites just above the GBZ ranges between -27.5 and -28.2‰ (Tab. 5.6). This shift towards less negative values in the GBZ correlates with changes in the C27:C28:C29 sterane biomarker distribution and with a decrease in the amount of hopanes which indicate a change to more normal marine conditions (see section in section 5.4.3.2).

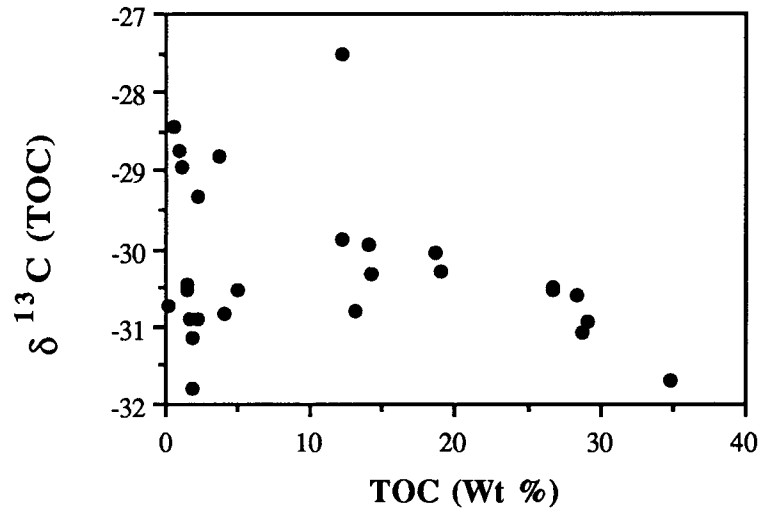


Fig. 5.11 Scatter plot of $\delta^{13}\text{C}_{\text{TOC}}$ vs total organic carbon content. Note the wide scatter in the samples with low organic carbon content and the tendency to more negative compositions with increasing TOC in the samples with TOC > 10%

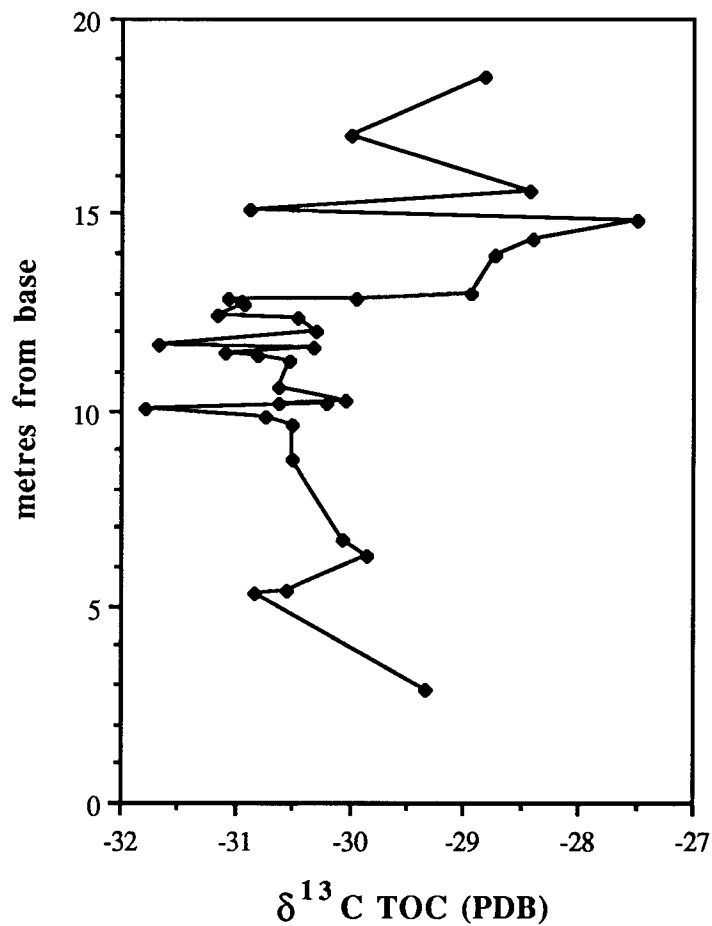


Fig. 5.12 Variations in $\delta^{13}\text{C}_{(\text{TOC})}$ in the profile at Miriglioli (P.902). The trend to less negative $\delta^{13}\text{C}$ composition in the upper Grenzbitumenzone is interpreted as due to a decrease in bacterial activity and to an opening of the basin to more open marine conditions.

Table 5.6.

Carbon isotope composition of TOC, saturated (SHC) and aromatic (AHC) hydrocarbon fractions.

Layer No	m from base	$\delta^{13}\text{C}$ (PDB)	TOC %	$\delta^{13}\text{C}$ (PDB) SHC	$\delta^{13}\text{C}$ (PDB) AHC
23	2.90	-29.34	2.18		
51	5.30	-30.84	3.97		
52	5.40	-30.54	4.95	-32.87	-32.76
56	6.25	-29.86	12.09		
60	6.70	-30.05	18.60		
75	8.75	-30.52	26.70		
82	9.60	-30.50	26.70	-32.27	-32.23
84	9.85	-30.74	0.25		
88 u	10.05	-31.79	1.78		
88 o	10.15	-30.21			
93 u	10.20	-30.63			
93 o	10.25	-30.04			
97	10.60	-30.61	28.30		
106	11.25	-30.54	1.42		
108 u	11.40	-30.81	13.00		
108 o	11.50	-31.10			
109	11.60	-30.32	14.26		
110	11.70	-31.68	34.90	-32.52	-32.21
115	12.00	-30.30	18.98		
120	12.35	-30.45	1.50		
122	12.40	-31.16	1.78		
129	12.70	-30.92	1.70		
130	12.75	-30.95	29.04		
132	12.80	-31.07	28.80	-32.96	-32.89
134	12.85	-29.95	14.02		
136	13.00	-28.95	1.05	-31.31	-31.35
142	13.90	-28.74	0.84		
146	14.35	-28.40			
153	14.80	-27.50	12.20	-28.15	-27.61
155	15.10	-30.89	2.22	-29.79	-30.0
162	15.55	-28.44	0.52	-29.25	-28.71
185	17.00	-29.99			
226	18.50	-28.82	3.66	-31.38	-31.30
S. Giorgio dolomite					
	35.00*	-27.51			
	40.00*	-28.04			
	50.00*	-28.20			

* m from base of the Grenzbitumenzone

5.5.2 Saturated and aromatic hydrocarbon fractions

The carbon isotope compositions of the extracts range from -28.2 to -33.0‰ (PDB) for saturated fractions and -27.6 to -32.9‰ for aromatic fractions with an excellent positive correlation between the two (Fig. 5.13). The saturated and the aromatic fractions have $\delta^{13}\text{C}$ values 0.8 to 2.4 ‰ and 0.5 to 2.3 ‰, respectively, more negative than those for TOC. The composition of aromatic and saturated fraction likewise correlates positively with TOC composition (Fig. 5.14). Therefore, it can be assumed that in general the isotopic compositions of the extracts closely mirror those of the TOC.

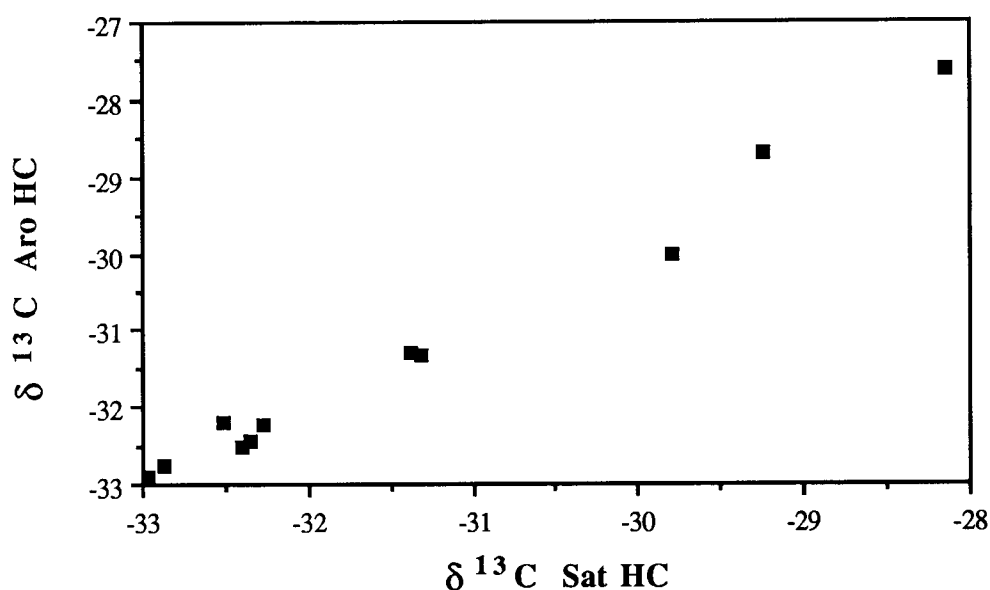


Fig. 5.13 Scatter plot of $\delta^{13}\text{C}$ of aromatic and saturated hydrocarbon fractions showing an excellent correlation.

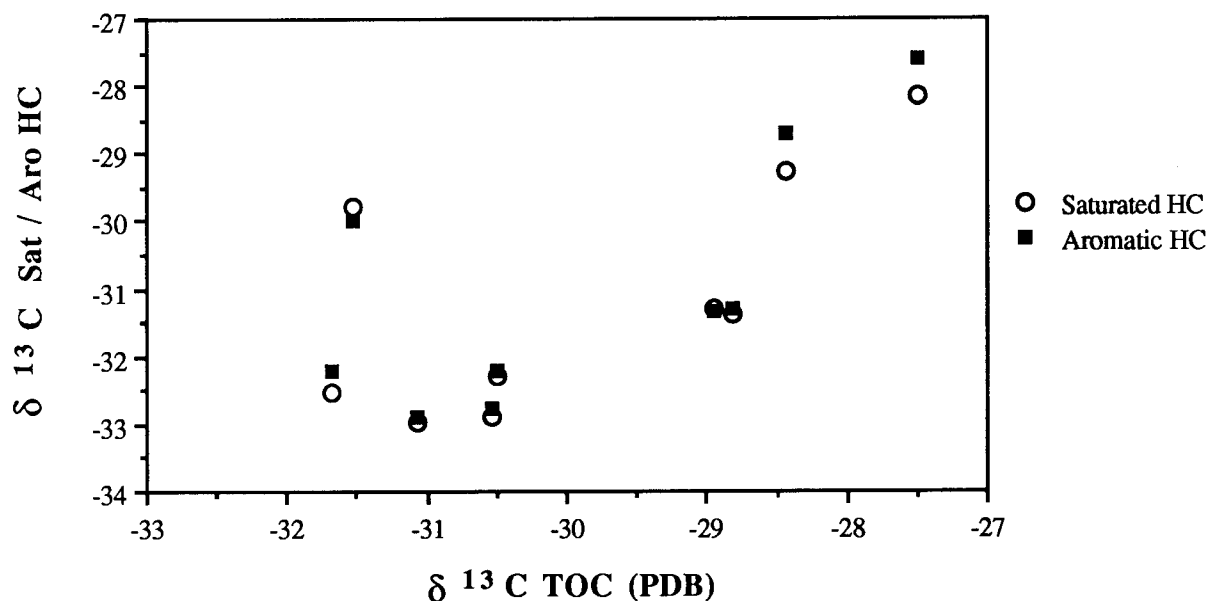


Fig. 5.14 Scatter plot of $\delta^{13}\text{C}_{\text{TOC}}$ vs $\delta^{13}\text{C}$ of aromatic and saturated hydrocarbon fractions. The good correlation suggests that the variations seen in the isotopic composition of the extract fractions are representative of the bulk isotopic composition of the total organic matter.

Correlations between input-related biomarker parameters and isotopic composition of the extracts are depicted in Figs 5.15 to 5.19. The most negative values for the extract fractions are found in samples with the highest amount of hopanes (represented by the C30 hopane) relative to normal alkanes (represented by the C20 normal alkane) (Fig. 5.15) and highest Ph/n-C18 ratios (Fig. 5.16) and Pr/n-C17 (Fig. 5.17) and in the samples with the lowest tricyclic-terpanes/hopanes (Fig. 5.18) and tetracyclic-terpanes/hopanes ratios (Fig. 5.19). Cross plots of the isotopic composition of the saturated hydrocarbons with C27/C29 sterane ratio (Fig. 5.20), terpane/sterane ratios (Fig. 5.21) and Pr/Ph ratio (Fig. 5.22) show a relatively wide scatter probably reflecting the multiple sources of these compounds and complex chemical controls on their formation during diagenesis. The correlation between these parameters and the isotopic composition of the extracts indicate that the carbon isotope composition of the organic matter in the GBZ is controlled by variations in organic matter input. In particular, the most negative carbon isotope compositions are found in samples with the highest concentrations of biomarkers indicative for a significant input of bacterial biomass.

The correlation between the maturity parameters C29 (20S)/(20S+20R) and Ts/Tm with the carbon isotope composition of the extracts (Figs. 5.23 and 5.24) indicate that the variations in these parameters observed in the GBZ may be a consequence of changes in bacterial activity during the earliest stages of diagenesis and that the significance of these parameters as maturity indicators should be regarded with caution.

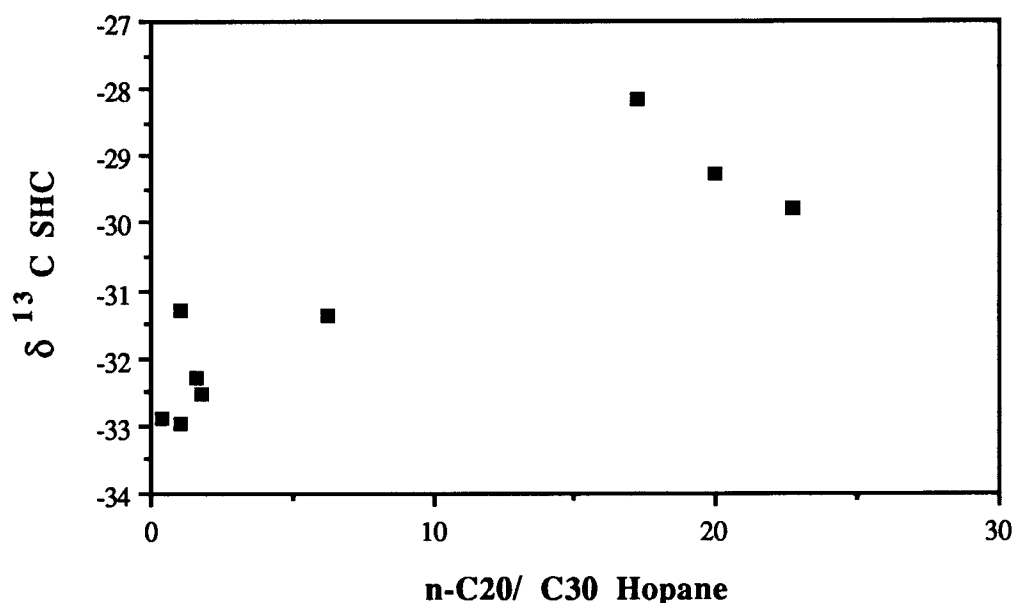


Fig. 5.15 Scatter plot of $\delta^{13}\text{C}$ of the saturate hydrocarbon fraction vs the C20 normal alkane/C30 hopane ratio. The n-C20 alkane is taken as an approximation of the primary algal input whereas the C30 hopane is a proxy of the bacterial input. The data clearly define two groups of samples: a group with light $\delta^{13}\text{C}$ compositions and high hopane concentrations and a group with heavy $\delta^{13}\text{C}$ compositions and low hopane concentrations.

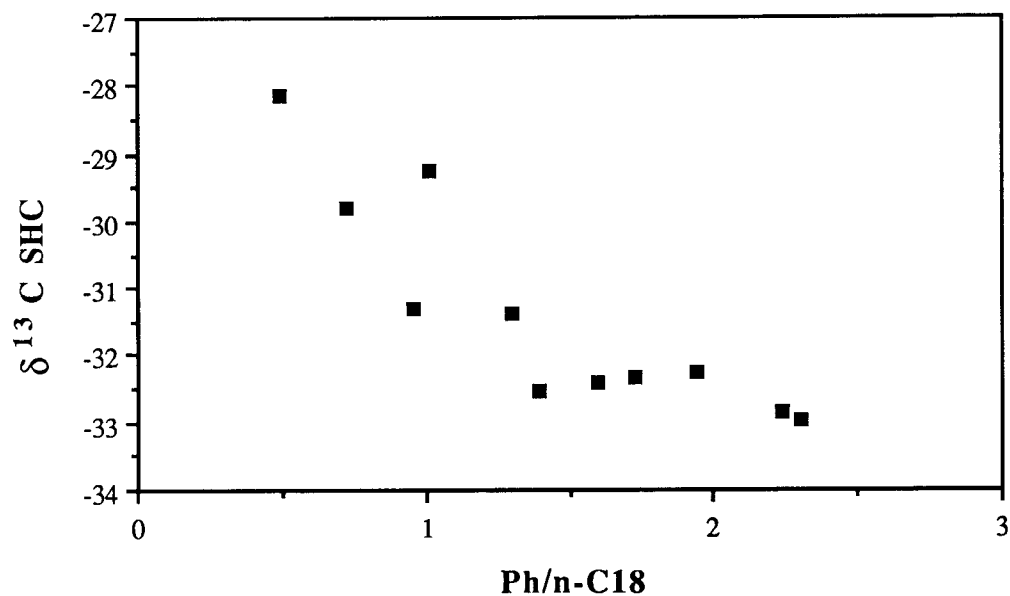


Fig. 5.16 Cross plot of $\delta^{13}\text{C}$ of saturated hydrocarbons versus Ph/n-C18 ratio. The correlation between high phytane concentrations and negative carbon isotope composition suggests a control of the bacterial activity on phytane production during early diagenesis.

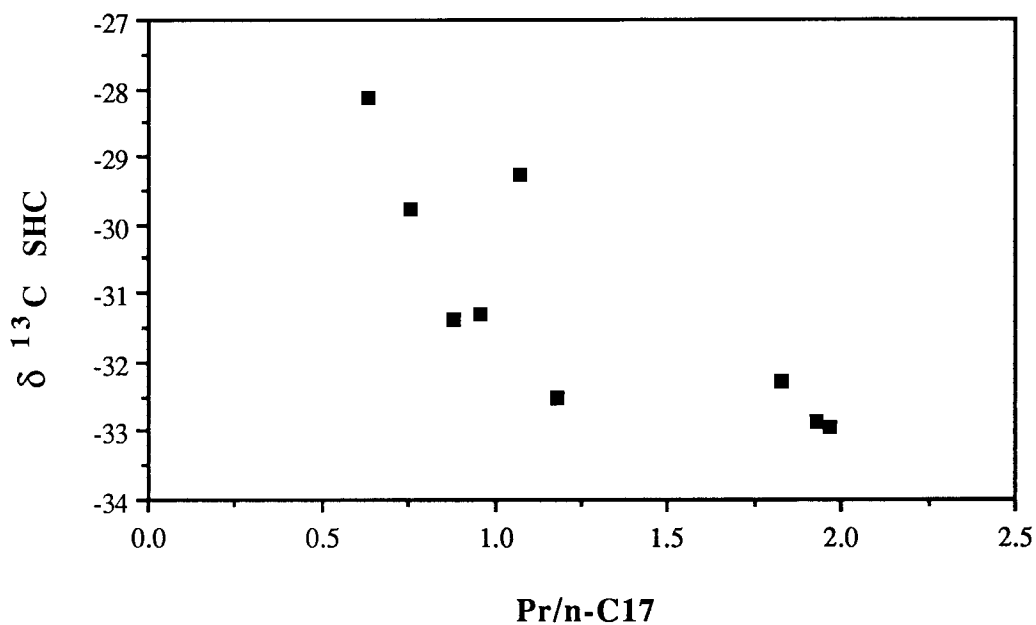


Fig. 5.17 Cross plot of $\delta^{13}\text{C}$ of saturated hydrocarbons versus Pr/n-C17 ratio.

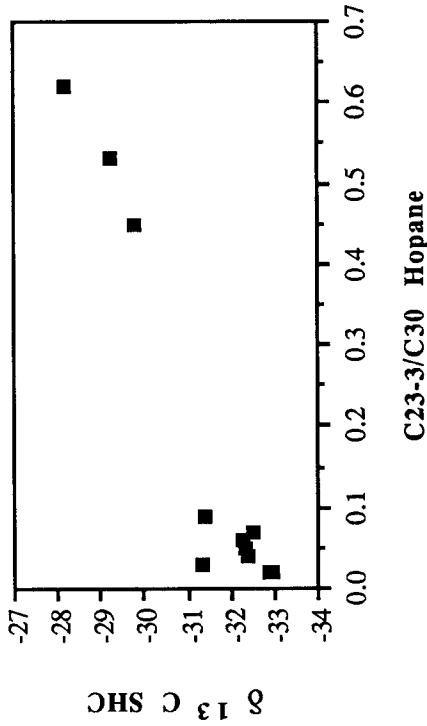


Fig. 5.18 Cross plot of $\delta^{13}C$ of saturated hydrocarbons versus tricyclic/pentacyclic triterpane ratio.

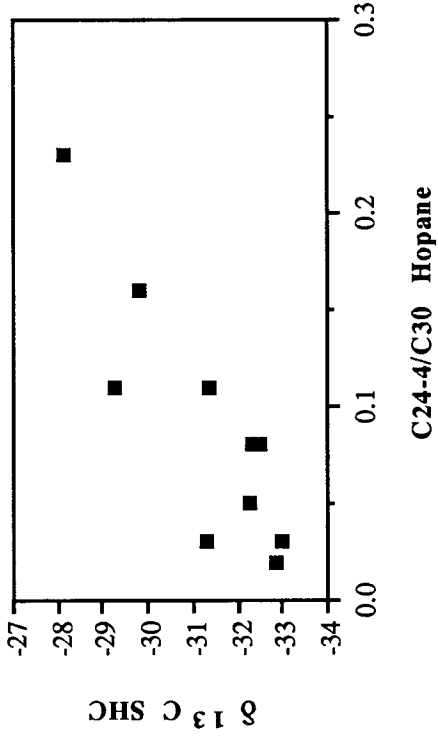


Fig. 5.19 Cross plot of $\delta^{13}C$ of saturated hydrocarbons versus tetracyclic/pentacyclic triterpane ratio.

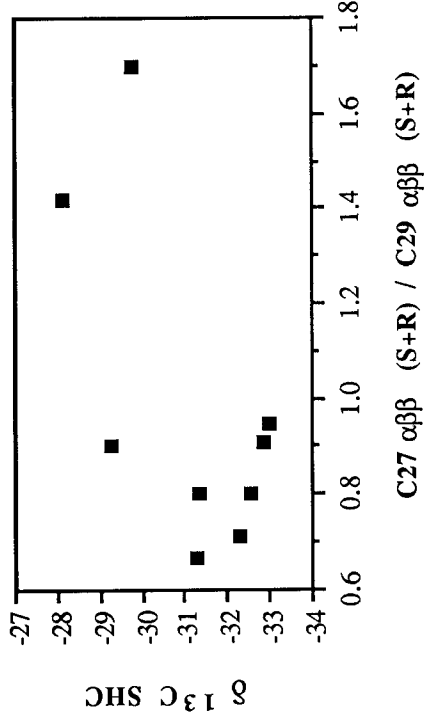


Fig. 5.20 Cross plot of $\delta^{13}C$ of saturated hydrocarbons versus C27/C29 sterane ratio. The group with the lowest $\delta^{13}C$ composition indicates that the sterane distribution is at least partially controlled by bacterial activity and does not solely reflect variations in primary input variations.

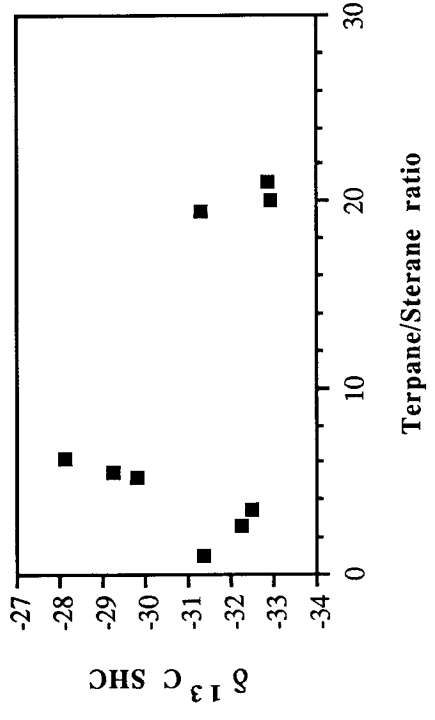


Fig. 5.21 Cross plot of $\delta^{13}C$ of saturated hydrocarbons versus terpane/sterane ratio.

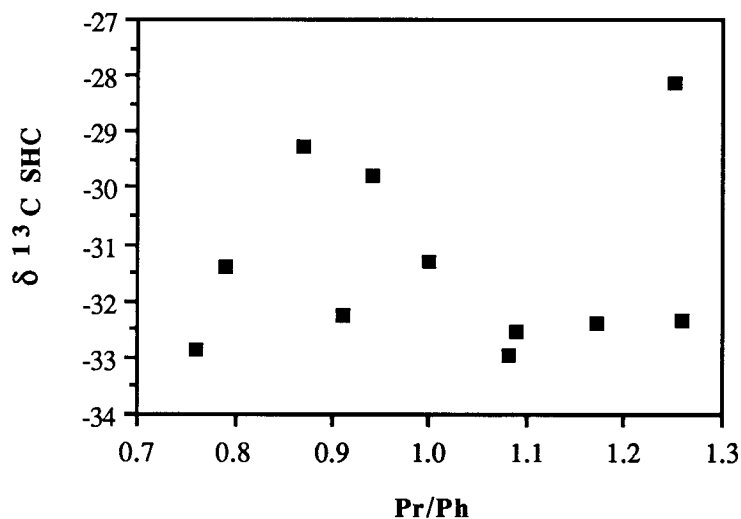


Fig. 5.22 Cross plot of $\delta^{13}\text{C}$ of saturated hydrocarbons (SHC) versus pristane/phytane ratio. The wide scatter is attributed to the composite sources of these isoprenoids.

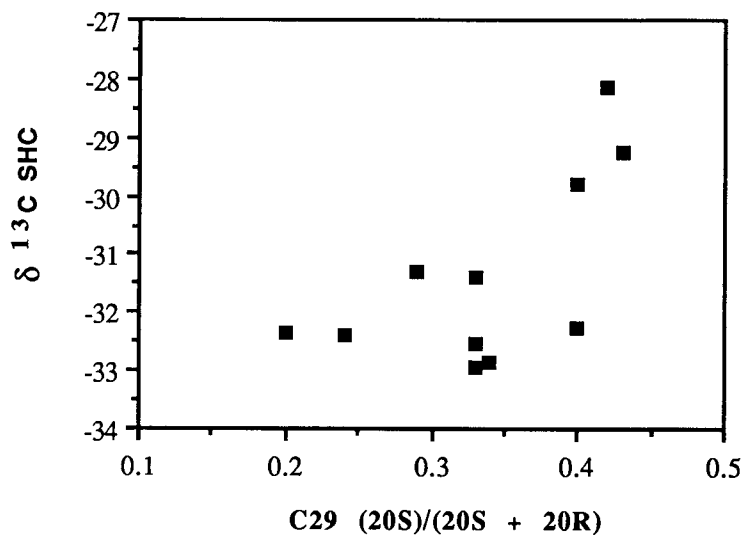


Fig. 5.23 Cross plot of $\delta^{13}\text{C}$ of saturated hydrocarbons (SHC) versus C29 sterane isomerization ratio.

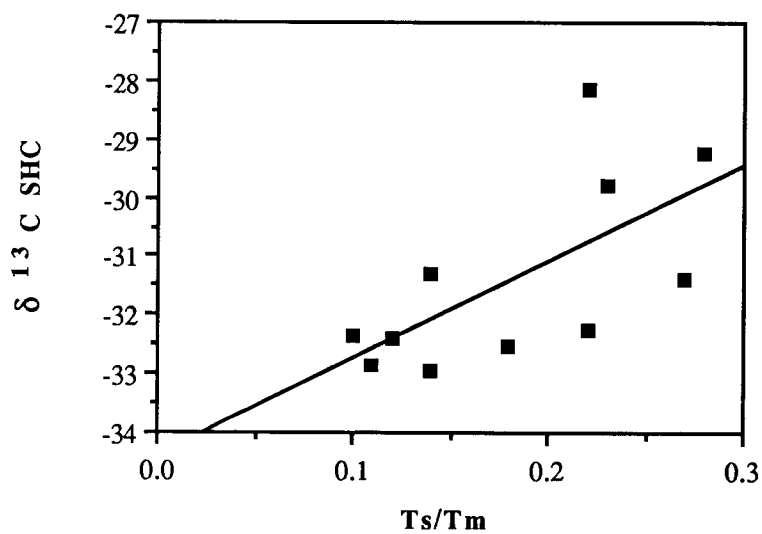


Fig. 5.24 Correlation between $\delta^{13}\text{C}$ of saturated hydrocarbons (SHC) and Ts/TM ratio.

5.5.3 Discussion

The carbon isotope composition of sedimentary marine organic matter is controlled by a large number of factors. The most important are: (1) the relative proportion of terrestrial to marine organic matter, (2) variations in plankton species and water temperature, (3) selective preservation of organic compounds during diagenesis, (4) extent of bacterial reworking, (5) concentration of CO₂ in the water column and (6) changes in the CO₂ sources for organic matter synthesis. It is therefore clear that the isotopic composition of sedimentary organic matter is the result of a combination of primary input-related variations and syndepositional to early diagenetic overprinting. Thermal maturation can be excluded as a influencing factor as many studies have shown that no significant changes in the isotopic composition of kerogen occur until metamorphic conditions are reached (e.g. Hoefs and Frey, 1976).

Modern terrestrial organic matter is on the average lighter than marine organic matter by about 7 ‰ (Degens, 1969), but the opposite relationship has been documented for different epochs in the Phanerozoic (Lewan, 1986; Dean et al., 1986). Although the carbon isotope composition of terrestrial organic matter has remained roughly constant through geologic time (Degens, 1969; Schoell, 1984), the composition of the marine organic matter has widely varied (Lewan, 1986; Dean et al., 1986). Lewan (1986) postulated that marine organic matter was isotopically lighter than terrestrial matter during periods when stagnation and sluggish circulation led to a reduction of gas exchange with the atmosphere. In this case, the water column stratification caused an enrichment of organically-derived carbon in the photic zone, which decreased the isotopic composition of the dissolved carbon used by the primary producers to synthesize new organic matter. An alternative explanation was put forward by Arthur et al. (1985), Dean et al. (1986) and Popp et al. (1989) who related variations in carbon isotope composition of marine organic matter to variations in the pCO₂ in the atmosphere. The carbon isotope composition of the primary organic matter is thought to be best represented by the composition of the porphyrins (Hayes et al., 1987). Based on porphyrin data, Popp et al. (1989) estimated the isotopic composition of primary Triassic marine organic matter to be -24.5 ‰ to -25.5 ‰. On the other hand, Lewan (1986) determined the isotopic composition of average Triassic marine organic matter to be -27.2 ‰ on the basis of amorphous kerogen composition

Many questions arise concerning the isotopic composition of the organic matter in the GBZ: What is the origin of the very negative $\delta^{13}\text{C}$ compositions (as low as -32 ‰) of total organic carbon? These are up to 10 ‰ more negative than recent marine organic matter, between 1.2 and 4.6 ‰ more negative than average Triassic marine organic matter (-27.2 ‰ PDB; Lewan, 1986) and more negative than average terrestrial organic matter (Avg -27.0 ‰; Degens, 1968). What are the causes of the variations within the GBZ

Formation? Are these primary signals or the result of early diagenetic processes after the organic matter was deposited?

The organic geochemical studies indicate a predominantly marine organic matter input with only minor terrestrial contribution for the entire GBZ, with limited variations among samples. These isotope results confirm the conclusions of Lewan (1986) that marine organic matter was more negative than terrestrial organic matter in the Middle Triassic. The values in some of the samples of the upper part of the GBZ and in the San Giorgio Dolomite (-27.5 to -28.5‰) are in the range determined by Lewan (1986) for Triassic marine organic matter. The more negative values found in the lower GBZ, however, must reflect a further organic matter source other than marine phytoplankton or terrestrial higher plant debris.

Temperature variations can be excluded as a cause for the isotopic shifts because of the very low temperature dependence of carbon isotopic composition of OM. Wong and Sackett (1978) have shown that the temperature dependence of carbon isotope fractionation range between -0.13 and +0.15 ‰/°C for different types of phytoplankton. An unrealistic change in temperature of 22 to 26°C is required to explain the 3.4 ‰ variations found in the GBZ.

Different biochemical components of organisms have different carbon isotopic compositions. For example, Degens et al. (1968) found that lipids of marine organisms can be enriched in ^{12}C by 8 to 10‰ relative to the carbohydrates and proteins. Selective preservation in the sediments of different fractions of the original organic matter could, therefore, produce a significant isotope shift compared to the value of the originally deposited organic matter. Spiker et al. (1984), for example, have shown that a 4 ‰ enrichment of ^{12}C occurs in algal remains preserved under optimum anaerobic conditions compared to the primary total organic matter. This preservation effect could explain the difference in composition between the primary producers inferred from porphyrin composition (Popp et al., 1989) and the TOC found in the upper GBZ. Assuming a possible depletion of 4 ‰ during early diagenesis, a composition of -29.5 ‰ could be expected from preferential preservation of lipid compounds during early diagenesis.

The correlation between the isotopic composition of the extracts and the relative concentration of hopanes (Fig. 5.15) and other biomarker parameters, which are considered to be at least partly dependent on bacterial activity (see section 5.3.1), indicate that the extremely negative compositions found in the GBZ reflect an important contribution of bacterial biomass in the preserved organic matter. Three alternative models are possible to explain the observed depletion. The high contribution of bacterial biomass in the GBZ organic matter is derived from:

- (1) methanotrophic bacteria living at the oxic-anoxic interface in the water column, and/or

- (2) autotrophic bacteria (cyanobacteria) which used a ^{13}C depleted source of CO_2 , and/or
- (3) a ^{13}C -depleted biomass of chemoautotrophic bacterial origin.

A definite answer to this question could only be found by analyzing the isotopic composition of individual organic molecules (e.g hopanes) with a known biological precursor, as the available data do not enable an unambiguous interpretation.

Methanogens have two main metabolic pathways of methane generation: by fermentation of acetate and by reduction of CO_2 (Balch et al., 1979), whereby in marine sediments methane production by CO_2 -reduction appears to be the dominant mechanism (Whiticar et al., 1986 and references therein). The fractionation between CO_2 and CH_4 varies between 45 and 80‰, and the range in $\delta^{13}\text{C}$ for biogenic methane in marine environments is -45 to -100 ‰ depending on the carbon source (Whiticar et al., 1986). Methane-oxidizing bacteria (methanotrophs) incorporate methane-derived carbon in their bodies and as a result are greatly depleted in ^{13}C . The incorporation of a significant amount of methanotrophs in kerogen would, therefore, depress the overall isotopic composition of the organic matter.

The presence of methylated hopanoids in the GBZ (McEvoy and Giger, 1987), which may be derived from methylotrophic bacteria (Bisseret et al., 1985; Zundel and Rohmer, 1985), would support hypothesis (1). Methylotrophs are bacteria that live in the water column at the oxic-anoxic interface and can grow at the expense of reduced carbon compounds containing one or more carbon atoms but no carbon-carbon bonds. Methane-oxidizing bacteria are one strain of methylotrophs. This hypothesis would also be supported by the correlation of the isotopic composition with Ph/n-C18 (Fig. 5.8), if phytane is assumed to be derived primarily from methanogens (Freeman et al., 1990). On the other hand, the sulfur isotope composition of pyrite and organic matter (Section 4.2) and the carbon isotopes of dolomite (Fig. 4.10), together with the lack of other biomarkers indicative of methanogenic activity such as squalane and 2,6,10,15,19-pentamethyleicosane, suggest that methanogenic activity was limited in the GBZ sediments. Thus, it appears unlikely that a process of methane recycling could have produced the large negative shift observed in the overall carbon isotopic compositions of organic matter in the GBZ.

It is not possible to constrain the relative importance of the contribution of chemoautotrophic bacteria (e.g denitrifying bacteria, sulfur oxidizers) and autotrophic bacteria (Cyanobacteria) because hopanes have been detected in species belonging to both of these groups of bacteria (Ourisson et al. 1987) and no other biomarkers specific to one of these groups are known. An indication of the presence of cyanobacteria in the GBZ is the high content of methylated hopanoids, which have also been detected in cyanobacteria (Zundel and Rohmer, 1985). In lacustrine basins with permanently stratified water columns, these bacteria have been observed to form a bacterial plate

suspended at the anoxic-oxic interface in the water column and carbon stable carbon isotope compositions of these bacteria are up to 20‰ lighter than algal biomass (Fry, 1986). Modern examples of bacterial plates in marine environments have been described in the Black Sea (Dickmann and Artuz, 1978) and in a stratified estuary (Inderbø et al., 1970). Because a combination of hypothesis (2) and (3) is compatible with the sedimentological and geochemical data, I suggest that in the GBZ basin, a high concentration of cyanobacteria and/or chemoautotrophs were present as a suspended bacterial layer in the water column, and that these contributed considerably to primary productivity.

5.5.4 Estimate of the bacterial contribution to total organic matter

A tentative estimate of the contribution of bacterial biomass to the total organic matter of the GBZ can be made on the basis of the isotopic compositions of the extracts (Table 5.6). Little data are available on the isotopic composition of individual hopanes in the rock record. The only useful data are those of Freeman et al. (1990), who measured the isotopic composition of various biomarkers in extracts from the Messel Shale in Germany. A weighted average of all hopanes gives a value of -47‰ (PDB). Using this value as a estimate of the isotopic composition of the bacterial biomass, a rough estimate of the bacterial contribution to the GBZ can be made. Because the isotopic composition of the primary producers in the GBZ is unknown three different values for the isotopic composition of the primary marine organic matter will be used:

1) $\delta^{13}\text{C}$ of primary producers: -25‰ (PDB), based on porphyrin compositions (Popp et al. 1989),

2) $\delta^{13}\text{C}$ of primary producers: -27‰ (PDB), based on composition of amorphous organic matter Middle Triassic marine sediments (Lewan, 1986),

3) $\delta^{13}\text{C}$ of primary producers: -28.5‰ (PDB) (based on isotopic composition of OM in the San Giorgio Dolomites.

Using the formula:

$$\delta^{13}\text{C}_{\text{Extract}} = x \delta^{13}\text{C}_{\text{primary producers}} + (1-x)\delta^{13}\text{C}_{\text{hopanes}}$$

the amount of bacterial biomass is estimated to lie between 18 and 37% of the total organic matter, depending on the initial value considered.

5.6 Summary

The following conclusions can be derived from the organic geochemical studies of the Grenzbitumenzone:

- (1) The organic matter is immature and can be classified as type II. It is dominated by a marine source with a large bacterial contribution.
- (2) The GBZ can be considered to be a good source rock.
- (3) The organic geochemical data indicate deposition in a restricted environment with a trend towards more open marine conditions and a decrease of bacterial contribution in the upper part of the formation, above layers 130-140.
- (4) The organic-carbon content of the sediments was not controlled by differing degrees of preservation but rather was a result of carbonate dilution of a relatively constant organic matter-detrital sedimentation.
- (5) No evidence for the presence of methanogenic bacteria was found in the biomarker distributions.
- (6) Variations observed in closely spaced samples within the GBZ indicate that environmental and/or primary organic matter input variations influenced some biomarker parameters, such as the Ts/Tm and the C29 sterane isomerization ratios, which are commonly thought to be only maturity dependent.
- (7) The carbon isotopic composition of the primary organic matter was strongly modified through incorporation of biomass derived from cyanobacteria and/or chemoautotrophic bacteria which formed a suspended bacterial layer in the water column.

CHAPTER 6

SUMMARY AND CONCLUSIONS

6.1 Introduction

This chapter summarizes the main results of this study and discusses the GBZ depositional environment and the possible links between the formation of the cyclic bedding and sea-level variations. This is followed by a discussion of the environmental parameters that promoted the preservation of high quantities of organic matter in the GBZ; then a model of the influence of bacterial activity on the accumulation, carbon isotope composition and quality of organic matter in sediments is presented. Finally, the origin of dolomite in the GBZ and the factors controlling dolomite formation in anoxic sediments are discussed. Carbonate, sedimentation in shallow water environments is strongly climate dependent thus, before discussing the depositional environments and the possible links between cyclicity in the GBZ and climatic variations, a brief discussion of the paleogeographic position of the Southern Alps and the climate in the Triassic is presented.

Paleogeographic reconstructions of the Middle Triassic indicate that the Southern Alpine realm was located between the equator and 20° latitude north (Scotese et al., 1979; Parrish et al., 1986). At this time all of the larger continents formed a unique continental mass, the supercontinent Pangea. This land mass distribution resulted in a very different atmospheric circulation pattern and climate zoning than today. Atmospheric circulation and paleoclimatological modeling by Parrish et al. (1986) and Kutzbach and Gallimore (1989) suggest that the climate during the Middle Triassic was characterized by a strong monsoonal circulation possibly modulated by orbital variations. The absence of therapsid fauna from paleolatitudes between 35° north to 35° south has been taken by Parrish et al. (1984) as evidence for a hot dry equatorial climate during Lower and Middle Triassic time. In agreement with the above authors, Tucker and Benton (1982) concluded that the equatorial humid belt was poorly developed in the Triassic, that a subtropical arid belt occupied an expanded low- to mid-latitude location between 25 and 50 degrees and that the land configuration could have produced warmer global temperatures and a generally lower rainfall than during other geological periods. In the Southern Alps, the upper Scythian and lower Anisian are characterized by the presence of evaporites (Carniola di Bovegno) and evaporitic lagoons (parts of the Elto Dolomite_x (Brack, 1984)), indicating a dry and warm climate and widespread sabkha-type environments. In the whole Southern Alps, the Anisian and Ladinian are characterized by the widespread occurrence of carbonate platforms indicative of a warm climate, but lithological indications for aridity are absent. However, a detailed study of the palynological

assemblages in the Middle Triassic of the western Dolomites by Van Der Eem (1983) shows a floral distribution dominated by xerophytic plants suggesting a warm arid climate at the end of the Anisian, followed by a progressive increase in humidity, at least locally, during the Ladinian and again an increased aridity towards the Carnian. This late Ladinian-Carnian arid phase is consistent with the presence of evaporites in the upper part of the Calcare di Meride (Kalkschieferzone) and the gypsum of the Raibl beds. Summarizing, the climate in the Lugano region during the deposition of the GBZ was probably tropical and rather poor in precipitation but possibly with periodic high rainfall during monsoon seasons.

6.2 The GBZ Depositional Environment and Basin Geometry

The sedimentological, geological and geochemical data indicate that the GBZ was deposited in a silled marine basin with extremely restricted circulation. Due to the lack of outcrops the extension of the basin cannot be exactly constrained. The available outcrops constrain the minimal E-W and N-S dimensions of the GBZ to be approximately 10 x 10 kilometers. The maximum possible E-W extension of the basin is 20 km if a connection with the basin in which the Perledo-Varenna Limestone was deposited is assumed. The extension towards the south cannot be constrained because of the thick Tertiary and Quaternary cover in the Po plain.

The fine grain-size of the sediments, the lack of evidence for sediment reworking as well as the lack of disruption and orientation of the vertebrate skeletons suggest limited current activity at the bottom of the basin and sedimentation below wave base. Based on model calculations and geological data, the depth of the basin can be constrained to be between 30 and 100m with a progressive deepening towards the top. The presence of an abundant cosmopolitan and varied normal marine fauna (ammonoids, *Daonella*, fish, saurids) indicates that the surface waters in the GBZ basin were connected to the Triassic Paleotethys and maintained a relatively normal marine salinity. On the other hand, the undisturbed laminations, the lack of benthonic fossils and bioturbation structures, the high organic sulfur content and the trace element signature of the black shales and laminated dolomites indicate that the GBZ was deposited under permanently anoxic conditions in H₂S-rich bottom waters. These data indicate the presence of a stable stratified water column in the basin for a very long period of time.

For a stable stratification to be maintained, a density gradient in the water column, due to variations in temperature and/or salinity, is necessary. In equatorial or tropical environments, as in the case of the GBZ, strong temperature gradients in the water column are unlikely. Therefore, the stratification observed in the GBZ can be considered primarily a consequence of salinity gradients in the water column. However, no petrographic or geochemical evidence for hypersalinity of the bottom waters have been

observed. For example, pseudomorphs of evaporite minerals are missing, and the oxygen isotopic compositions of dolomite are inconsistent with the presence of highly evaporated waters. Moreover, biomarker distributions in recent hypersaline settings are substantially different from those in the GBZ. For example, these settings, in contrast to the GBZ, are characterized by: 1) very low pristane to phytane ratios of 0.1-0.3 (GBZ: 0.76-1.25), 2) a high abundance of regular C25 isoprenoid (absent in the GBZ), 3) $R_{22} > 1.5$ (GBZ: 1.03-1.21), 4) relatively high abundances of gammacerane (present only in low concentrations in one sample of the GBZ), and (5) C31-C35 $14\beta(H), 17\alpha(H)$ hopane distributions maximizing at C35 (maximum at C31 in GBZ) (ten Haven, 1989). Thus, it can be assumed that the GBZ was deposited in a normal saline or at the most slightly hypersaline environment.

Silled basins have a number of physical barriers that influence water circulation patterns and restrict vertical mixing, thereby promoting water stratification. Silled basins can be divided into two main groups, those in humid zones with a positive water balance and those in arid zones with a negative water balance (Grasshoff, 1975). Basins with a positive water balance have a strong salinity contrast between outflowing fresh or brackish surface waters and deeper inflowing more saline and nutrient-rich marine water. In modern environments, such basins are often characterized by the development of anoxic conditions in the bottom waters (Demaison and Moore, 1980). Typical recent examples are the Black Sea (Degens and Ross, 1972) and Saanich Inlet, British Columbia (Nissenbaum et al., 1972). In basins with a negative water balance, such as the Mediterranean and Red Sea, inflowing seawater replaces the hypersaline surface water which sinks to the bottom and flows out as an undercurrent. In these basins the bottom waters are generally oxygenated and nutrient-poor and no enrichments of organic carbon are observed in the sediments. This circulation is generally induced by the winter cooling of the higher saline surface waters formed during the summer and is therefore efficient only if strong seasonal temperature variations are present. If seasonal temperature variations are absent, the overturn may not take place and therefore the bottom waters tend to become anoxic. This is the case for example in Johnson Pond, Gainesville, Florida where overturn of the water column takes place only in cold winters, whereby the bottom waters become anoxic again very rapidly, due to the high rates of oxygen consumption (J. McKenzie, pers. comm. 1991).

The sedimentological and geochemical data presented in this study indicate that there may be no unequivocal modern day marine basin similar to the GBZ. The permanently anoxic conditions of the bottom waters in the GBZ as well as the lack of evidence for hypersalinity could be considered evidence for deposition in a basin with a positive water balance. On the other hand, there is no evidence for freshwater or riverine input as the detrital input is very low and the fauna indicates normal marine salinity. The climate modelling of the Middle Triassic indicates an arid climate with evaporation

exceeding precipitation (Kutzbach and Gallimore, 1989). It is possible that a negative water balance due to evaporation exceeding precipitation associated with only small seasonal temperature variations produced denser higher saline bottom waters which stagnated in the basin. Overturns of the water column, which would replenish oxygen in the bottom waters, were probably relatively rare due to the lack of temperature variations. This, together with high productivity and long renewal times for the water (residence time for the waters can be estimated to be 30 to 60 years), could have induced oxygen depletion in the bottom waters and promoted the development of anoxia.

6.3 Sedimentation Rates

Calculations of trace metal accumulation rates (Section 4.1.3) and primary productivities, together with paleontological data of Rieber (1968), indicate that the sedimentation rate for the black shales was approximately 1m/m.y. Assuming that most of the time is contained in the black shales, a bulk compacted sedimentation rate between 5 and 7m/m.y. is estimated. The preservation style of the ammonoid and the lack of compaction features in the slump folds indicate that compaction in the dolomites was minor. Assuming a compaction factor of approximately 10 for the black shales, the original uncompact thickness of the GBZ can be estimated to be at the most 40-50 m.

Low sedimentation rates are supported by other geochemical data. It has been proposed that the sedimentation rate exerts a control on the carbon isotopic composition of the dolomites (Kelts and McKenzie, 1984). In slowly deposited sediments, dolomite will mostly form in the sulfate reduction zone carrying a negative $\delta^{13}\text{C}$ signature, whereas dolomite formed in areas with high accumulation rates dominantly have positive $\delta^{13}\text{C}$ signatures with strong gradients across beds. The lack of these trends and the constantly negative carbon isotope composition of the dolomites in the GBZ support this hypothesis. Moreover, in subtidal settings where diffusion of Mg from seawater into the sediments can be considered the major source of magnesium for dolomite formation (Baker and Burns, 1985; Burns and Baker, 1987; Compton and Siever, 1986), the formation of significant quantities of early diagenetic dolomite is only possible with extremely slow sedimentation rates where the pore waters form an open system with the overlying seawater for a long period of time. In addition, the very negative sulfur isotope composition of the pyrite and organic matter (Section 4.2) support the hypothesis of an open system diagenesis.

Similar low sedimentation rates are found in other coeval basins across the entire Southern Alps (e.g. Buchenstein beds) (Brack and Rieber, 1986, Brack, pers comm. 1990, Brack and Rieber in prep.). Higher bulk sedimentation rates are observed only in basins close to volcanic eruption centers with a high volcanic input (Brack pers. comm. 1990). These low sedimentation rates imply that the anoxic conditions were present in the GBZ

basin for 2 to 3 Ma and suggest that a high sedimentation rate is not a necessary condition to preserve high quantities of organic matter in sediments.

6.4 Origin of cyclicity

Cyclic sediments occur world-wide in most stratigraphic systems. The deposition of cyclic sediments is mainly attributed to rhythmic climatic oscillations, named Milankovitch cycles, which are produced by variations in the earth orbital parameters (e.g. many papers in Einsele and Seilacher, 1982). The periodicity of these variations is 21, 40, 100 and 400 Kyr (e.g. Berger, 1977). The major factors controlling fourth- and fifth-order cyclicity in shallow marine sediments are glacio-eustatic sea-level variations. Therefore, exact information on the presence or absence of polar ice-caps during the Triassic would be of primary importance to explain the cyclicity in the GBZ. No positive evidence for the presence of ice caps during the Triassic has yet been found. Studies on flora by Retallack (1975) and on amphibians by Colbert and Cosgriff (1974) indicate that the general climate was probably too warm for ice and snow to be present in polar regions during Triassic time.

In contrast to data indicative of an ice-free Triassic epoch, Goldhammer et al. (1987, 1990) postulated that the cyclic recurrence of emersion surfaces in the Ladinian Latemar platform in the Dolomites can be attributed to composite glacio-eustatic sea-level fluctuations on the order of few meters. Based on a combination of field data and numeric modeling of the observed cycles, they postulate two orders of cyclicity: a dominant component with a 20,000 year periodicity corresponding to variations in the earth axis tilt and a less important component reflecting the 100,000 years eccentricity cycle. A similar interpretation has tentatively been proposed for the Middle Triassic carbonate platforms in the Catalan Basin, Spain (Calvet et al., 1990).

The sedimentological study of the GBZ has shown that the lamination and the bedding probably reflect variations in carbonate supply over a more or less constant detrital and organic matter input. Although it must be considered that diagenesis could have enhanced or erased details of the cyclicity (Ricken, 1986), as a first approximation, we can assume that the bedding in the GBZ has a primary origin. Because the oldest known calcareous plankton is found in Carnian and Rhaetian sediments and only from only one location in the world (Wombat Plateau, Northern Australia, ODP Leg 122) and because many laminae and beds show evidence of resedimentation, it is concluded that the carbonate was produced on the Salvatore-Esino Platform and was transported into the basin by normal and/or "detached turbidity currents" (see Section 3.3). The amount of carbonate found in the GBZ is, therefore, directly dependent on the primary production on the platform, which in turn is dependent on variations in sea-level. No cyclicity is observed in the Salvatore Dolomite because extensive dolomitization has more or less

completely erased primary structures and no evidence of widespread emersion surfaces have been found. However emersion is suggested by the presence of indicators for vadose diagenesis (Zorn, 1971).

The first order cyclicity of black shales alternating with dolomites could be the result of variations in sea-level, whereby the black shales represent times of sea-level low stand with reduced or inhibited carbonate production on the platform and limited carbonate transport into the GBZ basin. Low sea-level, lowering the water depth above the sills, would restrict water circulation in the basin and enhance water stratification, which in turn would promote organic matter accumulation and preservation. Likewise, the dolomite beds may represent times of high sea-level stand when intense carbonate production on the platform took place. The fact that the black shale layers seem to represent a much longer time span than the dolomites may be a consequence of a slow recovery of the carbonate production on the platform after a sea-level rise. The minimum depth for carbonate production, sediment accumulation and sediment dispersal to begin on a carbonate platform is estimated to be 1-2m (Hardie and Shinn, 1986). Thus, a substantial length of time could have been necessary for the platform to resume carbonate production after a period of low stand, considering that sea-level variations in the Triassic were probably on the order of a few meters (Goldhammer et al., 1987).

6.5 Controls on Organic Matter Accumulation and Preservation

The main factors controlling accumulation of organic matter in sediments are:

1) *Primary productivity in the water column.* High primary productivity enhances organic matter accumulation; it not only provides a large flux of organic matter to the sediments but also has a large effect on the oxygen budget in the water column. Oxidation of a large amount of dead organic matter depletes oxygen in the water column which in turn inhibits further oxidation.

2) *Composition of organic matter.* Different organisms have widely varied compositions. Phytoplankton is particularly enriched in protein which forms 50 to 75 wt% of the dry body mass (Parsons et al., 1984). Proteins are preferentially used by aerobic bacteria, and marine organic matter is therefore readily remineralized under oxic conditions. On the other hand, higher plants contain a high amount of cellulose and other polymers which are more resistant to bacterial attack and are generally more easily preserved.

3) *Residence time of organic matter under oxic conditions.* Preservation of organic matter in shallow basins or in basins which have a redoxcline in the water column close to the water surface have a higher preservation potential for organic matter because the

residence time of the organic matter in the oxic water column is shorter and degradation of organic matter under anoxic conditions is slower.

4) *Sediment accumulation rates.* High accumulation rates generally favour the preservation of organic matter because even if the sediments are deposited under oxic conditions, the pore waters quickly become anoxic and organic matter degradation through aerobic bacteria and benthic burrowers is slowed down. On the other hand, above a certain threshold, the input of high quantities of sediment dilutes the organic matter content of the sediment.

5) *Extent of benthic animal feeding.* Experimental studies have shown that organic material that has been digested by benthic invertebrates is more readily degraded by subsequent bacterial activity (Hargrave, 1975; Swift et al., 1979). This suggests that the slower organic matter degradation observed in anoxic environments may not depend on a lesser efficiency of anaerobic bacteria compared to aerobic bacteria, but to the lack of an intermediate step of decomposition through metazoans before bacterial attack (Emerson and Hedges, 1988).

The high organic carbon content of the GBZ sediments is a consequence of the combination of different factors which promoted the preservation of organic matter. Firstly, they were deposited under permanently anoxic and sulphidic conditions. These conditions were lethal to any benthic metazoans and therefore suppressed an important source of degradation. Moreover, the shallow water and the dominance of anoxic conditions in the water column resulted in a short residence time of the dead organic matter in oxygenated waters.

A high contribution of bacterial biomass (methylotrophs and/or chemoautotrophs and/or cyanobacteria) living at the redoxcline in the water column can be inferred from the presence of high concentrations of hopanes in the GBZ. In some samples the hopanes are present in concentrations up to an order of magnitude higher than steranes. Hopanes are known only from prokariotic organisms and are thought to be reinforcers of the cell membranes. Sterols have the same function in eukariotic organisms and are exclusively present in eukariotes (Ourisson et al., 1987). Hopane and steranes occur in approximately the same proportions of the body weight of the respective organisms (0.1-2 mg/g dry wt). Assuming that the preservation potential of steranes and hopanes is the same, the dominance of hopanes over steranes would mean that the organic matter of the GBZ contains more bacterial than eukariotic biomass. Therefore, I suggest that cyanobacteria and possibly chemoautotrophic bacteria (which are known to produce hopanes; Ourisson et al., 1987) formed a bacterial plate at the anoxic-oxic interface and substantially contributed to the primary productivity in the GBZ (Fig. 6.1). Recent examples of high concentrations of bacteria (bacterial plates) at the oxic-anoxic interface such as the Black Sea (Dickman and Artuz, 1978), Jellyfish Lake, Palau (Burnett et al. 1989), Big Soda Lake, Nevada, USA (Zehr et al., 1987), Saelenvann Estuary, Norway (Indrebø et al.,

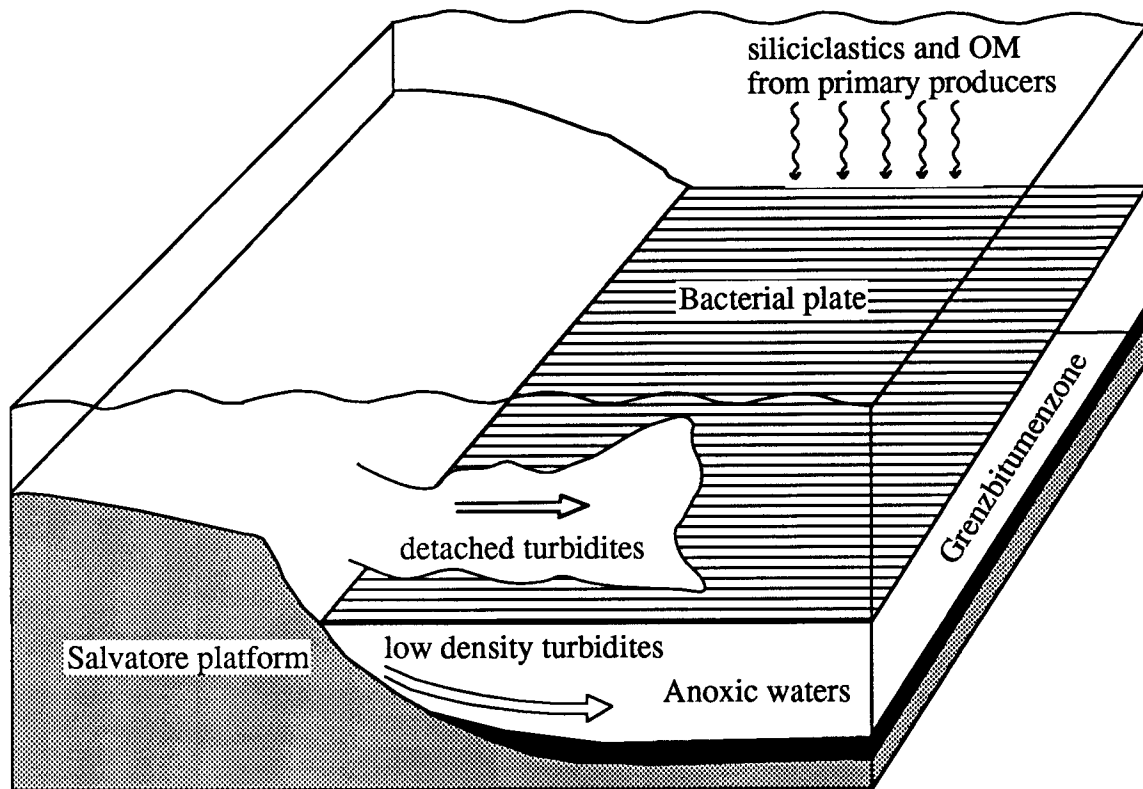


Fig. 6.1 Model of the depositional environment of the GBZ basin. Sedimentation in the basin was influenced by two main factors: the periodic deposition of carbonate mud turbidites and the presence of a bacterial plate at the anoxic-oxic interface in the water column.

(1979a,b) and Fayetteville Lake, New York (Culver and Brunskill, 1969) may represent present-day analogues of the GBZ. In some of the the above examples, anaerobic and aerobic photosynthetic bacteria living at the oxic-anoxic interface represent one of the main primary producers within the basins (e.g. Dickman and Artuz, 1976; Culver and Brunskill, 1968).

This model is also supported by the extremely high content of V0-porphyrins in the GBZ (approximately 1000 ppm; Thomas and Blumer, 1964). Water column studies in recent environments suggest that rapid transport into anoxic waters is essential for the preservation of chlorophyll and its derivatives (the precursors of porphyrins) in sediments (Baker and Louda, 1986). In analogy, considering cyanobacteria as the primary producers in the GBZ, they must also have been the major suppliers of chlorophyll. As the bacteria died, they sank directly into the anoxic waters, leading to the accumulation of high amounts of porphyrins. The existence of a bacterial plate in the GBZ basin is supported by the very negative carbon isotopic compositions of the organic matter and by the correlation between biomarkers parameters. In particular, the

terpane-sterane ratios and the n-alkane hopane ratios indicate the presence of high quantities of bacterial biomass in samples which are most depleted in ^{13}C .

In general, negative shifts in the isotopic composition of organic matter of planktonic organisms are observed at times of low productivity or when high concentrations of CO_2 in the surface waters are present (Arthur et al., 1988, Calder and Parker, 1973; Hollander, 1989). During periods of high productivity a general trend towards more positive carbon isotopic composition of OM and inorganic carbon is observed and is due to either a reservoir effect or a high demand of CO_2 from the photosynthetic organisms (e.g. Hollander, 1989). Thus, if the GBZ were characterized by high productivity, positive, rather than negative carbon isotope shifts in the organic matter would be expected. An isotopic study of the bacterial plate in the Fayetteville Lake has shown that the different bacterial species in the plate are depleted in ^{13}C by 10 to 20‰ with respect to phytoplankton (Fry, 1986). A significant contribution of bacterial biomass to the sediment would, therefore, result in a depletion of the overall carbon isotope composition of the resulting kerogen. By analogy, it can be concluded that the negative carbon isotope compositions of the organic matter in the GBZ is associated with the incorporation of bacterial biomass into the kerogen.

The preservation of OM can also be enhanced by the presence of chemolitho-heterotrophic bacteria which utilize inorganic compounds as an energy source and organic carbon as a source of carbon. Although they do not synthesize new organic carbon from CO_2 , they assimilate organic matter much more efficiently than the heterotrophs and, therefore, conserve biomass more efficiently (Jorgensen, 1989).

6.6 Controls on Dolomite Formation in the GBZ.

The geochemical, sedimentological and petrographic data indicate that dolomitization in the GBZ occurred soon after deposition of the sediments and close to the sediment-water interface. The sulfur isotope compositions of pyrite together with the carbon isotope compositions of dolomite indicate that dolomitization occurred in the sulfate reduction zone of organic matter diagenesis in a relatively open pore-water system. In recent sediments the depth of sulfate depletion in slowly deposited sediments is generally >2m, which is greater than the depth inferred for dolomitization in the GBZ. The lack of extreme values in $\delta^{13}\text{C}$ indicates that in the GBZ sediments the carbon isotope signature of the dolomite was controlled by the high carbonate content of the sediments prior to dolomitization. A contribution of approximately 20% of carbon derived from organic matter decomposition can be estimated by mass balance calculations.

Although dolomite is thermodynamically stable in seawater, which is approximately 20 times supersaturated with respect to dolomite (Bathurst, 1975), it forms only a minor

part of the carbonates in normal marine environments. Many different kinetic factors have been proposed as dolomite inhibitors and the interplay of all of these factors control the extent of dolomitization (e.g. Machel and Mountjoy, 1986; Hardie, 1987). The dolomite problem, however, is not only a chemical one but also a hydrological one because a major factor is always the source of Mg ions. Experimental studies have shown that sulfate retards dolomite formation at high temperatures (Baker and Kastner, 1981). On the basis of these experiments, the occurrence of dolomite in anoxic sediments has often been attributed to the depletion of sulfate in the pore-waters through bacterial activity. This interpretation has been challenged by various authors (e.g. Morrow and Ricketts, 1986; Compton, 1988) and is inconsistent with numerous occurrences of dolomite in sulfate-rich environments (Bathurst, 1975; Eugster and Hardie, 1978; Hardie, 1987). The geochemical evidence for an open-system diagenesis in the GBZ is in agreement with these latter studies and suggests that the most important control on dolomite precipitation was an increase in carbonate alkalinity produced by organic matter degradation through sulfate reduction rather than a depletion in SO_4 .

Pervasive early diagenetic dolomitization requires high quantities of Mg, whereby a lack of dolomitization is often a consequence of the low Mg-availability as a result of high sedimentation rates. The trace metal calculations suggest that the extensive dolomitization in the GBZ was possible because of extremely slow sedimentation rates. Slow sedimentation would have prolonged interaction with marine waters and permitted Mg diffusion into the sediments leading to complete dolomitization.

REFERENCES

- Aizenshtat Z., Lipiner G. and Cohen Y. (1984) Biogeochemistry of carbon and sulfur cycle in microbial mats of Solar Lake (Sinai). In: Cohen Y., Castenholz R. and Halvorson H. (eds): *Microbial mats: stromatolites*. Alan R. Liss, New York, 281-312.
- Al-Ashimi W. and Hemingway J.E. (1974) Recent dolomitization and the origin of the rusty crusts of Northumberland: a reply. *Jour. Sed. Petrol.*, 44, 271-274.
- Aquino Neto F.R., Trendel J.M., Restle A., Connan J. & Albrecht P.A. (1983) Occurrence and formation of tricyclic and tetracyclic terpanes in sediments and petroleum. *Adv. Org. Geochem.*, 1981, 659-667.
- Arthur M.A., Dean W. and Pratt L. (1988) Geochemical and climatic effects of increased marine organic carbon burial at the Cenomanian-Turonian boundary. *Nature*, 335, 714-716.
- Arthur M.A., Dean W.E. and Claypool G.E. (1985) Anomalous ^{13}C enrichment in modern marine organic carbon. *Nature*, 315, 216-218.
- Assereto R., Jadoul F and Omenetto P. (1977) Stratigrafia e metallogenese del settore occidentale del distretto a Pb, Zn, fluorite e barite di Gorno (Alpi bergamasche). *Riv. Ital. Paleont.*, 83, 395-532.
- Baker E.W. & Louda J.W. (1986) Porphyrins in the geological record. In: Johns R.B. (ed): *Biological markers in the sedimentary record. Methods in geochemistry and geophysics* (Elsevier), 24, 125-226.
- Baker P.A. & Burns S.J. (1985) Occurrence and formation of dolomite in organic-rich continental margin sediments. *Am. Assoc. Pet. Geol. Bull.*, 69(11), 1917-1930.
- Balch W.E., Fox G.E., Magrum L.J., Woese C.R. and Wolfe R.S. (1979) Methanogens: reevaluation of a unique biological group. *Microbiol. Rev.*, 43, 260-279.
- Barnes R.S.K. (1980) *Coastal lagoons*. Cambridge Univ. Press, 106 pp.
- Bassani F. (1886) Sui fossili e sull' età degli scisti bituminosi di Besano in Lombardia. *Mem. Soc. Ital. Sci. Nat.*, 7,1, 15-72.
- Bathurst R.G.C (1974) Marine diagenesis of shallow water carbonate sediments. *Ann. Rev. Earth and Plan. Sci.*, 2, 257-274.
- Bathurst R.G.C. (1975) Carbonate sediments and their diagenesis. *Developments in sedimentology*, 12, 658 p.
- Bathurst R.G.C (1980) Lithification of carbonate sediments. *Sci. Prog. Oxford.*, 66, 451-471.
- Beadle L.C. (1981) *The inland waters of tropical Africa*. 2nd ed. Longman, London.
- Bein A., Almogi-Labin A. and Sass E. (1990) Sulfur sinks and organic carbon relationships in cretaceous organic-rich carbonates: implications for evaluation of oxygen-poor environments. *Am. J. Sci.*, 290, 882-911.
- Berger A. (1977) Long term variation of the earth's orbital elements. *Celestial Mechanics*, 15, 53-74.
- Berner R.A. (1970) Sedimentary pyrite formation. *Am. J. Sci.*, 268, 1-23.
- Berner R.A. & Raiswell R (1984) C/S method to distinguishing freshwater from marine sedimentary rocks. *Geology*, 12, 365-368.

- Bernoulli D.B. (1972) North Atlantic and mediterranean Mesozoic facies: a comparison. *Init. Rep. DSDP*, 11, 801-871.
- Bernoulli D. (1964) Zur Geologie des Monte Generoso (Lombardische Alpen). *Beitr. zur Geol. Karte der Schweiz*, NF 118, 134 p.
- Bernoulli D. et al (1976) *Geol. Atlas der Schweiz* 1:25000. Blatt 1353 Lugano..
- Bertotti G. (1991) Early Mesozoic extension and alpine shortening in the western southern Alps: The geology of the area between Lugano and Menaggio (Lombardy, Northern Italy). *Mem. Sci. Geol.*, In press.
- Bertrand P., Pittion J-L and Bernaud C. (1986) Fluorescence of sedimentary organic matter in relation to its chemical composition. *Org. Geochem.*, 10, 641-647.
- Bisseret P., Zundel M., and Rohmer M. (1985) Prokaryotic triterpenoids 2.2 β -methylhopanoids from *Methylobacterium organophylum* and *Nostoc muscorum*, a new series of prokaryotic terpenoids. *Eur. J. Biochem.*, 150, 29-34.
- Blumer M. (1950) Porphyrinfarbstoffe un Porphyrin-Metallkomplexe in schweizerische Bitumina. *Helv. Chim. Acta*, 33(4), 1627-1637.
- Blumer M. & Omenn G.S. (1961) Fossil porphyrins: uncomplexed chlorins in a Triassic sediment. *Geochim. Cosmochim. Acta*, 25, 81-90.
- Blumer M. & Snyder W.D. (1965) Isoprenoid hydrocarbons in recent sediments: presence of pristane and probable absence of phytane. *Science*, 150, 35-45 1588-1589.
- Blumer M. & Snyder W.D. (1967) Porphyrins of high molecular weight in a Triassic oil shale: Evidence by gel permeation chromatography. *Chem. Geol.*, 2, 35-45.
- Bohlke J.K., Radke A.S., Heropoulos C. and Lamothe P.J. (1981) Spectroscopic geochemical of vanadiniferous marine sediments of the Gibellini Claims, southern Fish Creek Range, Eureka County, Nevada. *USGS Open File Report*, 81-32,.
- Botz R., Faber E., Whiticar M.J. and Brooks J.M. (1988) Authigenic carbonates in sediments from the Gulf of Mexico. *Earth Plan. Sci. Letters*, 88, 263-272.
- Boudreau B.P. and Westrich J.T. (1984) The dependence of bacterial sulfate reduction on sulfate concentration in marine sediments. *Geochim. Cosmochim. Acta*, 48, 2503-2516.
- Brack P. (1984) *Geologie der Intrusiva und Rahmengesteine des Südwest-Adamello*. Unpubl. Diss. ETH, Diss. Nr. 7612, 253 p.
- Brack P. and Rieber H. (1991) Refined age calibration of the South Alpine Middle Trias: new fossils and correlations of Anisian/Ladinian-boundary sections. In prep.
- Brack P. & Rieber H. (1986) Stratigraphy and ammonoids of the Lower Buchenstein Beds of the brescian Prealps and Giudicarie and their significance for the Anisian/Ladinian boundary. *Eclogae Geol. Helv.*, 79(1), 181-225.
- Bralower T.J. and Thierstein H.R. (1987) Organic carbon and trace metal accumulation rates in Holocene and mid-Cretaceous sediments: palaeoceanographic significance. In : Brooks J. and Fleet A.J. (eds): *Marine Petroleum source rocks*. *Geol. Soc. Spec. Publ*, 26, 345-370.
- Brassel S.C., Eglington G., Maxwell J.R. and Philp R.P. (1978) Natural background of alkanes in the aquatic environment. In: Hutzinger O., van Lelyveld L.H. and Zoeteman B.C.J. (eds): *aquatic pollutants, transformation and biological effects*. Pergamon, Oxford, 69-86.

- Brassel S.C., Wardroper A.M.K. Thomson I.D., Maxwell J.R. & Eglington G. (1981) Specific acyclic isoprenoids as biological markers of methanogenic bacteria in marine sediments. *Nature*, 290, 693-696.
- Broecker W. & Peng T.H. (1983) Tracers in the sea. Lamont-Doherty, Geol. Observ. N.Y., , 690 p.
- Brongersma-Sanders M. (1966) Origin of trace metal enrichments in bituminous shales. In Hobson G.D. and Speers G.C. (eds). *Advances in Organic Geochemistry*. Pergamon press., , 231-236.
- Brooks J.D., Gould K and Smith J.W. (1969) Isoprenoid hydrocarbons in coal and petroleum. *Nature*, 222, 257-259.
- Brumsack H.J. (1980) Geochemistry of Cretaceous black shales from the Atlantic ocean (DSDP Legs 11, 14, 36 and 41). *Chem. Geol*, 31, 1-25.
- Brumsack H.J. (1986) the inorganic geochemistry of Cretaceous black shales (DSDP leg 141) in comparison to modern upwelling sediments from the Gulf of California. In: Shackleton N.J. and Summerhayes C.P. (eds) *North Atlantic paleoceanography*. Geol. Soc. Spec. Publ., 21, 447-462.
- Brusca C., Gaetani M., Jadoul F. and Viel G. (1981) Paleogeografia e metallogenesi del Triassico Sudalpino. In: Omenetto P. (ed.) *Correlazioni tra paleogeografia e mineralizzazioni*. Mem. Soc. Geol It., 22, 65-82.
- Buletti M. (1985) Petrographisch-geochemische Untersuchungen im Luganer Porphyrgbiet. Unpubl. Diss. Univ. Bern 157 pp
- Bürgin T., Rieppel O., Sander P.M. and Tschanz K. (1989) The fossils of Monte San Giorgio. *Sci. Am.*, 260, 50-57.
- Burnett W.C., Landing W.M., Lyons W.B. and Orem W. (1989) Jellyfish Lake, Palau: A model anoxic environment for geochemical studies. *EOS, Transactions, American Geophysical Union*, 70/33, 777-783.
- Burns S.J. & Baker P.A. (1987) A geochemical study of dolomite in the Monterey Formation, California. *J.S.P.*, 57, 128-139.
- Burns S.J., Baker P.A. & Showers W.J. (1988) The factors controlling the formation chemistry of dolomite in organic-rich sediments: Miocene Drakes Bay Formation, California. In : *Sedimentology and geochemistry of dolostone*. SEPM Spec. Publ., 43, 41-52.
- Caby R. and Galli J. (1964) Existence de cinérites et de tufs volcaniques dans le Trias moyen de la zone Briançonnaise. *C.R. Acad. Sc. Paris*, 259/2, 417-420.
- Calder J.A. and Parker P.L. (1973) Geochemical implications of induced changes in C-13 fractionations by blue-green algae. *Geochim. Cosmochim. Acta*, 37, 133-140.
- Callegari E. and Der Pieri R. (1967) Unmixing in the sanidines of the "Pietra verde" of the Dolomites (Italy). *Schweiz. mineral. petrogr. Mitt.*, 47, 111-119.
- Calvert S.E. (1987) Oceanographic controls on the accumulation of organic matter in marine sediments. In : Brooks J. and Fleet A.J. (eds): *Marine Petroleum source rocks*. Geol. Soc. Spec. Publ, 26, 137-152.
- Carpenter A.B. (1980) The chemistry of dolomite formation I: the stability of dolomite. In: Zenger D.A., Dunham J.B. and Ethington R.G. (eds): *Concepts and models of dolomitization*. SEPM Spec. Publ., 28, 111-121.
- Cassani F., Gallango O., Talukdar S., Vallejos C. & Ehrmann U. (1988) Methylphenantrene index of marine source rock extracts and crude oils from the Maracaibo Basin. *Org. Geochem.*, 13, 73-80.

- Chicarelli M.I. and Maxwell J.R. (1984) Naturally occurring, chlorophyll b related porphyrin. *Tetrahedron Lett*, 25/41, 4701-4704.
- Chicarelli M.I., Eckardt C.B., Owen C.R., Maxwell J.R., Eglington G., Hutton R.C. and Eaton A.N. (1990) Application of inductively coupled plasma-mass spectrometry in the detection of organometallic compounds in chromatographic fractions from organic-rich shales. *Org. Geochem.*, 15/3, 267-274.
- Chicarelli M.I., Kaur S. & Maxwell J.R. (1987) Sedimentary porphyrins: unexpected structures, occurrence and possible origins. In : Filby R.H. & Branthaver J.F. (eds): *Metal complexes in fossil fuels*, Am. Chem. Soc. Symposium Series, 344, 40-67.
- Chicarelli M.I., Wolff G.A., Murray M. and Maxwell J.R. (1984) Porphyrins with a novel exocyclic ring system in an oil shale. *Tetrahedron*, 40 no. 20, 4033-4039.
- Claypool G.E., Holser W.T., Kaplan I.R., Sakai H. and Zak I. (1980) The age curves of sulfur and oxygen isotopes in marine sulfate and their mutual interpretation. *Chem. Geol.*, 28, 199-260.
- Clayton R.N., Jones B.F. and Berner R.A. (1968) Isotope study of dolomite formation under sedimentary conditions. *Geochim. Cosmochim. Acta*, 32, 415-432.
- Colbert E.H. and Cosgriff J.W. (1974) Labyrinthodont amphyblans from Antarctica. *Amer. Mus. Novit.*, 2611, 1-20.
- Collier R & Edmond J (1984) The trace element geochemistry of marine biogenic particulate matter. *Prog. Oceanogr.*, 13, 113-199.
- Cook H.E. and Mullins H.T. (1983) Basin margin environment. In: Scholle P.A., Bebout D.G. and Moore C.H. (eds): *Carbonate depositional environments*. Am. Assoc. Pet. Geol. Memoir, 33, 539-618.
- Coveney R.M. Jr and Glascock M.D. (1989) A review of the origins of metal-rich Pennsylvanian black shales, central USA, with an inferred role for basinal brines. *Applied Geochemistry*, 4, 347-367.
- Coveney R.M. Jr, Leventhal J.S. Glascock M.D. & Hatch J.R. (1987) Origin of metals and Organic matter in the Mecca Quarry shale member and stratigraphically equivalent beds across the Midwest. *Econ. Geol.*, 82, 915-933.
- Craig H. (1957) The geochemistry of stable carbon isotopes. *Geochim. Cosmochim. Acta*, 3, 53-92.
- Culver D.A. and Brunskill G.J. (1969) Fayetteville Green Lake, New York. 5. Studies of primary production and zooplankton in a meromictic marl lake. *Limnol. Oceanogr.*, 14, 862-873.
- Curiale J.A. & Odermatt J.R. (1989) Short-term biomarker variability in the Monterey Formation, Santa Maria Basin. *Org. Geochem.*, 14, 1 - 13.
- Curioni G. (1863) Sui giacimenti metalliferi e bituminosi nei terreni triasici di Besano. *Mem. R. Istituto Lombardo di Scienze*, 9, 241-268.
- De Zanche V. And Farabegoli E. (1988) Anisian paleogeographic evolution in the central-western Southern Alps. *Mem. Sci. Geol.*, 40, 399-411.
- Dean W.E. & Arthur M.A. (1989) Iron-sulfur-carbon relationship in organic-carbon-rich sequences I: Cretaceous western interior seaway. *Am. J. Sci.*, 289, 708-743.
- Dean W.E., Arthur M.A. and Claypool G.E. (1986) Depletion of ^{13}C in Cretaceous marine organic matter: source diagenetic or environmental signal?. *"Mar. Geol."*, 70, 119-157.

- Degens E.T. (1969) Biochemistry of stable carbon isotopes. In: Eglinton G. and Murphy M.J.T. (eds). *Organic geochemistry methods and results.*, Springer Verlag, New York, 304-356.
- Degens E.T. and Ross D.A. (1972) Chronology of the Black Sea over the last 25,000 years. *Chem. geol.*, 10, 1-16.
- Demaison G.J. & Moore G.T. (1980) Anoxic environments and oil source bed genesis. *Am. Assoc. Pet. Geol. Bull.*, 64, 1179-1209.
- Deuser W.G. (1975) Reducing environments. In: Riley J.P., Chester R.(Eds): *Chemical Oceanography*, 3, 1-37 Academic Press, London.
- Dickmann M. and Artuz I. (1978) Mass mortality of photosynthetic bacteria as a mechanism for dark lamina formation in the sediments of the Black Sea. *Nature*, 275, 191-195.
- Dinur D., Spiro, B. & Alzenshtat Z. (1980) The distribution and isotopic composition of sulfur in organic-rich sedimentary rocks. *Chem. Geol.*, 31, 37-51.
- Duncan A.D. and Hamilton R.F.M. (1988) Palaeolimnology and organic geochemistry of the Middle Devonian in the Orcadian Basin. In: Fleet, A.J., Kelts K. and Talbot M.R. (eds) *Lacustrine Petroleum Source Rocks*. *Geol. Soc. Spec. Publ.*, 40, 173-201.
- Durand B. (1980) *Kerogen*. Editions Technip, Paris.
- Dydik B.M., Simoneit B.R.T., Brassel S.C. and Eglinton G. (1978) Organic geochemical indicators of paleoenvironmental conditions of sedimentation. *Nature*, 272, 216-222.
- Einsele G. & Seilacher A. (1982) *Cyclic and event stratification*. Springer Verlag, 536 p.
- Emerson S. & Hedges J.I. (1988) Processes controlling the organic carbon content of open ocean sediments. *Paleoceanography*, 3, No.5, 621-634.
- Espitalié J. (1986) Use of Tmax as a maturation index for different types of organic matter. Comparison with vitrinite reflectance. In Burrus J.(ed) *Thermal modeling in sedimentary basins*. IFP Expl. Res. Conf. Technip. Paris, 44, 565-583.
- Espitalié J., Deroo G. & Marquis F. (1985) La pyrolyse Rock-Eval et ses applications. Partie 1 et 2. *Revue Inst Fr. Petr.*, 40/5-6, .
- Espitalié J., Deroo G. & Marquis F. (1986) La pyrolyse Rock-Eval et ses applications. Partie 3. *Revue Inst Fr. Petr.*, 41/1, .
- Eugster H.P. & Hardie L.A. (1978) Sedimentation in an ancient playa-lake complex: the Wilkins Peak Member of the Green River Formation of Wyoming. *Geol. Soc. Am. Bull.*, 86, 319-334.
- Farabegoli E. & De Zanche V. (1984) A revision of the Anisian stratigraphy in the western southern Alps (west of Lake Como). *Mem. Ist. Geol. Min. Univ. Pavia*, 36, 391-401.
- Folk R.L. & Pittman J.S. (1971) Length-slow chalcedony: a new testament for vanished evaporites. *J. Sed. Petrol.*, 41, 1045-1058.
- Frauenfelder A. (1916) Beiträge zur Geologie der tessiner Kalkalpen. *Eclogae Geol. Helv.*, 14, 247-367.
- Freeman K.H., Hayes J.M., Trendel J-M. and Albrecht P. (1990) Evidence from carbon isotope measurements for diverse origin of sedimentary hydrocarbons. *Nature*, 343, 254-256.

- Frisia-Bruni S., Jadoul F. and Weissert H. (1989) Evinosponges in the Triassic Esino limestone (Southern Alps): documentation of early lithification and late diagenetic overprint. *Sedimentology*, 36, 685-700.
- Fry B. (1986) Source of carbon and sulfur nutrition for consumers in three meromictic lakes of New York state. *Limnol. Oceanogr.*, 31(1), 79-88.
- Gaetani M. (1982) Elementi stratigrafici e strutturali della galleria Bellano-Varenna (Nuova ss36) (Como). *Riv. It. Pal. Strat.*, 88, 1-10.
- Gaetani M., Gianotti R., Jadoul F., Ciarapica G., Cirilli S., Lualdi A., Passeri L., Pellegrini M. and Tannoia G. (1986) Carbonifero superiore, Permiano e Triassico nell' area lariana. *Mem. Soc. Geol. It.*, 32, 5-48.
- Galbiati B. and Vanossi M. (1986) Caratteristiche sedimentologiche e strutturali del calcare di Perledo -Varenna. *Convegno di Geologia Lariana, Guida alle escursioni*, 104-109.
- Garrison R.E., Kastner, M. and Zenger D.H. (eds) (1984) Dolomites of the Monterey Formation and other organic-rich units. *Pac. Sect. SEPM spec. publ.*, 41, 215p.
- Garzanti E. (1985) The sandstone memory of the evolution of a Triassic volcanic arc in the Southern Alps, Italy. *Sedimentology*, 32, 423-433.
- Gianotti R. & Tannoia G. (1988) Elementi per una revisione stratigrafico-paleontologica del Trias medio superiore della regione compresa tra il Lario e il Ceresio. *Mem. Soc. Geol. It.*, . . .
- Giger W., Schaffner C. & Wakeham S.G. (1980) Aliphatic and olefinic hydrocarbons in recent sediments of Greifensee, Switzerland. *Geochim. Cosmochim. Acta*, 44, 119-129.
- Glenn C.R., Arthur M.A., Yeh H. & Burnett W.C. (1988) Carbon isotopic composition and lattice-bound carbonate of Peru-Chile margin phosphorites. *Mar. Geol.*, 80, 287-307.
- Goldhaber M.B. and Kaplan I.R. (1974) The sulfur cycle. In: Goldberg E.D. (ed): *The Sea*, . . . vol. 5, 569-655.
- Goldhammer R.K., Dunn P.A. and Hardie L.A. (1990) Depositional cycles, composite sealevel changes, cycle stacking patterns, and the hierarchy of stratigraphic forcing: examples from the Alpine Triassic platform carbonates. *GSA Bull.*, 102, 535-562.
- Goldhammer R.K. Dunn P.A. & Hardie L.A. (1987) High frequency glacio-eustatic sealevel oscillations with Milankowitch characteristics recorded in middle triassic carbonates of Northern Italy. *Am. Jour. Sci.*, 287, 853-892.
- Grasshoff K. (1975) The hydrochemistry of landlocked basins and fjords. In: Ryley J.P. and Chester R. (eds). *Chemical Oceanography*, Vol. 2, Academic press, London, 456-598.
- Grossman E.T. and Ku T.L. (1981) Aragonite-water isotopic paleotemperature scale based on the benthic foraminifera *Hoeglundia elegans*. *Geol. Soc. Am. Abstr. Prog.*, 13, 464.
- Gulbrandsen R.A. (1970) Relation of carbon dioxide content of apatite of the Phosporia Formation to regional facies. *USGS Prof. Pap.*, 700(B), B9-B13.
- Hardie L.A. (1987) Perspectives: Dolomitization: a critical view of some current views. *Jour. Sed. Petr.*, 57, 166-183.
- Hardie L.A. and Shinn E.A. (1986) Carbonate depositional environments, modern and ancient, 3, Tidal Flats. *Colorado School of Mines Quart.*, 81(1), 74p.

- Hardy R. and Tucker M.E. (1988) X-ray powder diffraction of sediments. In Tucker M.E. (ed) *Techniques in sedimentology*. Blackwell Sci. Publ., Oxford.
- Hargrave B.T. (1975) The central role of invertebrate faeces in sediment decomposition In: Anderson J.M. and MacFadden (eds): *The role of Terrestrial and aquatic organisms in decomposition processes*. Blackwell Scientific Publications, Oxford, 301-321.
- Hayes J.M., Takigiku R., Ocampo R., Callot H.J. & Albrecht P. (1987) Isotopic compositions and probable origins of organic molecules in the Eocene Messel Shale. *Nature*, 329, 48-51.
- Hellmann K.N. & Lippolt H.J. (1981) Calibration of the Middle Triassic time scale by conventional K-Ar and Ar/Ar Dating of alkali feldspars. *J. Geophys.*, 50, 73-88.
- Hoefs J. and Frey M. (1976) The isotopic composition of carbonaceous organic matter in metamorphic profile from the Swiss Alps. *Geochim. Cosmochim. Acta*, 40, 1019-1029.
- Hofmann F. (1956) Zur Frage der Entstehung des glimmerartigen Tons in der Trias des Monte Caslano, Kanton Tessin. *Schweiz. mineral. petrogr. Mitt.*, 36/2, 489-496.
- Hollander D.J. (1989) Carbon and nitrogen isotopic cycling and organic geochemistry of eutrophic lake Greifen: Implications for preservation and accumulation of ancient organic carbon-rich sediments. Unpubl. Diss. ETH, 318 p.
- Indrebø G., Pengerud B. and Dundas I. (1979a) Microbial activity in a permanently stratified estuary. 1. Primary production and sulfate reduction. *Mar. Biol.*, 51, 295-304.
- Indrebø G., Pengerud B. and Dundas I. (1979b) Microbial activity in a permanently stratified estuary. 2. Microbial activities at the oxic-anoxic interface. *Mar. Biol.*, 51, 305-309.
- Irwin H, Curtis C.D. and Coleman M.L. (1977) Isotopic evidence for source of diagenetic carbonates formed during burial of organic-rich sediments. *Nature*, 269, 209-213.
- Jacobs L., Emerson S. and Skei J. (1985) Partitioning and transport of metals across the O₂/H₂S interface in a permanently anoxic basin: Framavaren Fjord, Norway. *Geochim. Cosmochim. Acta*, 49, 1433-1444.
- Jadoul F & Rossi P.M. (1982) Evoluzione Paleogeografico strutturale e vulcanismo Triassico nella Lombardia centro-occidentale. In Castellarin & Vai(eds): *Guida al sudalpino centro-orientale*. Guide Geol. Reg. S.G.I., 143-155.
- Jarvis J. and Higgs N. (1987) Trace element mobility during early diagenesis in distal turbidites: Late Quaternary of Madeira abyssal plain, North Atlantic. In: Waver P.P.E. and Thomson J. (eds): *geology and geochemistry of abyssal plains*. Geol. Soc. Spec. Publ., 31, 179-213.
- Jongmans W.J. (1960) Die Karbonflora der Schweiz. *Beitr. Geol. Karte Schweiz*, NF108, 97 p.
- Jorgensen B.B. (1989) Biogeochemistry of chemoautotrophic bacteria. In: Schlegel H.G. and Bowien B. (Eds): *Autotrophic bacteria.*, Brock/Springer Series in Contemporary Bioscience, 117-146.
- Karhu J. & Epstein S. (1986) The implication of the oxygen isotope records in coexisting cherts and phosphates. *Geochim. Cosmochim. Acta*, 50, 1745-1756.
- Kastner M., Keene J.B. & Gieskes J.M. (1977) Diagenesis of siliceous oozes I. Chemical controls on the rate of opal-A to opal-CT transformation - an experimental study. *Geochim. Cosmochim. Acta*, 41, 1041-1059.

- Kelly M. and Naguib M. (1984) "Eutrophication in coastal marine areas and lagoons: a case study of Lac de Tunis.". *Unesco reports in marine science*, 29, 54p.
- Kelts K. & McKenzie J.A. (1982) Diagenetic dolomite formation in quaternary anoxic diatomaceous muds of DSDP leg 64, Gulf of California. *Init. Rep. DSDP*, 64, 553-569.
- Kelts K. & McKenzie J.A. (1984) A comparison of anoxic dolomite from deep-sea sediments: Quaternary Gulf of California and Messinian Tripoli Formation of Sicily. In: Garrison R.E., Kastner M and Zenger D.H. (Eds.): *Dolomites of The Monterey Formation and other organic-rich units.*, SEPM Pac. Sect. Spec. Publ., 19-28.
- Knaut L.P. & Epstein S. (1976) Oxygen and hydrogen isotope ratios in nodular and bedded cherts. *Geochim. Cosmochim. Acta*, 40, 1095-1108.
- Kolodny Y & Epstein S. (1976) Stable isotope geochemistry of deep sea cherts. *Geochim. Cosmochim. Acta*, 40, 1195-1209.
- Krebs B. (1965) *Ticinosuchus ferox* nov. gen. nov. sp. In: Kuhn-Schnyder E. and Peyer B. (Eds): *Die Trias Fauna der Tessiner Kalkalpen XIX*. Schweiz. Paläont. Abh., 81, 1-140.
- Kuhn-Schnyder E. (1974) *Die Triasfauna der Tessiner Kalkalpen*. VrtJh. Natf. Ges. Zürich, 119 pp.
- Kutzbach J.E. & Gallimore R.G. (1989) Pangaeian climates: Megamonsoon of the megacontinent. *Jour. Geophys. Res.*, 94, 3341-3357.
- Land L.S. (1985) The origin of massive dolomite. *J. Geol. Education*, 33, 112-125.
- Langford F.F. & Blanc-Valleron M.M (1990) Interpreting Rock-Eval pyrolysis data using graphs of pyrolyzable hydrocarbons vs. total organic carbon. *Am. Assoc. Pet. Geol. Bull.*, 74, 709-806.
- Lehner P. (1952) Zur Geologie des Gebietes der Denti della Vecchia, des M. Boglia, des M. Bre und des M. San Salvatore bei Lugano. *Eclogae. Geol. Helv.*, 45, 85-159.
- Leuzinger P. (1926) Geologische Beschreibung des M. Campo dei Fiori und der Sedimentzone Luganersee-Valcuvia. *Eclogae geol. Helv.*, 20, 90-157.
- Leventhal J.S. (1979) Carbon and sulfur relationships in Devonian shales from the Appalachian Basin as an indicator of environment of deposition. *Am. J. Sci.*, 287, 33-49.
- Leventhal J.S. (1983) An interpretation of carbon and sulfur relationships in Black Sea sediments as indicator of environments of deposition. *Geochim. Cosmochim. Acta*, 47, 133-138.
- Lewan M.D. (1986) Stable carbon isotopes of amorphous kerogens from Phanerozoic sedimentary rocks. *Geochim. Cosmochim. Acta.*, 50, 1583-1591.
- Leythaeuser D. and Schwarzkopf Th. (1986) The pristane/n-heptadecane ratio as an indicator for recognition of hydrocarbon migration effects. *Org. Geochem.*, 10, 191-197.
- Lijmbach G.W.M. (1975) On the origin of petroleum. *Proc. 9th. world petrol. congress*, 357-369.
- Lipiner G., Willner I. and Aizenshtat Z. (1988) Correlation between geochemical environments and controlling factors in the metallation of porphyrins. *Org. Geochem.*, 13, 747-756.

- MacKenzie A.S. and Maxwell J.R. (1981) Assessment of thermal maturation in sedimentary rocks by molecular measurements. In: Brooks J. (ed): Organic maturation studies and fossil fuel exploration., 239-253.
- MacKenzie A.S., Brassel S.C., Eglington G. and Maxwell J.R. (1982) Chemical fossils: the geological fate of steroids. *Science*, 217, 491-504.
- MacKenzie A.S., Brassel S.C., Eglington G. & Maxwell J.R. (1982) Chemical fossils: the geological fate of steroids. *Science*, 217, 491-504.
- MacKenzie A.S., Hoffman C.F. & Maxwell J.R. (1981) Molecular parameters of maturation in Toarcian shales, Paris Basin, France. III- Changes in aromatic hydrocarbons. *Geochim. Cosmochim. Acta.*, 45, 1345-1355.
- MacKenzie A.S., Patience R.L., Maxwell J.R., Vandenbroucke M. & Durand B. (1980) Molecular parameters of maturation in Toarcian shales, Paris Basin, France. I- Changes in the configuration of acyclic isoprenoid alkanes, steranes and triterpanes. *Geochim. Cosmochim. Acta*, 44, 1709-1721.
- Mallory F.B., Gorton J.T. and Conner R.L. (1963) The isolation of a pentacyclic triterpenoid alcohol from a protozoan. *J. Am. Chem. Soc.*, 85, 1326-1363.
- Martin J.H. and Knauer G.A. (1973) The elemental composition of marine plankton. *Geochim. Cosmochim. Acta*, 37, 1639-1653.
- Mattews A. and Katz A. (1977) oxygen isotope fractionation during the dolomitization of calcium carbonate. *Geochim. Cosmochim. Acta*, 41, 1431-1438.
- McCrea J.N. (1950) On the isotopic chemistry of carbonates and a paleotemperature scale. *J. Chem. Phys.*, 18, 849-857.
- McEvoy J. & Giger W (1985) Origin of hydrocarbons in Triassic Serpiano oil shales: Hopanoids. *Org. Geochem.*, 10, 943-949.
- McKenzie J.A. (1981) Holocene dolomitization of calcium carbonate sediments from the coastal sabkhas of Abu Dhabi, U.A.E.: a stable isotope study. *Jour. Geol.*, 89, 185-198.
- McRea J.M. (1950) On the isotope chemistry of carbonates and a paleotemperature scale. *J. Chem. Phys.*, 18, 849-857.
- Mekhtiyeva V.L., Gavrilov Y.Y. and Pankina R.G. (1976) Sulfur isotope composition in land plants. *Geochem. Int.* 13, 85-88.
- Middelburg J.B.M. (1990) Early diagenesis and authigenic mineral formation in anoxic sediments of Kahu Bay, Indonesia. *Geologica Ultratrectina*, 71, 177 pp.
- Middelburg J.J., de Lange G.J. & Kreulen R. (1990) Dolomite formation in anoxic sediments of Kau Bay, Indonesia. *Geology*, 18, 399-402.
- Moldowan J.M., Seifert W.K. & Gallegos E.J. (1983) Identification of an extended series of tricyclic terpanes in petroleum. *Geochim. Cosmochim. Acta.*, 47, 1531-1534.
- Moldowan J.M., Sundararaman P. and Schoell M. (1986) Sensitivity of biomarker properties to depositional environment and/or source input in the Lower Toarcian of SW Germany. *Org. Geochem.*, 10, 915-926.
- Müller W. (1964) Conodonten aus der mittleren Trias der Tessiner Kalkalpen. *Eclogae Geol. Helv.*, 57/2, 747-753.
- Müller W. (1965) Beitrag zur Sedimentologie der Grenzbitumenzone vom M. S. Giorgio (Kt. Tessin) mit Rücksicht auf die Beziehung Fossil-Sediment. Unpubl. Diss, Basel, unknown, 228 pp.

- Müller W., Schmid R & Vogt P. (1964) Vulkanogene Lagen aus der Grenzbitumenzone (Mittlere Trias) des M. S. Giorgio in den Tessiner Kalkalpen. *Eclogae Geol. Helv.*, 57/2, 431-450.
- Murata K.J., Friedman I & Gleason J.D. (1977) Oxygen isotope relations between diagenetic silica minerals in Monterey Shale, Tremblor Range, California. *Am. J. Sci.*, 277, 259-272.
- Murata K.J. & Randall R.G. (1975) Silica mineralogy and structure of the Monterey shale, Tremblor Range, California. *U.S.G.S. J. of Res.*, 3 (5), 567-572.
- Nelson R.B. & Lindsley-Griffin N. (1987) Biopressured carbonate turbidite sediments: A mechanism for submarine slumping. *Geology*, 15, 817-820.
- Nissenbaum A., Presley B.J. and Kaplan J.R. (1972) Early diagenesis in a reducing Fjord. Saanich Inlet, British Columbia - I Chemical and isotopic changes in major components of interstitial waters. *Geochim. Cosmochim. Acta*, 36, 1007-1027.
- Orr W.L. (1974) Changes in sulfur content and isotopic ratios of sulfur during petroleum maturation - Study of Big Horn basin paleozoic oils. *Am. Assoc. Pet. Geol. Bull.*, 50(11), 2295-2318.
- Ourisson G., Albrecht P. and Rohmer M. (1982) Predictive microbial biochemistry a forensic approach to prokaryotic membrane constituents. *Trends Biochem. Sci.*, 7, 236-239.
- Ourisson G., Rohmer M. and Poralla K. (1987) Prokaryotic hopanoids and other polyterpenoid sterol surrogates. *Ann. Rev. Microbiol.*, 41, 301-333.
- Palacas J.G., Anders D.E. and King J.D. (1985) South Florida Basin - a prime example of carbonate source rocks of petroleum. In Palacas J.G. (ed.) *Petroleum potential and source rock potential of carbonate rocks*. Am. Assoc. Pet. Geol. Studies in Geology, 18, Tulsa, 71-86.
- Parrish J.M., Parrish J.T. & Ziegler A.M. (1986) Permian-Triassic paleogeography and paleoclimatology and implications for therapsid distribution. In: Hotton N., MacLean P.D., Roth J.J. & Roth C. E. (eds): *The ecology and biology of mammalian-like reptiles.*, Smithsonian Inst. Press, 109-131.
- Parsons T.R., Taskahashi M. and Hargrave B. (1984) *Biologic oceanographic processes*. Pergamon press., 330 p.
- Pedersen T.F. and Calvert S.E. (1990) Anoxia vs. productivity: What controls the formation of organic-carbon-rich sediments and sedimentary rocks?. *Am. Assoc. Pet. Geol. Bull.*, 74, 454-466.
- Philp R.P. (1985) Fossil fuel biomarkers, application and spectra. *Methods in geochemistry and geophysics*, (Elsevier), 23, 294 pp.
- Pieri M. & Mattavelli L. (1986) Geologic framework of Italian petroleum resources. *Am. Assoc. Pet. Geol. Bull.*, 70, 103-130.
- Pisciotta K.A. (1981) Review of secondary carbonates in the Monterey Formation, California. In: Garrison et al (eds): *The Monterey formation and related siliceous rocks of California*. SEPM, Pac. Sect., 273-283.
- Pisciotta K.A. and Mahoney J.L. (1981) isotopic survey of diagenetic carbonates, Deep Sea Drilling Project Leg 63. *Init. Reports DSDP*, 63, 595-609.
- Popp B.N., Takigiku R., Hayes J.M., Louda J.W and Baker E.W. (1989) The post-Paleozoic chronology and mechanism of ^{13}C depletion in primary marine organic matter. *Am. J. Sci.*, 289, 436-454.

- Pratt L.M. (1984) Influence of paleoenvironmental factors on preservation of organic matter in Middle Cretaceous Greenhorn Formation. *Am. Assoc. Pet. Geol. Bull.*, 68, 1146-1159.
- Pratt L.M., Claypool G.E. and King J.D. (1986) Geochemical imprint of depositional conditions on organic matter in laminated-bioturbated interbeds from fine-grained marine sequences. *Mar. Geol.*, 70, 67-84.
- Premovic P.I., Pavlovic M.S. & Pavlovic N.Z. (1986) Vanadium in ancient sedimentary rocks of marine origin. *Geochim. Cosmochim. Acta*, 50, 1923-1931.
- Radke M., Welte D.H. & Willsch H. (1986) Geochemical study on a well in the Western Canada Basin: Relation of the aromatic distribution pattern to maturity of organic matter. *Geochim. Cosmochim. Acta*, 46, 1831-1848.
- Raiswell R. (1988) Chemical model for the origin of minor limestone-shale cycles by anaerobic methane oxidation. *Geology*, 16, 641-644.
- Raiswell R. & Berner R.A. (1987) Organic carbon loss during burial and thermal maturation of normal marine shales. *Geology*, 15, 853-856.
- Reeder J. & Grams J.C. (1987) Sector zoning in calcite cement crystals: implication for trace element distribution in carbonates. *Geochim. Cosmochim. Acta.*, 51, 187-194.
- Reinhard (1953) Ueber das Grundgebirge des Sottoceneri im südlichen Tessin. *Eclogae Geol. Helv.*, 46, 214-222.
- Retallack G. (1975) The life and times of a Triassic lycopod. *Alcheringa*, 1, 3-29.
- Ricken W. (1986) Diagenetic bedding. a model for marl-limestone alternations. Lecture notes in Earth Sci. 6, Springer Verlag, 210 p.
- Rickenbach E. (1947) Vorkommen von bituminösen Schiefern. In: *Erdölgeologische Untersuchungen in der Schweiz-Beitr. Geol. Schweiz, Geotechn. Serie*, 26-1 .
- Rieber H. (1968b) Zur Entstehung der Grenzbitumenzone der Mittleren Trias der Tessiner Kalkalpen. *Bull. Ver. Schweiz. Petrol. Geol.u. Ing.*, 35/87, 55-62.
- Rieber H. (1968a) Die Artengruppe *Daonella Elongata* Mojs. aus der Grenzbitumenzone der mittleren Trias des Monte San Giorgio (Kt. Tessin, Schweiz). *Paläont. Z.*, 42, 33-61.
- Rieber H. (1973) Ergebnisse palaeontologisch-stratigraphische Untersuchungen in der Grenzbitumenzone (Mittlere Trias) des Monte S. Giorgio (Kanton Tessin, Schweiz). *Eclogae Geol. Helv.*, 66/3, 667-685.
- Rieber H. (1973) Cephalophoden aus der Grenzbitumenzone (Mittlere Trias) des Monte S. Giorgio (Kanton Tessin, Schweiz) .In Peyer & Kuhn-Schnyder (eds): *Die Triasfauna der Tessiner Kalkalpen. XXII. Schweiz. Pal. Abh.*, 93, 1-96.
- Rieber H. and Sorbini L. (1983) Middle Triassic bituminous shales of Monte San Giorgio(Tessin, Switzerland. *First. Int. Congr. Paleoecol. Excursion*, 11A, 1-40.
- Rieppel O. (1987) The pachypleurosauridae: an annotated bibliography. with comments on some Lariosaurs. *Eclogae. Geol. Helv.*, 80, 1105-1118.
- Risatti J.B., Rowland S.J., Yon D.A. and Maxwell J.R. (1983) Stereochemical studies of acyclic isoprenoids-XII. Lipids of methanogenic bacteria and possible contributions to sediments. *Org. Geochem.*, 6, 93-104.
- Riva A., Salvatori T. Cavaliere R., Ricchiuto T. & Novelli L. (1986) Origin of oils in Po basin, Northern Italy. *Org. Geochem.*, 10, 391-400.

- Roedder E. (1984) Fluid inclusions. Rev. in Mineral., Mineralogical Society of America, 12, 645 pp.
- Sander P.M. (1989) The pachypleurosaurids (Reptilia: Nothosauria) from the Middle Triassic of Monte San Giorgio (Switzerland) with the description of a new species. Phil. Trans. Roy. Soc. London, 325/1230, 561-670.
- Scherrer M. (1977) Preservation, alteration and multiple cementation of aragonite skeletons from the Cassian Beds (Southern Alps), petrographical and geochemical evidence. Neues Jb. Geol. Paleont. Abh., 154, 233-262.
- Scheuring B.W. (1978) Mikrofloren aus den Meride Kalken des Monte S. Giorgio (Kanton Tessin). Schweiz. Pal. Abh., 100, 1-203.
- Schieber J. (1986) The possible role of benthic microbial mats during the formation of carbonaceous shales in shallow Mid-Proterozoic basins. Sedimentology, 33, 521-536.
- Schieber J. (1989) Facies and origin of shales from the mid-Proterozoic Newland Formation, Belt basin, Montana, USA. Sedimentology, 36, 203-219.
- Schoell M. (1984) Stable isotopes in petroleum research. In: Brooks J. and Welte D. (eds): . Advances in petroleum geochemistry, Vol 1, Academic Press, London, 215-245.
- Schoell M., Faber E. and Coleman M.L. (1983) Carbon and hydrogen isotopic compositions of the NBS 22 and NBS 21 stable isotope reference materials: an interlaboratory comparison. Org. Geochem., 5/1, 3-6.
- Schwarz H-U. (1982) Subaqueous slope failures- experiments and modern occurrences. Contrib. to Sedimentology, 11, 116 pp.
- Schwarz W. (1970) *Birgeria stensiöi* ALDINGER. In: Kuhn-Schnyder E. and Peyer B. (Eds): Die Trias Fauna der Tessiner Kalkalpen XX. Schweiz. Paläont. Abh., 89, 1-93.
- Seifert W.K. & Moldowan J.M. (1978) Applications of steranes, terpanes and monoaromatics to the maturation, migration and source of crude oils. Geochim. Cosmochim. Acta, 42, 77-92.
- Seifert W.K. & Moldowan J.M. (1980) The effect of thermal stress on source rock quality as measured by hopane stereochemistry. In: Douglas A.D. and Maxwell J.R. (eds): "Adv. in Org. Geochemistry 1979", Pergamon press, Oxford, 229-237.
- Seifert W.K. & Moldowan J.M. (1986) Use of biological markers in petroleum exploration. In: Johns R.B. (ed): Biological markers in the sedimentary record. Methods in geochemistry and geophysics (Elsevier), 24, 261-290.
- Senn A. (1924) Beiträge zur Geologie des Alpen Südrandes zwischen Mendrisio und Varese. Eclogae Geol. Helv., 18, 550-632.
- Shackleton N.J. and Kennett J.P. (1975) Paleotemperature history of the Cenozoic and the initiation of Antarctic glaciation: oxygen and carbon isotope analyses in DSDP sites 277, 279 and 281. In: Kennett et al. (eds). Init. Rep. DSDP, 19, 743-755.
- Shemesh A., Kolodny Y. & Luz B. (1988) Isotope geochemistry of oxygen and carbon in phosphate and carbonate of phosphorite francolite. Geochim. Cosmochim. Acta, 52, 2565-2572.
- Shimmield G.B and Price N.B. (1984) Recent dolomite in hemipelagic sediments of Baja California. In: Garrison R.E., Kastner M and Zenger D.H. (Eds.): Dolomites of The Monterey Formation and other organic-rich units. SEPM Pac. Sect. Spec. Publ., 5-18.
- Sinninghe-Damsté J.S. (1988) Organically bound sulfur in the geosphere: a molecular approach. Unpubl. Diss, Delft, 287 pp.

- Smith I.R. and Sinclair I.J. (1972) Deep water waves in lakes. *Freshwater Biology.*, 2, 387-399.
- Spiker E.C. and Hatcher P.G. (1984) Carbon isotope fractionation of sapropelic organic matter during early diagenesis. *Org. Geochem.*, 5, 283-290.
- Stach E. (1969) Fortschritte der Auflicht-Fluoreszenz microscopie in der Kohle Petrographie. *Freiberger Forsch.*, C242, 35-55.
- Stanley D.J. (1983) Parallel laminated deep-sea muds and coupled gravity flow-hemipelagic settling in the Mediterranean. *Smithsonian Contributions to Marine Sciences*, 19, 1-19.
- Swift M.J., Heal O.W. and Anderson J.M. (1979) Decomposition in terrestrial ecosystems. University of California Press, Berkeley, 465 p.
- ten Haven H.L., de Leeuw J.W., Rullkötter J. & Sinninghe-Damsté J.S. (1987) Restricted utility of the pristane/phytane ratio as palaeoenvironmental indicator. *Nature*, 330, 641-643.
- ten Haven H.L., de Leeuw J.W., Sinninghe-Damsté J.S., Schenk P.A., Palmer S.E. & Zumberge J.E. (1988) Application of biological markers in the recognition of palaeo-hypersaline environments. In: Fleet et al (Eds): *Lacustrine petroleum source rocks*. Geological Soc. Spec. Publ., 40, 123-130.
- Tissot B.P. & Welte D.H. (1984) *Petroleum formation and occurrence*. Springer, 699 p.
- Tucker M. and Benton M.J. (1982) Triassic environments, climates and reptile evolution. *Palaeogeography, Palaeoclimatology, Palaeoecology*, 40, 361-379.
- Van Deer Eem J.G.L.A. (1983) Aspects of middle and late Triassic palynology. 6. Palynological investigations in the Ladinian and lower Carnian of the western dolomites. *Review of Paleobotany and Palynology*, 39, 189-300.
- Venkatesan M.I. (1989) Tetrahymanol: its widespread occurrence and geochemical significance. *Geochim. Cosmochim. Acta*, 53, 3095-3101.
- Vine J.D. & Turtelot H.A. (1970) Geochemistry of black shale deposits - a summary report. *Econ. Geol.*, 65, 253-272.
- Volkman J.K. (1988) Biological marker compounds as indicators of the depositional environments of petroleum source rocks. In: Fleet et al (Eds): *Lacustrine petroleum source rocks*. Geological Soc. Spec. Publ., 40, 103-122.
- Volkman J.K. & Maxwell J.R. (1986) Acyclic isoprenoids as biological markers. In: Johns R.B. (ed): *Biological markers in the sedimentary record*. Methods in Geochemistry and Geophysics (Elsevier), 24, 1 - 42.
- Wedepohl K.H. (1970) Environmental influences on the chemical composition of shales and clays. In: Ahrens L.H., Press F., Runcorn S.K. and Urey H.C. (eds). *Physics and Chemistry of the Earth*, 8, 305-333.
- Wetzel A. (1982) Cyclic and discyclic Black shale formation. In: Einsele G. & Seilacher A. (eds): *Cyclic and event stratification*. Springer Verlag., , 431-455.
- Whiticar M.J., Faber E. and Schoell M. (1986) Biogenic methane formation in marine and freshwater environments: CO₂ reduction vs. acetate fermentation - isotope evidence. *Geochim. Cosmochim. Acta*, 50, 693-709.
- Williams L.A. (1984) Subtidal stromatolites in Monterey Formation and other organic rich rocks as suggested source contributors to petroleum formation. *Am. Assoc. Pet. Geol. Bull.*, 68, 1879-1893.

- Wirz A. (1945) Beiträge zur Kenntnis des Ladinikums im Gebiete des Monte S. Giorgio. In Peyer & Kuhn-Schnyder (eds): Die Triasfauna der Tessiner Kalkalpen. XV. Schweiz. Pal. Abh., 65, 1-84.
- Wolff G.A., Chicarelli M.I., Shaw R.P., Quirke J.M.E. and Maxwell J.R. (1984) Structure analysis of naturally occurring alkyl porphyrins by hydrogen chemical ionisation mass spectrometry. *Tetrahedron*, 40 no. 19, 3777-3786.
- Wolff G.A., Murray M., Maxwell J.R., Hunter B.K. & Sanders J.K.M. (1983) 15,17-Butano-3,8-diethyl-2,7,12,18-tetramethylporphyrin - a novel occurring tetrapyrrole. *J. Chem. Soc., Chem Commun.*, 623, 921-924.
- Wong W.W. and Sackett W.M. (1978) Fractionation of stable carbon isotopes by marine phytoplankton. *Geochim. Cosmochim. Acta*, 42, 1809-1815.
- Zander J.M., Caspi E., Pandey G.N. and Mitra C.R. (1969) The presence of tetrahymanol in *Oleandra wallichii*. *Phytochemistry*, 8, 2265-2267.
- Zingg A., Handy M.R., Hunziker J.C. and Schmid S.M. (1990) Tectonometamorphic history of the Ivrea zone and its relationship to the crustal evolution of the Southern Alps. *Tectonophysics*, 182, 169-192.
- Zorn H. (1971) Palaeontologische, stratigraphische und sedimentologische Untersuchungen des Salvatore dolomits (Mittlere Trias) der Tessiner Kalkalpen. Schweiz. Pal. Abh., 91, 1-90.
- Zundel M. and Rohmer M. (1985) Hopanoids of the methylotrophic bacteria *Methylococcus capsulatus* and *Methylomonas* sp. as possible precursor of C29 and C30 hopanoid chemical fossils. *FEMS microbiology letters*, 28, 61-64.

Appendix A Continued.

	MI 142	MI 56	MI 120	MI 23	PO 88	MI 129	PO134	MI 115	MI 115o	MI 51	MI 134	MI 136	MI 155o	MI 122	PO 106
SiO2	3.04	13.46	1.21	6.04	12.65	0.88	4.94	2.90	3.04	5.99	4.75	2.23	4.22	4.16	1.20
TiO2	0.04	0.05	0.01	0.05	0.05	0.01	0.06	0.04	0.04	0.03	0.06	0.03	0.05	0.04	0.02
Al2O3	0.95	1.36	0.40	1.78	1.40	0.38	1.35	0.84	0.89	0.87	1.33	0.69	1.10	1.14	0.43
Fe2O3	1.13	2.12	0.19	0.73	0.68	0.19	0.58	0.38	0.39	0.31	0.63	0.86	0.53	0.44	0.18
MnO	0.21	0.02	0.03	0.02	0.02	0.04	0.02	0.02	0.03	0.01	0.01	0.14	0.04	0.03	0.02
MgO	18.58	13.12	17.22	17.31	16.55	19.32	17.51	17.67	18.37	17.34	17.11	19.14	17.75	17.58	19.11
CaO	27.46	19.22	24.75	24.40	23.37	27.65	24.78	24.68	25.75	24.52	24.12	27.66	25.13	24.99	26.79
Na2O	0.05	0.04	0.05	0.07	0.05	0.04	0.07	0.05	0.05	0.05	0.05	0.04	0.04	0.10	0.05
K2O	0.24	0.51	0.09	0.60	0.46	0.08	0.42	0.27	0.30	0.21	0.48	0.13	0.36	0.35	0.08
P2O5	0.08	0.09	0.03	0.04	0.04	0.02	0.04	0.06	0.06	0.06	0.04	0.03	0.07	0.05	0.03
CO2	41.04	22.79	43.24	38.33	33.16	42.94	38.29	20.19	39.30	35.91	36.42	42.80	38.47	36.60	43.31
S	0.29	2.04	0.19	0.42	0.26	0.15	0.41	2.27	0.28	0.26	0.76	0.29	0.24	0.40	0.14
LOI	44.14	39.50	46.30	42.22	39.33	46.85	43.63	45.64	45.39	44.46	44.07	45.22	44.27	44.62	46.33
TOC	1.90	12.09	1.48	2.18	2.18	1.68	2.68	18.98	3.37	3.97	4.21	1.05	2.91	3.86	1.42

Trace elements (ppm)

F	3002	712	2994	2486	2708	3030	2583	201	< 10	2189	2268	2884	2779	2431	2980
Ba	18	20	< 10	35	4	< 10	42	247	< 10	7	73	9	1129	30	6
Rb	< 8	< 8	< 8	< 8	< 8	< 8	< 8	3	< 8	< 8	< 8	< 8	< 8	< 8	< 8
Sr	39	30	26	39	39	41	42	94	22	42	4 < 15	39	71	41	31
Pb	< 5	< 5	< 5	< 5	< 5	< 5	< 5	57	< 5	< 5	< 5	< 5	< 5	< 5	< 5
Th	< 5	< 5	< 5	< 5	< 5	< 5	< 5	< 5	< 5	< 5	< 5	< 5	< 5	< 5	< 5
U	< 10	< 10	< 10	< 10	< 10	< 10	< 10	< 10	< 10	< 10	< 10	< 10	< 10	< 10	< 10
Nb	< 4	< 4	< 4	< 4	< 4	< 4	< 4	< 4	< 4	< 4	< 4	< 4	< 4	< 4	< 4
La	< 20	< 20	< 20	< 20	< 20	< 20	< 20	< 20	< 20	< 20	< 20	< 20	< 20	< 20	< 20
Ce	< 15	< 15	< 15	< 15	< 15	< 15	< 15	< 15	< 15	< 15	< 15	< 15	< 15	< 15	< 15
Ni	< 25	< 25	< 25	< 25	< 25	< 25	< 25	< 25	< 25	< 25	< 25	< 25	< 25	< 25	< 25
Y	< 3	< 3	< 3	< 3	< 3	< 3	< 3	< 3	< 3	< 3	< 3	< 3	< 3	< 3	< 3
Zr	< 10	< 10	< 10	< 10	< 10	< 10	< 10	16	< 10	< 10	< 10	< 10	< 10	< 10	< 10
V	37	1367	50	456	119	117	62	2141	158	378	133	23	29	166	139
Cr	< 6	< 6	< 6	< 6	< 6	< 6	< 6	< 6	< 6	< 6	< 6	< 6	< 6	< 6	< 6
Ni	14	103	< 3	16	7	7	14	120	9	14	26	7	6	11	5
Co	14	15	5	7	5	9	6	13	< 4	6	6	10	8	9	8
Cu	< 3	238	< 3	< 3	< 3	< 3	< 3	169	< 3	87	< 3	< 3	< 3	< 3	3
Zn	28	32	26	32	37	132	40	203	29	39	47	< 5	27	38	208

Appendix B

Calculation method of trace metal bioconcentration.

$$\text{Excess Metal} = \text{Me}_{\text{samp.}} - (\text{TOC}_{\text{samp.}} \times [\text{Me}/\text{TOC}]_{\text{plankton}}).$$

$[\text{Me}/\text{TOC}]_{\text{plankton}}$ was calculated from the literature data compilation of Arthur et al 1990, assuming that carbon is 40 wt% of dry organic matter.

The ratio is then multiplied by 1.42 to take into account a carbon diagenetic loss of 30%.

The corrected Metal/OC ratios used are:

$$\text{Ni} = 0.27$$

$$\text{V} = 0.11$$

$$\text{Zn} = 3.92$$

$$\text{Cu} = 0.4$$

$$\text{Pb} = 0.21$$

Appendix C

Carbon and oxygen isotope composition of the carbonates from the San Giorgio Dolomite and Meride Limestone

Sample	Mineralogy	$\delta^{13}\text{C}$ (PDB)	$\delta^{18}\text{O}$ (PDB)	DOL %
SB 32-2	Dol	1.23	-4.51	
SB33	Dol	1.47	-1.23	
SB 59	Dol	1.01	-4.29	
SB 59	Dol	1.45	-6.74	
SB 35 U	Dol	1.19	-3.85	
SB 35 o	Dol	1.42	-2.55	
SB 36 U	Dol	1.15	-2.76	
SB 36 o	Dol	1.07	-4.54	
SB 37 U	Dol	0.77	-4.35	
SB 37 o	Cc + Dol	0.67	-3.63	69
SB 38	Cc + Dol	1.17	-3.15	60
SB 39	Cc + Dol	0.55	-4.54	12
SB 40	Cc + Dol	0.82	-3.22	22
SB 60	Cc + Dol	0.62	-4.28	10
SB 60 A	Dol	0.46	-5.50	
SB 62	Dol	1.40	-3.25	
SB 63	Dol	1.27	-3.43	
SB 64	Cc	2.21	-3.10	
SB 65	Cc	1.92	-3.69	
SB 66	Cc	1.76	-3.69	
SB 76	Cc	-0.36	-5.25	
SB 76	Cc + Dol	-0.96	-4.97	16
SB 77	Dol	-3.07	-3.43	
SB 77	Dol	-3.12	-3.75	
SB 78	Cc	0.06	-4.51	
SB 78	Cc + Dol	-0.01	-4.62	13
SB 79	Cc + Dol	-0.58	-5.28	43
SB 80	Cc + Dol	-0.13	-4.18	36
SB 83	Dol	1.28	-3.76	
SB83	Cc	-7.09	-8.59	
SB 84	Dol	2.46	-2.84	

Sample	mineralogy	$\delta^{13}\text{C}$ (PDB)	$\delta^{18}\text{O}$ (PDB)
CM 1	Cc	-1.49	-4.46
CM 3	Cc	-0.52	-3.88
CM 4	Cc	-1.38	-4.45
CM 6	Dol	1.83	-4.02
CM 2	Dol	-0.16	-7.35
SOS 1	Cc	-1.05	-3.35
SOS 2	Cc	0.77	-4.27
SOS 5	Cc	0.98	-5.25
SOS 5	Cc	0.94	-3.60
SOS 3	Cc	0.71	-4.68
SOS 4	Cc	0.74	-3.16
SOS 6	Cc	0.65	-3.98
MI 2	Dol	-7.57	-7.16
MI 2	Dol	-0.04	-8.44
MI4	Dol	-1.37	-6.35
MI4	Dol	0.66	-4.74
SB6A	Dol	1.11	-3.48
SB69	Dol	-3.17	-4.25
SB4B	Dol	1.15	-2.72
Mi 217 u	Dol	-0.31	-5.52
MI 217 m	Dol	-0.27	-7.62
MI 217 o	Dol	0.11	-7.70
SB59	Dol	1.14	-3.82
SB59	Dol	0.68	-5.72

Appendix C cont.

Carbon and oxygen isotope composition of the dolomites from the Salvatore Dolomite

Sample	$\delta^{13}\text{C}$ (PDB)	$\delta^{18}\text{O}$ (PDB)
SB23-1	-0.17	-3.45
SB23-1	0.52	-6.18
SB27-1	-0.80	-9.98
SB 27-2	-5.61	-7.20
SB27.1	1.12	-5.03
SB28	-0.86	-5.49
SB28	1.56	-3.45
Ro1	2.07	-4.33
RO1	1.63	-2.31
RO1	1.49	-5.05
RO 1-1	2.51	-2.68
RO 1-2	1.53	-2.65
RO 1-3	1.37	-4.69
RO4	1.48	-4.56
RO4	2.16	-1.71
SB 53	2.25	-2.46
SALV 3	0.29	-3.38
LAV2	1.28	-5.63
LAV 3	0.98	-4.46
LAV4	0.97	-4.26
SALV 5A	0.34	-5.24
SB52	0.78	-3.38
SB52	-0.01	-5.88
SB29	-0.98	-3.05
SB 30	-1.63	-5.45

Appendix C cont.

Carbon and oxygen isotope composition of the dolomites from the Grenzbitumenzone.

sample/layer	$\delta^{13}\text{C}$ (PDB)	$\delta^{18}\text{O}$ (PDB)
Mu 23	-2.07	-3.97
Vst 51	-3.65	-5.71
KK 52a	-2.83	-4.24
KK 52b	-2.94	-3.74
KK 52c	-2.51	-3.94
KK 52d	-2.50	-5.16
KK52-1	-2.49	-4.32
KK 52-2	-2.87	-4.78
KK 52-3	-3.22	-5.29
KK 52-4	-2.60	-3.52
KK 52-5	-3.10	-2.66
KK 52-6	-2.61	-3.61
KK 52-7	-2.44	-2.48
MI 57o-1	-2.84	-1.61
MI 57o-2°	-3.17	-3.59
MI 57o-3	-3.31	-3.35
MI 57o-4	-3.57	-3.92
MI 57o-5	-3.00	-3.21
MI 69	-3.05	-2.96
MI 69	-3.15	-1.20
MI 69	-3.57	-1.25
MI 69	-3.49	-0.97
MI 69	-3.44	-1.78
FO 71	-2.56	-4.11
MI 87	-4.27	-2.80
MI 87	-4.08	-2.04
MI 87	-3.86	-1.77
MIN 88	-3.97	-3.10
MI 88-1	-4.12	-1.35
MI 88-2	-3.85	-1.07
MI 88-3	-4.31	-2.49
102/46A	-3.73	-3.81
102/46A	-2.68	-3.16
POR 120	-5.63	-3.32

Appendix C cont.

sample/layer	$\delta^{13}\text{C}$ (PDB)	$\delta^{18}\text{O}$ (PDB)
122	-3.94	-3.19
131/1A	-3.82	-3.97
131/1A	-3.81	-4.19
131/1A	-3.77	-4.51
134 u	-2.61	-4.67
134m	-2.73	-3.04
134 o	-1.73	-2.86
138 °	-3.68	-2.91
138	-3.69	-4.58
138	-3.75	-4.79
138	-3.63	-4.50
138	-4.38	-5.81
138	-3.91	-5.13
138	-3.94	-5.05
138	-3.55	-4.91
138	-3.53	-4.26
138	-3.74	-3.45
138	-3.62	-3.41
MI 138/7	-4.15	-4.10
MI 138/7	-3.83	-3.31
MI 138/7	-3.65	-2.35
MI 138/7	-3.54	-2.79
MI 138/7	-3.66	-2.66
140 mu	-3.55	-2.01
140 mu	-4.16	-2.93
140 mu	-3.65	-1.61
143/2	-3.98	-2.05
143/2	-4.02	-2.10
MI 143	-3.99	-2.03
MI 143	-4.21	-1.88
MI 143	-4.28	-2.25
ALBIO 144	-3.31	-0.52
ALBIO 144 -2	-3.26	-0.73
ALBIO 144-3	-3.15	-2.42
BESANO 144	-3.32	-2.56

Appendix C cont.

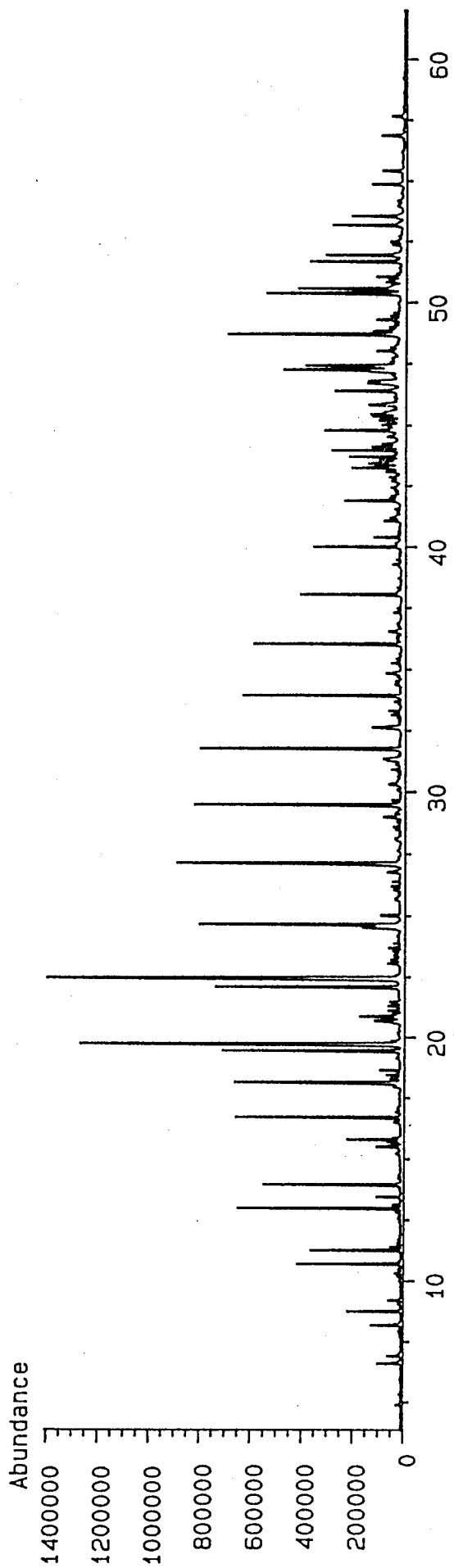
sample/layer	$\delta^{13}\text{C}$ (PDB)	$\delta^{18}\text{O}$ (PDB)
144/5b	-4.11	-3.75
144/5B	-4.33	-3.68
144/5B	-4.13	-2.81
144/5B	-4.38	-2.68
SB69	-3.17	-4.29
SB 68 STR 144	-3.44	-1.27
SB 68 STR 144	-4.06	-1.99
SB 68 STR 144	-3.49	-1.40
SB 68 STR 144	-4.11	-1.27
MI 144/4 A9	-3.81	-2.32
MI 144/4 A9	-4.04	-1.27
MI 144/4 A9	-4.43	-1.69
MI 146	-3.98	-1.45
MI 146	-3.78	-0.76
MI 162	-2.83	-2.18
MI 162 /2	-3.00	-1.61
178	-2.36	-2.73
MI 185	-1.36	-4.26
MI 185/2	-3.42	-4.59
MI 186	-2.08	-3.85
MI 187	-1.98	-5.69
MI 187/2	-1.19	-5.74
SB 74 /187	-0.83	-5.25
SB72	-3.72	-6.30
HG 1	-3.05	-4.67
SB 70	-3.91	-3.92
SB 70	-2.05	-4.93
SB 70	-3.31	-2.59
SB 70	-3.31	-6.53

APPENDIX D

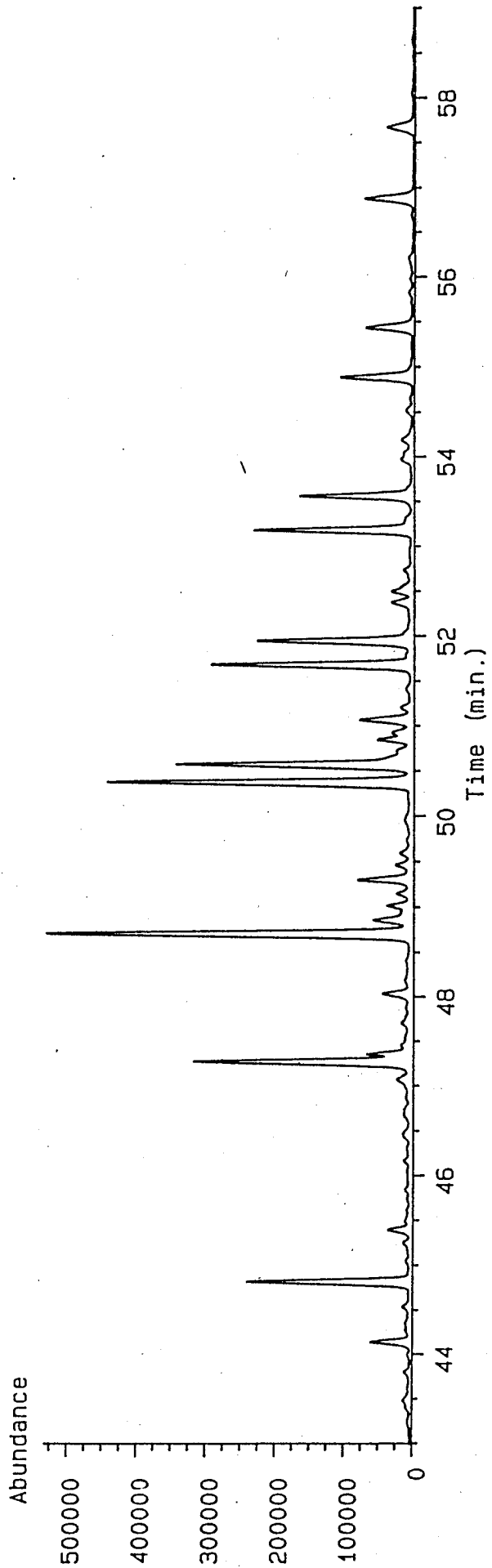
Total ion current gas chromatograms (TIC) of the saturated hydrocarbon fraction and mass fragmentograms of the Hopanes (m/z 191), steranes (m/z 217) and diasteranes (m/z 218) of the studied samples.

Layer 82

TIC of 689HCS.d

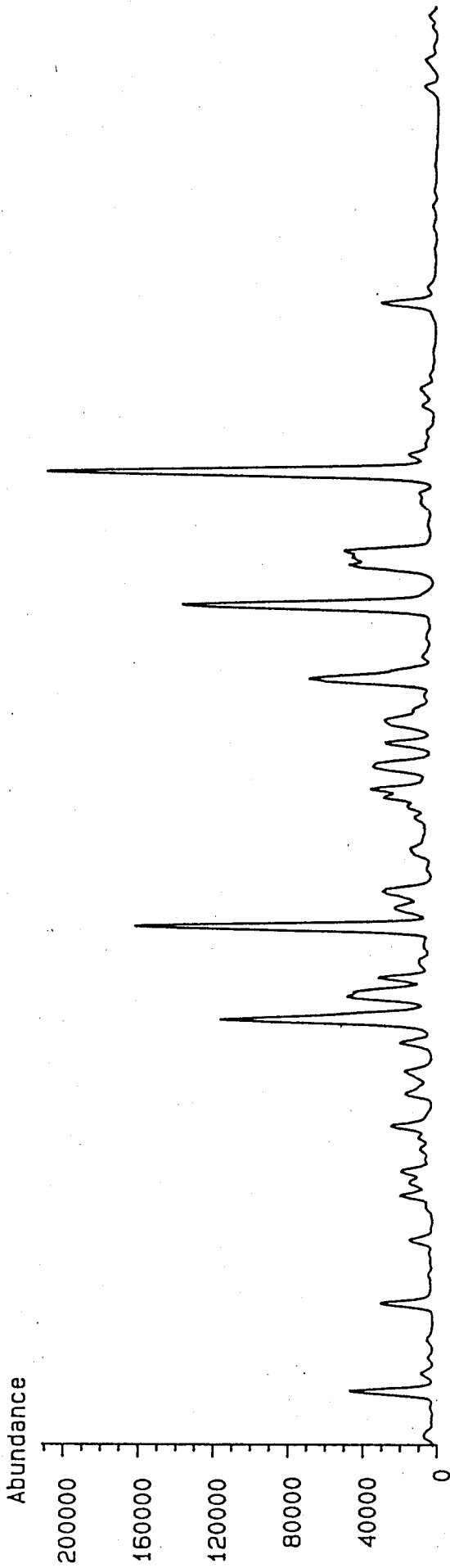


Ion 191.20 amu. from 689HCS.d

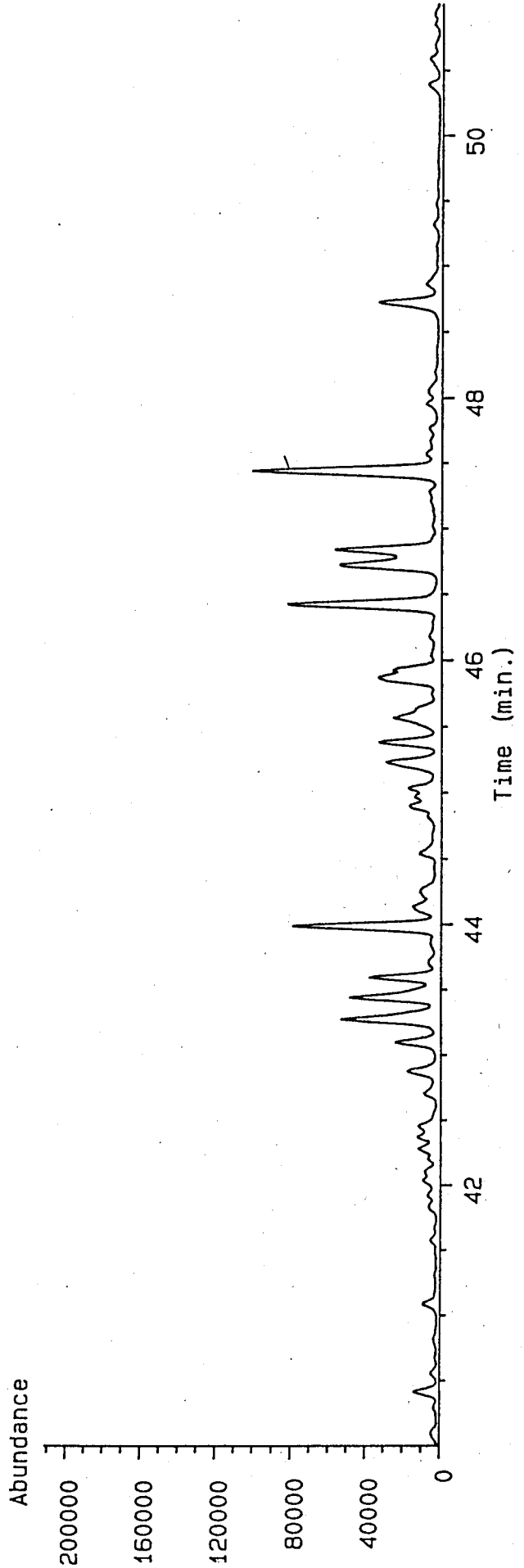


Layer 82

Ion 217.20 amu. from 689HCS.d

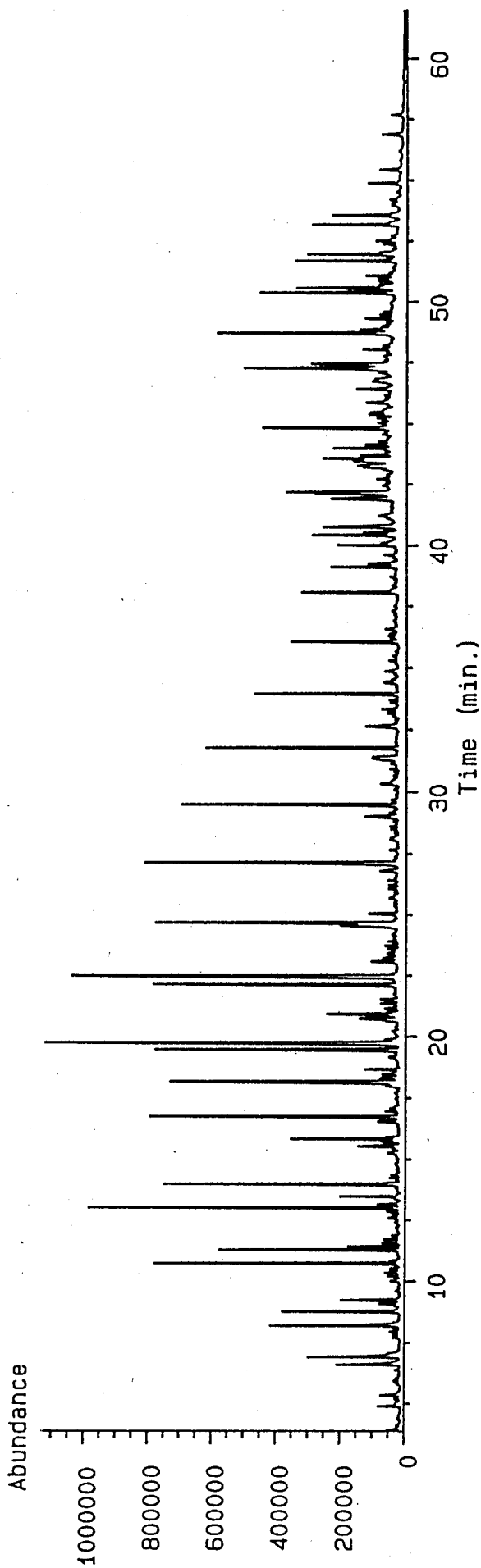


Ion 218.20 amu. from 689HCS.d

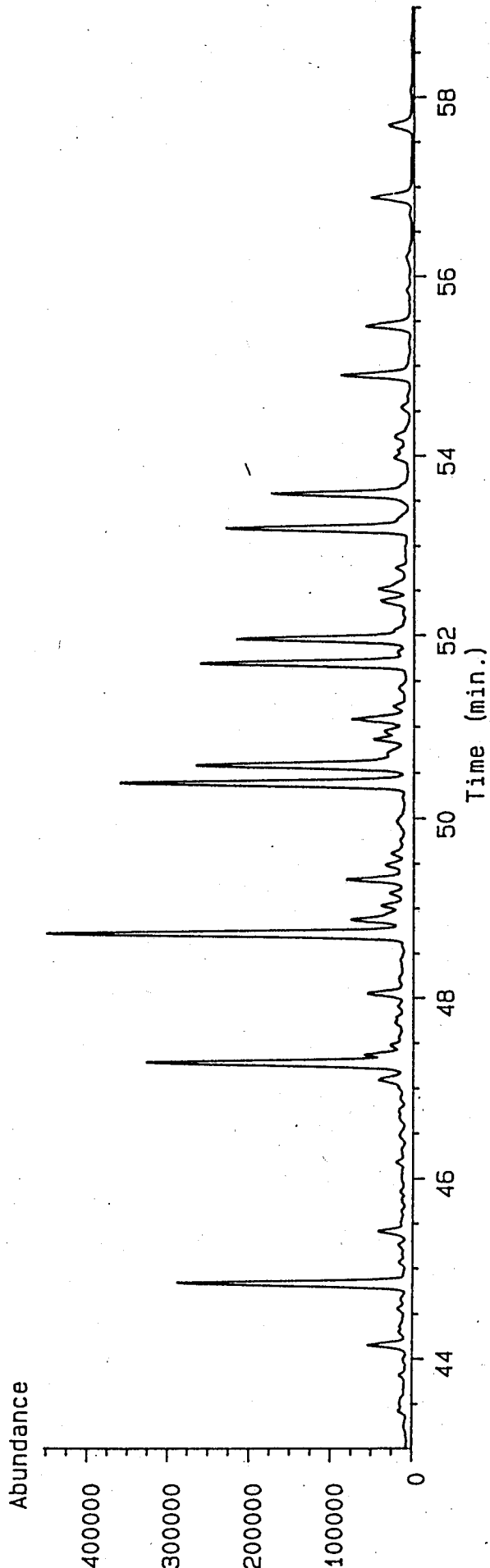


Layer 110

TIC of 690HCS.d

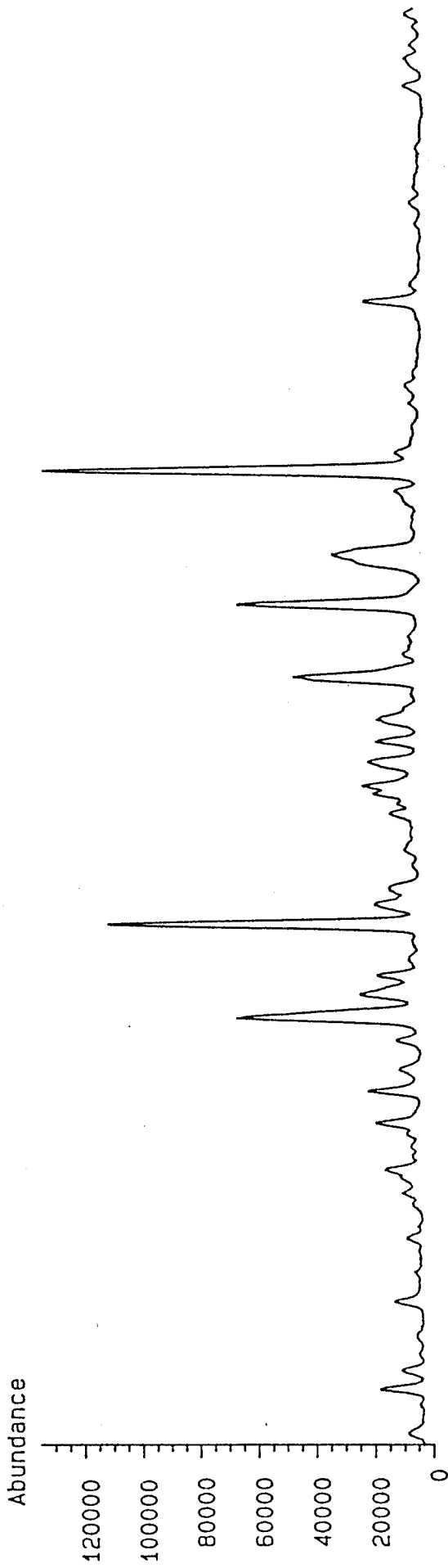


Ion 191.20 amu. from 690HCS.d

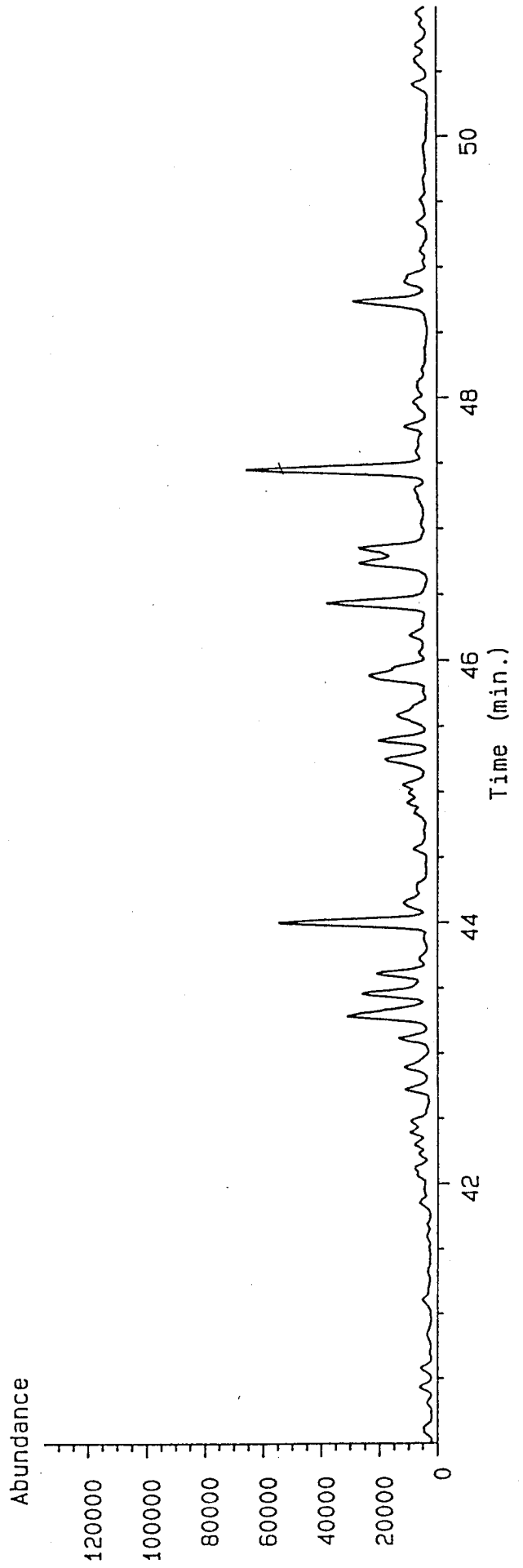


Layer 110

Ion 217.20 amu. from 690HCS.d

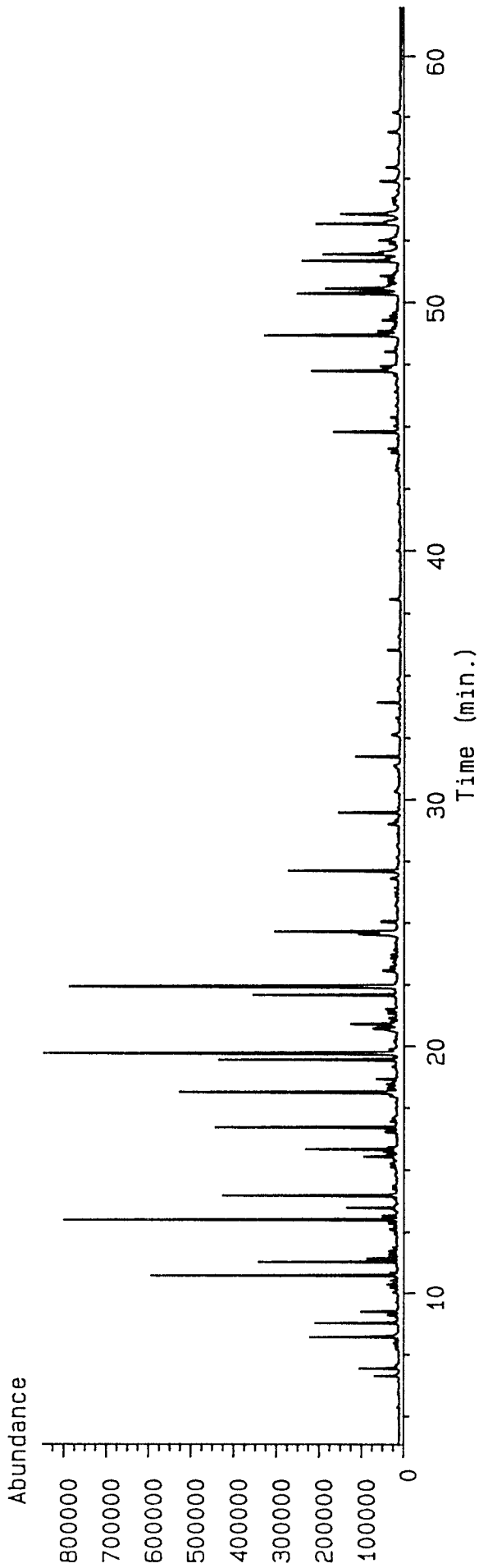


Ion 218.20 amu. from 690HCS.d

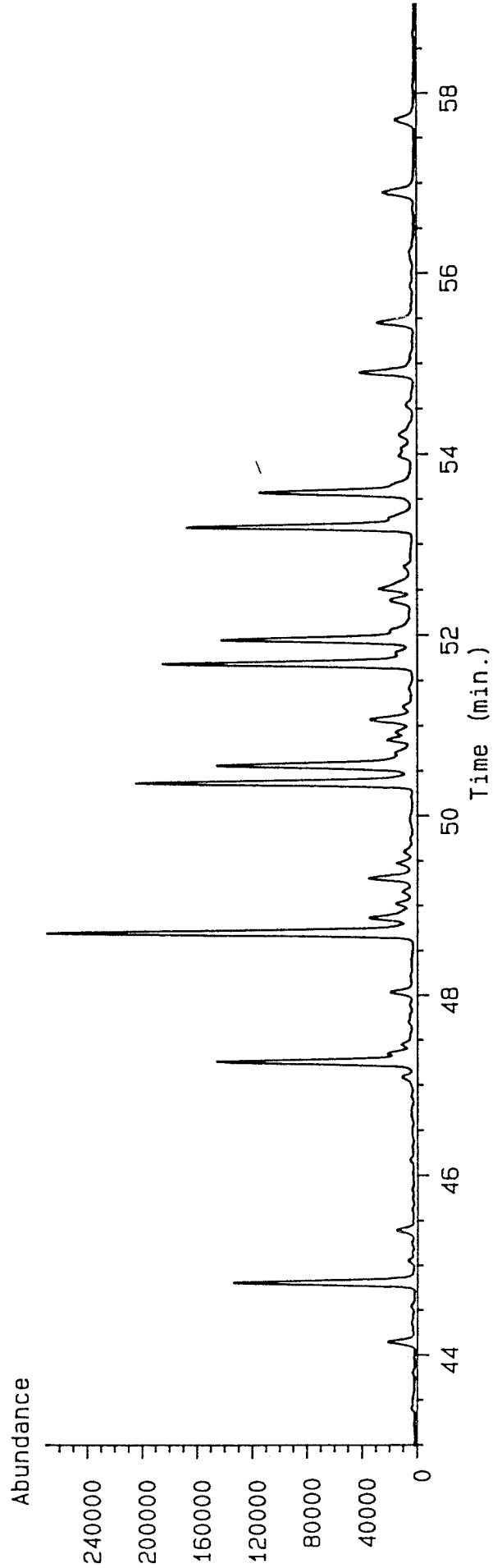


Layer 132

TIC of 695HCS.d

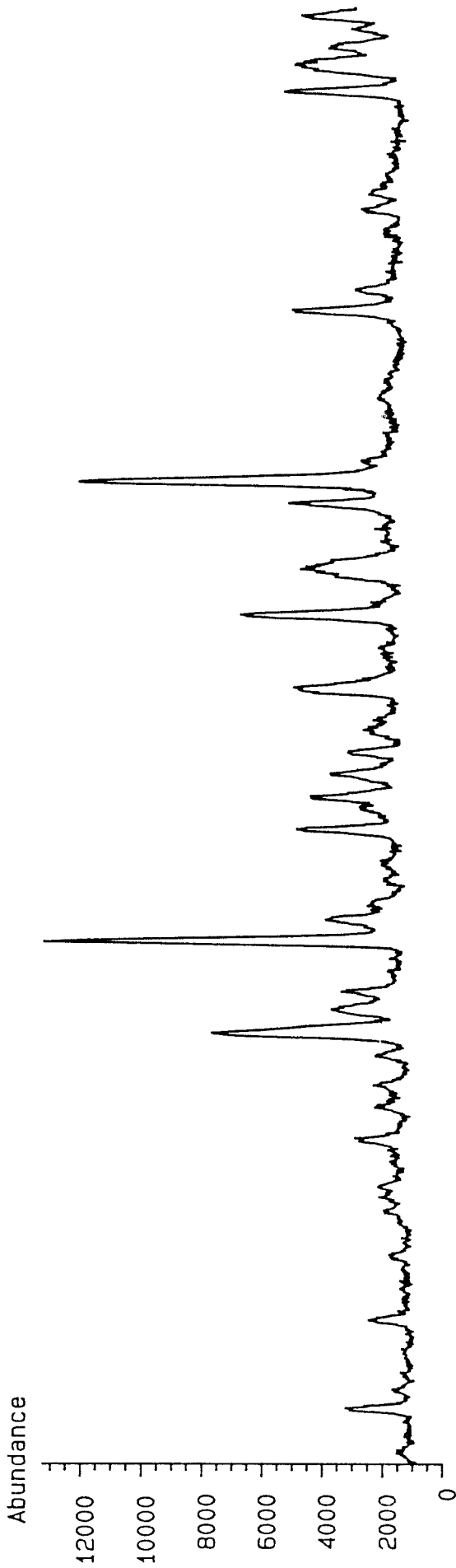


Ion 191.20 amu. from 695HCS.d

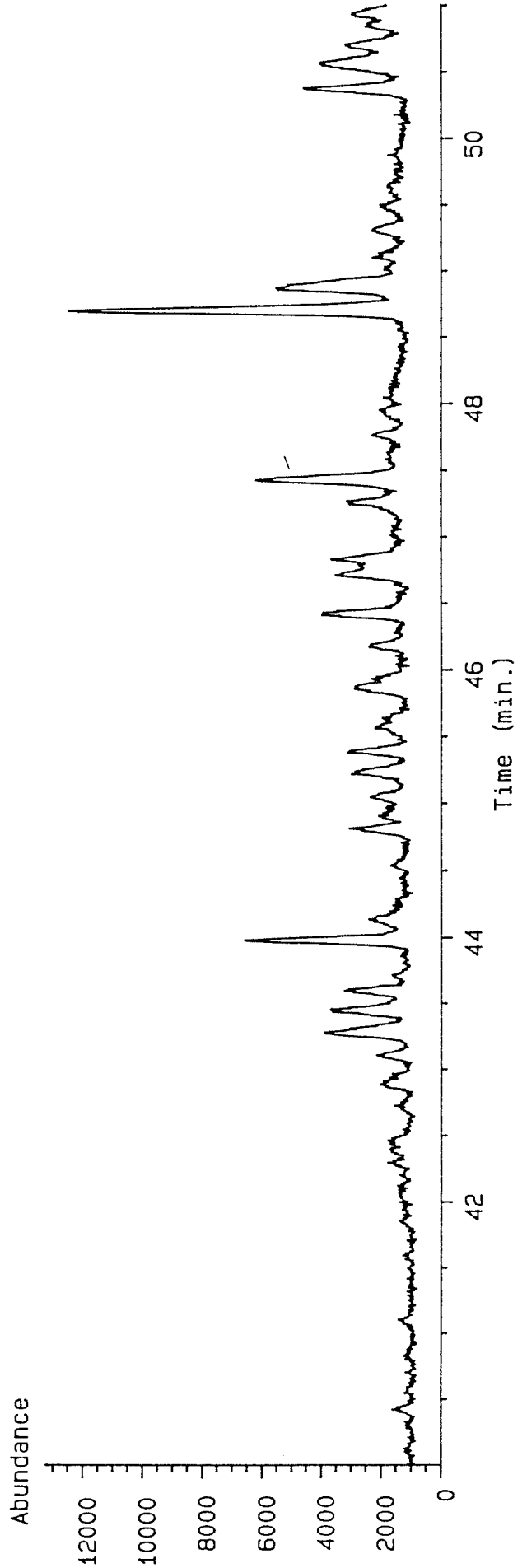


Layer 132

Ion 217.20 amu. from 695HCS.d

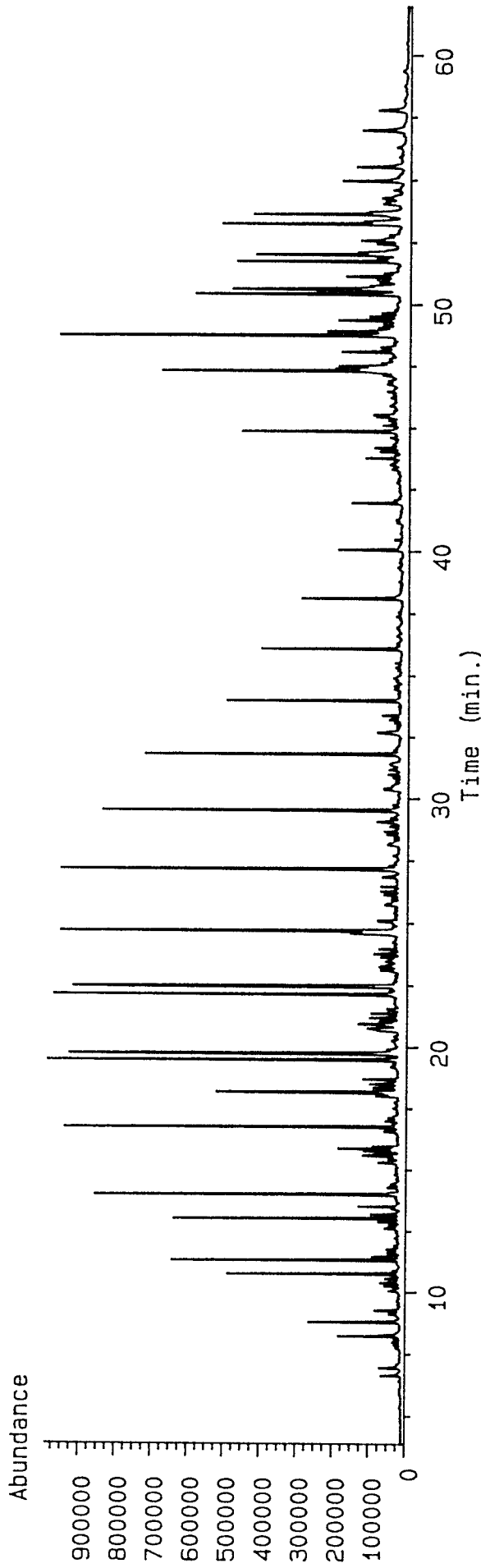


Ion 218.20 amu. from 695HCS.d

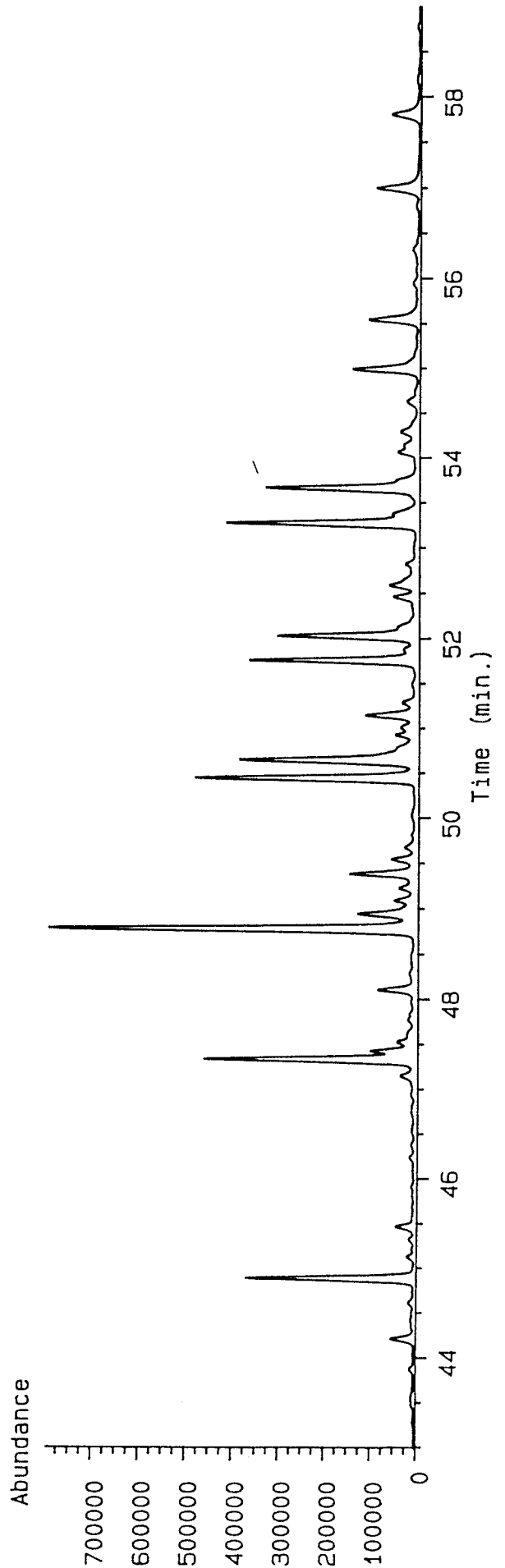


Layer 136

TIC of 694HCS.d

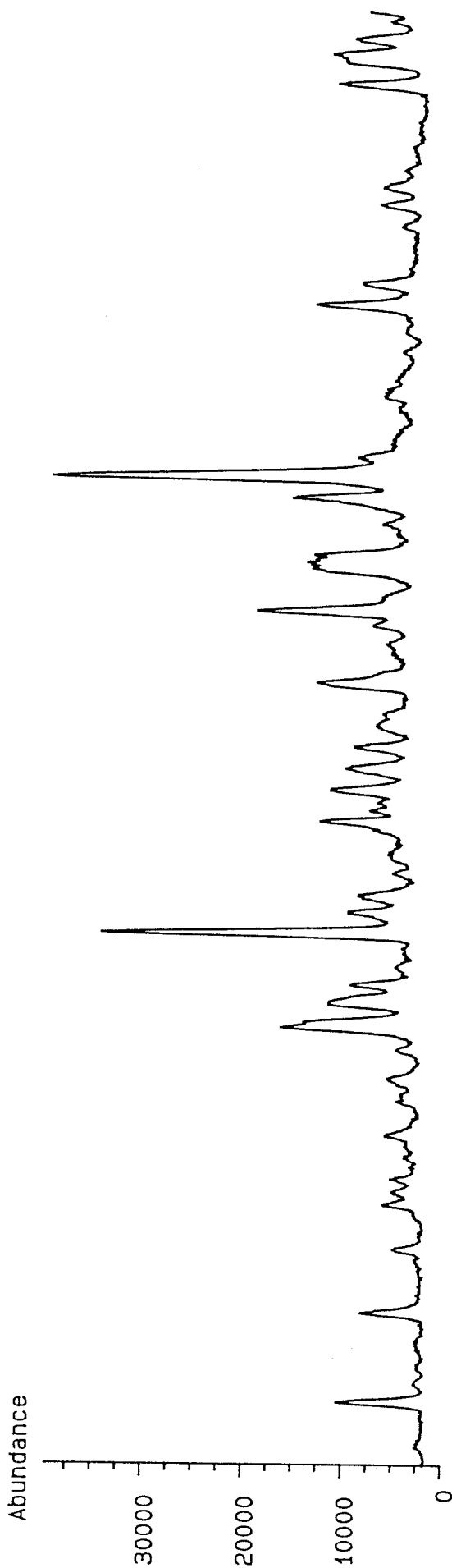


Ion 191.20 amu. from 694HCS.d

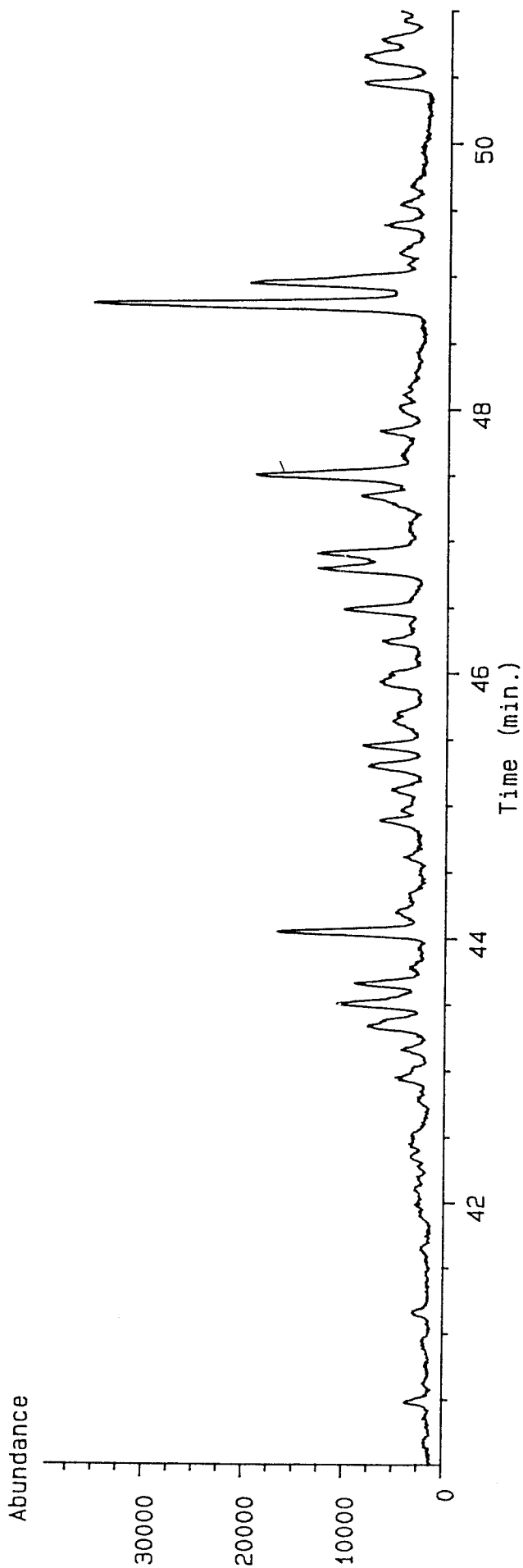


Layer 136

Ion 217.20 amu. from 694HCS.d

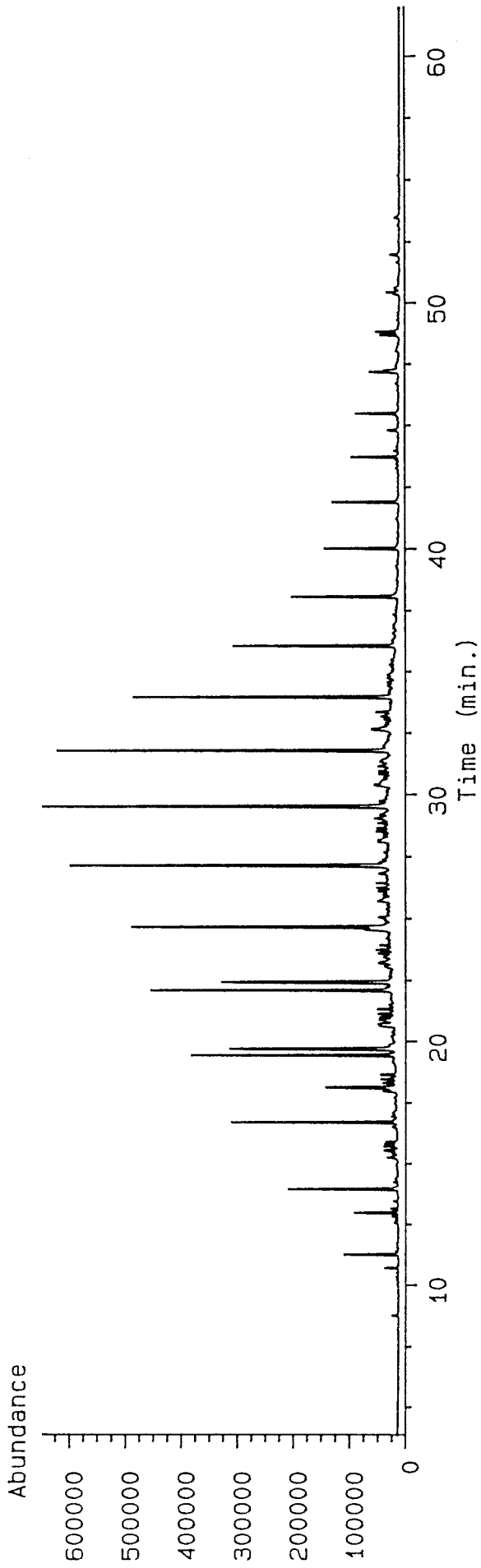


Ion 218.20 amu. from 694HCS.d

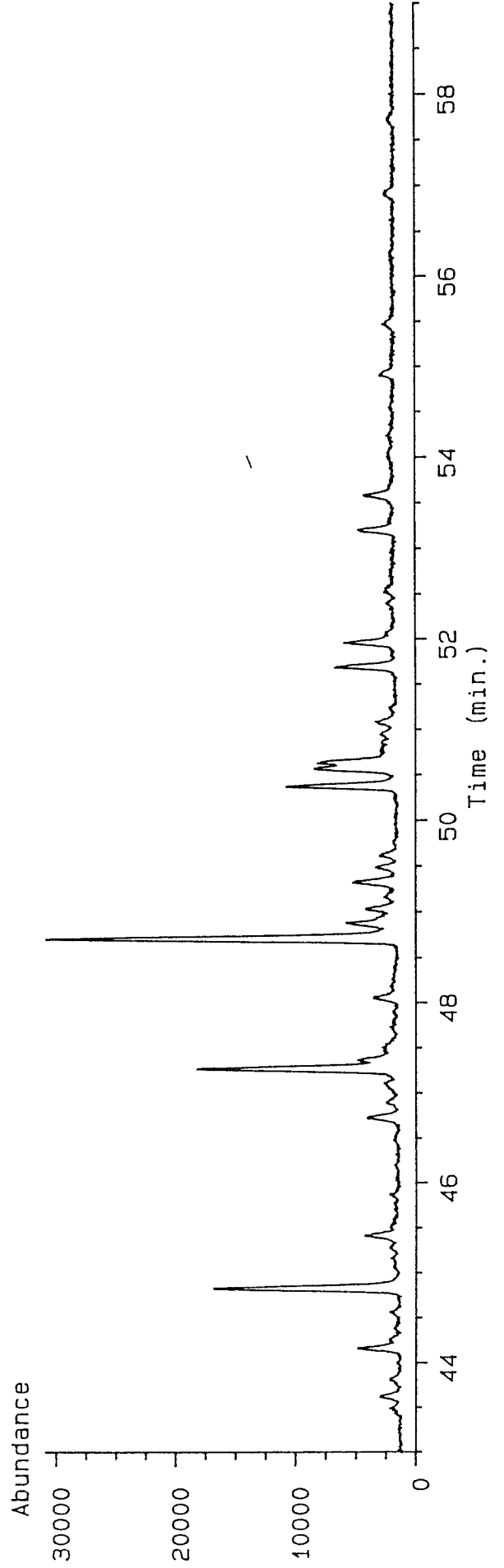


Layer 155

TIC of 805HCS.d

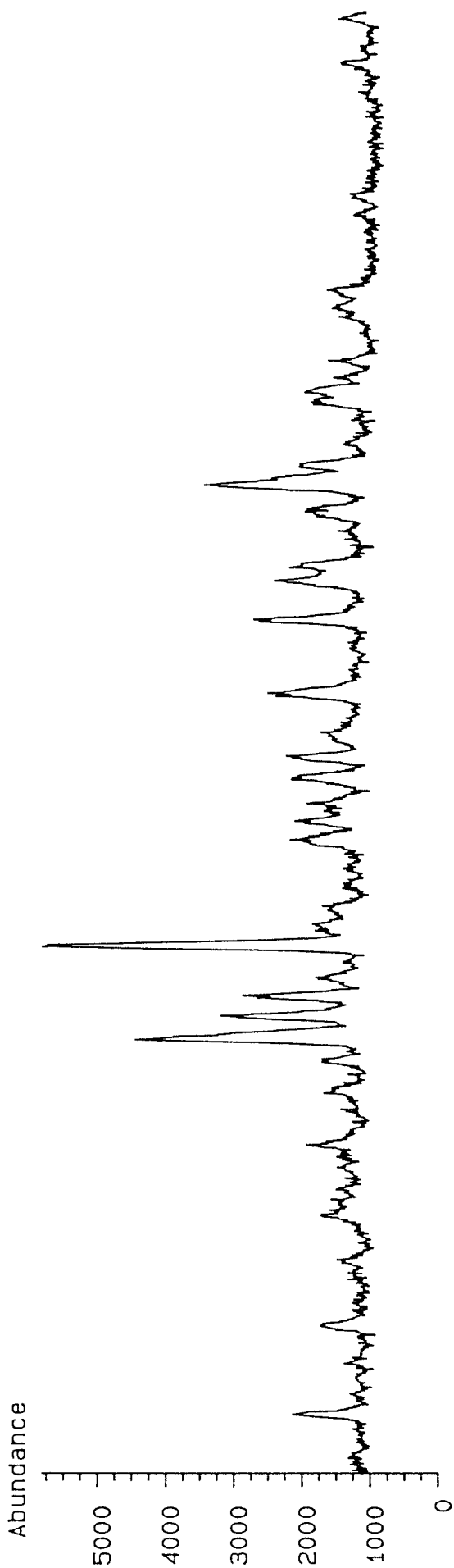


Ion 191.20 amu. from 805HCS.d

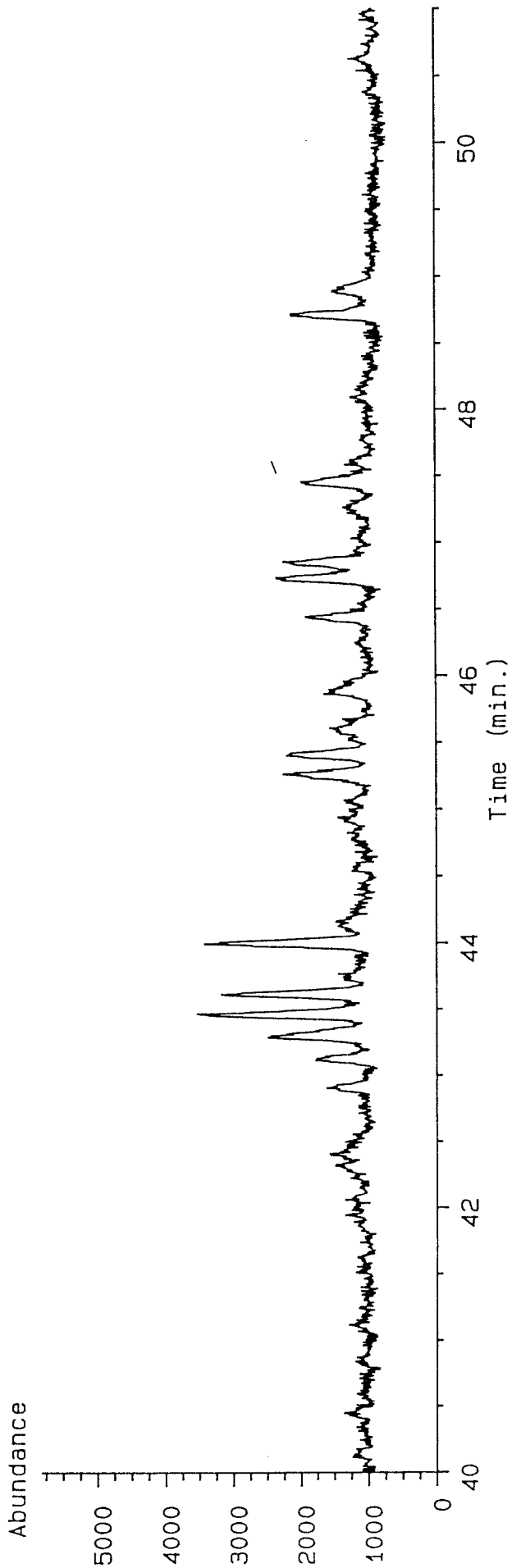


Layer 155

Ion 217.20 amu. from 805HCS.d

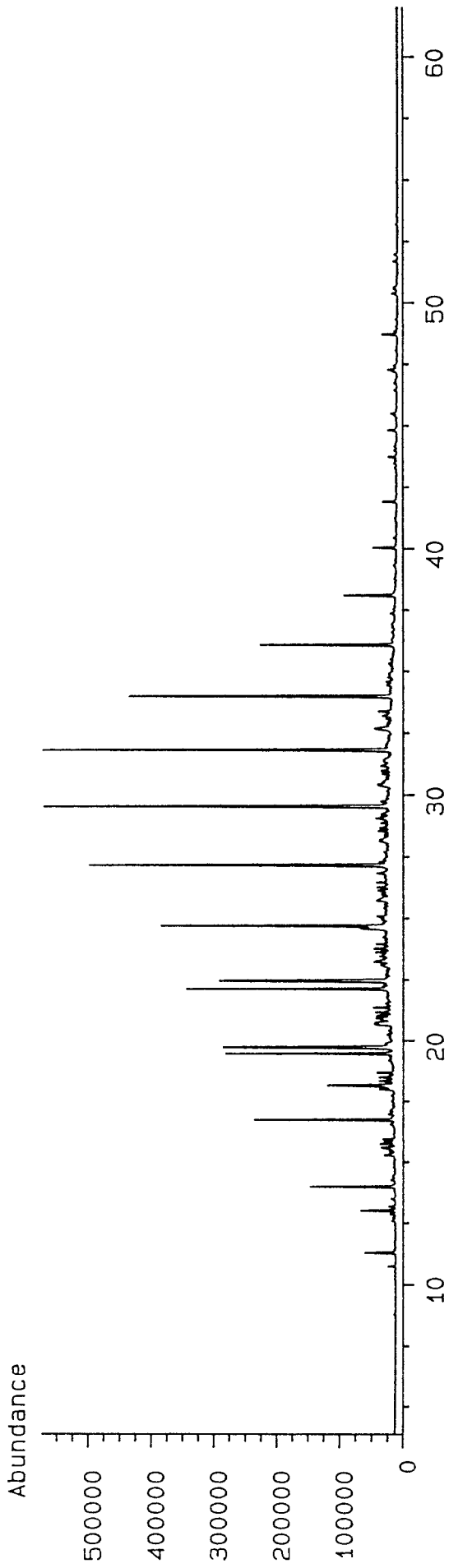


Ion 218.20 amu. from 805HCS.d

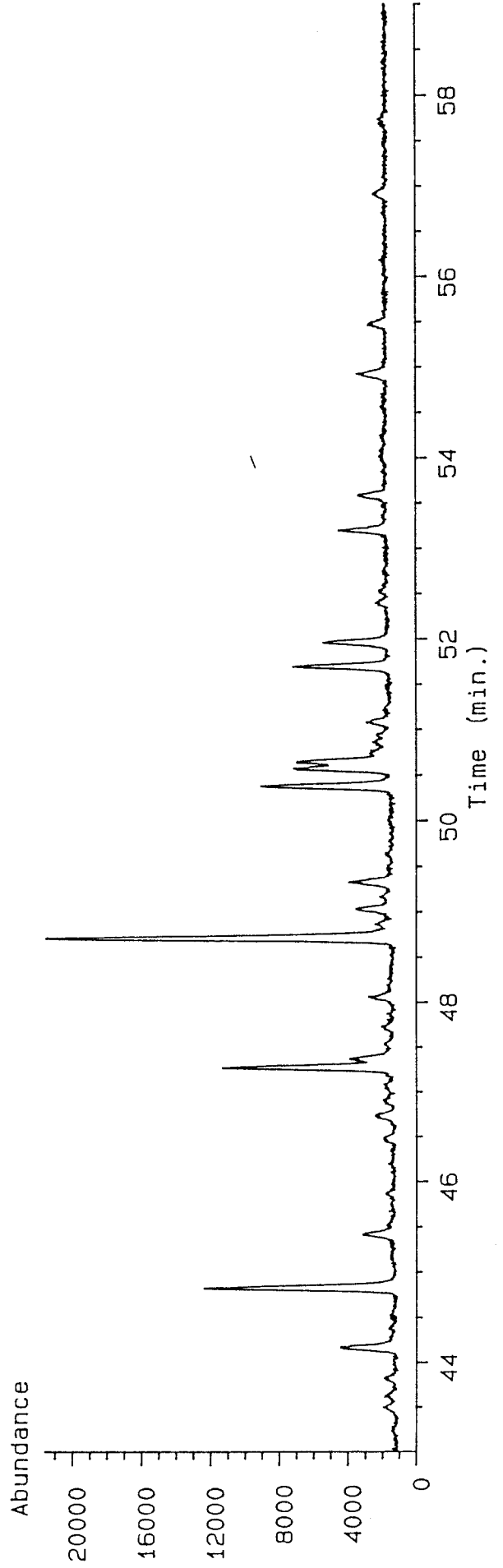


Layer 162

TIC of 806HCS.d

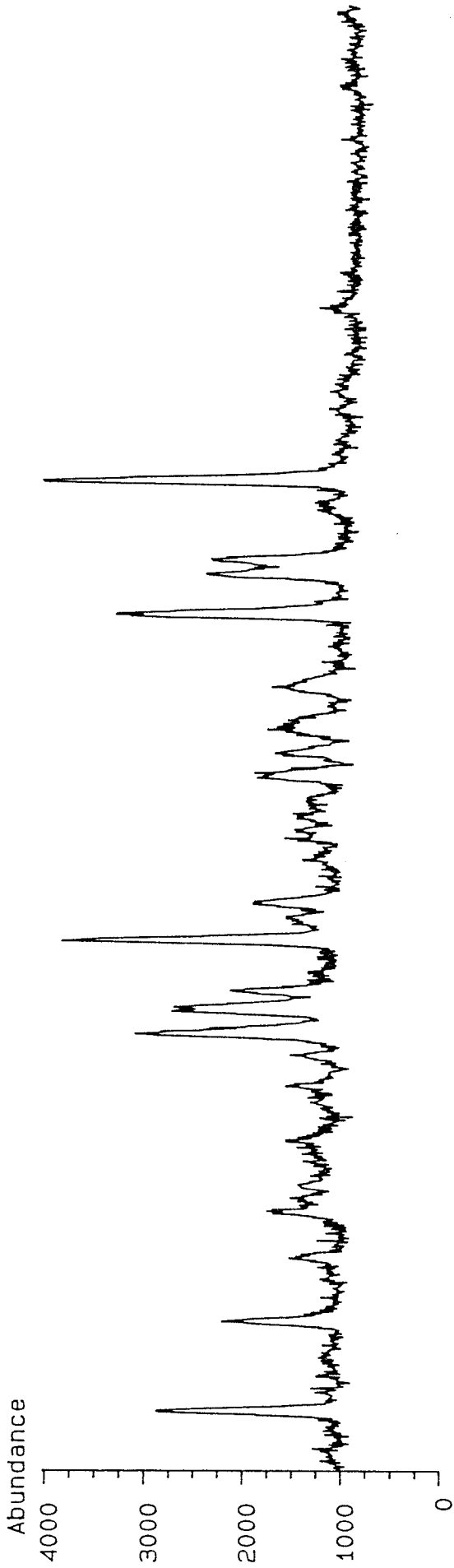


Ion 191.20 amu. from 806HCS.d

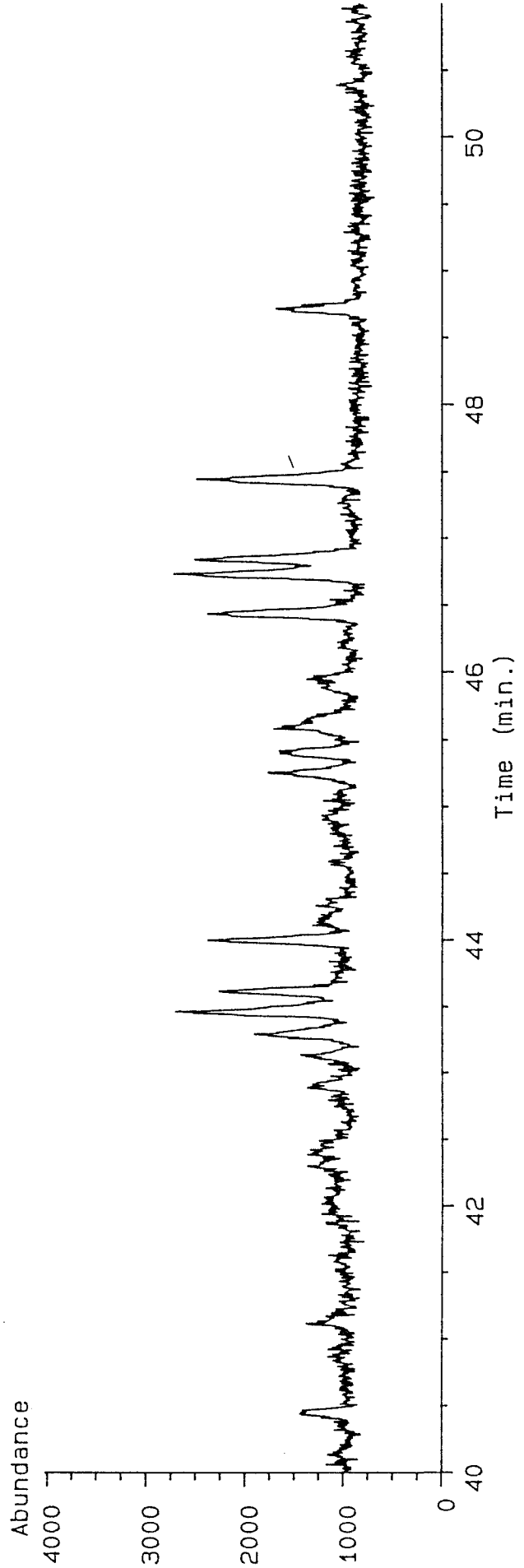


Layer 162

Ion 217.20 amu. from 806HCS.d

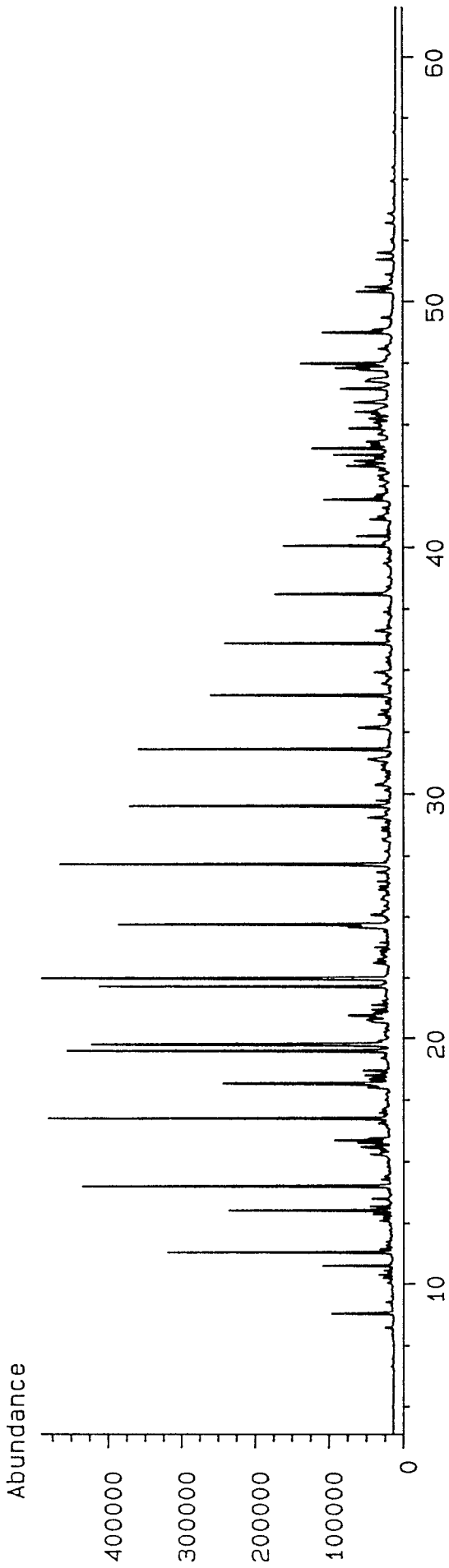


Ion 218.20 amu. from 806HCS.d

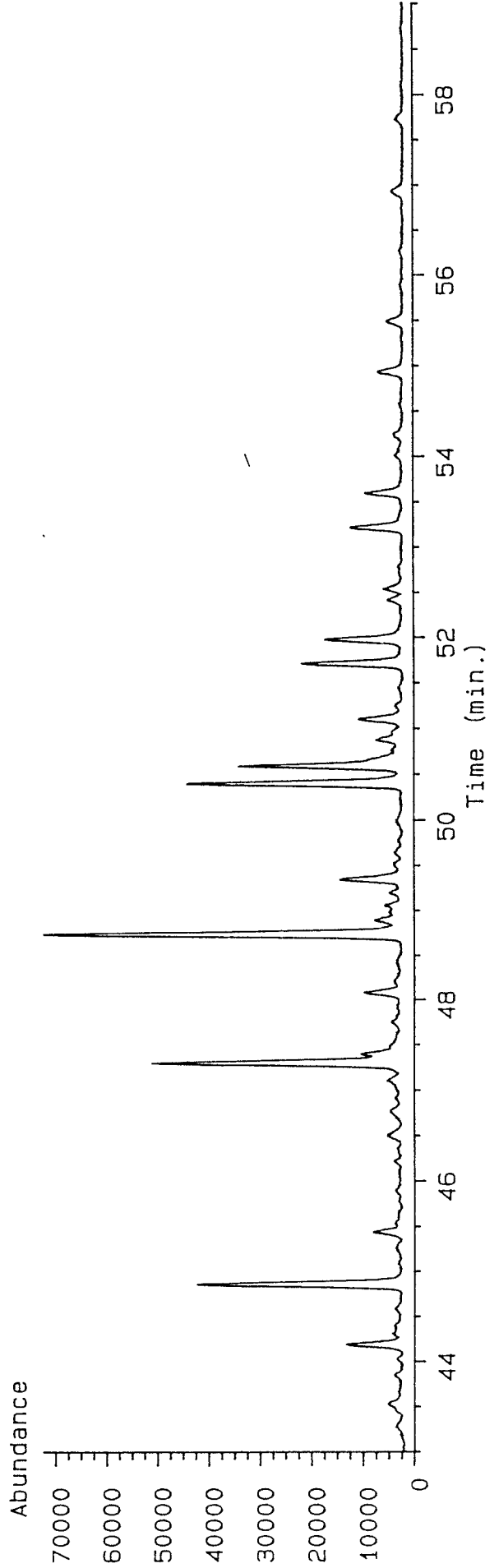


Layer 226

TIC of 807HCS.d

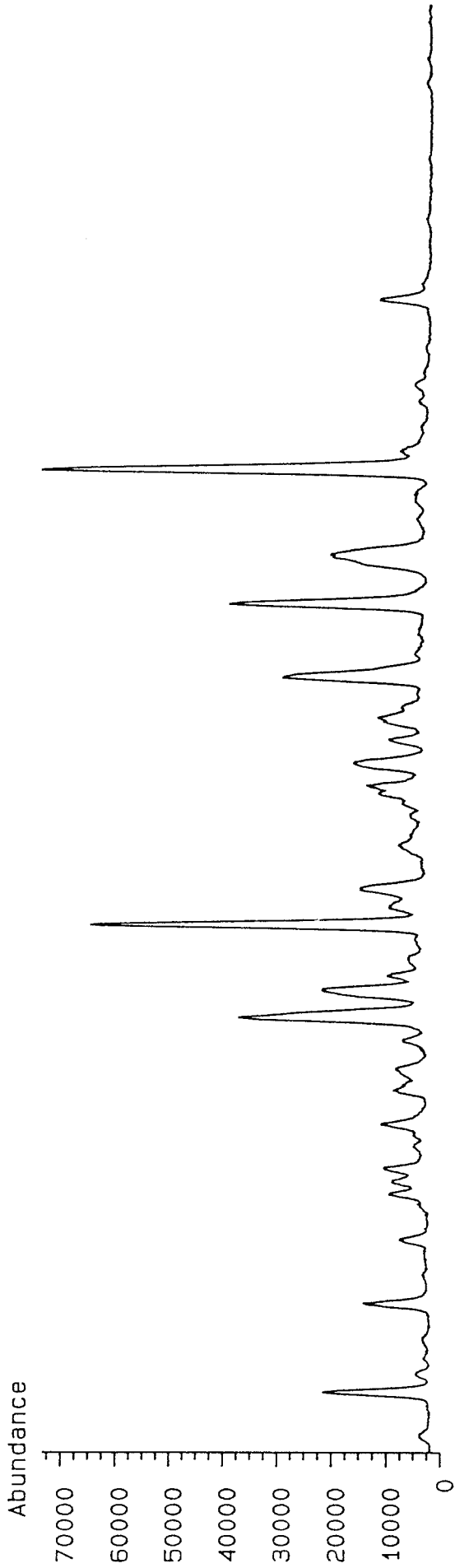


Ion 191.20 amu. from 807HCS.d

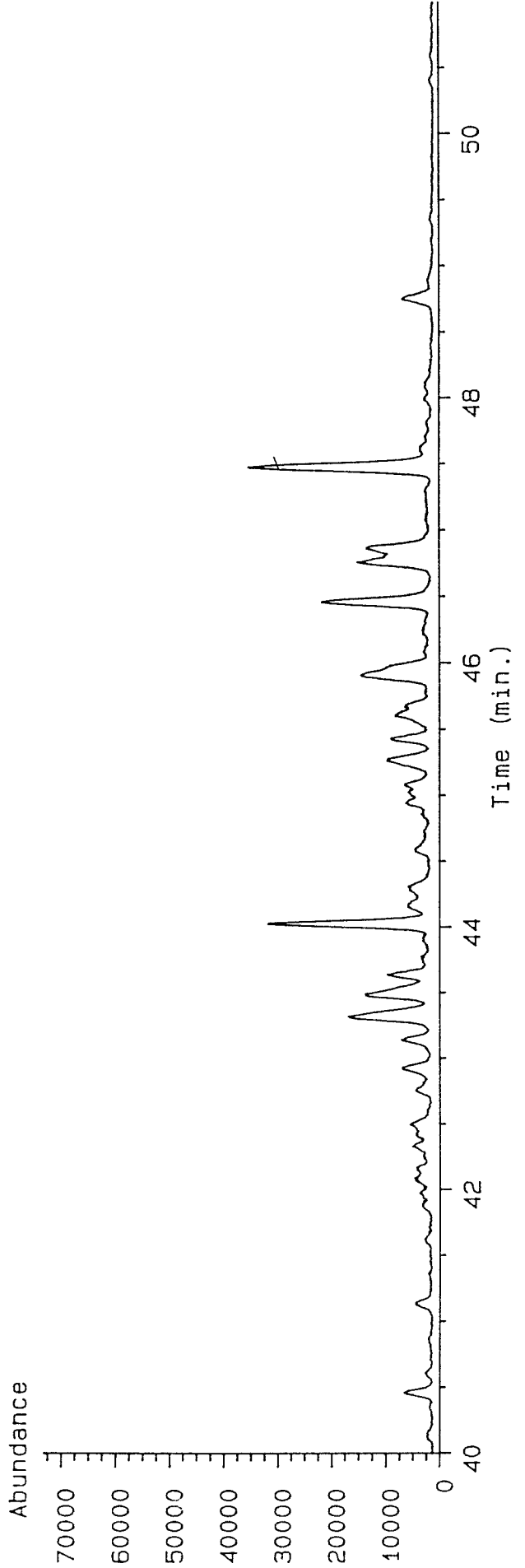


Layer 226

Ion 217.20 amu. from 807HCS.d



Ion 218.20 amu. from 807HCS.d



Curriculum vitae**Stefano Michele Bernasconi**

Born on June 16, 1961 in Sorengo, Ticino, Switzerland.

Education:

1967 - 1972: Scuole elementari di Neggio, Ticino, Switzerland.

1972 - 1977: Ginnasio cantonale di Agno, Ticino, Switzerland.

1977 - 1980: Liceo Cantonale di Lugano, Ticino, Switzerland.

1980 - 1986: Study of geology at the ETH-Zürich

1986: Diploma thesis: "Il metamorfismo di contatto dell' aureola termometamorfica del Monte Capanne, Isola d' Elba, Italia". supervisors: Prof. Dr. Volkmar Trommsdorff, Prof. Dr. Volker Dietrich.

1987 - 1991: Doctoral student at the Geological Institute, ETH-Zürich. Thesis: "Geochemical and microbial controls on dolomite formation and organic matter production/preservation in an anoxic environment: a case study from the Middle Triassic Grenzbitumenzone, Southern Alps (Ticino, Switzerland)" Supervisors: Prof. Dr. D. Bernoulli, Prof. Dr. J. McKenzie, and Dr. A Riva.